UNIVERSITY OF SOUTHAMPTON

ELECTRICAL PROPERTIESOF MINERAL OIL AND OIL/IMPREGNATED PRESSBOARD FOR HVDC CONVERTER TRANSFORMERS

By

Yuan Zhou

A thesis submitted for
the degree of Doctor of Philosophy

Electronics and Computer Science

Faculty of Physical Sciences and Engineering

University of Southampton

United Kingdom

Feburary 2014

UNIVERSITY OF SOUTHAMPTON

ABSTRACT

FACULTY OF PHYSICAL SCIENCES AND ENGINEERING
ELECTRONICS AND COMPUTER SCIENCE

Doctor of Philosophy

ELECTRICAL PROPERTIESOF MINERAL OIL AND OIL/IMPREGNATED PRESSBOARD FOR HVDC CONVERTER TRANSFORMERS

by Yuan Zhou

Modern power industry requires higher performance dielectric liquids. Mineral oil is one of those most important and widely used insulating materials. Recently, research on the dielectric properties of mineral oil insulation reveal that oil resistivity can greatly influence the field distribution within an oil-pressboard insulation system in a DC field environment, especially during polarity reversals. Basic test methods such as dielectric spectroscopy and polarization and depolarization measurement have already been used to test mineral oil and pressboard conductivity. However, the knowledge about the mechanism of electrical conduction ininsulating oil and pressboard is still limited. Therefore, the goal of this thesis is to gain a better understanding of the mechanism of electrical conduction in mineral oil and oil impregnated pressboard.

Polarization and depolarization current method (PDC) has gained huge popularity for insulation diagnosis. This time-dependent measurement may provide sufficient information about the dielectric properties of mineral oil and its electrical performance. Here, the dielectric characteristics of three types of mineral oils with different ageing times have been studied using the PDC method. A new polarization theory involving two kinds of charge carriers have been proposed to explain the dielectric behaviour observed in our measurements.

Dielectric spectroscopy is a powerful tool to study dipole relaxation, electrical conduction and structure of molecules. Electrode polarization, as a parasitic effect due to the blocking of charge carriers in the vicinity of an electrode, can make the frequency response at low frequency difficult to understand. Since charge carriers in mineral oil are

not only generated from dissociation but also from injection at electrodes, the current induced by the motion of the injected charge carriers should also be taken into consideration. The polarization caused by the injection current has been studied in this thesis. When the electric field is not intense, the injection current is proportional to the field and only contributes to the imaginary part of the complex permittivity. A new computer based calculation method and a modified space charge polarization theory have been proposed with this injection current being involved. The frequency responses of three different kinds of mineral oils have been measured and the experimental results have been compared with the simulation using the modified model. It seems the density of the injected charge carriers increases with the aging period. This new model enables one to gain a better understanding of electrical conduction in mineral oil.

The design and choice of an electrode system is important in DC conductivity measurement of insulating liquid. In this thesis, the electric field distribution of an electrode system which consists of two parallel circular metallic electrodes and a guard electrode has been studied using Comsol Multiphysics software. A new parameter which is not yet involved in current standards, the edge radius, has been investigated by means of field calculation. It has been found out that there are regions in the vicinity of the edges of the guard and measuring electrode at which the field is dramatically distorted. If the edges of these two electrodes are sharp, the maximum electric field in the test cell will be much higher than the average field between the measuring electrode and the high voltage electrode. An empirical equation has been proposed to calculate this maximum field. The classic correction expression of effective radius has been re-evaluated with the edge radius being taken into account. Experimental work has been performed to confirm this conclusion. Three kinds of mineral oils with different aging times have been tested under the DC field using a guarded electrode system and the electric strengths of these oils have been estimated. A recommendation has been made to current standards in insulating liquid measurement.

The dielectric properties of the oil impregnated pressboard sample have been evaluated with the PDC measurement under different temperatures and electric fields. The classic R-C equivalent model has used to explain the dielectric behaviour of the oil/pressboard sample in our PDC measurement. As the electrode effect should be taken into consideration in a DC field, a modified R-C equivalent model has been proposed and used to fit the experimental results and good fitting has been obtained.

Contents

List of Figures

List of Tables

Declaration of Authorship

I, Yuan Zhou, declare that the thesis entitled:

"Electrical Properties in Mineral Oil and Oil/Impregnated Pressboard for HVDC Converter Transformers"

and the work presented in it are my own, and have been generated by me as a result of my own original research. I confirm that:

- this work was done wholly or mainly while in candidature for a research degree at the University;
- where any part of this thesis has previously been submitted for a degree or any other qualification at this University or any other institution, this has been clearly stated;
- where I have consulted the published work of others, this is always clearly attributed;
- where I have quoted from the work of others, the source is always given. With the exception of such quotations, this thesis is entirely my own work;
- I have acknowledged all main sources of help;
- where the thesis is based on work done by myself jointly with others, I have made clear exactly what was done by others and what I have contributed myself;

parts of this work have been published as:

Journals:

Zhou, Y, Hao, M, Chen, G, Wilson, G and Jarman, P (2014) Study of the dielectric response in mineral oil using frequency-domain measurement. *Journal of Applied Physics*, 115

Zhou, Y, Hao, M, Chen, G, Wilson, G and Jarman, P (2014) Study of a guarded electrode system in the dc conductivity measurement of insulating liquid *IOP Measurement Science and Technology* 25 075005

Hao, M, Zhou, Yuan, Chen, G, Wilson, G and Jarman, P (2014) Space Charge behaviour in 1mm thick oil-impregnated pressboard under HVDC stresses *IEEE Trans DEI special issue HVDC,* accepted

Zhou, Y, Hao, M, Chen, G, Wilson, G and Jarman, P (2014)Study of the charge dynamics in mineral oil under a non-homogeneous field submitted to *Journal of Applied Physics*

Zhou, Y, Hao, M, Chen, G, Wilson, G and Jarman, P (2014)Quantitative study of electric conduction in mineral oil by polarization and depolarization current measurement submitted to *IEEE Trans DEI special issue Insulating Liquid*

Conferences:

Zhou, Y, Hao, M, Chen, G, Wilson, G and Jarman, P (2012) Frequency-dependence of conductivity of new mineral oil studied by dielectric spectroscopy. In, *Proceedings of 2012 International Conference on High Voltage Engineering and Application*.781-784.

Hao, M, Zhou, Y, Chen, G, Wilson, G and Jarman, P (2013) Space Charge Behaviour in Thick Oil-Impregnated Pressboard under HVDC Stresses. In, *IEEE 2013 International Conference on Solid Dielectrics,* 397-400.

Zhou, Y, Hao, M, Chen, G, Wilson, G and Jarman, P (2013) Space charge polarization in insulating mineral oil. At *2013 IEEE Conference on Electrical Insulation and Dielectric Phenomena,* 587-590.

Hao, M, Zhou, Y, Chen, G, Wilson, G and Jarman, P (2014) Space charge behaviour in oil and impregnated pressboard combined insulation system *ICDL 2014*1-4

Zhou, Y, Hao, M, Chen, G, Wilson, G and Jarman, P (2014) Study of the depolarization current of the mineral oils with different aging times *ICDL 2014* 1-4

Zhou, Y, Hao, M, Chen, G, Wilson, G and Jarman, P (2014) A new approach to understand the frequency response of mineral oil *ICDL 2014* 1-4

Hao, M, Zhou, Y, Chen, G, Wilson, G and Jarman, P (2014)Space charge dynamics in Oil and thick pressboard combined system *CEIDP 2014*867 - 870

Definitions and Abbreviations

A_{ASTM} : Effective area of measuring electrode obtained from ASTM D257 (m^2)

$A_{simulation}$: Effective area of measuring electrode obtained from simulation (m^2)

C_0 : Geometrical Capacitance (F)

c : Concentration of ionic pairs (m^{-3})

D : Diffusion coefficient (m^2/s)

D_+ : Diffusion coefficient of positive charge carriers (m^2/s)

D_- : Diffusion coefficient of negative charge carriers (m^2/s)

D_i : Diffusion coefficient of injected charge carriers (m^2/s)

d : Half of distance between the electrodes (m)

E_{ac} : Activation energy for temperature dependence of conductivity (eV)

E_{acv} : Activation energy for temperature dependence of Viscosity (eV)

E_{avr} : Average field between measuring electrode and high voltage electrode (V/m)

$E_{\max}$: Maximum electric field in a guarded electrode system (V/m)

E_0 : Magnitude of AC field (V/m)

F : Electric force (N)

F' : Friction force (N)

f : Frequency (Hz)

G : Total conductance (S)

g : Distance between measuring electrode and guard electrode (mm)

h : Distance between measuring electrode and high voltage electrode (mm)

I :Current (A)

I_1 : First kind modified Bessel function of order one. $I_a(x) = \sum_{m=0}^{\infty} \frac{1}{m!\Gamma(m+a+1)} \left(\frac{x}{2}\right)^{2m+a}$

i_{adep} : Added depolarization current (A)

i_{dep} : Depolarization current (A)

i_{diff} : Difference of magnitude of polarization and depolarization current (A)

i_p : Polarization current (A)

j : Current density (A/m^2)

j_d : Current density of dissociated charge carriers (A/m^2)

J_{dep} : Current density of depolarization (A/m^2)

j_i : Current density of injected charge carriers (A/m^2)

J_+ : Current density of positive charge carriers (A/m^2)

J_- : Current density of negative charge carriers (A/m^2)

J_i : Total current density of injection (A/m^2)

K_d : Dissociation coefficient (s^{-1})

K_d^0 : Dissociation coefficient at zero field (s^{-1})

K_r : Recombination coefficient (s^{-1})

K_1 : Modified Hankel function of second kind $K_a(x) = \frac{\pi}{2}\frac{I_{-a}(x) - I_a(x)}{\sin(a\pi)}$

k : Boltzmann constant (8.617×10^{-5} eVK^{-1})

l : Distance between electrodes (m)

l_B : $l_B = q^2 / 4\pi\varepsilon_0\varepsilon_r kT$ Bjerrum distance (m)

l_i : Distance between ionic pairs (m)

l_o : $l_o = (q / 4\pi\varepsilon_0\varepsilon_r E)^{1/2}$ Onsager distance (m)

n : Density of charge carriers (m^{-3})

n_+ : Density of positive charge carriers (m^{-3})

n_- : Density of negative charge carriers (m^{-3})

Q : Induced charge density at electrode (C/m^2)

q : Elementary charge (1.602×10^{-19} C)

q_i : Injected charge density (C/m^3)

q_i^0 : Charge density related to nature of electrode and liquid (C/m^3)

R : Effective radius (m)

R_i : Effective radius calculated from simulation (m)

R_0 : Geometrical radius (m)

r : Edge radius (mm)

r_{ion} : Radius of charge carrier (m)

S : Surface area of electrode (m^2)

T : Absolute temperature (K)

t : Time (s)

t_p : Electrification time (s)

V : Electric voltage (V)

V_0 : Magnitude of AC electric voltage (V)

v : Velocity of charge carriers (m/s)

v_l : Velocity of liquid (m/s)

x_B : Minimum distance that a charge carrier can get to electrode (m)

α : Ratio of conductivity of injection over the total conductivity

ε : Permittivity (F/m)

ε_0 : Permittivity of vacuum (F/m)

ε^* : Relative complex permittivity

ε' : Real part of relative complex permittivity

ε'' : Imaginary part of relative complex permittivity

η : Viscosity (mPa·s)

κ : Ratio of field enhancement

λ : Eigenvalue

μ : Mobility of charge carriers (m^2 s^{-1} V^{-1})

μ_+ : Mobility of positive charge carriers ($m^2\ s^{-1}\ V^{-1}$)

μ_- : Mobility of negative charge carriers ($m^2\ s^{-1}\ V^{-1}$)

μ_d : Mobility of dissociated charge carriers ($m^2\ s^{-1}\ V^{-1}$)

μ_i : Mobility of injected charge carriers ($m^2\ s^{-1}\ V^{-1}$)

ξ : Ionic adsorption rate at the electrode

ρ : Total injected charge density (C/m^3)

ρ_1 : Total injected charge density from one electrode (C/m^3)

ρ_d : Total charge in charge layer (C)

ρ_{oppo} : Total injected charge density from the other electrode (C/m^3)

ρ_{tot} : Total injected charge density from two electrodes (C/m^3)

σ : Conductivity (S/m)

σ_i : Conductivity of injection (S/m)

σ_d : Dissociated conductivity (S/m)

ϕ : Electric potential (V)

ω : Angular frequency (rad/s)

Acknowledgements

Many thanks to my supervisor Prof George Chen. He has shown his great patience to my case. He also provides invaluable enlightenment of this study and to firm the confidence and determination for me to complete this report.

I would like to give my gratitude to many members of the Tony Davies High Voltage Laboratory who provided advice, interesting discussion and humour during my research. In particular the help of Dr Ian Hosier, Dr Celia Yeung, Dr Richard Chippendale, Dr Alex Holt, Dr Nicky Freebody, Dr Jack Hunter, Dr Martin Reading, Dr Matt Praeger, Dr Pedro Amaro, Mr Miao Hao, Mr Shekhar Mahmud, Mr Hisham Alghamdi, Mr Azwadi Mohamad, Mr Stelios Christou, Mr Cheng Chang; their help were greatly appreciated. Thanks also go to the technical support of the lab, in particular the help of Mike, Brian and Neil, without whom the experiment would not have been possible.

Finally thanks go out to my family and friends for their ongoing support and understanding throughout all of my studies. Specially thanks to my parents for their continued and unconditional support through the inevitable highs and lows of a PhD.

Lastly, I would like to thank NGC Company for financial support. I would like to acknowledge Dr Paul Jarman and Dr Gordon Wilson for their helpful suggestions and comments.

To you all I will be forever grateful.

Chapter 1 Introduction

1.1 HVDC power transmission and HVDC converter transformers

High voltage direct current (HVDC) technology has attracted more attention in long distance power transmission and the number of HVDC projects commenced or under consideration has steadily increased in recent years. Compared with the traditional HVAC transmission system, the HVDC transmission system can be advantageous on long distance electricity transmission, interconnecting separate power systems and long submarine cable crossings [1-4].

The two basic converters used in a HVDC transmission system are the line commutated current source converter (CSC) and self-commutated voltage source converter (VSC), which are shown in Figs. 1.1 - 1.2 [5]. A conventional HVDC converter station with CSC is shown in Fig. 1.1 and a HVDC converter station with VSC is shown in Fig. 1.2. The conversion process in a CSC relies on the line voltage on the AC side to effect the commutation from one switch device to another one. The thyristor is widely used as the switch device in a CSC. On the DC side of the CSC, the direction of DC current does not change and the magnitude of this DC current can be treated to be constant as it flows through a large inductance [5-6]. For this reason, CSC can be considered as a current source converter. Because the thyristor can only be turned on by control action, one limitation of a CSC converter is that a synchronous machine should always be involved in a HVDC converter to provide the commutating voltage. To solve this issue, the semiconductor device, the insulated gate bipolar transistor (IGBT), which can control both turn-on and turn off actions, has been used in the design of a VSC. In a VSC, the polarity of the DC voltage is always fixed and the DC voltage is smoothed by a large capacitance and it can be considered constant. Thus, the VSC with IGBTs is usually referred to as a voltage source converter [5-6].

The HVDC converter transformer is one of the most costly and important components in a HVDC transmission system. Carlson has summarized the primary functions a HVDC converter transformer serves as [7]:

- “Supply of AC voltages in two separate circuits with a relative phase shift of 30 electrical degrees for reduction of low order harmonics, especially the 5^{th} and 7^{th} harmonics.”[7]

- “Act as a galvanic barrier between the AC and DC systems to prevent the DC potential to enter the AC system”[7]
- “Reactive impedance in the AC supply to reduce short circuit currents and to control the rate of rise in valve current during commutation”[7]
- “Voltage transformation between the AC supply and the HVDC system” [7]
- “A fairly large tap range with small steps to give necessary adjustments in supply voltage”[7]

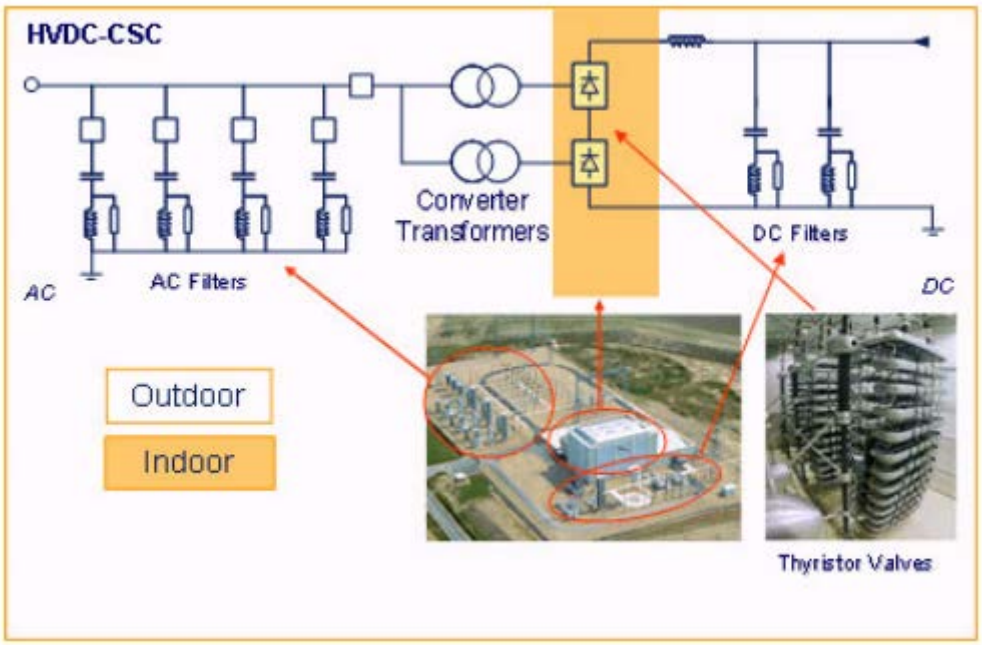

Fig. 1.1 Scheme of CSC transmission system [ref 5]

A HVDC converter transformer suffers from the normal AC electric field and the extra DC electric field generated by the DC potentials. The DC electric field is mainly determined by the resistivities of the insulating materials in a steady state condition, which is different from the capacitance-governed AC electric field [8-9].

It is commonly accepted that space charge can be easily formed under a DC field and the field distribution can be distorted by the presence of the space charge. The electric conduction can also be affected by the space charge effect, and the mechanism of the DC conduction in oil or oil impregnated pressboard is still not clearly understood. Therefore, research on the DC conductivity of oil and oil/pressboard insulation can benefit the quality diagnostics of the HVDC converter transformer and the HVDC power transmission.

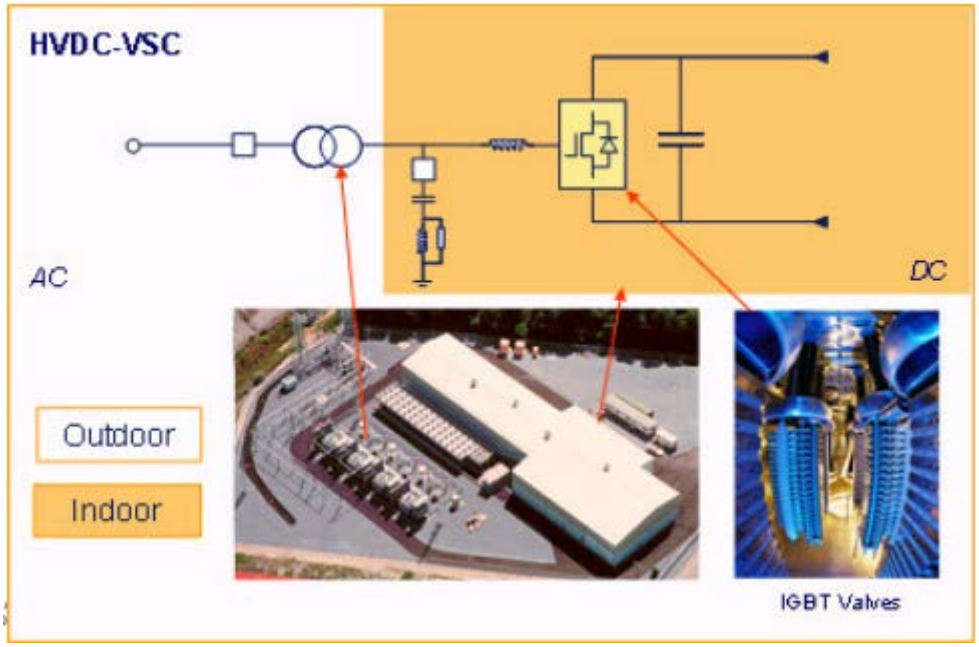

Fig. 1.2 Scheme of VSC transmission system [ref 5]

1.2Mineral oil and oil impregnated pressboard insulation in transformer

The mineral oil and the oil impregnated pressboard, as the insulation materials, have been used in the HVDC converter transformer for their low cost and good dielectric properties.

1.2.1 Mineral oil in transformer

Mineral Oil, a highly insulating material and non-conductive coolant, is widely used in power industry. In the majority of cases, mineral oil is a product of petroleum and is a complex mixture of paraffin, naphthene, and aromatic and naphthenoarmoatic compounds. Small amounts of derivatives of hydrocarbons that include atoms of other elements, such as nitrogen, sulphur and oxygen, also can be found in mineral oil [10]. When mineral oil is exposed to surrounding environment, gaseous molecules, such as oxygen, nitrogen and water vapour, may also be dissolved into the mineral oil and the dielectric property of the oil will change. Evidently, since the quality of the mineral oil affects the performance of a transformer, how to estimate the status of the mineral oil has become a worthy issue in recent decades [10-12].

1.2.2 Pressboard in transformer

Pressboard is a class of cellulose based material constructed of several layers of paper which have been compressed using a combination of heat and pressure to form a stiff and dense media. Pressboard consists of cellulose and hemicellulose. The tensile strength and electric strength of pressboard decrease with aging and finally the pressboard can no longer withstand the high electric field[13]. The mechanism of aging of pressboard is complex and relies on the operating conditions [13]. An important parameter to indicate the paper degradation is the degree of polymerization [14]. IEC 60450 states that the average value of degree of polymerization for new pressboard is expected to be 1000~ 2000 [15]. If this value reaches 150~ 200, the pressboard is considered to be defective and needed to be replaced [15-16].It is generally accepted that temperature, moisture and oxygen are major factors that can affect the aging of pressboard in transformers [17-24]. Degradation is a chemical reaction, which obeys the Arrhenius theory of reaction kinetics, meaning that the reaction rate is related to the reciprocal of the absolute temperature. It was reported that above 140 ℃, the oxidation reaction and hydrolytic reaction could be enhanced and the degradation rate could be accelerated [17-21]. Fabre and Pichon found that reducing the oxygen level from saturation level in oil can effectively prevent the degradation of the pressboard. [20]. When a transformer is aged, the water content in pressboard increases resulting in a low electrical strength [22-24]. The degradation rate of pressboard at normal service temperature with moisture of 4% has been shown about 20 times higher than that with only 0.5% moisture, so water content is a significant factor that can affect the pressboard aging [24].

1.3 Definition of DC conductivity in oil impregnated pressboard

DC conductivity measurement is one of the simple methods to evaluate the dielectric quality of the oil/pressboard insulation. Different international standards have been developed to provide guidance in DC conductivity measurement. IEC 61620, IEC 60247 and ASTM D 1169 are the standards for the measurement of insulating liquid, whilst IEC 60093 and ASTM D257 are the standards for the measurement of solid sample [25-29]. Here, a brief description about the definition of the conductivity in these standards will be given.

1.3.1 IEC 61620

The conductivity defined in IEC 61620 is related to an initial current density during a very short period of time, which is also known as the initial conductivity. The electric field used in the measurement is below 100 V/mm and the electrification time is below 5 s [25].

1.3.2 IEC 60247

IEC 60247 relates conductivity to a steady state current density. The maximum electric field defined in this standard for measurement is below 250 V/mm. The time of electrification is 1 min [26].

1.3.3 ASTM D 1169

ASTM D 1169 relates the conductivity to a current density at a given instant of time. The electric field recommended by this standard is 1.2 kV/mm, which is slightly higher than those used in other standards. The electrification time is 1 min [27].

1.3.4 IEC 60093

IEC 60093 states that the conductivity should be calculated from steady state current density. The maximum voltage recommended by this standard is 15 kV. In this standard, current will be measured at 1, 2, 5, 10, 50, 100 min until steady state is reached. If steady state is not reached within 100 min, the conductivity should be reported as a function of electrification time [28].

1.3.5 ASTM D 257

ASTM D 257 defines that the conductivity should be related to “a current without respect to time” [26]. The maximum electric field suggested by this standard is 15 kV/mm. The electrification time is 1 min [29].

If the standards for the liquid conductivity measurement (IEC61620, IEC60247 and ASTM D 1169) are scrutinized, the procedures for liquid conductivity measurement are all performed under very short times of electrification and at very low electric strength. The electrification time defined in the standards for insulating liquid is not long enough for the current to truly reach a steady state [30]. Non- linear behaviour of electric

conduction in mineral oil can be observed when the field is high, which is also not involved in these standards [30].

1.4Electrical conduction in mineral oil

1.4.1 Dissociation and recombination

The creation of charge carriers in liquids is usually governed by physical and chemical processes. When the electric field is low, the dissociation of impurities or of the liquid itself determines the conductivity.

Electrolytes are substances that can ionize when added to suitable ionizing solvents. Thus, even before the impurities are introduced in the electrolyte, there are ions existing in the electrolyte. The dissociation process can be described as

$$(A^+B^-) \Leftrightarrow A^+ + B^- \tag{1.1}$$

where (A^+B^-) stands for the density of ionic pairs, A^+ and B^- are the concentration of free ions [31].

In non-polar liquids, the molecules are usually formed by covalent bonds and they can hardly generate free ions. However, these molecules might react with other substances to produce ionic pairs and the newly generated ionic pairs can be dissociated into free ions. Thus, the dissociation in non-polar liquid can be described as

$$C + D \Leftrightarrow (A^+B^-) \Leftrightarrow A^+ + B^- \tag{1.2}$$

where C and D stand for the impurity molecule and non-polar molecule in the liquid [31].

As the free ions are usually generated from the dissociation of ionic pairs, the dissociation and recombination of ionic pairs can be described using the following equation:

$$\frac{dn_+}{dt} = \frac{dn_-}{dt} = K_d c - K_r n_+ n_- \tag{1.3}$$

where c is density of ionic pairs, n_+ and n_- is density of positive and negative ions in the liquid. K_d (s^{-1}) is the dissociation coefficient and K_r (s^{-1}) is the recombination coefficient [31].

Debye [32] obtained the recombination coefficient by calculating the collision frequency as a result of Brownian motion and the Coulomb interaction with the rest charge. The recombination coefficient can be denoted as

$$K_r = q\frac{\mu_+ + \mu_-}{\varepsilon}(1 - e^{-\frac{l_B}{l_i}})^{-1} \tag{1.4}$$

where l_i (m) is the distance between ions in an ionic pair and l_B (m) is the Bjerrum distance at which the Coulombian interaction electrostatic energy between two ions of opposite polarity equals to their thermal energies, $l_B = q^2 / 4\pi\varepsilon_0\varepsilon_r kT$, ε is the permittivity. μ_+ ($m^2s^{-1}V^{-1}$) and μ_- ($m^2s^{-1}V^{-1}$) are the mobility of positive and negative ions. For nonpolar liquid, such as mineral oil, Bjerrum distance is much higher than distance between the ions, and then this recombination coefficient becomes [33]

$$K_r = q\frac{\mu_+ + \mu_-}{\varepsilon} \tag{1.5}$$

In the presence of the electric field, the dissociation coefficient can also change. Onsager [34] has studied this effect. When an electric field is present, the dissociation coefficient can be written as [34]

$$K_d = K_d^0 \frac{I_1(2b)}{b} \tag{1.6}$$

with $b = l_B / l_o$, l_o (m) is Onsager distance at which the force due to electric field equals to the attractive force between two ions of opposite polarity, $l_o = (q / 4\pi\varepsilon_0\varepsilon_r E)^{1/2}$ (m). I_1 is the first kind modified Bessel function of order one.

1.4.2Charge transportation

Assuming that ions are the only charge carriers in the liquid and the movement of these ions behaves like spheres moving in a continuum. The expression for the ionic transportation can be denoted as

$$v = \mu E - D\frac{\nabla n}{n} \tag{1.7}$$

where D (m^2s^{-1}) is the diffusion coefficient. According to Einstein relation, the diffusion coefficient can be written as

$$D = \frac{\mu kT}{q} \tag{1.8}$$

When it comes to a fluid in motion, ions are advected with the liquid, which means the transportation equation should be modified as

$$v = \mu E - D\frac{\nabla n}{n} + v_l \tag{1.9}$$

where v_l (m/s) is the velocity of liquid. As seen from the above equation, the first term is due to the drift of the ions, the second term accounts for molecular diffusion and the last term is caused by the motion of the liquid [31].

1.4.3 Charge injection

In nonpolar liquids, charge transportation and injection are different from that in solid and gas. A two-step process can be used to explain the injection in non-polar liquid: the charge carriers are first created at the interface of the metal electrodes and the liquid, and then these charge carriers will be extracted by the electrical force [35-36]. The second step has been fully studied; whilst the mechanism of charge transfer at electrodes is still not clearly understood [35]. The second step of the injection process in liquid was first studied in 1978 by Felici [37]. In Felici's theory, the field distortion in the vicinity of the metal electrodes and the charge transportation mechanisms participating under a non-homogeneous field have been taken into account and a general expression for charge injection was derived [37-38]. Later, detailed studies on the electric conduction when both injection and dissociation are present in dielectric liquid have been carried out by many researchers [36-46]. Alj et al compared the experimental results and this injection theory and they found the injection current might be proportional to the concentration of ions at thermodynamic equilibrium [35]. Nemamcha et al confirmed that this theory was valid under different temperatures [36]. Pontiga and Castellanos suggested that Onsager's field enhanced dissociation theory should also be involved in the charge injection of non-polar liquid [45-46].

In liquids, the diffusion of ions can affect the electrical conduction due to a high mobility of charge carriers. By taking consideration of the diffusion and the electrical drift, the current density can be denoted as:

$$j = \mu nqE - Dq\frac{dn}{dx} \tag{1.10}$$

where μ ($m^2s^{-1}V^{-1}$) is the mobility of ions, E ($V*m^{-1}$) is the electric field, n is the charge density, D (m^2s^{-1}) is the diffusion coefficient. In the vicinity of the electrode, ions are not only driven by electric field, but also image force from the electrode. Therefore, if there is no presence of space charge, the electrical potential can be written as:

$$\phi(x) = -\frac{q}{16\pi\varepsilon x} - xE \tag{1.11}$$

where x(m) is distance between ion and electrode. After a long time of drift, the current flow enters a quasi- equilibrium state. By calculating the ratio of the current near the electrode and the quasi- constant current in a long distance from the electrode, the charge at considerable long distance can be described as [35]:

$$q_i = \frac{q_i^0}{2b \times K_1(2b)} \tag{1.12}$$

with

$$b = \sqrt{\frac{q^3 E}{16\pi\varepsilon_0\varepsilon_r k^2 T^2}} \tag{1.13}$$

where q_i (C/m^3) is the charge density that is considerable far away from the electrode where the charge density could be treated as constant, q_i^0 is a constant that is determined by the nature of the electrode and liquid, K_1 is the modified Hankel function of the first order [35].

1.5Factors of influence on the conduction in mineral oil

Transformer failures can result in power stoppage and asset losses with damage from power outage or fire. Using of oil impregnated pressboard in transformer can increase the reliability of transformer at a reasonable cost. Correct evaluation of the conditions of a transformer would be of enormous importance to the power industry. To minimize the costly maintenance and to plan the replacement rationally in future, it is necessary to have knowledge on the factors that can affect the dielectric properties of the mineral oil.

1.5.1 Electric field

Theoretical studies and experiments carried out by various researchers have indicated that the conductivity values of insulating liquid measured with increasing electric field follows a particular trend [47-52]. As seen from the experimental results obtained by Briere and Gaspard [47] shown in Fig 1.3, the field dependence of the current density of nitrobenzene can be distinguished into three regions: a low field region where the current density is proportional to the electric field; a medium field region where the current density seems to be saturated; and a high field region in which the total density of charge

carriers increases dramatically with the electric field and leads to breakdown finally [47]. The saturated region might not be observed sometimes due to the interference of impurities in insulating liquid [48-50].

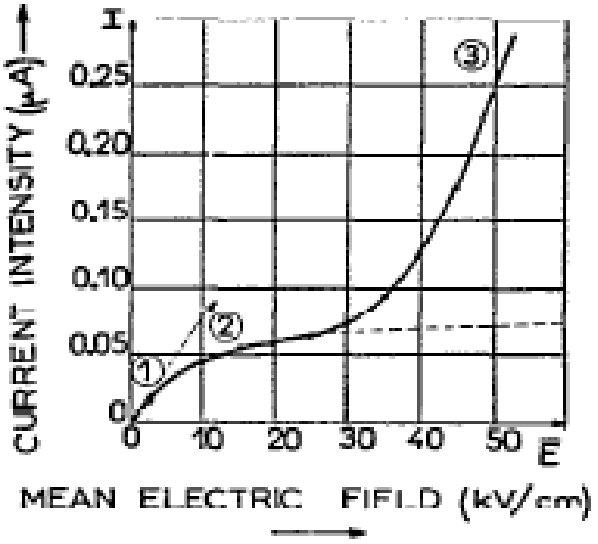

Fig. 1.3 A typical curve of current-voltage of nitrobenzene [ref 47]

In the first region, the free ions extracted by electric field can be replaced by the newly produced ones in the insulating liquid, thus, the conductivity remains at a constant value. In the next region, the density of free ions decreases as the ions are drifted away from the bulk at a faster rate than their generating rate. As the newly generated charge carriers are majority free charge carriers in the mineral oil, the conductivity of the mineral oil depends on the ionic dissociation rate. Hence, if the dissociation rate and recombination rate do not change, the current density seems to enter a saturated region and the conductivity decreases with the electric field. In the third region, the charge injection and ionic dissociating rate increase enormously, and consequently, more charge carriers are generated from dissociation and injection and the conductivity increases with the electric field [51-53].

1.5.2 Temperature

The viscosity of insulating liquid decreases with the temperature, thus, the mobility of the charge carriers becomes high when the temperature rises [54-55]. The dissociating coefficient also increases with the temperature, so there would be more charge carriers under a higher temperature [56]. Then, more charge can be transported at a higher

temperature and the conductivity increases with the temperature. As seen from Fig 1.4, the temperature dependence of Benzene can be depicted using the following equation [53]:

$$\sigma(T) \approx A_T \cdot e^{(-E_{ac}/kT)} \tag{1.14}$$

where T (°C) is the absolute temperature in Kelvin, A_T is a constant related to the nature of ions in liquid, k is the Boltzmann constant and E_{ac} (eV) is the activation energy. The temperature dependence of the conductivity of most insulating liquids also satisfies Eq. (1.1) [54-55].

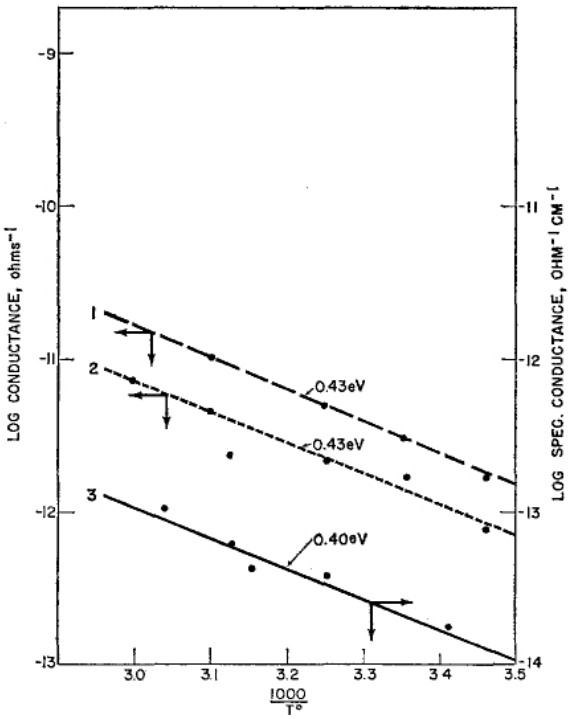

Fig. 1.4 The temperature dependence of the conductivity of Benzene[ref 53]

1.5.3 Moisture and water

It has been accepted that the deterioration of electrical properties of insulating liquid is affected by the moisture. As seen from Fig 1.5, DC conductivity of hydrocarbon liquid increases with water content. For new mineral oil, a water content of 20 ppm can be responsible for a conductivity enhancement by one order of magnitude [57-62].

The relationship between water content and mineral oil conductivity is still not clearly understood. Itahashi and his colleagues investigated the effect of strength of hydrogen bonding energy on the electric conduction [60]. According to their experimental result, it seems that the conductivity under nano-second pulsed field increases exponentially with the water content.

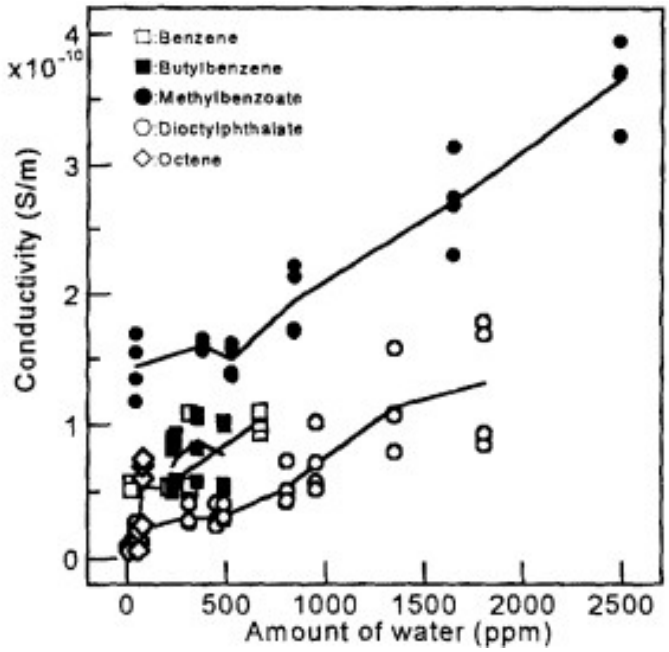

Fig. 1.5 The conductivity of hydrocarbon liquid can be affected by the water content[ref 59]

Kleinheins has claimed that when water concentration is well below the saturation concentration, the current increases linearly with the water content and the mobility of charge carriers shows a linear dependence on the water content [61]. Stannett has studied the resistivity of the insulating oil with the presence of the water droplet and an inverted "V" shape resistivity-temperature characteristic was observed in his experiment [62]. Stannett thought that more water droplets were dissolving into the oil when the temperature increased and the total conductivity would decrease as there would be fewer water droplets to carry the charges [62].

Craig confirmed the study of Kleinheins and Stannett, and found once an emulsion of water and oil was formed, the conductivity decreased rapidly. He claimed that the emulsion had a completely different electric conduction based on the movement of the water droplet and the formation of extra chains among the water droplets [63].

1.6 Factors of influence on the conduction of oil/pressboard insulation

To withstand the high electric field, paper and pressboard are used widely in transformers. The dielectric properties of oil/pressboard insulation can affect the breakdown strength greatly, especially during polarity reversal [64-66]. It is commonly acknowledged that the electrical conduction in oil/pressboard insulation can be affected

by temperature, moisture and oxygen [17-24]. The DC conductivity measurement of oil/pressboard insulation is usually performed using polarization and depolarization current (PDC) measurement techniques. Here, the factors that can affect the PDC measurement will be discussed.

1.6.1 Temperature

The experimental results obtained from PDC measurement are strongly influenced by the temperature [67]. The equilibrium of moisture between oil and pressboard is temperature dependent [68]. Increase in the temperature will break the balance of water content between oil and pressboard. Also, the dissociation coefficient and the mobility of the charge carriers are also temperature-dependent. Hence it is essential to study the effect of the temperature.

As seen from Fig 1.6, the polarization current increase with the temperature [69]. The temperature dependence of conductivity of oil/ pressboard insulation can also be described using Arrhenius equation (Eq. 1.1), which has been verified by many researchers [68-74]. For outdoor performed experiment, the temperature of oil and pressboard might not be constant. Therefore, Fofana et al have studied the effect of thermal transient in the PDC measurement for the oil/pressboard insulation [73-76]. They suggested using the temperature values at the beginning of the measurement to analyse the polarization current and the temperature after the measurement for the depolarization current [75-76].

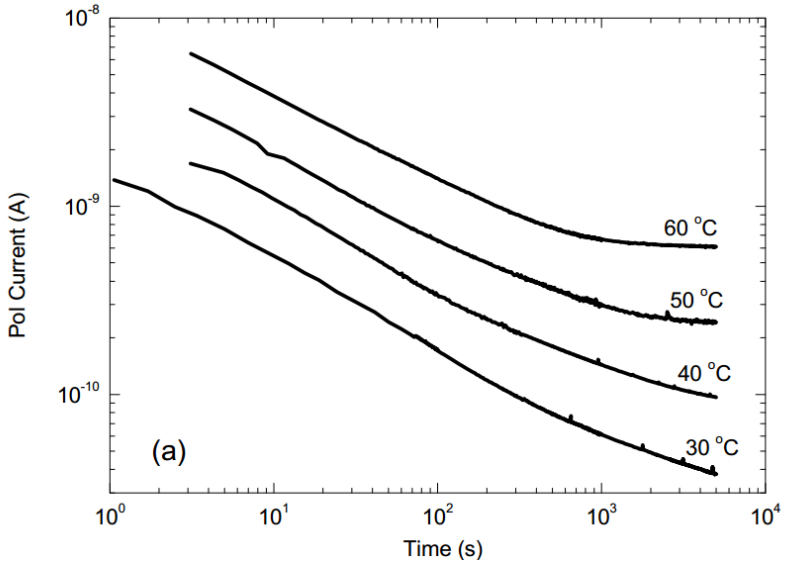

Fig. 1.6 Temperature dependence of polarization current in oil [ref 69]

1.6.2 Moisture

Pressboard is vulnerable to moisture. It has been observed that the expected life period of dry pressboard can be reduced if its moisture content is high [77-79]. PDC measurement is sensitive to moisture and the experimental results can be affected by the water content. Itahashi et al have investigated the effect of moisture on the conductivity of the oil/pressboard insulation and found out that the conductivity becomes larger when the water content increases [58]. It has been reported that moisture in pressboard might form bridge inside the pressboard and charge carriers could move faster through these bridges [58]. Jadav et al have studied the impact of moisture to the dielectric response of oil and paper insulation [77].

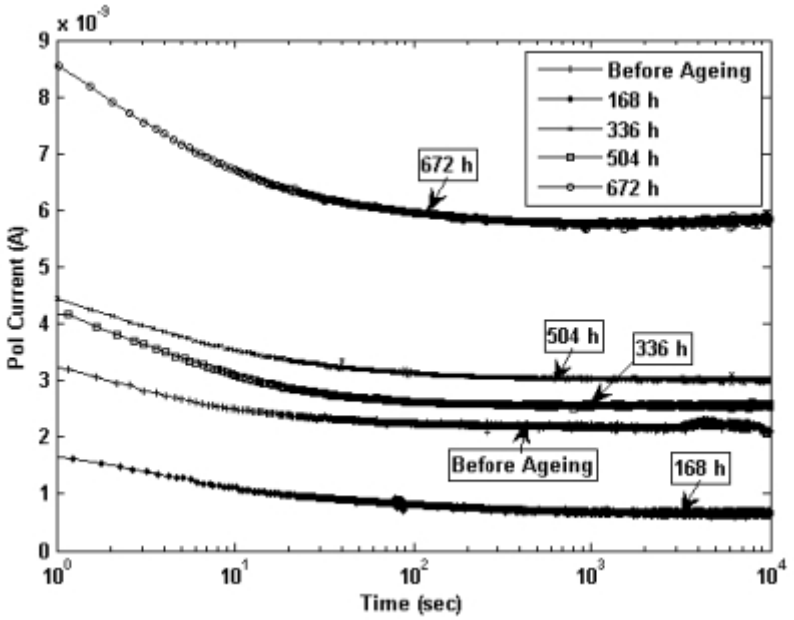

Fig. 1.7 Magnitude of the polarization current decreases at the initial stage of aging and then increases when the aging period is over 336 h. [ref 77]

As seen from their experimental results which are shown in Fig. 1.7, the polarization current is decreasing with aging at the initial stages of aging. After a certain period of time, the polarization current starts to increase. They thought the drop of polarization current for the initial stage of aging is due to the migration of the moisture from the paper to the oil [77]. Fig. 1.8 shows the moisture change of the pressboard during the aging [77]. A1 and B2 pressboard sample have different water content the aging [77]. As seen from Fig. 1.8, the moisture of the pressboard fluctuated, which suggested that the water solubility of the pressboard and oil changed with the ageing time and the water equilibrium of oil/pressboard could be disturbed during the ageing period [77]. Saha et al

have found out that solubility of oil increases with aging and the aged mineral oil hold more water in comparison with fresh oil [80]. The phenomenon that the oil can absorb water from the pressboard has been reported in several literatures [81-83].

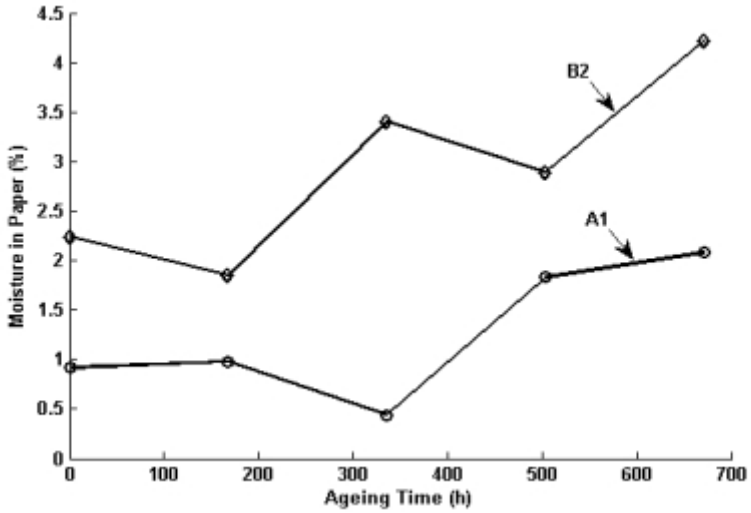

Fig. 1.8 Moisture of paper decreases at the initial stage of aging and then starts to increase with the aging time. [ref77]

1.6.3 Conductivity of pressboard and oil

As the conductivity of oil impregnated pressboard is determined by the dielectric properties of both pressboard and oil, the conductivity of pressboard and oil can affect the polarization current that flows through an oil impregnated pressboard sample. Gafvert et al suggested that PDC measurement should be considered as a preferred method as the dielectric characteristic of oil and pressboard can be evaluated separately from the experimental results [84]. Saha et al have claimed that the time domain dielectric response of oil/pressboard insulation could be correlated to a response function which describes the fundamental property of a dielectric system [85]. The response function for oil/pressboard system can be denoted using a parametric form as [85]

$$f(t) = \frac{A}{\left(\frac{t}{t_0}\right)^n + \left(\frac{t}{t_0}\right)^m} \tag{1.15}$$

with $A > 0$, $t_0 > 0$, $m > n > 0$ and $m > 1$.

Earlier researches have reported that the condition of mineral oil mainly influences the initial parts of polarization and depolarization currents, whilst the long-term values of these current are sensitive to the condition of the pressboard [86-88]. Saha et al have

simulated the theoretical curves for the polarization and depolarization current based on different conductivity of oil and paper and compared their simulation results with the experimental results [88]. A good agreement with experimental results can be found in their work [88].

1.7Aim of thesis

The general objectives of the present study are as follows:

1. Establish a methodology for measuring oil DC conductivity and guidance for interpretation and evaluation of the measured oil DC conductivity characteristics.
2. Understand the relationship between oil status (ageing) and its DC conductivity.
3. Establish the relationship between the DC conductivity and the applied electric fields.
4. Understand charge carrier generation and transportation in the oil.
5. Make recommendation for new standards.
6. Establish a methodology for measuring DC conductivity of the oil/pressboard insulation and guidance for interpretation and evaluation of the measured DC conductivity characteristics of the oil/pressboard insulation.

1.8 Structure of thesis

This thesis reports the research work on dielectric characteristics in oil/pressboard insulation under both high and low electric field by quantitative numerical modelling and experimental investigations. It is structured in several chapters describing the following work.

Chapter 2 describes the experimental procedure for DC conductivity measurement of mineral oil and the experimental results are provided and analysed.

Chapter 3 reports the frequency dependent characteristics of the mineral oil. The initial conductivity obtained using time-domain measurement has been compared with that acquired from frequency-domain measurement.

In chapter 4, the classic ionic drift and diffusion model has been used to explain the frequency response of mineral oil. A theory of injection induced polarization has been derived using ionic injection models under both homogeneous field and non-

homogeneous field. A modified Coelho model has been proposed and compared with the computer based simulation.

In chapter 5, the depolarization current has been studied. A depolarization model has been developed and used to fit the experimental results. The dissociation conductivities of different kinds of oils have been calculated and analysed.

Chapter 6 suggests the field enhancement in a guarded electrode system can be quite serious for insulating liquid measurement. An empirical equation has been provided to calculate the maximum field in a guarded electrode system when this system is submerged in dielectric liquid.

Chapter 7 gives a brief description of the procedure of DC conductivity measurement for oil/pressboard insulation and relevant experimental results have been presented. A modified R-C model has been proposed to fit the experimental results.

Chapter 8 summarizes the conclusions from the above work on the electrical conduction in mineral oil and oil/pressboard insulation.

Chapter 2 DC Test System and Measurement on Mineral Oil

2.1 Mineral oil and its degradation

Mineral oil has been widely used in power transformer for its excellent insulation properties and as it is a low viscosity coolant. Basically, mineral oil is made of hydrocarbons and these hydrocarbon molecules can be divided into three main groups as shown in Fig. 2.1.

- Paraffin

  Paraffins, which are also known as alkanes, consist of only single bonds. All these bonds are hydrogen and carbon bond.

- Naphthene

  Naphthenes, which are also called as cycloalkanes, have one or more rings of carbon atoms.

- Aromatics

  Aromatics are kind of hydrocarbons that have carbon rings with alternating double and single bonds between the carbon atoms.

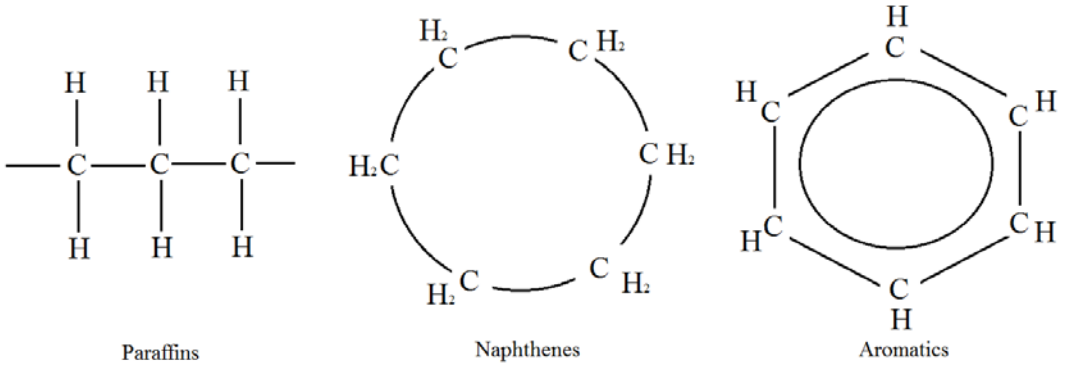

Fig. 2.1 Hydrocarbon compounds in mineral oil

It is commonly accepted that the dielectric properties of mineral oil deteriorates under the impact of electrical, thermal and chemical stress in service.

2.1.1 Electrical stress

In non-polar liquid, molecules are formed by covalent bonds. Free electrons that escape from the conduction band of the metal electrode are injected into the liquid and accelerated by the electric field. If the energy on the free electrons is large enough, the electron collision with the molecules can break the vulnerable bonds in the molecules and resulting in pairs of free radicals [89-90]. This process can be described as

$$\text{M-N} \xrightarrow{e} \text{M}\bullet + \text{N}\bullet \tag{2.1}$$

where M-N is the vulnerable molecules in non-polar liquid, $\text{M}\bullet$ and $\text{N}\bullet$ are the free radicals. In chemistry, a free radical is any atom or molecule that has a single unpaired electron in an outer shell. In mineral oil, once free radicals are formed, they can act as initiators for chain reactions involving free radicals and hydrocarbons to accelerate oil ageing [90].

2.1.2 Thermal stress

When the insulating liquid is used in high voltage apparatus, sometimes the temperature of the insulating liquid is quite high (usually below 100 °C). Occasionally, the energy accumulated on the molecules with weak covalent bonds can be large enough to reach the excitation level and free radicals can be generated through the breakdown of the covalent bonds [90].

2.1.3 Chemical stress

In insulating liquid, the dissolved chemical aggressive oxygen molecules can react with the free radicals that generated from the hydrocarbon molecules and participate in the formation of soluble oxidation products and insoluble sludge [90-92]. Sanghi has given some general reactions [92]

$$\begin{cases} \text{R-H+X} \rightarrow \text{R}\bullet + \text{HX} \\ \text{R}\bullet + \text{O}_2 \rightarrow \text{R-O-O}\bullet \\ \text{ROO}\bullet + \text{RH} \rightarrow \text{ROOH+R}\bullet \\ \text{ROOH} \rightarrow \text{R-O}\bullet + \text{OH}\bullet \\ \text{RO}\bullet + \text{RH} \rightarrow \text{ROH+R}\bullet \\ \text{OH}\bullet + \text{RH} \rightarrow \text{H}_2\text{O+R}\bullet \end{cases} \tag{2.2}$$

Some of the oxidation products are acidic material and they can damage the component of the high voltage equipment [92]. As the oxidation process generates more free radicals and these free radicals form extra ions, the oxidation products affect the

characteristic of the insulating liquid and the dissipation factor of the liquid increases. The accumulation of the free radicals can also increase the chance that a covalent bond is formed between two large radicals to generate insoluble sludge, which can impair the heat transfer and the insulating properties [92]. As the DC conductivity is one of the important parameters used in the quality diagnostics of the insulating liquids, understanding the correlation between the DC conductivity and the aging effect has become a crucial issue.

2.2 DC measurement system

Our DC conductivity test system contains two parts, treatment part and measurement part.

2.2.1 Oil filtration

In order to remove contaminants, oil samples will undergo a filtration process. The oil filtration system includes a beaker, a vacuum pump, filter paper and a filter funnel. The filter system is illustrated in Fig. 2.3. First, a filter paper shaped like a disk is folded in the cone and placed inside the funnel. Oil is then poured into the filter funnel with the vacuum pump assisting to increase the speed of the filtration. Small particles are left on the paper because they are too large to pass the paper. The smaller liquid particles are able to go through. The liquid then goes into the glass beaker. When the glass beaker is half filled with oil, the filtered oil is removed and the used filter paper is discarded. When all the oil sample has been filtered, the oil is inserted into the pressure vessel for degassing.

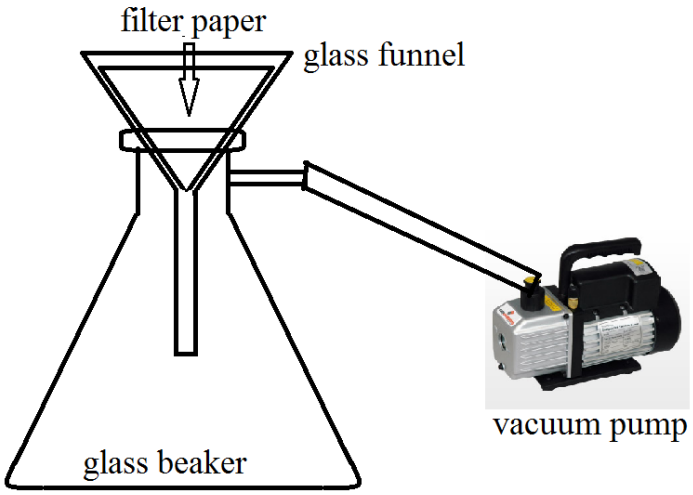

Fig. 2.2 Oil filtration system

2.2.2 Treatment of oil

The degassing of oil sample follows the procedures proposed by CIGRE working group A2/1.41 to reduce the influence from dissolved air. The oil treatment system consists of a vacuum pump, an electromagnetic hotplate, a pressure vessel and a vacuum gauge. The pressure vessel and the electromagnetic hotplate are shown in Fig. 2.3. There are five steps in the oil treatment. First, fill the pressure vessel with the 500 mL oil to be tested, and then place the pressure vessel on the electromagnetic hotplate and pump it to vacuum without turning on the stir knob. According to the test procedures given by CIGRE working group A2/1.41, the maximum pressure in the pressure vessel should below 100 Pa. Second, turn on the stir knob when the pressure vessel has been vacuumed at least 10 minutes. Third, turn on the heat knob after another 10 minutes and heat the pressure cell to 90 °C. Fourth, keep the pressure vessel vacuumed for at least3 hours and then switch off the valve on the pressure cell. Fifth, fill up the pressure cell with Nitrogen gas. During the treatment, avoid exposing the oil to air, because oxygen and moisture from air will introduce more charge carriers in mineral oil and then increase its conductivity [93, 94].

2.2.3 Measurement system

In our DC measurement, a three-electrode system will be used to get a more accurate result. First, connect the vacuum pump to the test cell and vacuum the test cell, and then, use the pressure vessel to inject the oil. When the oil is injected into the test cell, keep vacuuming the test cell for another 3 hours. A PTFE spacer will be used to create an oil

gap between the measuring electrode and high voltage electrode. The test cell which is modified from Kuchler's DC test cell is shown in Fig. 2.4 and Fig. 2.5 [95].

Fig. 2.3 Oil pre-treatment system

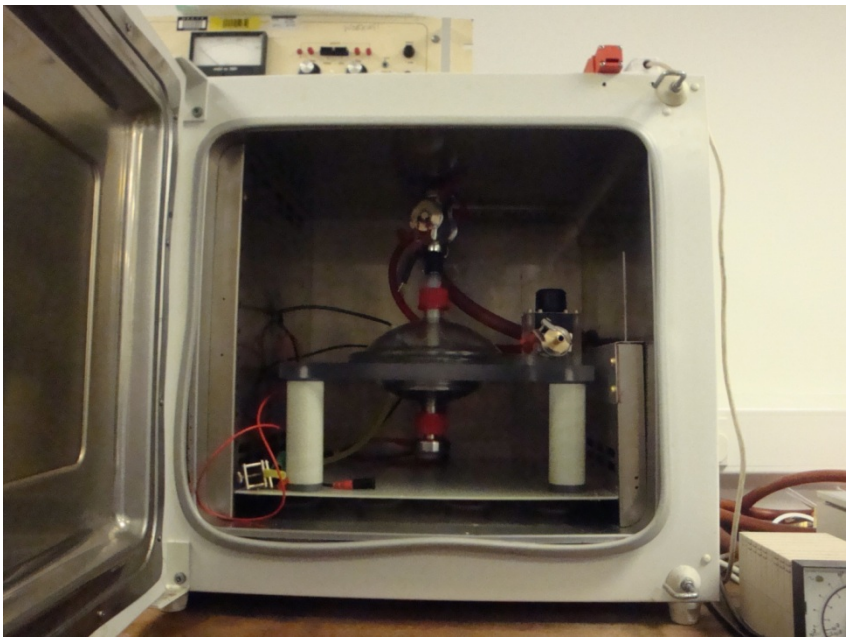

Fig. 2.4 Photograph of the oil test cell in oven

The DC Conductivity measurement system follows the test system designed by Li and his colleagues [96]. This system consists of a test cell, an oven, a vacuum pump, a pico-ammeter, a high voltage supply. The system is connected as that shown in Fig. 2.4. When the test starts, the pico-ammeter is turned on first to record the current, and then turn on the power supply so that the current at the very beginning can be recorded.

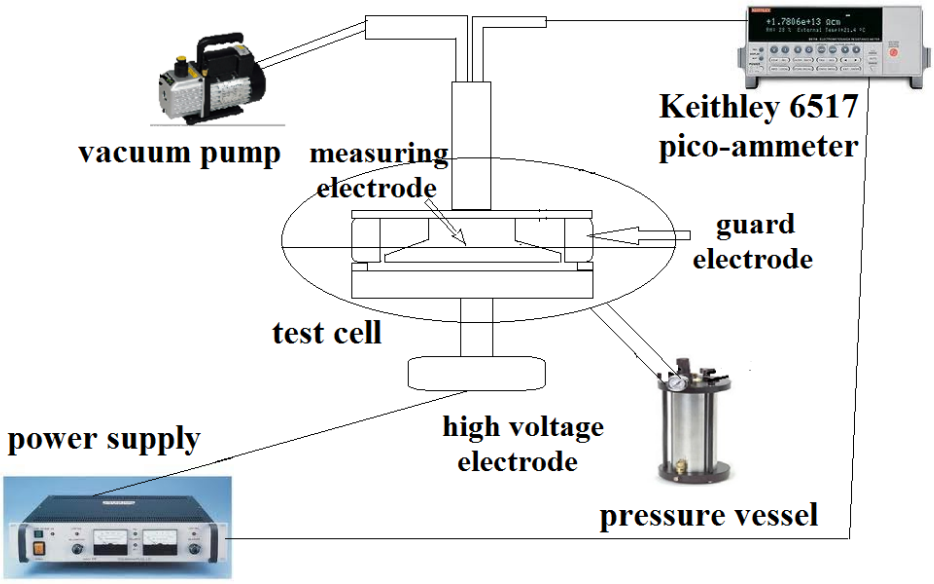

Fig. 2.5 DC conductivity test setup with electrode system

According to the requirement of Round Robin Test organized by CIGRE A2/1.41, the depolarization time should be at least 3 hours. If the time for depolarization is not sufficiently long, the remaining polarization in the oil can affect the next measurement.

2.3 Local field enhancement in a guarded electrode system

In the test of dielectric liquid, it is necessary to submerge the entire electrode system into the tested liquid to ensure a good contact of the liquid sample with the metal electrodes. If the electrodes have sharp edges, local field enhancement can be observed in the vicinity of that edge. In the past, increasing the edge radius of the measuring electrode is a good measure to avoid the local field enhancement which can bring parasitic influences of nonlinearities under high electric field [95].

Here, the distribution of the electric field in a guarded electrode system will be simulated using Comsol Multiphysics software. Three parameters that can affect the field distribution in the guarded electrode system have been studied. A guarded electrode system has been used to test the electric strength of three different kinds of mineral oils and the experimental results have been used to compare with the simulation results.

2.3.1 Field distribution in a guarded electrode system

The field distribution in two parallel metal electrodes with a guard ring will be studied here. This guarded electrode system includes three components: a high voltage electrode, a measuring electrode and a guard electrode. The structure of the test cell is illustrated in Fig 2.6. In this section, the influence of a new parameter, edge radius, r (m), will be investigated in depth. The other two parameters that can affect the field in the bulk are the distance between the high voltage electrode and the measuring electrode, h (m), and the width of the gap between the measuring and guard electrode, g (m). These three parameters are shown in Fig 2.7. If the measuring electrode and the guard electrode are large enough, the distribution of the electric field in the gap shown in Fig 2.6 may only be affected by these three parameters.

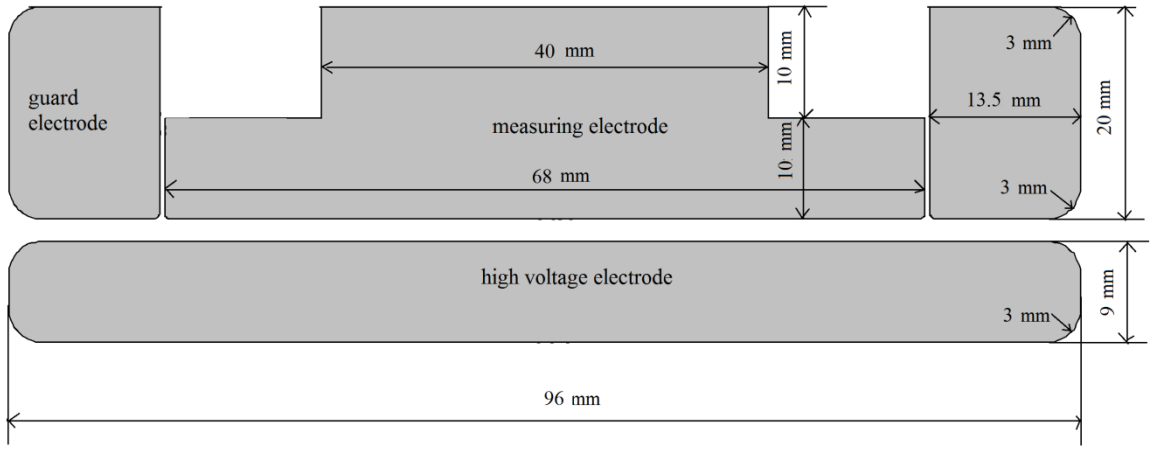

Fig. 2.6 Structure of parallel electrodes with a guard electrode.

Here, the conductivity of the insulating liquid is set to be constant and no presence of space charge is assumed in our simulation. All three metal electrodes are totally submerged in the insulating liquid. The electric potential of the high voltage electrode is set to be proportional to h, whilst the guard and measuring electrode are connected to the ground. Therefore, the average field between the measuring electrode and the high voltage electrode is supposed to be constant. This average field is set to 1 kV/mm. The relative permittivity of the insulating liquid is set to 2 and its conductivity is assumed as 10 fS/m. In our simulation, g = 0.5 mm, h = 2 mm, r = 0.1 mm.

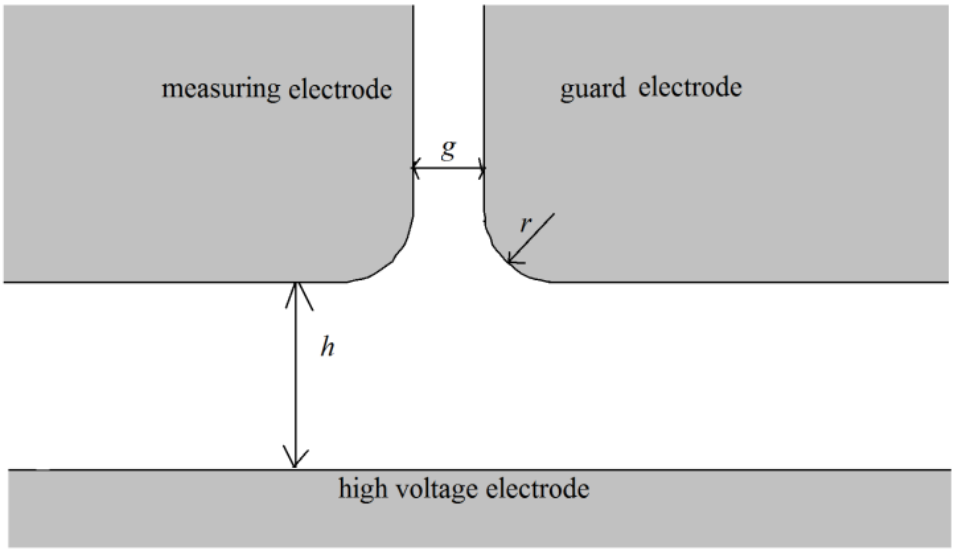

Fig. 2.7 Edge radius, *r* (m), gap width between guard electrode and measuring electrode, *g* (m) and distance between the measuring electrode and high voltage electrode, *h* (m).

The simulation was performed with 2D axial symmetry configurations in Comsol Multiphysics software. As the field near the edge of the guard electrode and measuring electrode might be seriously distorted, a very fine finite element analysis mesh is required to guarantee the accuracy of the simulation. The distribution of the mesh is shown in Figs 2.8 and 2.9. As seen from Fig. 2.9, the mesh at the edge of the measuring electrode and the guard electrode has been made extremely finest. The simulated field results converged numerically to the fourth significant figure in this simulation. Thus, the accuracy of the simulating result is acceptable.

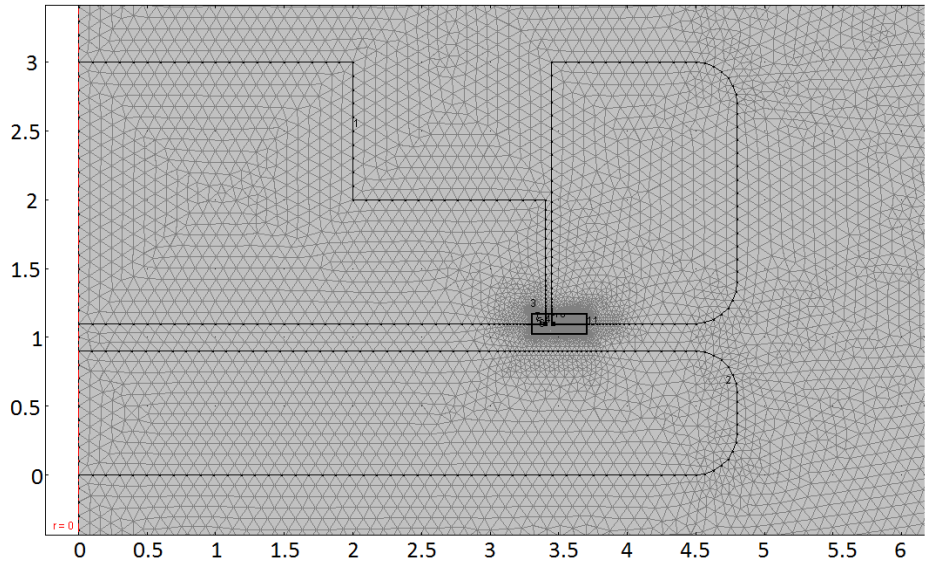

Fig. 2.8 Comsol Multiphysics mesh distribution of the guarded electrode system in the model

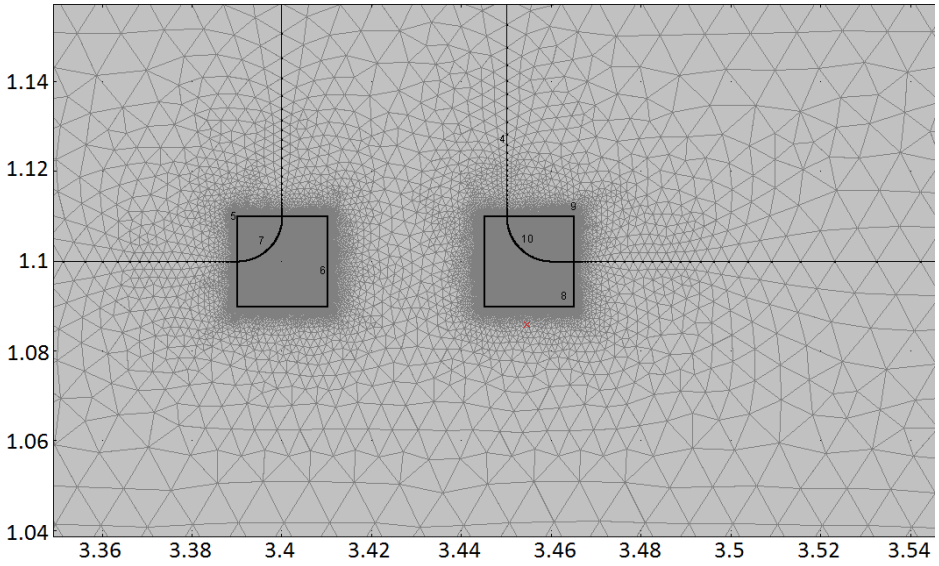

Fig. 2.9 Comsol Multiphysics mesh distribution of the edge of the measuring electrode and guard electrode in the model

The simulating results are shown in Fig. 2.10. Evenly distributed electric field has been observed between the measuring electrode and the high voltage electrode. It seems that the field distortion can be ignored when using a guarded electrode system. However, the maximum electric field, which is much higher than the average electric field, is around 1.62 kV/mm. Therefore, these must be places at which the field has been seriously enhanced. The electrode in Fig. 2.11 is the measuring electrode and the electrode in Fig. 2.12 is the guard electrode. As seen from Figs. 2.11 and 2.12, the field distortions become significant at the edge of the measuring electrode and the guarded electrode. It seems the electric field can be enhanced near the edge of the measuring or the guard electrode.

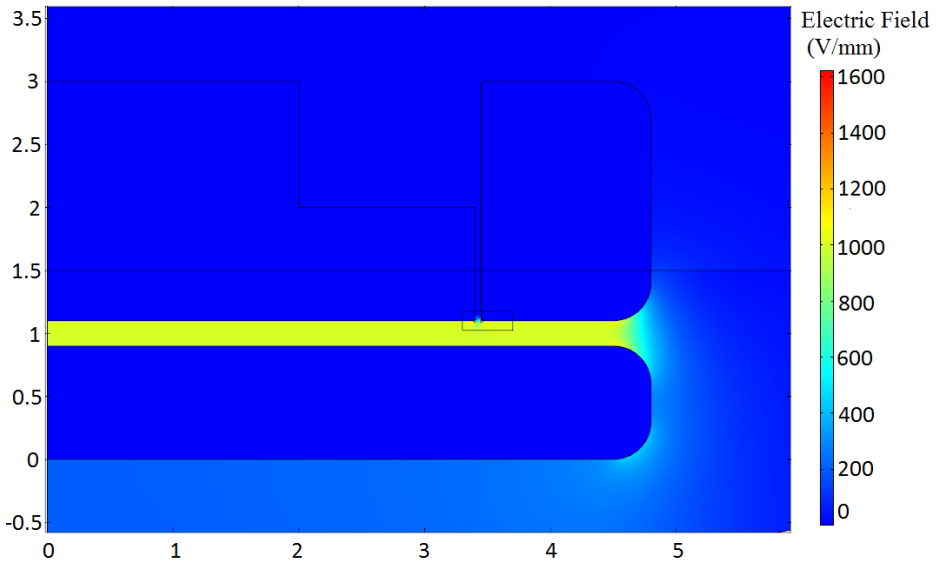

Fig. 2.10 Electric field distribution in the guarded electrode system

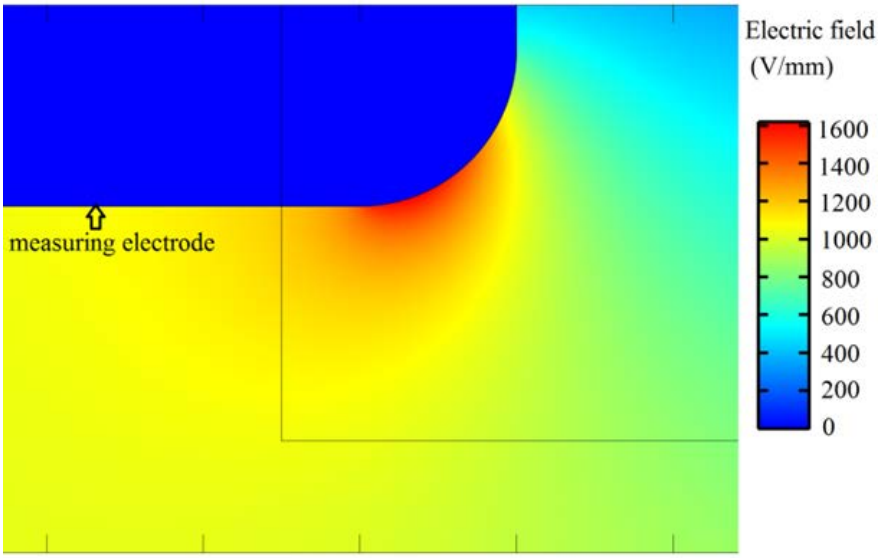

Fig. 2.11 Field distortion at the edge of the measuring electrode.

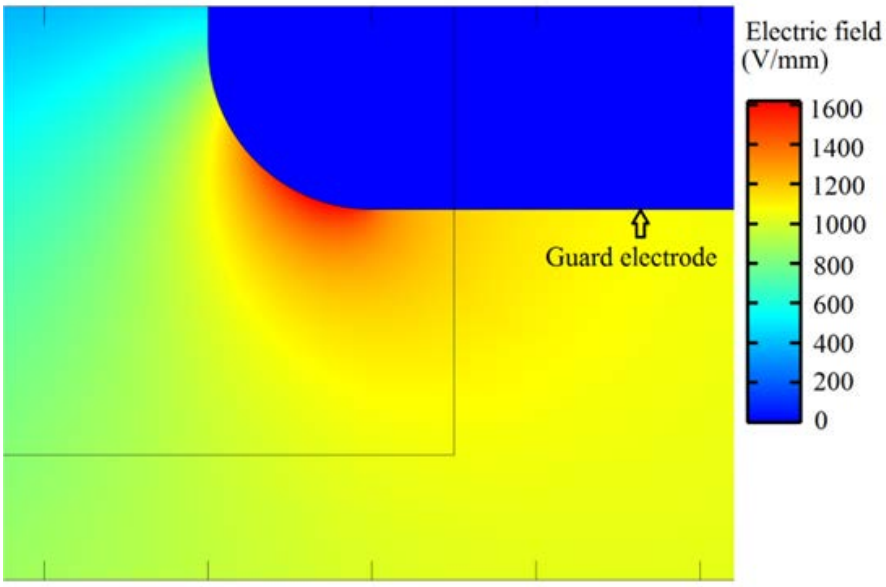

Fig. 2.12 Field distortion at the edge of the guard electrode.

As seen from Figs.2.11 and 2.12, if the measuring electrode and guard electrode have the same edge radius, there is not much difference between the field distributions in the vicinity of their edges. The maximum electric fields obtained in a region that is close to the edges of those two electrodes are also quite similar. For simplicity, only the maximum field at the edge of the measuring electrode will be studied here. This field enhancement in a guarded electrode system can lead to an unexpected breakdown in high voltage DC conductivity measurement. According to Thomson's work [97], the field from the middle of the lower surface of measuring electrode to the edge of the measuring electrode should

be homogeneous. As the electric field distribution is no longer homogeneous near the edge of the measuring electrode, the classical conductivity calculation approaches might be no longer valid and this will be verified later.

2.3.2 Maximum field in a guarded electrode system

As seen from the above simulation result, the maximum electric field in the insulating liquid is about 1.6 times higher than the average electric field between the high voltage electrode and the measuring electrode. Thus, in order to avoid the local field enhancements, these three parameters, *g*, *h* and *r*, should be chosen wisely. However, how the edge radius affects the field distribution has not been carefully studied in the past.

If two variables are set to be constant and the third one varies so that the influence of these three factors on the maximum field in the insulating liquid can be studied separately. First, *h* and *r* are set to be 2 mm and 0.05 mm and the maximum electric field is calculated when *g* changes from 0.02 mm to 2 mm. The values of these three parameters are selected based on the real guarded electrode system for HVDC conductivity measurement.

The simulation results are plotted in Fig 2.13. If *g* increases, the maximum electric field also increases. When *g* is 2 mm, the maximum field is about 2.77 kV/mm, which is almost three times of the average field. When *g* is large enough, the field distribution can be approximated by using the case in which a conductor that has a limited size at zero potential stays above an infinite metal plane at potential V. According to Thomson's study, *g* will not affect the field distribution in this case [97]. Therefore, when *g* is large enough, its influence on the maximum field is negligible.

Secondly, g = 0.5 mm and r = 0.05 mm. The maximum field will be calculated as *h* varies from 0.02 mm to 2 mm. As shown in Fig 2.13, when the value of *h* becomes larger, the maximum electric field also goes higher. If *h* is larger than 0.5 mm, the maximum field can still increase, but the increase can be hardly noticed. Therefore, if *h* is much higher than the other two variables, its influence on the maximum field in the insulating liquid is negligible. In order to reduce the maximum electric field, a small gap between the measuring electrode and the high voltage electrode is desirable.

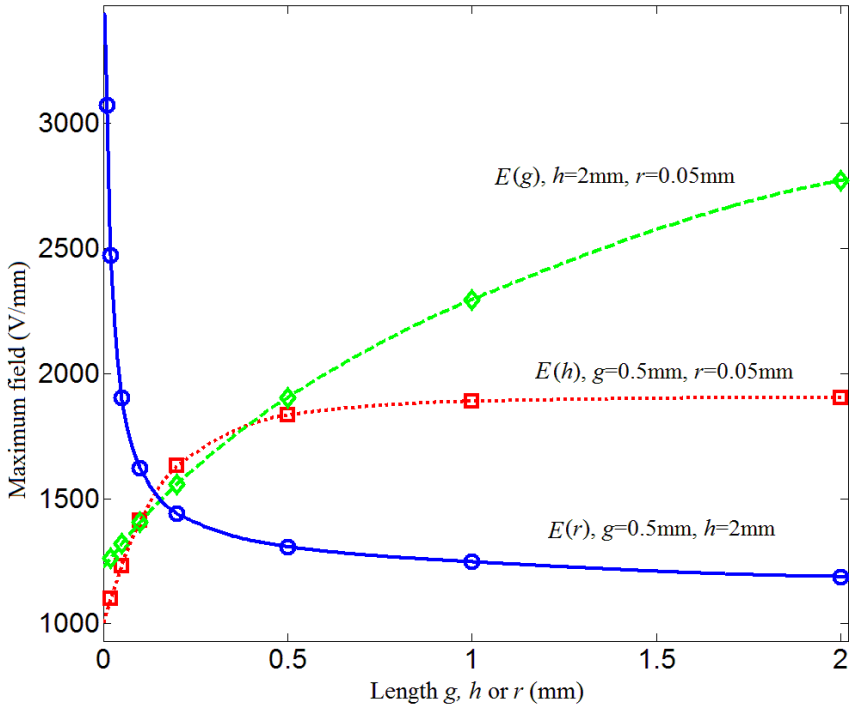

Fig. 2.13 Dependence of the maximum field on different *g*, *h* and *r*

Finally, the simulations are carried out for h = 0.5 mm and g = 2 mm when r varies from 0.01 mm to 2 mm. As seen from Fig. 2.13, when r increases, the maximum electric field decreases. When r is smaller than 0.5 mm, a notable drop of the maximum electric field can be observed. If r is larger than 0.5 mm, the decrease of the maximum field will be slowed and becomes unnoticeable. Apparently, a large edge radius can cause uneven field distribution between the high voltage electrode and measuring electrode. At the edge of the measuring electrode, the gap distance between the high voltage electrode and measuring electrode is not homogeneous in a rigid way. Increasing the edge radius can result in a decrease of the gap distance, thus, the actual effective surface area of the measuring electrode can be smaller for a larger edge radius. Consequently, in order to minimize the local field enhancement by raising r up to a much higher value is not recommended.

If the simulation results are combined together, it is easy to find out that there are three measures to reduce the local field enhancement in a guarded electrode system: (1) increase the edge radius of the measuring electrode and guard electrode, *r*; (2) decrease the distance between the measuring electrode and high voltage electrode, *h*; (3) reduce the gap width between the measuring electrode and the guard electrode, *g*.

Based on the simulation result, an empirical equation has been proposed to assess the maximum field easily without resorting to the electric field simulation in a guarded electrode system. As seen in Fig. 2.13, if *h* gets close to zero, the maximum field decreases. Bearing in mind that the maximum field cannot be lower than the average field, the maximum field should approach the average field as *h* gets close to zero. If the other two parameters are much smaller than *h*, *h* will no longer be a crucial parameter that can affect the maximum field. The influence of variable *g* on the maximum field can be studied similarly. As illustrated in Fig 2.13, the decrease of the edge radius can enhance the field distortion in a close region to the edge of the measuring electrode or the guard electrode. Having taken all these facts into account, the empirical equation can be expressed as,

$$E_{\max} = (\kappa + 1) E_{avr} \tag{2.2}$$

with

$$\kappa = \frac{(0.1/r) + 1/\sqrt{gh}}{1.5/g + 1.3/h} \quad , \tag{2.3}$$

in which, $E_{\max}$ (V/m) is the maximum field in the bulk , E_{avr} (V/m) is the average field between the high voltage electrode and the measuring electrode and κ is the ratio of the field enhancement.

The plot of the calculated maximum field using the empirical equation is illustrated in Fig. 2.14. It seems this empirical equation can fit the simulation result quite well. However, the maximum field calculated from the above equation is only an approximation and this equation is based on the assumption that there is no space charge among these three electrodes; thus, it might not indicate the exact highest field in the test cell. Since charge carriers in the liquid can be blocked by the electrode and form a charge layer, extra space charge might accumulate around that edge and affect the total current that flows through the measuring electrode. Therefore, the real maximum field in a guarded electrode system might be higher than that obtained in simulation or the empirical equation due to the presence of the space charge [31].

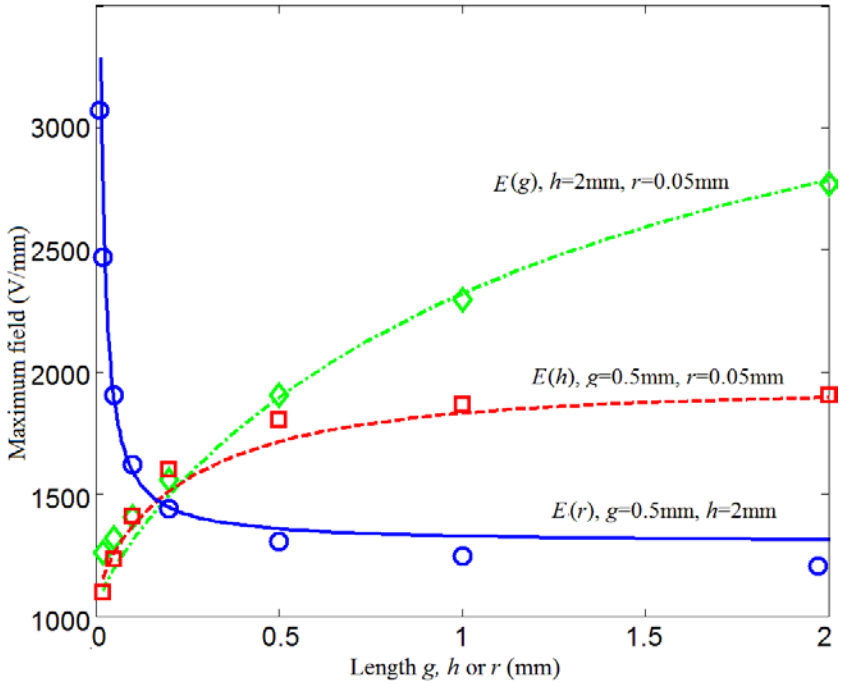

Fig. 2.14 Comparison between the maximum field calculated from the empirical equation and that are obtained through the field simulation using Comsol Multiphysics. Points are obtained through the computer based simulation. Curves are empirically calculated from Eq. (2.2).

2.3.3 Evaluation of conductivity calculation equations in the international standards

A guarded electrode system is usually used to perform accurate measurement of the DC conductivity of insulating liquid [26]. In order to calculate the conductivity, the knowledge about the thickness of the sample and the effective area of the measuring electrode is required [98]. Due to the edge fringing effect, the effective area of the measuring electrode is actually larger than its geometrical surface. The effective area of the measuring electrode has been well studied and correction expressions for different types of electrode system have been proposed [97-105]. Thomson calculated the field distribution among different types of electrode systems [97]. Based on Thomson's work, Lauritzen and Endicott developed the correction expressions for both thin and thick electrodes, separately [99-100]. For a sample that has a high relative permittivity, Amey developed an analytical expression to calculate the effective area of the measuring electrode [101]. The previous studies on the correction of the effective area are reviewed and these correcting equations have been applied on the capacitance measurement by Goad [102]. Lisowski studied the effective radius of the measuring electrode when the sample has a relative permittivity of 1 and proposed modifications to IEC 60093 [103-104]. All the previous studies were carried out with the presumption that the guard

electrode and measuring electrode both had sharp corners, but all components have finite radii at their corners in reality. To the knowledge of the author, the distribution of the electric field within a guarded electrode system has not been carefully studied under the condition that the corner of the measuring electrode and the guard electrode are rounded. The distortion of the electric field might be serious if a guarded electrode system was used in DC conductivity measurement of insulating liquid and the previous correcting expressions might not be valid. Therefore, it is necessary to re-verify the validity of the correction equations proposed in the current international standards.

The effective radius of the measuring electrode depends on the structure of the electrodes and the dielectric properties of the sample. For concentric cylinder electrodes, IEC 60093 defines the effective radius as,

$$R = R_0 + g/2 \ , \tag{2.4}$$

where R (m) is the effective radius and R_0 (m) is the geometrical radius of the measuring electrode [28].

However, Lisowski states that the effective radius is smaller than $R_0 + g/2$. This error could be substantial when $h << g$ [103]. ASTM D257 gives a more accurate equation and the effective radius can be denoted as

$$R = R_0 + \frac{Bg}{2} \ , \tag{2.5}$$

with

$$B = 1 - \frac{4}{\pi}\frac{h}{g} \cdot \ln\cosh\left(\frac{\pi}{4}\frac{g}{h}\right). \tag{2.6}$$

where B is the factor determining increase of the measuring electrode spreading margin [29].

The structure of the guarded electrode system is shown in Fig. 6.1. The distribution of the electric field has been simulated using finite element 2D axisymmetric analysis in Comsol Multiphysics software. The current that flows through the entire surface of the measuring electrode should be equal with the current that flows in the external measuring circuit. Thus, the measured current can be obtained through the integration of the current density over the entire surface of the measuring electrode. If there is no presence of space charge in the insulating liquid and the conductivity of the insulating liquid is homogenous, the current is proportional to the electric field and the total current becomes,

$$I = \sigma \int_S E_s dS \,, \tag{2.7}$$

where, I (A) is the measured current, σ (S/m) is the conductivity of the insulating liquid, E_s (V/m) is the electric field at the surface of the measuring electrode and S (m^2) is the total surface area of the measuring electrode.

With Ohm's law, the total conductivity obeys

$$G = I/U = \sigma \frac{\pi R_i^2}{h} \,. \tag{2.8}$$

in which, R_i (m) is the effective radius calculated from the simulation. If Eq. (2.7) and (2.8) are put together, the simulated effective radius can be written as

$$R_i = \left(\frac{h}{U\pi} \int_s E_s dS \right)^{1/2} \,, \tag{2.9}$$

where U (V) is the electric potential of the high voltage electrode.

To verify the validation of the correcting expression provided by ASTM standard, the simulations using Eq. (2.9) will be carried out for g = 1 mm, for r varies from 0.1 mm to 3 mm and for h between 0.1 mm to 5 mm. The appropriate characteristics $B(r) = f(g/h)$ are shown in Fig. 2.15.

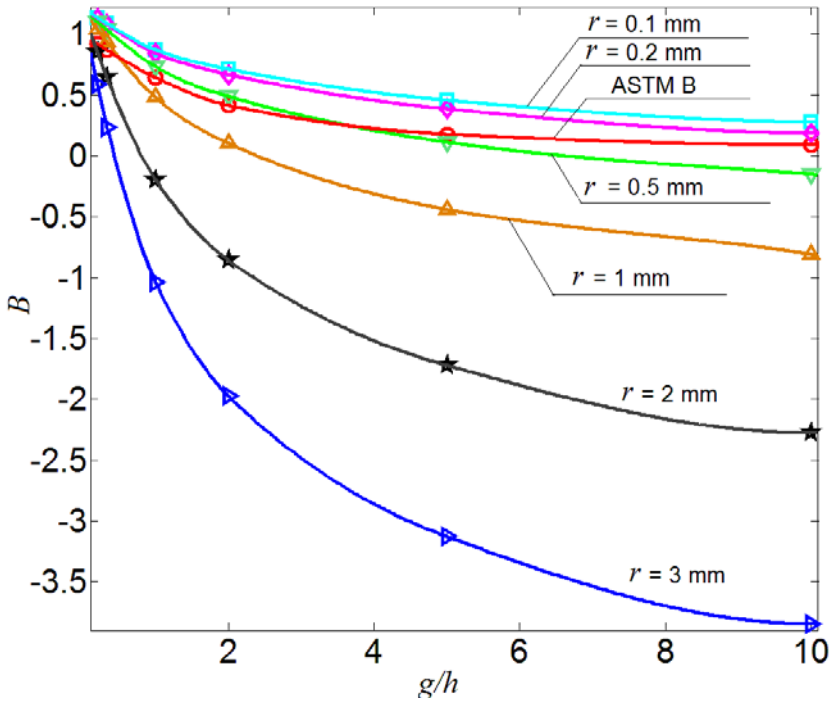

Fig. 2.15 Dependence of the B factor on the ratio of g/h (gap width/sample thickness).g = 1 mm.

As seen in Fig 2.15, when *r* is 0.1 mm or 0.2 mm, the value of *B* obtained from the simulation is slightly higher than that is acquired from ASTM standards. When *r* is 0.5 mm, the value of *B* calculated from the ASTM standard is still slightly lower than the simulated value if *g/h* is below 2. As *g/h* increases, a fast decrease of the simulated value of *B* can be observed and the value of *B* that calculated from the ASTM standard will be higher than that obtained from the simulation. When *r* is larger than 0.5 mm, the simulation results reveal great deviation of the value of *B* from that provided by the ASTM standard. The differences among the value of *B* calculated for different values of *r* are negligible when *g/h* is small. When the ratio of *g/h* is higher than 0.5, a great disparity of *B* can be observed. Thus, the parameter *r* can affect the effective edge radius of the measuring electrode. If the edge radius of the measuring electrode is large, a substantial error can be caused when the correction equation given by the ASTM standard is used.

As observed from Fig. 2.15, the coefficient *B* takes negative value and the effective radius seems to shrink. That is because Eq. 2.8 is flawed. Eq. 2.8 has been developed based on two assumptions: (1) only the measuring electrode radius can change; (2) the distance between the high voltage electrode and the measuring electrode, h , is homogeneous. This cannot be true in a rigorous way. When the edge of the measuring electrode is rounded, the distance *h* increases near the edge of the electrode. Thus, assumption of a constant *h* only means that it is a contractual distance between the high voltage electrode and the measuring electrode. The effective radius of the measuring electrode is shrunk as *h* increases near the edge of the electrode. Therefore, the parameter *B* is affected by both the edge fringing effect and the change of the gap distance *h* that is due to the rounded edges.

To study this effect in depth, the relative error of the effective area of the measuring electrode will be investigated and this relative error can be denoted as,

$$\delta A = \frac{A_{simulation} - A_{ASTM}}{A_{simulation}} \times 100\%, \tag{2.10}$$

with

$$\begin{cases} A_{simulation} = \pi(d + B_{simulation} g)^2 / 4 \\ A_{ASTM} = \pi(d + B_{ASTM} g)^2 / 4 \end{cases}, \tag{2.11}$$

where δA is the relative error of the effective area of the measuring electrode, *d* (m) is the diameter of the measuring electrode, the value of $B_{simulation}$ is obtained from simulation and the value of B_{ASTM} is acquired from the ASTM D257 standard, $A_{simulation}$ and A_{ASTM}

represent the effective area of the measuring electrode calculated from the computer based simulation, and that obtained from ASTM D257 standard, respectively. Fig. 2.16 depicts the dependencies of the relative errors of the effective area of the measuring electrode on *g/h*. It seems that if *g/h* or the edge radius is too large, the correction equation in the ASTM standard can cause a significant error. If the ratio of *g/h/r* is chosen as 1:3:1, a minimum relative error can be obtained. The ratio of the field enhancement is 0.301, if *g/h/r* = 1:3:1. According to our simulation results, the field distortion among the electrodes is not severe for this choice. IEC 60093 suggests the smallest practical gap between the measuring electrode and the high voltage electrode is 1 mm, therefore, the recommended values for the edge radius of the guard and measuring electrode, the distance between high voltage electrode and measuring electrode and the distance between the measuring electrode and guard electrode are 0.5mm, 0.5mm and 1.5mm, respectively.

Most of the correction equations to calculate the effective surface area of the measuring electrode are developed using the Schwarz and Christoffel transformation [97-104], and this transformation needs to be modified if it is going to transform the polygon with rounded corners [106-108]. Nevertheless, the current studies upon the field distribution in a guarded electrode system have not taken account this modification.

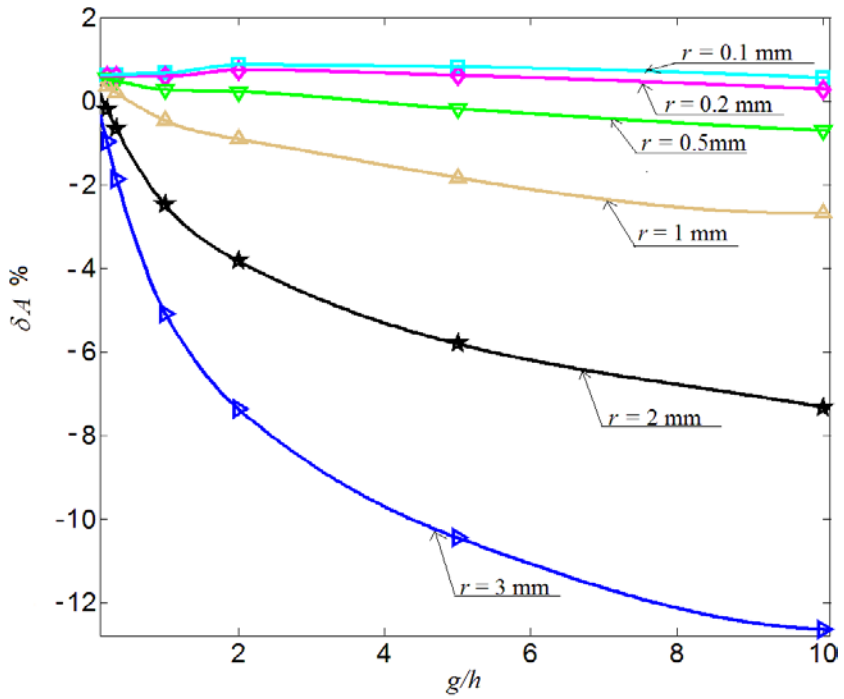

Fig. 2.16 Dependence of the relative error of the effective surface area of measuring electrode on the *g/h* ratio (gap width/sample thickness). *g* = 1 mm.

To sum up, edge radius is a new parameter that needs to be considered in the correction equation for the effective radius. Because the parameters *h*, *r* and *g* can significantly affect the effective radius, they should be chosen carefully in the design of a guarded electrode system. On considering both the effect on the maximum field and the effective radius, a ratio of *g/h/r* = 1:3:1 is recommended

2.3.4 Experimental confirmation

The DC conductivity test system shown in chapter 2 has been used to perform the verification test. The DC conductivity measurements were last for 3 hours and the tests were performed at different electric fields (1 kV/mm, 2 kV/mm, 3.5 kV/mm and 5 kV/mm) and different temperatures (30 °C and 90 °C). Here, the electric strength of the insulating liquid has been redefined as the maximum field at which the liquid sample can survive for 3 hours without breakdown. The pressure of the test cell is below 100 Pa during the test. Each of these tests has been repeated at least twice.

The electric strength of the mineral oils introduced in Chapter 2, Shell ZX-I oil, Hydro Quebec oil and Terna oil, have been tested. The distance between the high voltage electrode and the measuring electrode is 1 mm and the gap between the measuring electrode and guard electrode is 0.5 mm. The edge radiuses of the measuring electrode and the guard electrode are set to be 0.05 mm first and then are modified to 0.5 mm. According to our simulation, the ratio of the field enhancement is 0.89 for r = 0.05 mm and 0.27 for r = 0.5 mm, which means the electric strength measured for r = 0.5 mm should be about 1.5 times of that measured for r = 0.05 mm.

The electric strengths of these three mineral oils have been given in table 6.1. As seen from table 2.1, the electric strengths of the Shell ZX-I oil are higher than 5 kV/mm for both edge radiuses. Since the resistivity of Shell ZX-I oil is high and the breakdown strength of Shell ZX-I that listed on the data sheet that provided by the manufacturer is much higher than 10 kV/mm, the distortion caused by the application of an average field of 5 kV/mm might not be high enough to cause breakdown in Shell ZX-I oil. The Hydro Quebec oil has been aged for 10 years and it has a medium conductivity. As seen from Table 2.1, the electric strength of Hydro Quebec oil seems to be doubled as the edge radius goes up from 0.05 mm to 0.5 mm, which suggests the maximum field in the guarded electrode system is higher than the breakdown strength of the Hydro Quebec oil

when r = 0.05 mm. Terna oil has been in service for almost half century, so its quality is the worst in all three oils and the conductivity of this oil is the highest. When r = 0.05 mm, breakdown happened in less than a minute as the lowest external potential, 1 kV/mm, was applied across the sample. Increasing the edge radiuses of the measuring electrode and guard electrode has made the electric strengths of Terna oil to be higher than 1 kV/mm at both 30°C and 90 °C. For the Hydro Quebec oil and Terna oil, the electric strengths for r = 0.5 mm seem to be about 2~3 times of those for r = 0.05 mm based on experiments. On considering that the presence of space charge could also contribute to the distortion of the electric field among the electrodes, the real maximum field in the experiment can be higher than that obtained from the simulation work.

Table 2.1 Electric strength of different mineral oil

Temperature	30 °C		90 °C	
Edge Radius	0.05 mm	0.5 mm	0.05 mm	0.5 mm
Shell ZX-I	> 5 kV/mm	> 5 kV/mm	> 5 kV/mm	> 5 kV/mm
Hydro Quebec	2~3.5 kV/mm	>5 kV/mm	2~3.5 kV/mm	> 5 kV/mm
Terna	<1 kV/mm	1~2 kV/mm	< 1 kV/mm	1~2 kV/mm

To sum up, by increasing the edge radiuses of the measuring electrode and guard electrode, the electric strength of the insulating liquid that can be measured experimentally will increase. The existence of the local field enhancement in the vicinity of the edge of the guard electrode and measuring electrode has been confirmed. Therefore, the ratio of the field enhancement is one of the important parameters that need to be taken into account in the design of a guarded electrode system for the DC conductivity of the dielectric liquid measurement.

Cigre working group A2/1.41 requires a oil gap of 1 mm in the DC conductivity measurement. In our DC conductivity measurement, the high voltage electrode and measuring electrode and the distance between the measuring electrode and guard electrode have been set to 0.5mm, 0.5mm and 1 mm, respectively. The field enhancement ratio calculated by using Eq. (2.2) is 0.36.

2.4 Experimental settings for DC conductivity measurement

In order to understand the influence of aging on DC conductivity of mineral oil, CIGRE A2/1.41 proposed a Round Robin Test on three kinds of mineral oils: Shell Diala S3 ZX-I oil, aged oil from transformers in Hydro Quebec and aged oil from transformers of Terna. These three kinds of mineral oils have different aging period. Shell Diala S3 ZX-I oil (Shell ZX-I oil) is the fresh oil provided by the Shell company. Aged oil from transformers in Hydro Quebec (Hydro Quebec oil) has been in service for almost 10 years. Aged oil from Terna transformer (Terna oil) has been in service in transformers for over 50 years. These mineral oils have gone through different types of stresses and their original conditions can also be different from each other. The conductivity of these three mineral oils can give a brief view of oil condition when they are fresh, in service for several years and heavily aged that are needed to be replaced. Therefore, it can be quite helpful if the DC conductivity of these three mineral oils are compared and analysed. As shown in Fig. 2.17, these three kinds of mineral oils have different colours. Shell ZX-I oil is transparent; Hydro Quebec oil is yellow and Terna oil is dark brown.

The distance between upper and lower electrodes is 1mm; the measuring temperature will be 30℃ and 90℃. The electrification time is 3 hours. The average water contents of these mineral oils are measured prior to the measurement 4.5 ppm (Shell oil), 12 ppm (Hydro Quebec oil) and 24.5 ppm (Terna oil) by Karl –Fischer titration. The water content measured after the experiment are 6 ppm (Shell oil), 14 ppm(Hydro Quebec oil) and 27 ppm (Terna oil). The sampling rate of the DC conductivity measurement is 0.5s. The current range of Keithley pico-ammeter is selected to "auto-range". The conductivity of Shell ZX-I oil were measured in current range of 0 - 2 nA or 2 - 20 nA; the conductivity Hydro Quebec oil were measured in a current range of 2 - 20 nA, 20 - 200 nA or 200 - 2000 nA; the conductivity of Terna oil were measured in a current range 20 - 200 nA, 200 - 2000 nA or 2 μA - 20 μA. In order to avoid fluctuation, the current range of the pico -ammeter will be set manually if the measured long- term current is close to the bound of any current range.

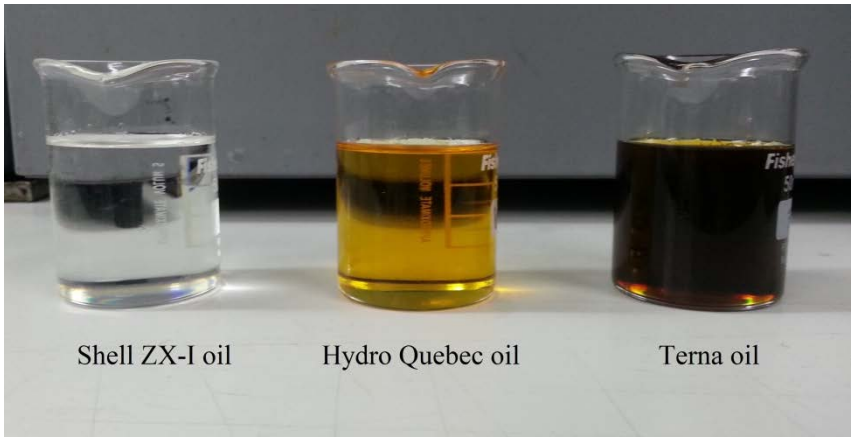

Fig. 2.17 Mineral oil with different aging times

Ultra violet/visible (UV/vis) spectroscopy was carried out in quartz cells of path length 10 mm using a Perkin Elmer Lambda 35 spectrometer.

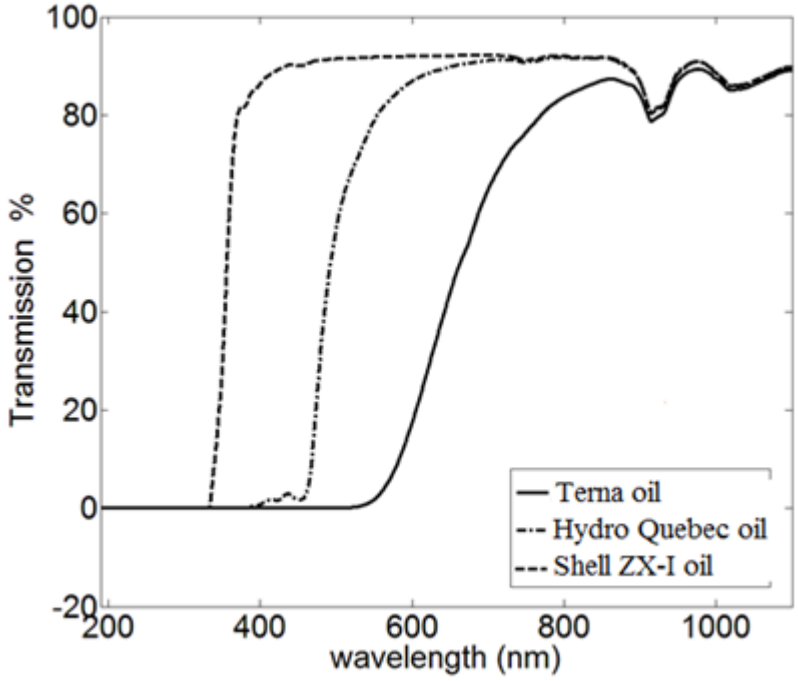

Fig. 2.18 UV/vis spectroscopy of three kinds of mineral oil

Ultraviolet- visible spectroscopy is an absorption spectroscopy or reflectance spectroscopy in the ultraviolet- visible spectral region [109-112]. The absorption in the visible range is directly affected by the colour of the chemical involved. As seen in Fig. 2.5, the fresh oil is almost transparent, the colour of Hydro Quebec oil is yellow and the colour of the Terna oil is dark brown. In UV/vis spectra measurement, a shift in the absorption edge to longer wavelengths can be observed. As seen in Fig. 2.27, the oils absorb most radiation below a certain wavelength and display a broad absorption edge.

The position of these edges relates to the character of the mineral oil and shift from the ultra violet into the visible range as the aging time goes longer. The result of the UV/vis spectroscopy is coherent with the colour of the oil. As the oil is aged, the DC conductivity increases and the colour of the oil is darkening [111-112]. As observed in our DC conductivity measurement: Terna oil has the highest conductivity and is dark brown, Hydro Quebec oil has a medium conductivity and is yellow, Shell ZX-I oil has the lowest conductivity and is transparent. Therefore, the result from the DC conductivity measurement is also consistent with the UV/vis spectroscopy result.

2.5 Experimental results for DC conductivity measurement

2.5.1 System repeatability

As seen from Fig. 2.19, the DC conductivity of Shell ZX-I oil under an electric field of 1 kV/mm has been measured at three different days. The measured electric current is quite noisy, however, if the average value of every ten seconds is calculated, the relative difference between each curves are less than 25%. On considering there are other factors, such as, water content, humidity, temperature and external voltage, et al, that can affect the conductivity measurement, the repeatability of this test system is acceptable.

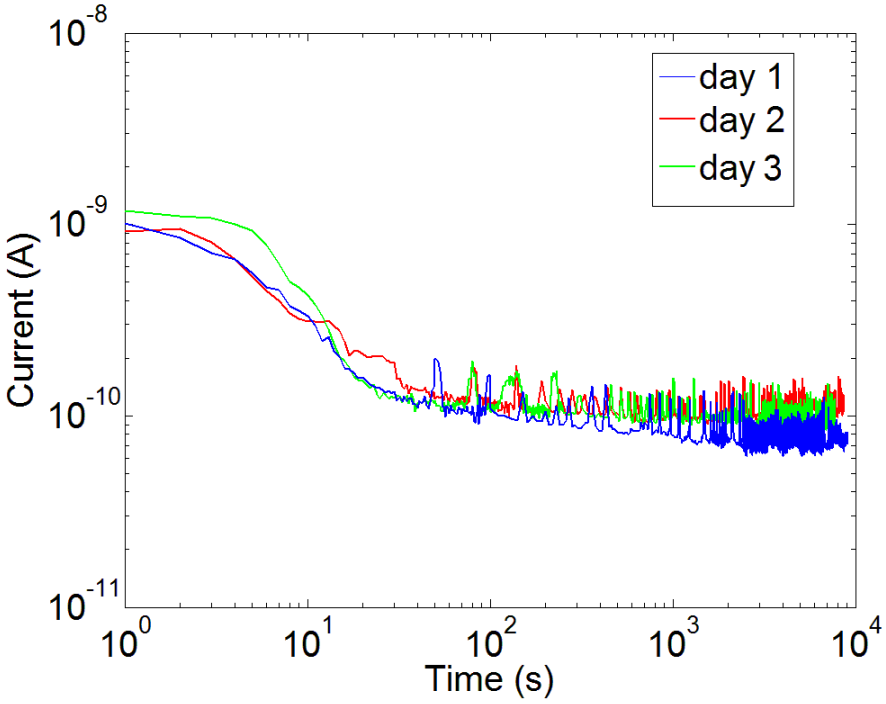

Fig. 2.19 Polarization current of Shell ZX-I oil under 1kV/mm at 30°C measured at three different days.

2.5.2 Shell ZX-I oil

Fig 2.20 and Fig 2.21 show the time dependence of the polarization current of Shell ZX-I oil under different field and temperature. The experimental results of the current that are measured at 30 ℃ are quite noisy and the curves are overlapped, thus, to reduce the noise level the average value of every 10 second after 80 second has been calculated and shown in Fig. 2.20. The values in the first 80 second are the original value. When the measuring temperature is low, the long -term current does not change much with the electric field (above 1000 V/mm), and it seems the current enters the saturated region in which the current increases slightly with the electric stress and no longer obeys ohm's law. The initial current seems to increase with the electric field at 30 ℃, which indicates the velocity of the charge carriers can increase with the electric field. The long-term current increases with the electric field at 90℃, which suggests that the long -term current has passed the saturated region and starts to increase again.

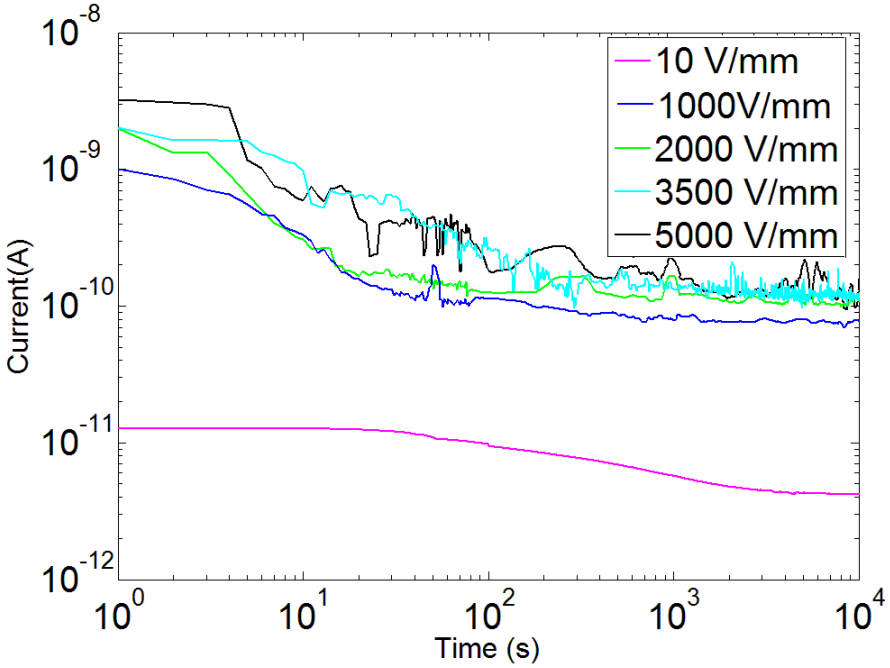

Fig. 2.20 Time dependence of polarization currentof Shell ZX-I oil at 30℃

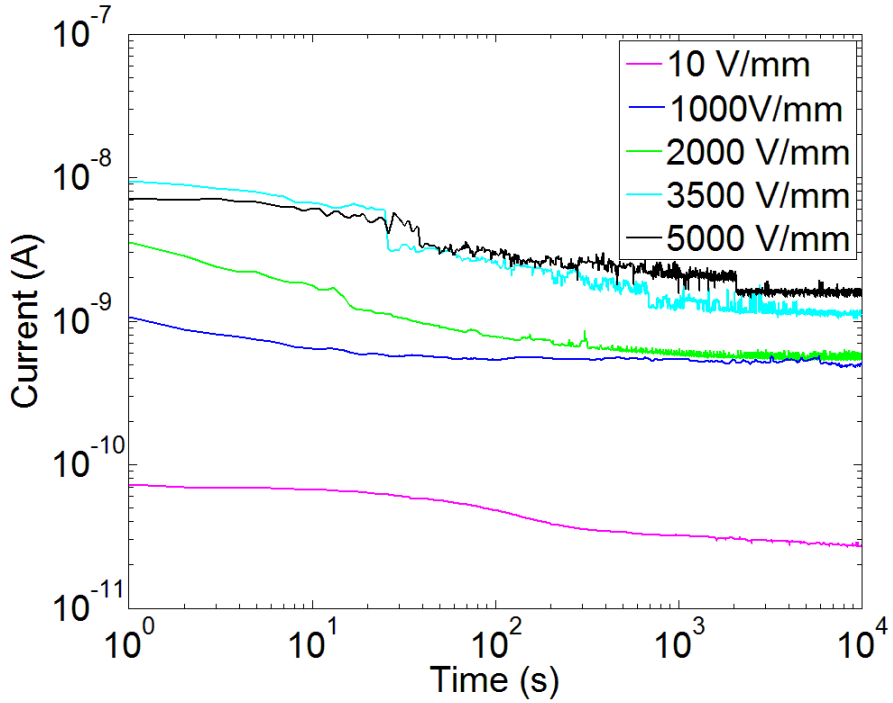

Fig. 2.21Time dependence of polarization current of Shell ZX-I oil at 90°C

2.5.3 Hydro Quebec oil

Fig. 2.22 and Fig. 2.23 show the correlation between the polarization current and the electric field of the mineral oil from Hydro Quebec. The initial current and the long –term current increase with the electric field at both 30°C and 90°C.It seems there is no saturated region for the field dependence of the DC conductivity of Hydro Quebec oil. In contrast with the experimental results of Shell ZX-I oil, the curves of the time dependence of the polarization are smooth under a field of 1 kV/mm and 2 kV/mm. The measured current becomes unstable when the field is higher than 3.5 kV/mm, as the non- linear behaviour can affect the electric conduction at a high field. The current also increase with the temperature. The current measured at 90°C is about 10 times higher than that measured at 30°C.

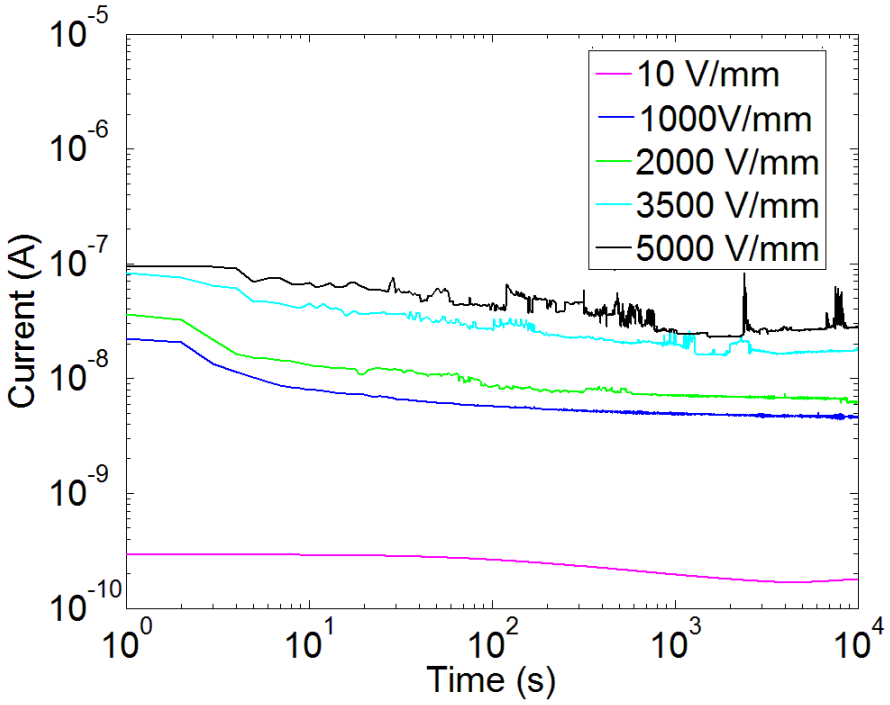

Fig. 2.22 Time dependence of polarization current of Hydro Quebec oil at 30℃

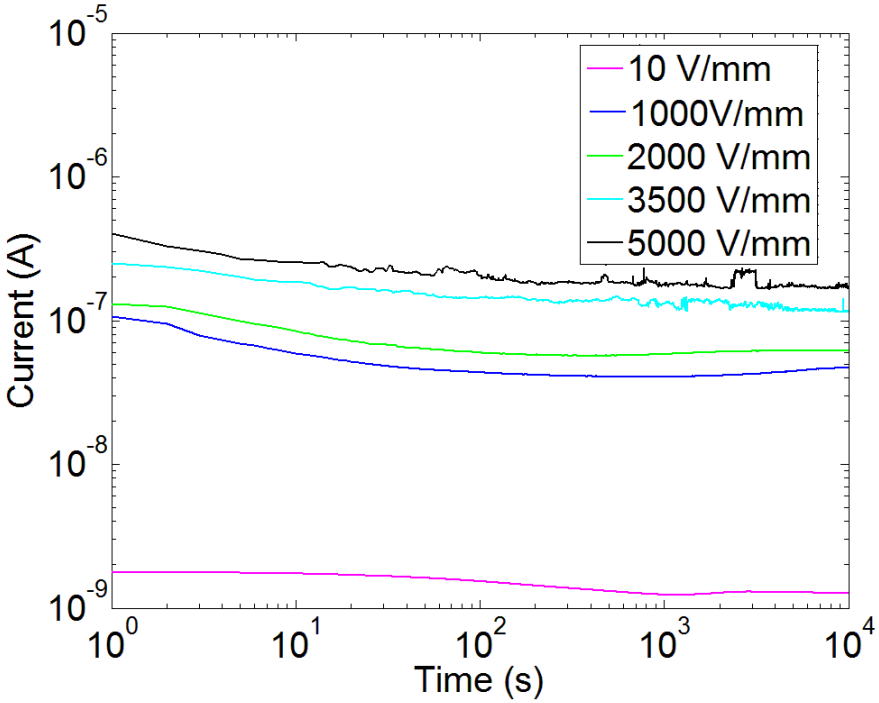

Fig. 2.23 Time dependence of polarization current of Hydro Quebecoil at 90℃

2.5.4 Terna oil

Due to a very low breakdown strength (around 3kV/mm), the measurement under a high electric field (above 2kV/mm) is unable to be carried out. The experimental data has been shown in Figs. 2.24-2.25, and it seems Terna oil has an even higher conductivity

than that of Hydro Quebec oil. The initial and long –term current increase with the electric field. The field dependent current of Terna oil also does not enter the saturated region. The polarization current decreases with the time at the beginning, reaches a minimum value and then starts to increase. As there are more charge carriers in Terna oil, the space charge effect could be enormous leading to a strong field distortionin the vicinity of the electrode. Thus, the charge injection can be enhanced at the electrode and the total current also becomes higher. However, the mechanism of charge injection is still not well understood and more studies are needed.

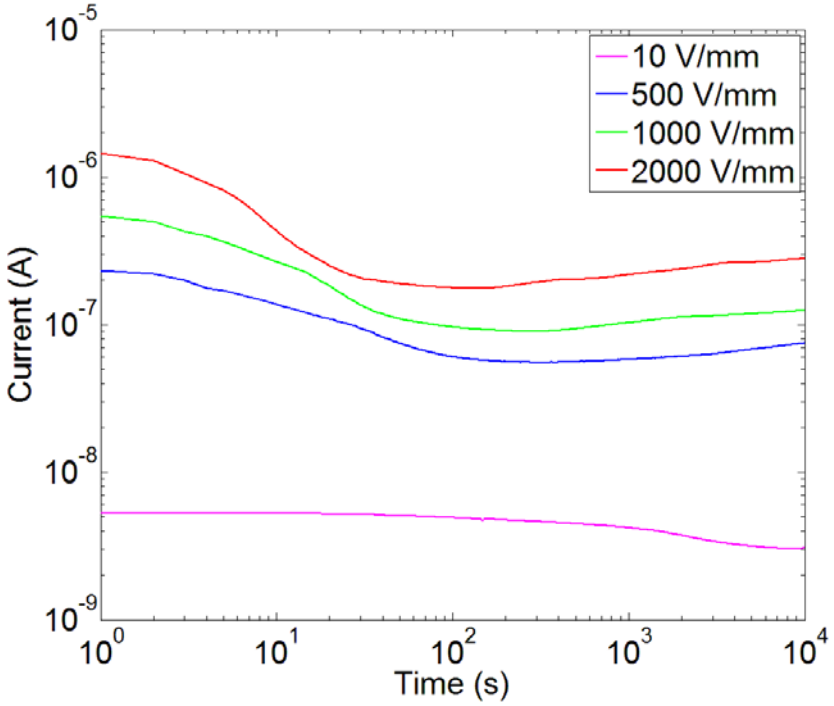

Fig. 2.24 Time dependence of polarization current of Terna oil at 30°C

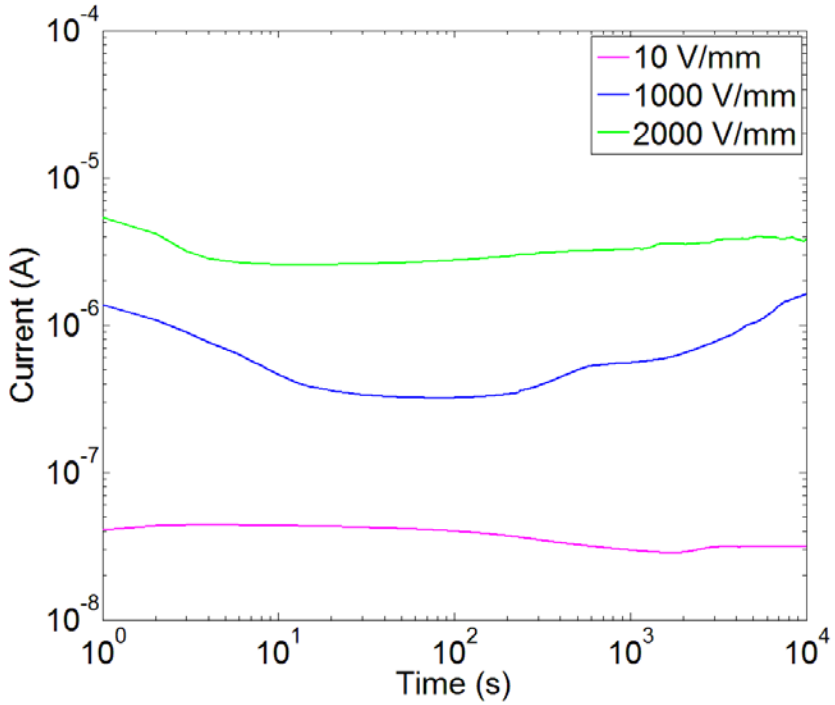

Fig. 2.25 Time dependence of polarization current of Terna oil at 90°C

To sum up, the conductivity will increase with the aging period and temperature. When the oil is aged, its DC conductivity rises. Besides, the improvement of oil manufacturing techniques can also play an important part, oil manufactured later may have better dielectric properties. Thus, Shell ZX-I oil has the highest resistivity, Hydro Quebec oil has a medium resistivity and Terna oil has the lowest resistivity.The polarization current of the aged oil (Hydro Quebec oil and Terna oil) don't enter the saturated region and the polarization current always increase with the electric field, whilst that of the Shell ZX-I oil doesn't change with the field at 30°C. Also, space charge might be formed in the bulk during long-term DC conductivity measurement.

2.6 Initial and long-term DC conductivity

According to IEC 61620, the initial conductivity is the conductivity measured in the beginning few seconds. The definition of long-term conductivity based on current international standards cannot provide sufficient information to characterize the status of mineral oil for short electrification time and low electric field. Kuchler et al stated that the electrification time for DC conductivity measurement is not sufficient enough to reach the equilibrium state in mineral oil [95]. As suggested by CIGRE group A2/ 1.41, conductivity that measured at 1 min, 2 min, 1 hour and 3 hour should be recorded and one

hour of electrification time is believed to be the minimum measuring time for long-term conductivity measurement. Here, the initial conductivity the conductivity measured at 1 minute, 1 hour and 3 hours of these three kinds of mineral oils will be studied.

2.6.1 Shell ZX-I oil

Fig 2.26 shows the field dependence of the electric conductivity of Shell ZX-I oil at 30℃.The line with the circular marker stands for the initial conductivity measured at the very beginning, the line with square marker is the conductivity measured at 1 minute, the line with triangular marker of denotes the conductivity measured at 1 hour and the line with star marker shows the conductivity measured at 3 hours.

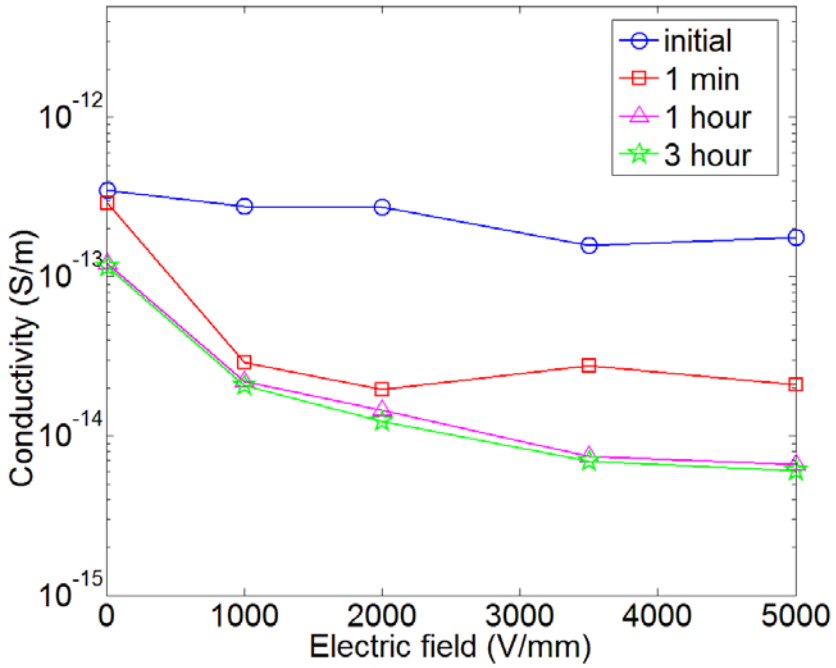

Fig.2.26 Conductivity for the Shell ZX-I oil at different electric field under 30 ℃

As seen from Fig. 2.26, the initial conductivity for the fresh oil does not change much with the electric field at 30 ℃. The conductivities of Shell ZX-I oil measured at 1 hour and 3 hours are similar and the long –term conductivity decreases with the electric field. The conductivity measured at 1 minute is close to that measured at 1 hour and 3 hours under a field of 1 kV/mm or 2 kV/mm, which indicates that the process by which the polarization reaches the equilibrium state can be accelerated by the electric field. As the field increases, non –linear behaviour can affect the electric conduction, the mineral oil needs longer time to reach the equilibrium state. Also, the electrification time of 1 hour is sufficient long enough to obtain a steady state conductivity. The steady state conductivity

decreases with the electric field. When the conducting current enters the saturated region, the current is determined by the dissociation rate. If the dissociation rate does not change very much, the current seems to be constant with the electric field. Thus, the conductivity decreases with the electric field once the saturated region has been reached.

Fig. 2.27 shows the field dependence of the electric conductivity of Shell ZX-I oil at 90℃. The initial conductivity measured under a field of 10V/mm are higher than those obtained under other electric fields. As the temperature increases, the mobility of the charge carriers also increases. Therefore, the time for the extraction of the pre-existing charge carriers at 90℃ is much shorter than that at 30℃. The initial current due to the drift of these pre-existing charge carriers might not be recorded by the pico-ammeter at a high temperature due to a short extraction time and the magnitude of the initial current cannot be related to the density of the pre-existing charge carriers any longer. The conductivity measured at 1 hour is also very close to that measured at 3 hours and a quasi -equilibrium state can be reached within 1 hour. There is a big gap between the conductivity measured at 1 minute and that measured at 3 hours when the electric field is above 2 kV/mm, which indicates that the non-linear behaviour of high electric field can also affect the electric conduction at 90 ℃. The steady state conductivity decreases with the electric field first and reaches a minimum value at 2 kV/mm. When the field is higher than 2 kV/mm, the conductivity seems to become constant. As the dissociation rate increases with the temperature, more charge carriers will be generated by the dissociation. Also, the injection can also be enhanced by the increase of the temperature [35-36]. Consequently, the long-term conductivity is determined by both the dissociation and the injection and the saturated region is not clearly observed at 90 ℃.

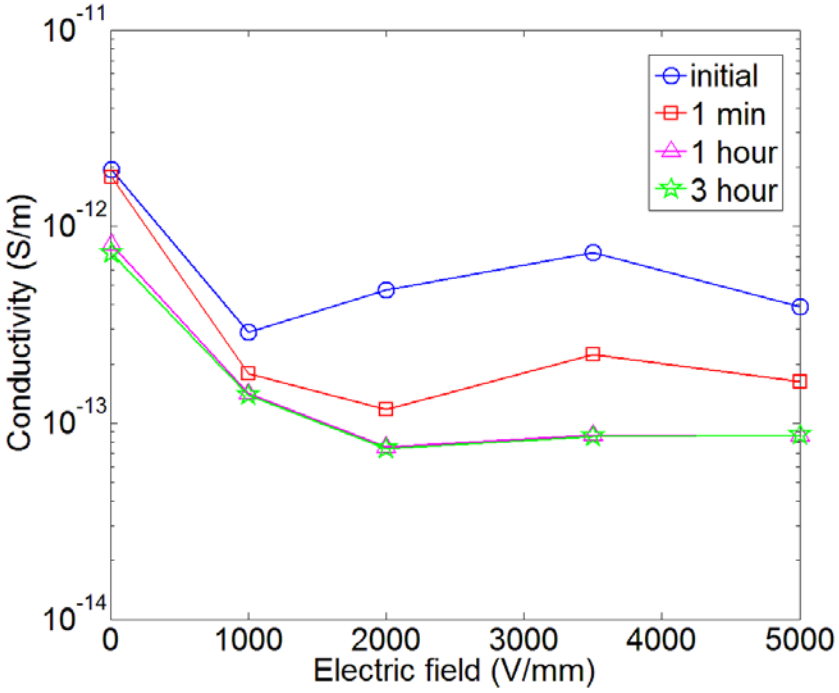

Fig. 2.27 Conductivity for the Shell ZX-I oil at different electric field under 90 ℃

2.6.2 Hydro Quebec oil

Fig. 2.28 shows the field dependence of the electric conductivity of Hydro Quebec oil at 30℃.The initial conductivity of Hydro Quebec oil at 30 ℃ does not change much with the electric field, which is similar to that observed from the experimental results of Shell ZX-I oil at 30 ℃ and the initial current depends on the density of the pre-existing charge carriers. There is notable difference between the conductivity measured at 1 minute and 1 hour, whilst the gap between the conductivity measured at 1 hour and that measured at 3 hours is negligible. Thus, the steady state can be reached within 1 hour and the electrification time of 1 minute is not long enough to reach the steady state conductivity. The steady state conductivity decreases to a minimum value at 2 kV/mm and then it increases with the electric field. When mineral oil is in service, vapour, such as oxygen, water, can be absorbed. Also, oxidation of hydrocarbon molecules can result in soluble oxidation products and increase of oil acidity. Acids have an impact on the degradation of cellulosic materials and may also be responsible for the corrosion of metal parts in a transformer, which bring derivatives of hydrocarbons that include atoms of other elements, such as nitrogen, sulphur and oxygen [89-92]. As Hydro Quebec oil has been aged for 10 years, the quantity of impurities in the oil is high. These impurities may have high dissociation coefficients and they will become free ions more easily. As pointed out

by other researchers, if there are sufficient impurities in the oil, the saturated region may not be observed [48-51].

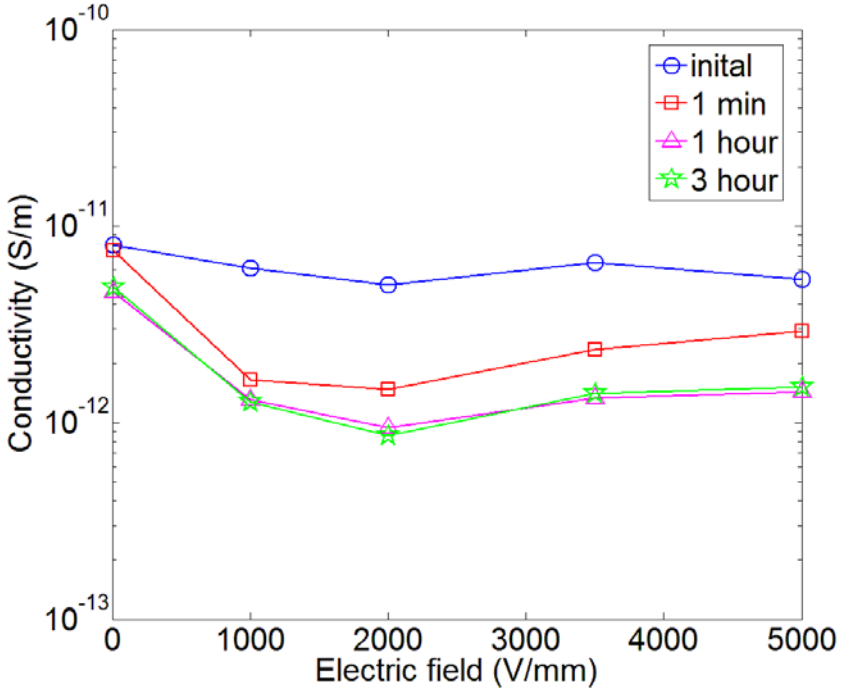

Fig. 2.28 Conductivity for the Hydro Quebec oil at different electric field under 30 ℃

Fig. 2.29 depicts the field dependence of the conductivity of Hydro Quebec oil at 90 ℃. The long –term conductivity decreases with the electric field first, and then reaches a minimum value at 2 kV/mm, after that the conductivity increases with the electric field. The field dependence of the DC conductivity does not have a saturated region, As more charge carriers are generated from the impurities and the ionic injection under a higher electric field, the current can increase with the electric field and the electric conduction is not determined by the ions dissociated from ionic- pairs. The conductivity measured at 1 minute is similar to that measured at 1 hour and 3 hours, therefore, the conductivity obtained at 1 minute can be used as the steady state conductivity.

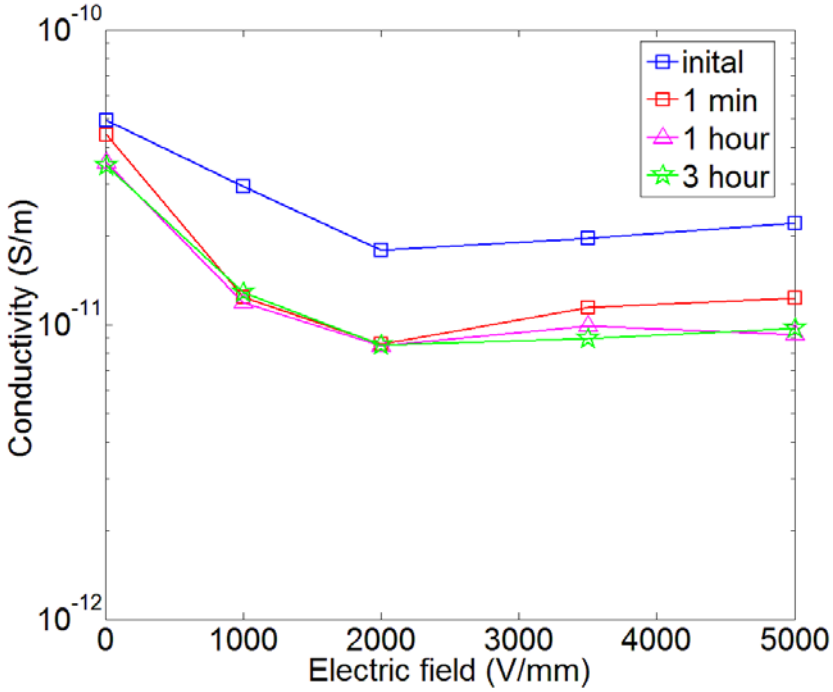

Fig. 2.29 Conductivity for the Hydro Quebec oil at different electric field under 90 ℃

2.6.3 Terna oil

Fig. 2.17 shows the field dependence of the electric conductivity of Terna oil at 30℃. Unlike the other two kinds of mineral oil, the initial conductivity of Terna oil increases with the field. However, the difference between the initial conductivity under different electric field is negligible and the initial conductivity still depends on the density of the pre-existing charge carriers. The minimum conductivity can be obtained around 1 or 2 minutes, and then the conductivity starts to increase. The conductivity measured at 1 minute decreases with the electric field, whilst the conductivity measured at 1 hour and 3 hour under a field not lower than 500 V/mm does not change much with the electric field. As the conductivity of Terna oil is very high, there are more charge carriers participating in the electric conduction which can result in a serious field distortion. Thus, the influence from the presence of the space charge cannot be ignored in the severely aged oil.

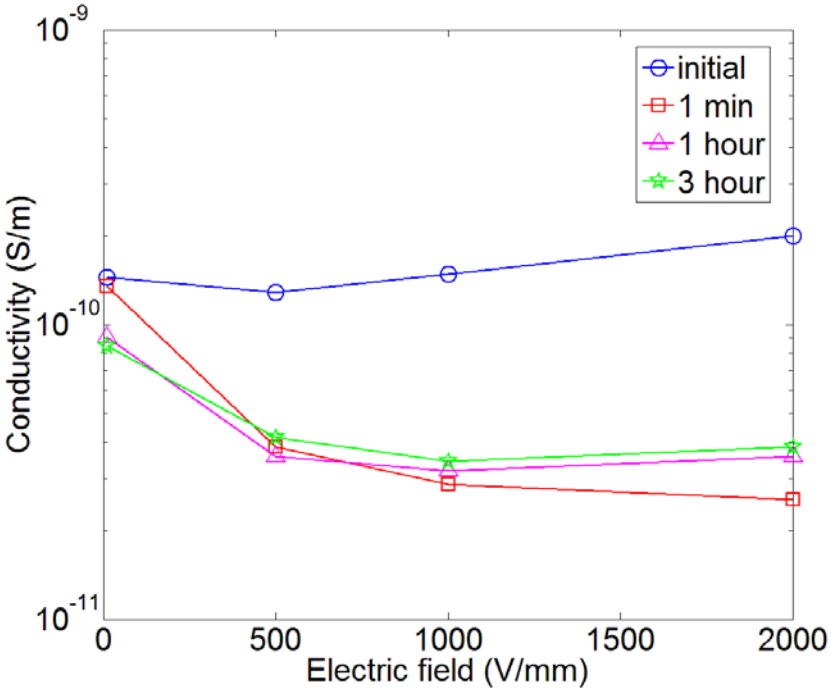

Fig. 2.30 Conductivity for the Terna oil at different electric field at 30 ℃

The field dependent conductivity of Terna oil at 90 ℃ is depicted in Fig 2.16. The conductivity measured at 1 minute is much lower than that measured at 1 hour and 3 hours. Even after 3 hours of polarization, the current still could not reach a steady state. Thus, the recommended electrification time given in current international standards is not long enough to obtain the steady state conductivity in the severely aged oil. The mechanism of the electric conduction in the Terna oil is still not very clear and more research is needed.

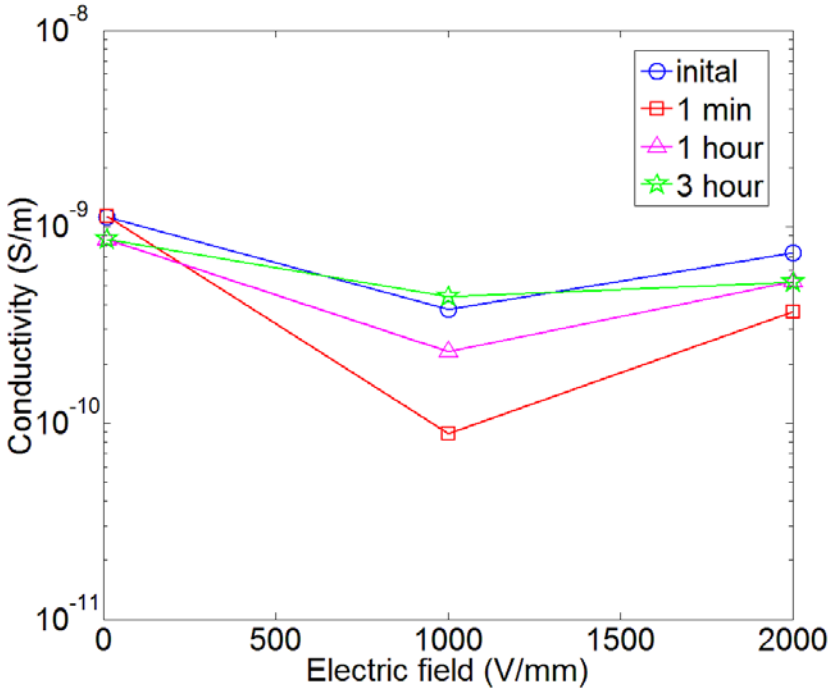

Fig. 2.31 Conductivity for the Terna oil at different electric field under 90 ℃

To sum up, the initial conductivity measured at low temperature (30 ℃) does not change much with the electric field in all three types of oil, which indicates that at the very beginning, the ionic conduction plays a crucial role in mineral oil. The conductivity of Shell ZX-I oil and Hydro Quebec oil decreases with the time, whilst that of Terna oil reaches a minimum value first and then starts to increase. The steady state conductivity can be obtained within an hour for Shell ZX-I oil and Hydro Quebec oil, whereas, it takes more than three hours for the electric conduction in Terna oil to reach an equilibrium state. The electrification time defined in current international standards is not long enough [25-27], the author suggests that an electrification time of 1 hour is required to obtain the long-term DC conductivity of mineral oil.

2.7 Depolarization current measurement

Polarization and depolarization current (PDC) measurement as a time-domain test method has been widely used in the diagnosis of dielectric properties of insulating materials. The principle of PDC measurement is to apply a DC voltage across a test media. The current, arising from different types of polarizations, can reveal the dielectric properties and the motion of charge carriers in the test object. Then, the applied voltage is removed and the test object is short –circuited. The previous activated polarization gets

relaxed and releases a discharging current in the opposite direction. Fig 2.32 is a scheme of a simple polarization and depolarization current measurement system.

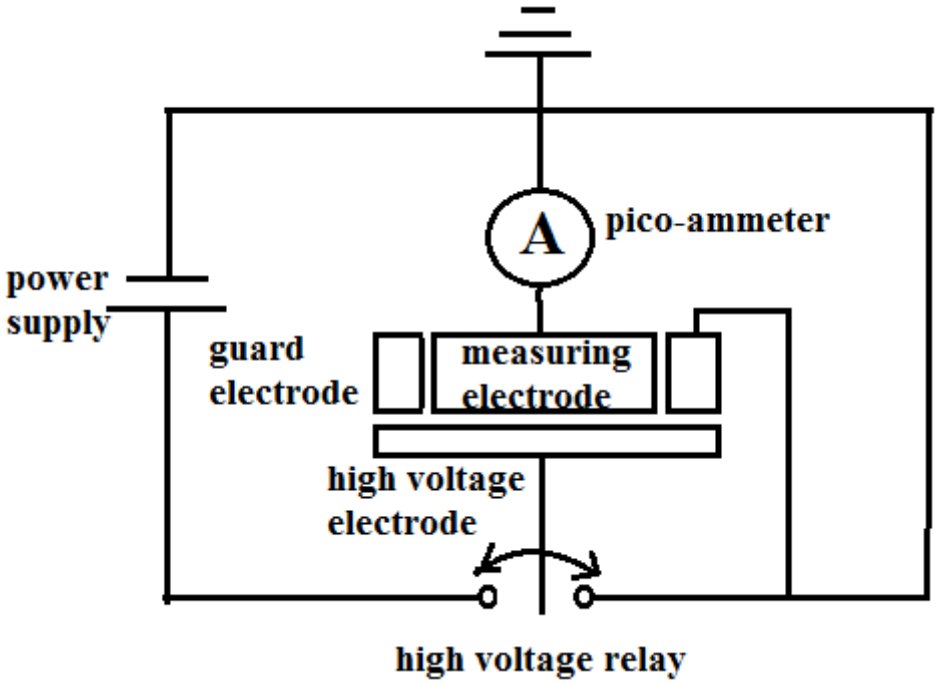

Fig. 2.32 Scheme of polarization and depolarization current measurement system

In our experiment, a high voltage relay is used as the switch in the above circuit. The polarization time is 3 hours. The influence from the electric field and temperature on the depolarization current will be investigated. Figs. 2.33-2.34 depict the time dependence of the depolarization current of Shell ZX-I oil at 30 °C and 90 °C. Figs. 2.35-2.36 show the time dependence of the depolarization current of Hydro Quebec oil at 30 °C and 90 °C. As seen from Figs. 2.33-2.36, the maximum value of the magnitude of the depolarization current of both Shell ZX-I oil and Hydro Quebec oil increase with the electric field and they decrease faster under a higher electric field. It has been widely accepted that the dissociation rate and the ionic injection rate increase with the field [34, 45-46], and consequently there should be more charge carriers participating in the electrical conduction process under a higher field. If more charge carriers have been involved in the electric conduction, the amount of the charge carriers that can be blocked by the electrode to form the charge layer will increase. When the oil sample is short circuited, the charge carriers that are stuck in the vicinity of the electrodes will start to drift backwards to the bulk and result in a depolarization current. Thus, the depolarization current should

increase with the field. It seems this explanation is consistent with the measurement results of Shell ZX-I oil and Hydro Quebec oil.

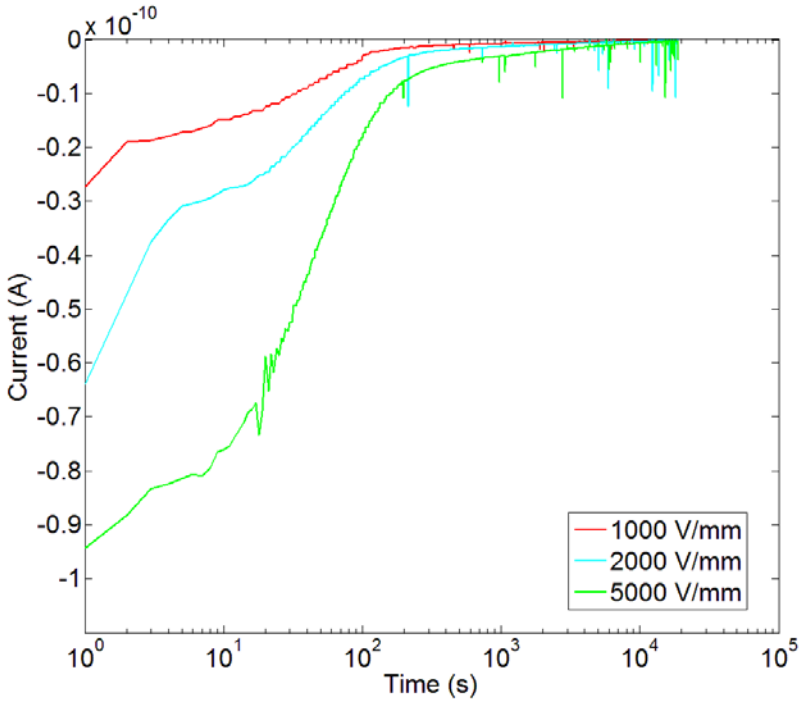

Fig. 2.33 Depolarization current for Shell ZX-I oil under different electric field at 30 ℃

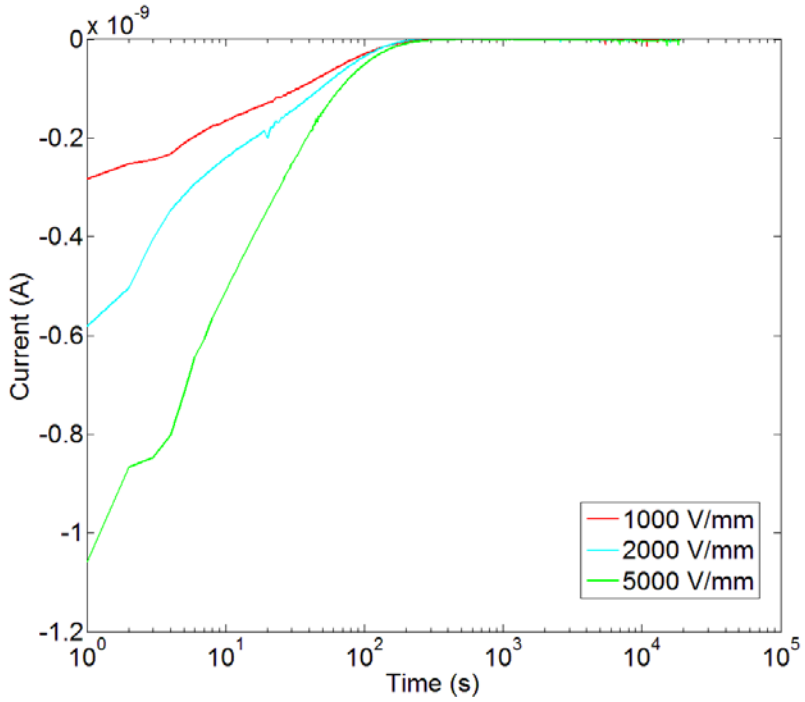

Fig. 2.34 Depolarization current for Shell ZX-I oil under different electric field at 90℃

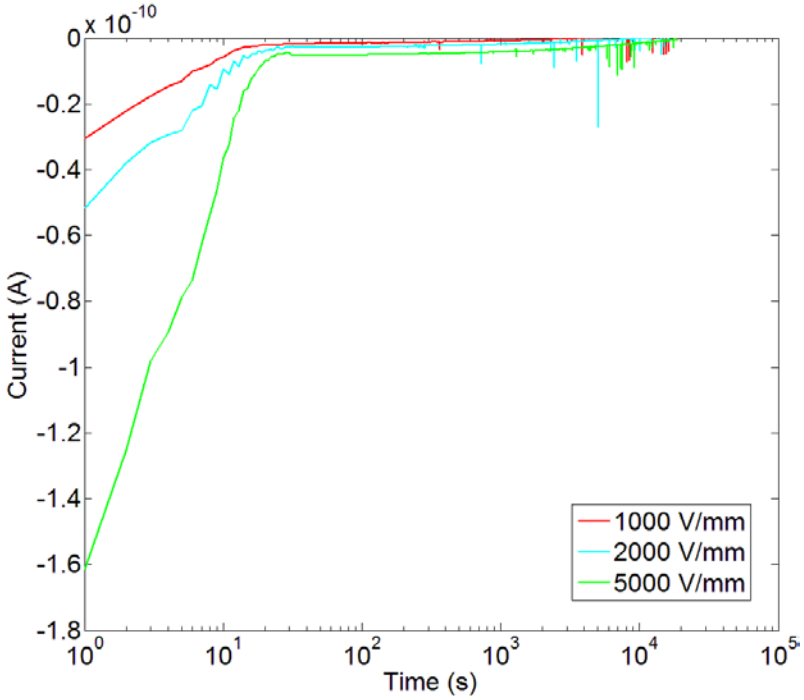

Fig. 2.35 Depolarization current for Hydro Quebec oil under different electric field at 30 °C

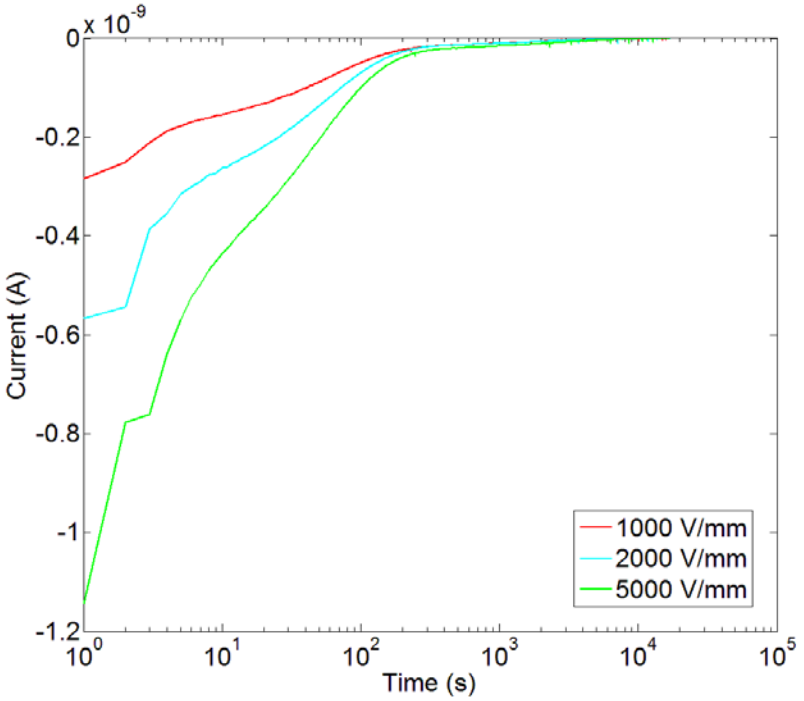

Fig. 2.36 Depolarization current for Hydro Quebec oil under different electric field at 90 °C

The time dependence of the depolarization current of Terna oil is shown in Figs. 2.37-2.38. The magnitude of the depolarization current first decreases and reaches a minimum value. Then the magnitude of this depolarization current increases. After a long period of increase, the magnitude of the depolarization current gets to another peak and starts to

decreases again and finally approaches to zero. When the electric field is removed, the space charge accumulated at the interface of oil/electrode will start to drift back into the bulk. If hetero-charge has been formed, the depolarization current should be negative. In a few seconds at the beginning, the magnitude of the depolarization current decreases fast at 30 °C. This is probably due to the ionic diffusion in the charge layer. The mobility of charge carriers in oil increases with temperature so that the diffusion coefficient is high at 90 °C. Thus, this diffusion happens much quicker and may not be observed if the pico-ammeter has a low resolution (the sampling rate is 0.5 s). After this fast current decrease, the magnitude of the depolarization current will start to increase. As Terna oil has been heavily aged and needs to be replaced, there can be charge carriers with very low mobility in this oil. There slow charge carriers will remain at the electrode for a long time and cause an internal electric field resulting a positive current. If the magnitude of the positive current decreases slower than that of the negative current, the magnitude of the total current can increase. Jaffe et al proposed a polarization theory to explain this phenomenon. They thought the internal field was distorted by the distribution of space charge in the dielectric liquid, thus an extra current caused by the internal field should be involved in the analysis of the depolarization process. In their work, an exponential equation has been given to describe this space charge induced current in the depolarization process [113-115].

As seen from Figs 2.33 -2.38, when the temperature becomes higher, the magnitude of the depolarization current also increases. The viscosity of the mineral oil decreases when the temperature rises, thus the friction force due to the viscosity is reduced at a high temperature [54-55]. Then the charge carriers can move faster when the temperature of the oil is higher. Also, the dissociation rate increases with the temperature and more charge carriers are generated at a higher temperature [32-33]. Consequently, there is more charge in the charge layer when the temperature is higher. Therefore, when the test media is depolarized, the depolarization current caused by the drift and diffusion of the charge carriers in the charge layer increases with the temperature. Although the conductivity of Hydro Quebec oil is much higher than that of Shell ZX-I oil, the magnitudes of the depolarization current of these two oils obtained at the same temperature and electric field are similar. This coincidence will be further studied in Chapter 5.

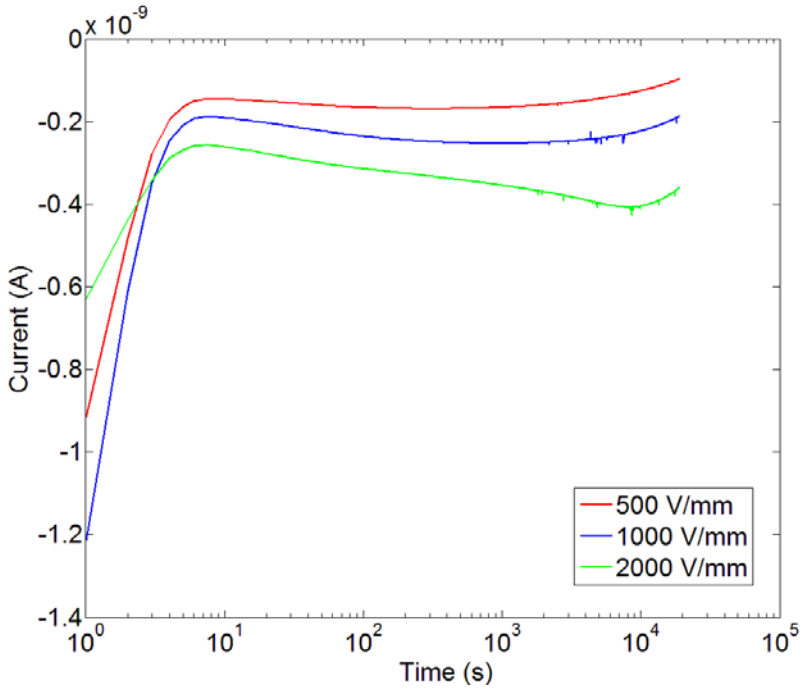

Fig. 2.37 Depolarization current for Terna oil under different electric field at 30 ℃

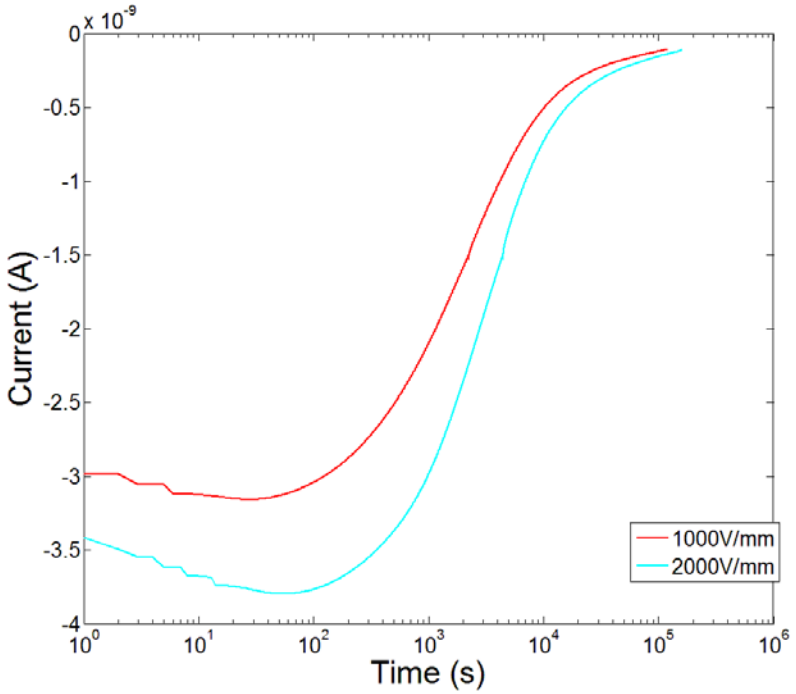

Fig. 2.38 Depolarization current for Terna oil under different electric field at 90 ℃

2.8 Viscosity of mineral oil

In order to carry out a quantitative study of the electric conduction mechanism of mineral oil in following chapters, the knowledge about the temperature dependence of the

mobility is required. As mobility is proportional to the inverse of viscosity in liquid, an experimental study on the viscosity of three oil samples has been performed.

The viscosity of a fluid is a measure of its resistance to deformation by shear stress or tensile stress. Viscosity is also an important parameter for oil quality analysis. Like the relationship between conductivity and temperature, viscosity of mineral oil can also be denoted using the Arrhenius Equation. Harrap and Heymann [54] have indicated that viscosity of liquid obeys the following equation:

$$\eta = Ae^{-\frac{E_{acv}}{kT}} \tag{2.12}$$

where η (mPa·s) is the viscosity, E_{acv} (eV) is the activation energy for the liquid flow, k is the Boltzmann constant, T (°C) is the temperature, A is a constant that relates to the property of material. Gutmann and Simmons [55] verified this equation in various dielectric liquids.

In our experiment, viscosity will be measured at 20°C, 30°C, 40°C, 50°C and 60°C using a rheometer. Before the measurement, all three types of mineral oil should be degassed for at least three hours in vacuum oven. The experimental data will be fitted using the Arrhenius equation.

As seen from the Fig. 2.39, the viscosity of all three types of oil fit this equation quite well. Based on these results, it might be possible to calculate the viscosity for a higher temperature approximately.

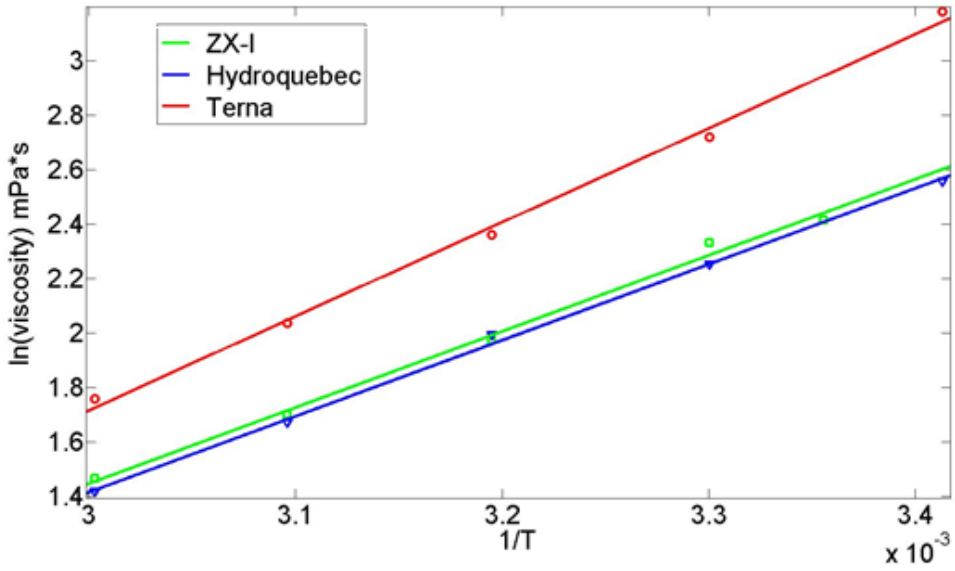

Fig. 2.39 Relationship between viscosity and temperature

According to Table 2.2, the viscosity for fresh oil from Shell ZX-I and Hydro Quebec oil is similar, whilst, the viscosity for Terna oil is higher. Thus, when the mineral oil is aged, its viscosity increases.

Table2.2 Viscosity for three different types of mineral oil

Viscosity(mPa·s)	Experimental data					Calculated data	
Temperature (℃)	20	30	40	50	60	75	90
Shell ZX-I	14.2	10.3	7.2	5.48	4.33	2.98	2.14
Hydro Quebec	12.9	9.5	7.33	5.31	4.12	2.89	2.09
Terna	24.1	15.2	10.6	7.67	5.8	3.60	2.38

2.9 Summary

As seen from the result of DC conductivity measurement, the DC conductivity of mineral oil increases with its aging time. The initial DC conductivity which is measured at the very beginning of the polarization process does not change much with the electric field and temperature. This indicates that at the very beginning when a DC field is applied, the space charge effect is negligible and the electrical conduction is determined by the drift of charge carriers. The long-time conductivity of mineral oil decreases with the electric field first, and then enters a quasi-constant region. If the electric field increases even higher, an increase of the conductivity can be observed. The time-dependent current of Terna oil can reach a minimum value within 1 hour of electrification and then start to increase. This may be attributed to space charge formation around electrode that can enhance charge injection process. The depolarization current of Shell ZX-I oil and Hydro Quebec oil decrease with time. When it comes to Terna oil, the magnitude of the depolarization current first decreases and reaches a minimum value. Then the magnitude of this depolarization current start to increase. After a long period of increase, the magnitude of the depolarization current gets to another peak and starts to decrease again and finally approaches to zero. This implies a serious field distortion in the Terna oil. However, the electrical conduction mechanism in mineral oil is still not very clear.

Chapter 3 AC Measurement on Mineral Oil

Starting in the late nineteenth century, dielectric spectroscopy techniques were developed for measuring polarization of various materials, such as liquid and solid insulation materials. Nowadays, a typical measurement can cover an extensive range of frequency from several GHz to several micro-Hz. It is a powerful tool to study dipole relaxation, electrical conduction and the structure of molecules. This frequency-domain method has been used to investigate dielectric properties of mineral oil and to estimate the remaining life period of a transformer in service [116-122].

In the case of a media with a constant conductivity and permittivity within certain frequency range, the real and imaginary parts of the relative complex permittivity obey the following expression.

$$\varepsilon'' = \frac{\sigma}{\varepsilon\omega} \tag{3.1}$$

$$\varepsilon' = \text{constant} \tag{3.2}$$

in which, ε' and ε'' are the real part and the imaginary part of the relative complex permittivity, respectively, σ (S/m) is the conductivity, ε (F/m) is the vacuum permittivity, ω (rad/s) is the angular frequency.

3.1 Existing models for dielectric spectroscopy measurement

Dielectric relaxation processes are usually analysed using relaxation functions. The basic function has been developed by Debye. The expression given by Debye for the frequency dependence of complex permittivity ε^* can be denoted as[123]

$$\varepsilon^*(\omega) = \varepsilon_\infty + \frac{\Delta\varepsilon}{1 + i\omega\tau_D} \tag{3.3}$$

where $\Delta\varepsilon = \varepsilon_S - \varepsilon_\infty$, $\varepsilon_S = \lim_{\omega\tau \to 1} \varepsilon'(\omega)$, $\varepsilon_\infty = \lim_{\omega\tau \to 1} \varepsilon'(\omega)$, and τ_D is a constant related to the frequency at which the dielectric loss reaches a peak value. However, only by assuming the object is composed by ideal, non-interacting dipoles can this equation be valid. Sometimes, the experiment data reveal a clear deviation from this equation, which is called non-Debye relaxation behaviour. Some researchers have proposed modified

expressions to explain this non- Debye dielectric behaviour, for instance, the Cole/Cole function, which leads to a symmetrical broadening for the relaxation function compared to Debye function. Cole/Davidson developed their function by describing an asymmetric broadening of the frequency dependent relaxation function. A more general model function was introduced by Havriliak and Negami, which is in fact a combination of the Cole/Cole and the Cole/Davidson function [124-126].

Over the past few decades, many researchers suggested the frequency- dependent dielectric response can be equalized with a combination of different resistors and capacitors, which is shown in Fig 3.1 [127-133]. This model consists of several different resistor- capacitor (RC) branches, a high frequency (50 Hz) capacitor and a DC resistor. Different RC branches stand for different polarization processes in the frequency range of the interested. The long term DC conductivity is considered as a DC resistance. The high frequency capacitor can be referred to the total polarization above 50 Hz. However, this equivalent circuit cannot reveal the motion of charge carriers. To reach a better understanding of the dielectric response in dielectric liquid, more research is required.

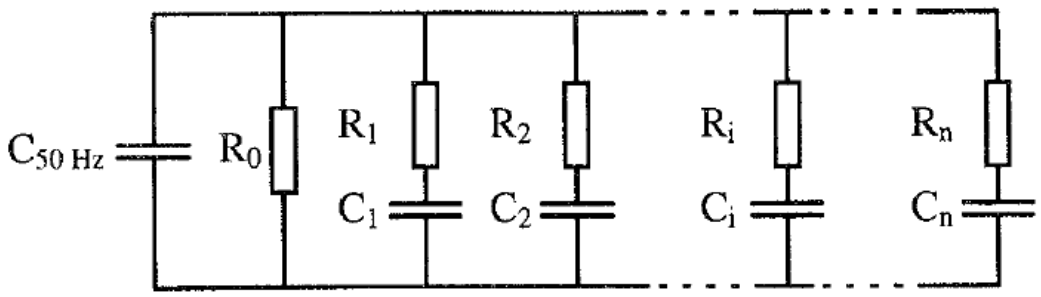

Fig. 3.1 Equivalent circuit for insulating liquid

Mobile charge carriers in insulating liquid can form charge layers at the electrodes when the frequency is low resulting in an increase of the real part of the complex permittivity. This effect is known as the space charge polarization or electrode polarization [121]. The dielectric response of the space charge polarization can be significant such that the contributions to the complex permittivity arising from electronic, atomic and dipole polarizations may be masked [121]. This space charge polarization has been studied both theoretically and experimentally by many researchers [113-115, 134-152]. Jaffe proposed a theoretical solution of the space charge polarization and his theory has been used to analyze the dielectric response of electrolytic solutions and dielectric

liquid [113-115]. Later, Macdonald presented more general expressions and his theory has been widely accepted and used to analyze the experimental result [134]. The previous polarization theories were developed based on linear approximations and they are only valid under a low electric field, thus, a computer-based method to calculate the effective complex permittivity of insulating media under high electric field has been provided by Stern and Weaver [135]. Sawada further developed the space charge polarization theory using computer based simulation and stated that the bound charge on the electrode should also be taken into consideration in analyzing the frequency response in liquids [141-145]. Coelho assumed that the mobile charges that move towards the electrode of opposite sign can accumulate in the vicinity of the electrode and finally result in a macro dipole finally [146]. Frood and Gallagher discovered that the experimental results are in fair agreement with Coelho's theory only when an additional contribution to the permittivity arising from DC conductivity has been taken into account [147]. Many researchers have reported that the dielectric loss induced from DC conductivity can be added to the total polarization to gain a better fit of the experimental results of the complex permittivity [148-152].

3.2 Experimental setting up

Figs 3.2-3.3 show the measuring equipment used in the experiment. Solartron 1296 dielectric interface and model 1260A impedance/gain- phase analyser has been used to perform the dielectric response test and transfer data to a computer through IEEE488 cable. The sample was heated up using a heating cylinder. A parallel electrode system was used in this frequency domain measurement. A PTFE ring was used as the spacer to create a gap between the two electrodes. Oil was always kept in the heating cylinder during the test to prevent exposure to the surrounding environment.

In our experiment, the thickness of the PTFE spacer is 0.5mm, the test temperatures are 25℃, 50℃, 75℃ and 90℃. The magnitude of the applied electric potential is 1V. When the temperature of the cylinder reaches the setting temperature, an extra half an hour is waited to achieve a steady temperature in the test cell.

The measured results do not change significantly after 3 hours of degassing. Thus, the oil should be vacuumed for at least three hours to remove dissolved air before the experiment. Also, the test cell should be thoroughly cleaned and dried according to the standard procedure from IEC 60247 Annex B [26].

Fig. 3.2 Solartron 1296 dielectric interface and model 1260A impedance / gain- phase analyzer

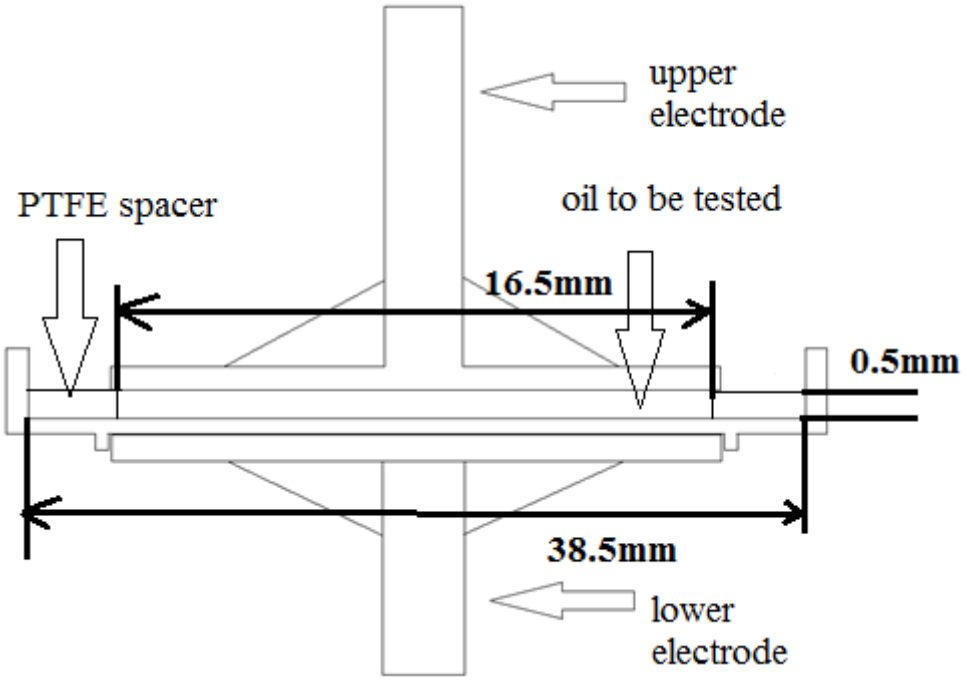

Fig. 3.3 Test cell

3.3 Experimental data and analysis

As seen from Figs 3.4-3.6, the real parts of the complex permittivity of Shell ZX-I oil and Hydro Quebec oil are quite similar, whilst that of Terna oil are much higher and increase faster when the frequency is below 1 Hz. The frequency response of all three kinds of mineral oil share the same pattern, the real part of complex permittivity of mineral oil is about 2.1-2.4 within a frequency range 100 Hz – 1 Hz and increases when the frequency is below 1Hz. The experimental data reveal that a longer aging period

results in a shift of the real part of the complex permittivity to the high frequency. When mineral oil is in service, the hydrocarbon molecule in the oil undergoes the thermal, electric and chemical stresses. Exact amount of charge carriers can be generated through the breakdown of the weak covalent bond and the oxidation of the hydrocarbon molecules [89-92]. Therefore, if there are more charge carriers participating in the electric conduction, the polarization due to space charge formation will be more significant. When the temperature goes higher, the dissociation rate increases and more charge carriers are created. Also, the viscosity of mineral oil decreases with the temperature leading to a high mobility of the charge carriers, therefore, the frequency response also seems to shift towards high frequency when the temperature rises. When the charge carriers drift to the interface of metal/oil and get blocked, these charge carriers will form a charge layer in the vicinity of the electrode. The measured capacitance will increase when more charge carriers move to the interface, therefore, the real part of the complex permittivity increase at low frequency range (0.01 Hz- 1 Hz).

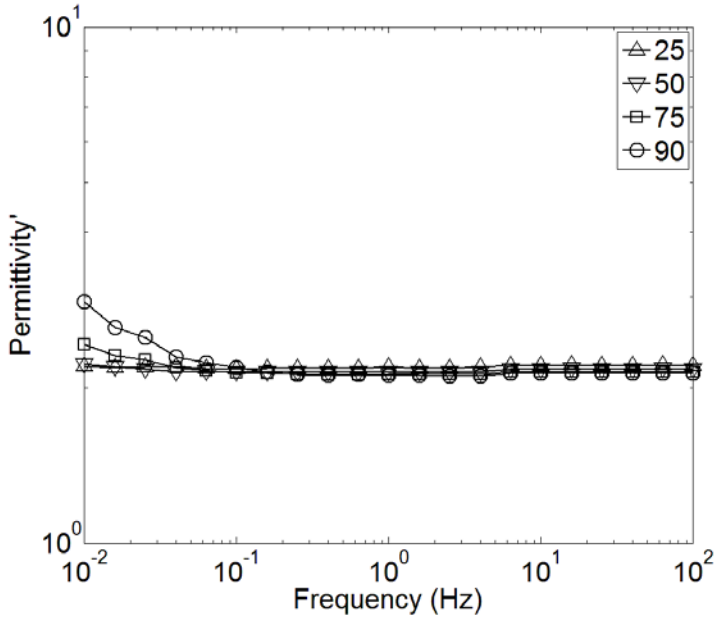

Fig. 3.4The real part of permittivity of fresh Shell ZX-I oil at different temperatures

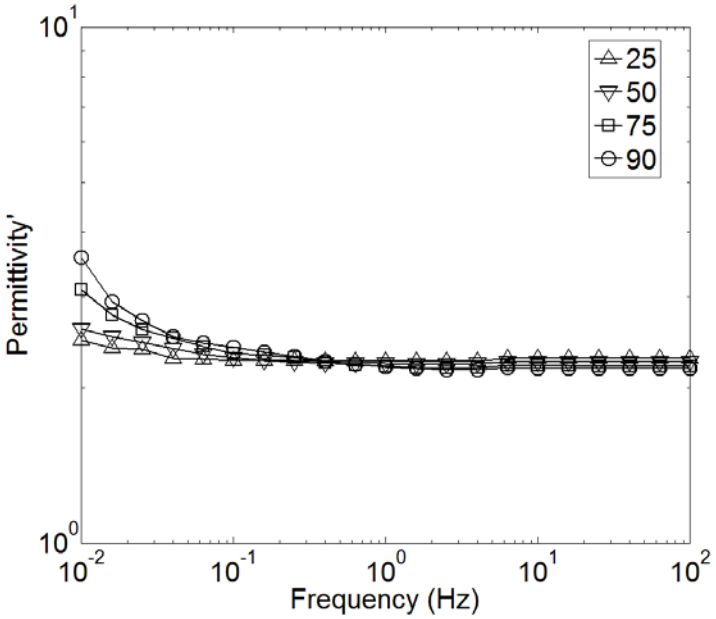

Fig. 3.5The real part of permittivity of Hydro Quebec oil at different temperatures

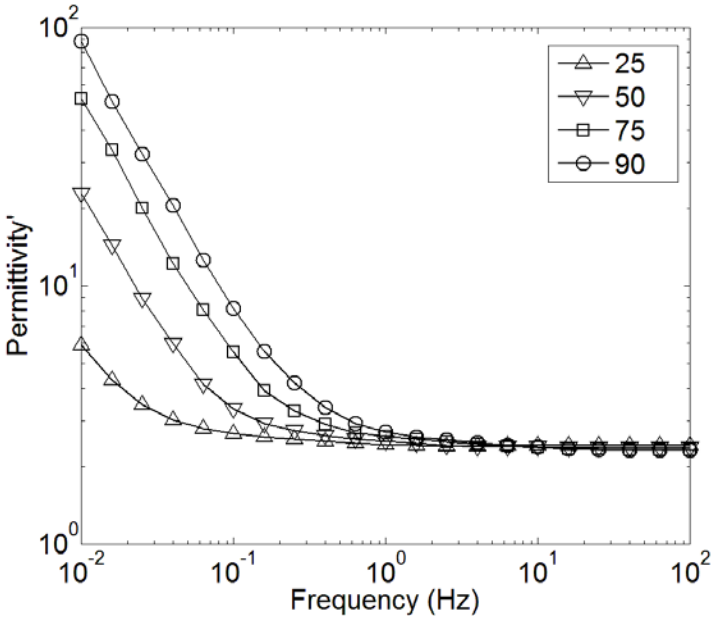

Fig. 3.6The real part of permittivity of Terna oil at different temperatures

As observed from Figs. 3.7-3.9, the imaginary parts of the complex permittivity of these mineral oils decrease with the frequency with a slope of approximately -1 in a log-log scale regardless of the conductivity. It indicates that the conductivity plays an important role in the frequency response of mineral oil in a range of 0.01Hz-100Hz and the mechanism that governs the electric conduction does not change much [152]. According to the experimental results under DC field shown in Chapter 2, Shell ZX-I oil has the lowest conductivity, Hydro Quebec oil has a medium conductivity and Terna oil

has the highest conductivity. The conductivity of mineral oil increases with aging due to the generation of the extra charge carriers from contamination or physical and chemical degradation in mineral oil [89-92]. As the conductivity of mineral oil increases with the temperature, the dielectric loss induced by the electric conduction also increases with the temperature. As pointed out by Sawada, within the frequency range studied here, the dielectric loss contributed by other polarizations, such as electronic polarization, atomic polarization and dipole polarizations, is negligible, the main dielectric loss is due to the electric conduction [140]. The imaginary part of the complex permittivity can be used to estimate the AC conductivity of mineral oil.

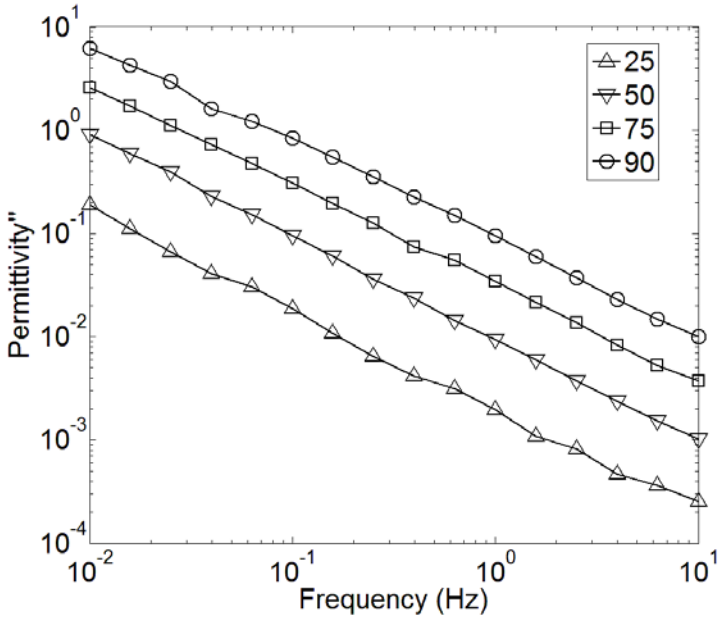

Fig. 3.7The imaginary part of permittivity of Shell ZX-I oil at different temperatures

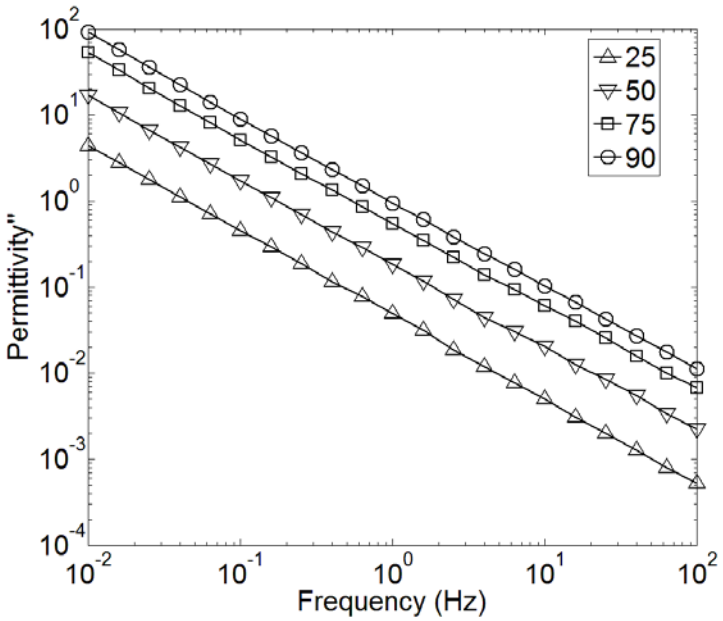

Fig. 3.8The imaginary part of permittivity of Hydro Quebec oil at different temperatures

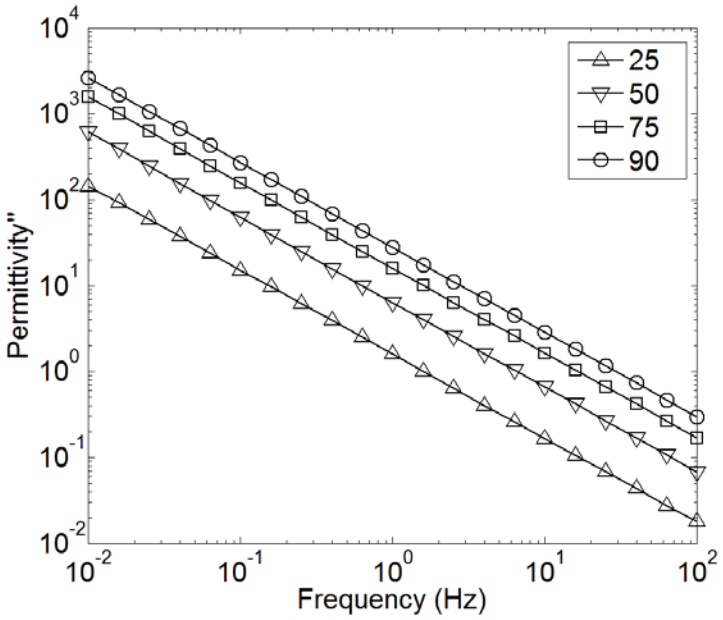

Fig. 3.9The imaginary part of permittivity of Terna oil at different temperatures

To sum up, there are several characteristics of frequency response that mineral oil share. First, the real part of permittivity does not change much at high frequency (1Hz-100Hz) and increases significantly when the frequency decreases further. Second, the imaginary part of complex permittivity will decrease with the frequency with a slope that is close to -1. Third, when the temperature increases, the frequency response of mineral oil will shift towards high frequency region.

The correlation between the conductivity and the temperature can be described using exponential equations. Here, the Arrhenius equation will be used to obtain the activation energy for these three kinds of mineral oil. This activation energy is the minimum energy that required for the separation of ions to overcome the potential barriers from the molecules. The obtained values are plotted in Arrhenius plot with natural logarithm of conductivity versus reciprocal of temperature as shown in Fig. 3.10. The slope of the fitted line can be related to the calculation of the activation energy. The activation energy for Shell ZX-I oil is 0.419eV, that for Hydro Quebec oil is 0.380 eV and for Terna oil is 0.359 eV. Therefore, the activation energy of the mineral oil decreases with its aging time and the energy needed for ionic dissociation is lower for aged mineral oil when compared with that for fresh oil.

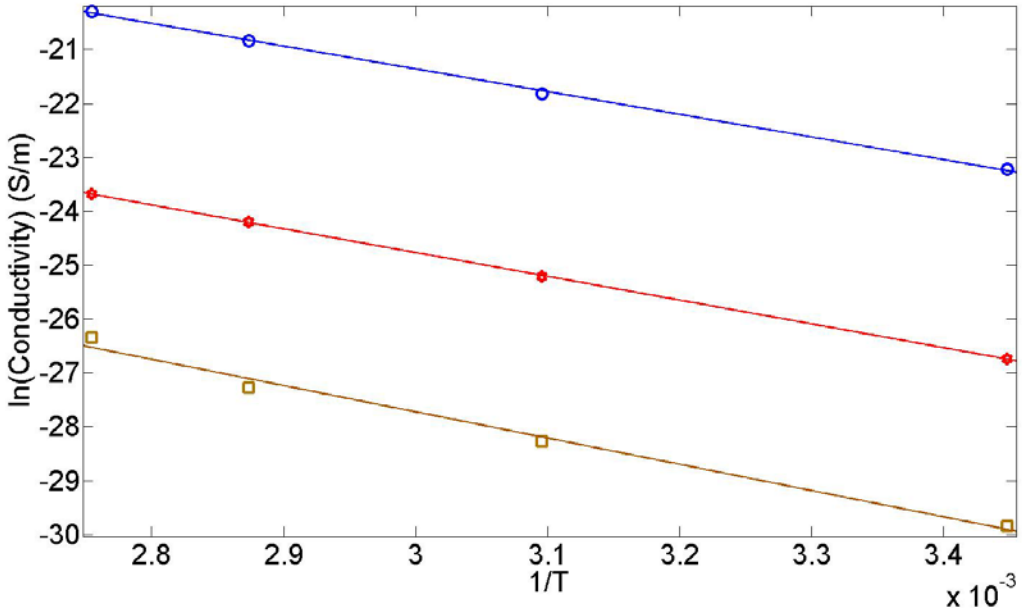

Fig. 3.10 Temperature dependence of AC conductivity of mineral oilsis fitted by Arrhenius equation.

3.4Correlation between AC and DC conductivity in mineral oil

The conductivities measured under DC or AC field are two important parameters to quantify the dielectric properties of insulating media. Here, the DC and AC conductivity of the mineral oil will be compared

In frequency- domain measurement, the ions in the oil, which are supposed to be the main charge carriers, move back and forth between the two electrodes. At high frequency,

most of these charge carriers do not have enough time to travel to the electrode and form a charge layer in the vicinity of the electrode. If the density of the ionic charge carriers does not change very much, the current induced by the motion of these charge carriers is proportional to the external voltage. When it comes to DC test that are carried out under a low electric field (10V/mm), most of the pre-existing charge carriers are unable to be extracted instantaneously when a voltage is applied across the oil. As electronic, atomic and dipole polarizations become fully polarized in less than several micro second and the current induced by those polarizations is hard to be observed by a pico-ammeter with a resolution of 0.5s. Therefore, the DC conductivity measured at the very beginning when a low voltage is applied is correlated to the initial charge density in the mineral oil and it should be similar to the AC conductivity obtained from the frequency- domain measurement. The calculated conductivity have been given in Table 3.1

Table 3.1 Comparison between conductivity measured from dielectric spectroscopy and initial DC conductivity (DC conductivity was measured under an electric field of 10 V/mm)

Conductivity (S/m)	Shell ZX-I	Hydro Quebec	Terna
30 °C AC	2.1e-13	4.6e-12	1.4e-10
30 °C DC	3.1e-13	7.6e-12	1.5e-10
90 °C AC	3.6e-12	5.1e-11	1.5e-9
90 °C DC	2.1e-12	4.2e-11	1.2e-9

As seen from Table 3.1, the conductivity measured through dielectric spectroscopy is close to the initial conductivity obtained from DC test under a field of (10 V/mm). Thus, our analysis of AC and DC conductivity is reasonable. The conductivity measured under the AC field is slightly lower than that measured under the DC field at 30 °C, whilst the conductivity measured under the DC field is slightly lower than that measured under the AC field at 90 °C. The frequency domain and time domain are performed under two different situations: the frequency domain measurement is carried out under atmospheric pressure, whilst the time domain measurement is performed under a pressure about 100 Pa. Several researchers have reported that the current decreases with the pressure[153-154]. Therefore, the current measured under the DC field might be lower than that measured under the AC field at 30 °C. However, as the oil sample is exposed to the atmosphere during dielectric spectroscopy measurement, gas and moisture can be adsorbed by the mineral oil and the conductivity of the oil increases. Consequently, the

conductivity measured under the DC field is slightly higher than that measured under the AC field at 90 °C.

Summary

Based on the experimental results, the characteristics of the frequency response of the mineral oil are similar. First, the real part of the complex permittivity doesn't change much at high frequency (1Hz-100Hz) and increases significantly when the frequency decreases further. Second, the imaginary part of complex permittivity will decrease with the frequency with a slope that is close to -1. Third, when the temperature increases, the frequency response of mineral oil will shift towards high frequency region. Also, the conductivity obtained by the dielectric spectroscopy measurement is similar to that measured by time-domain method under a low electric field. The imaginary part of the complex permittivity increases with aging, which means the aged oil has a high dielectric loss. When the oil is aged, more charge carriers will be generated due to chemical, electrical and thermal degradations. If more charge carriers can participate into the electric conduction, the space charge polarization can be more serious and the experimental results have revealed that the value of the real part of the complex permittivity increases with the aging period. However, the space charge effect in mineral oil has not been carefully studied and how to relate the results of the frequency domain measurement with the aging condition of the mineral oil is still not clear. In the following chapter, the space charge effect in mineral oil will be theoretically discussed.

Chapter 4 Injection Induced Polarization and Modified Space Charge Polarization Model

As discussed in previous chapter, the frequency responses of mineral oil share several common features. The real part of the complex permittivity remains constant when the frequency is above 1 Hz and starts to increase if the frequency becomes lower than 1 Hz, whilst the imaginary part decreases with frequency with a slope close to -1in a log-log scale. However, the curves of the imaginary part of the complex permittivity which is calculated by solving a Poisson- Nernst- Planck (PNP) model can unavoidably reach a peak value as the frequency decreases, which is against the experimental data. Therefore, there should be other charge transportation processes being involved. In this chapter, this new type of electric conduction is assumed to be the charge injection and these injected charge carriers are assumed to be charged in the region close to one electrode and discharged in the vicinity of the opposite electrode.

4.1General equations for PNP model

Dielectric spectroscopy measurement is a frequency-domain measurement and the field will change with the time. Thus, the inertia of the charge carriers can affect the instant speed when the force it is subjected to is not constant. In the following paragraphs, the field dependent velocity of a single charge carrier will be studied. Since the electric field changes with the time under AC field, it would be necessary to analyse the movement of charge carriers in an alternative field. The instant electric field can be written as:

$$E(t) = E_0 \sin(\omega t) \tag{4.1}$$

in which, $E(t)$ (V/m) is the electric field, E_0 is the magnitude of the electric field and ω (rad/s)is the angular frequency

Assuming there are only spherical charge carriers of mass m (kg) and diameter $2r_{ion}$ (m) in mineral oil and each of them has a charge q (C), the electrical force due to the electric field, $F(t)$ (N), can be denoted as

$$F(t) = qE(t) = qE_0 \sin(\omega t) \tag{4.2}$$

According to Stokes' law [121], the friction force, $F'(t)$ (N), caused by the viscosity can be described as

$$F'(t) = 6\pi\eta r_{ion} v \tag{4.3}$$

where η (mPa•s) is the viscosity, v (m/s) is the velocity of charge carrier. Combine these equations; a drift equation under AC field can be obtained as

$$F(t) - F'(t) = m\frac{dv}{dt} \tag{4.4}$$

With a boundary condition that $v = 0$ at $t = 0$, then the velocity with respect to time can be solved as

$$v(t) = \frac{k_1 k_2 \sin(\omega t)}{k_1^2 + \omega^2} - \frac{k_2 \omega \cos(\omega t)}{k_1^2 + \omega^2} + \frac{k_2 \omega}{k_1^2 + \omega^2} e^{-k_1 t} \tag{4.5}$$

with

$$\begin{cases} k_1 = 6\pi\eta r_{ion} / m \\ k_2 = E_0 q / m \end{cases} \tag{4.6}$$

In mineral oil, η has an order of 10mPa•s, the charge carrier has an ionic radius of 10^{-9}m, $E = 2\times10^3$ V/m, m has an order of 10^{-25} kg [31]. Thus, $k_1 \gg k_2$ and $k_1 \gg \omega$. When frequency is below 100Hz in mineral oil, Eq. (4.5) can be simplified as

$$v = \frac{E_0 q}{6\pi\eta r_{ion}} \sin(\omega t) \tag{4.7}$$

It means the velocity of charge carrier has a linear relationship with the electric field when the frequency is low. Thus, the relationship between velocity and mobility can be described as:

$$\vec{v} = \mu\vec{E} \tag{4.8}$$

in which $\vec{v}$ and $\vec{E}$ are both vectors.

Let us consider a parallel electrode system filled up with mineral oil. Assuming the charge carriers are distributed evenly between the two electrodes and there are two types of charge carriers that have the same properties except for their polarity are in the mineral oil, the density of positive charge carriers and negative charge carriers can be written as:

$$n_+ = n_- = n_0 = \sigma / q(\mu_+ + \mu_-) \tag{4.9}$$

where n_+ and n_- are density for positive charge carriers and negative charge carriers, σ is (S/m) is the conductivity of mineral oil, q (C) is the charge carried by a single charge

carrier and μ_+ ($m^2\ s^{-1}\ V^{-1}$) and μ_- ($m^2\ s^{-1}\ V^{-1}$) are the mobility for positive and negative charge carriers, respectively.

If the charge carriers are not evenly distributed between the two metal electrodes, the electric field is subject to the Poisson equation

$$\frac{\partial E(x,t)}{\partial x} = q[n_+(x,t) - n_-(x,t)] / \varepsilon_0 \varepsilon_r \tag{4.10}$$

where ε_0 (F/m) is the dielectric constant of vacuum and ε_r is the relative dielectric constant of the liquid. If the electric potential between the two electrodes is known as $V(t)$ (V) and the distance between the two electrodes is l (m), the electric field should obey the following equation

$$V(t) = \int_0^l E(x,t)dx \tag{4.11}$$

If assuming the charge carriers are dissociated from the ionic pairs, the relationship between the ionic pairs and the free charge carriers can be described as [31]

$$-\frac{dc}{dt} = \frac{dn_+}{dt} = \frac{dn_-}{dt} = K_d c - K_r n_+ n_- \tag{4.12}$$

where c is the concentration of ionic pairs, K_d (s^{-1}) is the dissociation rate and K_r (s^{-1}) is the recombination rate. Debye obtained the recombination constant by calculating the collision frequency as a result of Brownian motion and the Coulomb interaction with the rest charge [32]. The recombination rate can be denoted as

$$K_r = q\frac{\mu_+ + \mu_-}{\varepsilon}(1 - e^{-\frac{l_B}{l_i}})^{-1} \tag{4.13}$$

where l_i (m) is the distance between ions in an ionic pair and l_B (m) is the Bjerrum distance at which the Coulombian interaction electrostatic energy between two ions of opposite polarity equals to their thermal energies. For nonpolar liquid, such as mineral oil, Bjerrum distance is much higher than distance between the ions [33], and then this recombination rate becomes

$$K_r = q\frac{\mu_+ + \mu_-}{\varepsilon} \tag{4.14}$$

Since the mineral oil can be treated as weak electrolyte, therefore, the density of ionic pairs is much larger than the density of free charge carriers. Here, Eq. (4.12) can be rewritten as

$$-\frac{dc}{dt} = \frac{dn_+}{dt} = \frac{dn_-}{dt} \approx K_r n_0^2 - K_r n_+ n_- \tag{4.15}$$

When the flow of liquid can be ignored, the density of positive and negative charge carriers can be denoted as

$$\frac{dn_+(x,t)}{dt} = K_r n_0^2 - K_r n_+(x,t) n_-(x,t) + D_+ \frac{\partial^2 n_+(x,t)}{\partial x^2} - \mu_+ \frac{\partial [n_+(x,t) E(x,t)]}{\partial x} \tag{4.16a}$$

$$\frac{dn_-(x,t)}{dt} = K_r n_0^2 - K_r n_+(x,t) n_-(x,t) + D_- \frac{\partial^2 n_-(x,t)}{\partial x^2} + \mu_- \frac{\partial [n_-(x,t) E(x,t)]}{\partial x} \tag{4.16b}$$

where $D_\pm$ (m^2/s) is the diffusion coefficient. According to Einstein relation, the diffusion coefficient can be written as

$$D_\pm = D_0 = \frac{\mu kT}{q} \tag{4.17}$$

where, k is the Boltzmann constant, T (K) is the absolute temperature. If all the charge carriers can be blocked by the electrode, the boundary conditions can be described as

$$D_+ \frac{\partial n_+(x,t)}{\partial x} - \mu_+ n_+(x,t) E(x,t) \Big|_{x=0,l} = 0 \tag{4.18a}$$

$$D_- \frac{\partial n_-(x,t)}{\partial x} + \mu_- n_-(x,t) E(x,t) \Big|_{x=0,l} = 0 \tag{4.18b}$$

which means there is no current flow at the interface between electrode and mineral oil.

Because there is no charge exchange at the interface, the current flowing through the circuit can be calculated from the change of the induced charge at the electrode which is attracted by the space charge in the bulk. This induced charge, $Q(t)$ (C), can be denoted as

$$Q(t) = \frac{q}{l} \int_0^l x[n_+(x,t) - n_-(x,t)] dx \tag{4.19}$$

When there is no mobile charge carrier in mineral oil, the dielectric permittivity is contributed by electronic, atomic and dipole polarizations. As discussed in the previous chapter, the real part of the complex permittivity contributed by electronic, atomic and dipole polarizations can be approximated as a constant value and the dielectric loss caused by these polarizations is negligible within the frequency range studied here [141].

When the external electric potential applied upon the two electrodes is a simple sinusoidal voltage $V(t) = V_0 \sin(\omega t)$, the relative dielectric permittivity involving electrode polarization can be written as:

$$\begin{cases} \varepsilon''(\omega) = \dfrac{2I_{real}l}{\varepsilon_0 \omega V_0 S} \\ \varepsilon'(\omega) = \dfrac{2I_{imag}l}{\varepsilon_0 \omega V_0 S} + \varepsilon_\infty \end{cases} \tag{4.20}$$

with

$$\begin{cases} I_{real} = f\int_0^{1/f} \dfrac{dQ(t)}{dt} S\sin(\omega t)dt \\ I_{imag} = f\int_0^{1/f} \dfrac{dQ(t)}{dt} S\cos(\omega t)dt \end{cases} \tag{4.21}$$

where, f (Hz) is the frequency, S (m^2) is the surface area of the electrode, ω (rad/s) is the angular frequency. ε_∞ is the relative permittivity at high frequency. I_{real} (A) is the current that has the same phase with the electric potential and contributes to the imaginary part of the complex permittivity, while I_{imag} (A) is the current that leads the applied ac voltage by an angle of 90°and can affect the real part of the complex permittivity.

4.2 Calculation process of PNP model

To calculate the complex permittivity with Eqs. (4.20) and (4.21), the distribution function of positive and negative charge carriers needs to be obtained from Eqs. (4.9)-(4.19). It is difficult to find direct solution to these equations due to their non-linearity. Therefore, the computer based simulation proposed by Sawada is helpful to estimate the value of the density of the positive and negative charge carriers [141-145]. Here, the complex permittivity has been calculated in the same way as in his work by dividing the gap between the two parallel electrodes into *N* slabs equally, which is shown in Fig. 4.1. Let $n_{\pm}(i)$ be the average number of the positive and negative charge carriers in the *i*-th slab. The values of the electric field at the boundaries of each slab are denoted with $E(i)$. The current flux due to the drift and diffusion of the positive or negative charge carriers are denoted as $J_{\pm}(i)$ (A/m^2), respectively. Eq. (4.19) becomes

$$Q(t) = \frac{q}{l}\sum_{i=1}^{N}[i \times n_+(i) - i \times n_-(i)] \tag{4.22}$$

When $E(i) > 0$, the current flux can be given by

$$J_+(i) = q\mu_+ E(i) n_+(i) - qD_+\left[n_+(i+1) - n_+(i)\right]\frac{N}{l} \tag{4.23a}$$

$$J_{-}(i) = q\mu_{-}E(i)n_{-}(i+1) + qD_{-}\left[n_{-}(i+1) - n_{-}(i)\right]\frac{N}{l} \tag{4.23b}$$

Similarly, when $E(i) < 0$, the current flux can be given as

$$J_{+}(i) = q\mu_{+}E(i)n_{+}(i+1) - qD_{+}\left[n_{+}(i+1) - n_{+}(i)\right]\frac{N}{l} \tag{4.24a}$$

$$J_{-}(i) = q\mu_{-}E(i)n_{-}(i) + qD_{-}\left[n_{-}(i+1) - n_{-}(i)\right]\frac{N}{l} \tag{4.24b}$$

For a complete blocked electrode, the current flux at the two metal electrodes can be denoted as

$$J_{+}(0) = J_{+}(l) = J_{-}(0) = J_{-}(l) = 0 \tag{4.25}$$

In order to calculate the value for $n_{+}(x)$ and $n_{-}(x)$, the period T (s) will be separated with equal time intervals T / M. The changes of $n_{+}(x)$ and $n_{-}(x)$ can be expressed as

$$\Delta n_{+}(i) = \frac{NT}{qlM}\left[J_{+}(i-1) - J_{+}(i)\right] + K_r n_0^2 - K_r n_{+}(i)n_{-}(i) \tag{4.26a}$$

$$-\Delta n_{-}(i) = \frac{NT}{qlM}\left[J_{-}(i-1) - J_{-}(i)\right] - K_r n_0^2 + K_r n_{+}(i)n_{-}(i) \tag{4.26b}$$

With Poisson equation, the electric field can be calculated as

$$E(i) = E(i-1) + \frac{n_{+}(i) - n_{-}(i)}{\varepsilon_0 \varepsilon_r} \tag{4.27}$$

Eq. (4.27) can also be written in another form

$$E(i) = E(0) + \frac{1}{\varepsilon_0 \varepsilon_r}\sum_{a=1}^{i} n_{+}(a) - n_{-}(a) \tag{4.28}$$

Assuming the value of the average field in one slab is equal to the average value of the electric field at the boundary of this slab, the average field in the *i*-th slab can be denoted as

$$E_{avr}(i) = \frac{E(i) + E(i-1)}{2} \tag{4.29}$$

When Eq. (4.29) is substituted into Eq. (4.11),

$$\left(\frac{E(0) + E(N)}{2} + \sum_{a=1}^{N-1} E(a)\right) = \frac{N \times V(t)}{l} \tag{4.30}$$

If Eq. (4.28) is substituted into Eq. (4.30), $E(0)$ can be calculated as

$$E(0) = \frac{V(t)}{l} - \frac{1}{\varepsilon_0 \varepsilon_r}\sum_{a=1}^{N}\left[n_{+}(a) - n_{-}(a)\right] \times (N - a + 0.5) \tag{4.31}$$

Therefore, the electric field can be calculated using Eqs. (4.28) and (4.31). Repeated application of Eq. (4.22)-(4.31), the variation of the induced charge on the electrode with time can be specified.

With Eq. (4.20) and (4.21), the complex permittivity can be calculated.

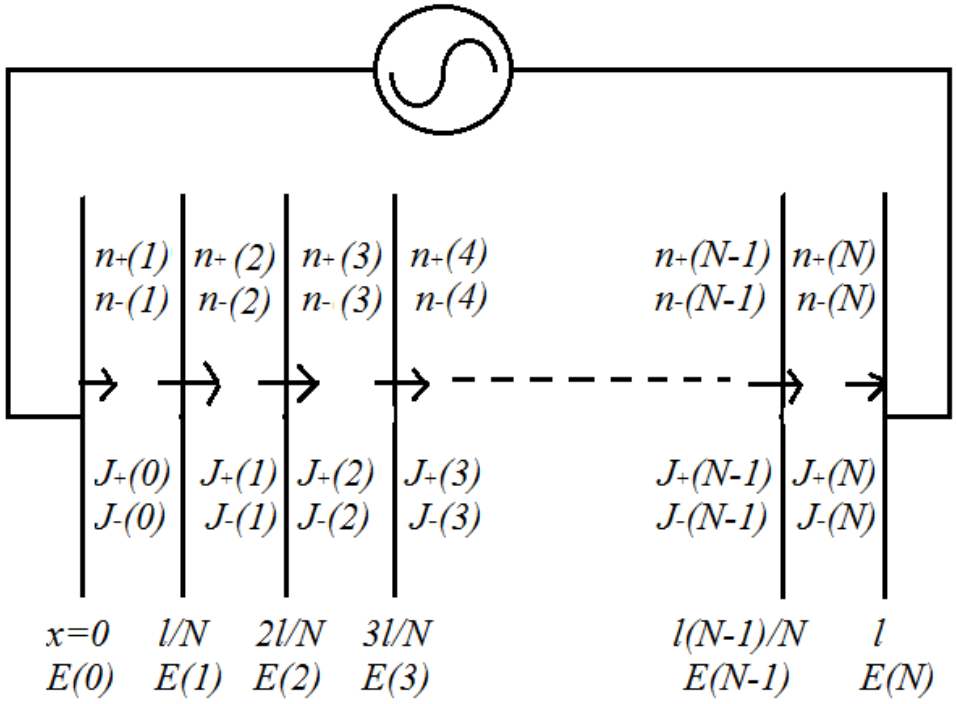

Fig. 4.1 Diagram showing the notation for the numerical calculation

As pointed out by Sawada, the necessary cycles needed to acquire the stationary values of the complex permittivity increases with the frequency [141-145]. Therefore, a wait cycle number *K*, introduced by Sawada, that depends on the frequency to obtain the stationary values is set in our simulation [141-145]. It is worth noting that the approximation involved in this chapter is valid only if the distance moved by a mobile charge in time Δt is sufficiently smaller than the slab width l / N. This implies

$$\Delta t << \frac{l^2}{\mu V_0 N} \quad . \tag{4.32}$$

The time interval and the number of slab should be set carefully so that Eq. (4.32) can be satisfied. The condition determined for the calculation in the steady state is summarized in Table 4.1.

The flow chart of the numerical calculation for obtaining the complex permittivity is shown in Fig. 4.2.

Table 4.1 Condition for the numerical calculation

Frequenc y (Hz)	Time coefficient *M*	Slab number *N*	Wait cycles *K*
100~1	10000	50	5
1~0.01	100000	50	3

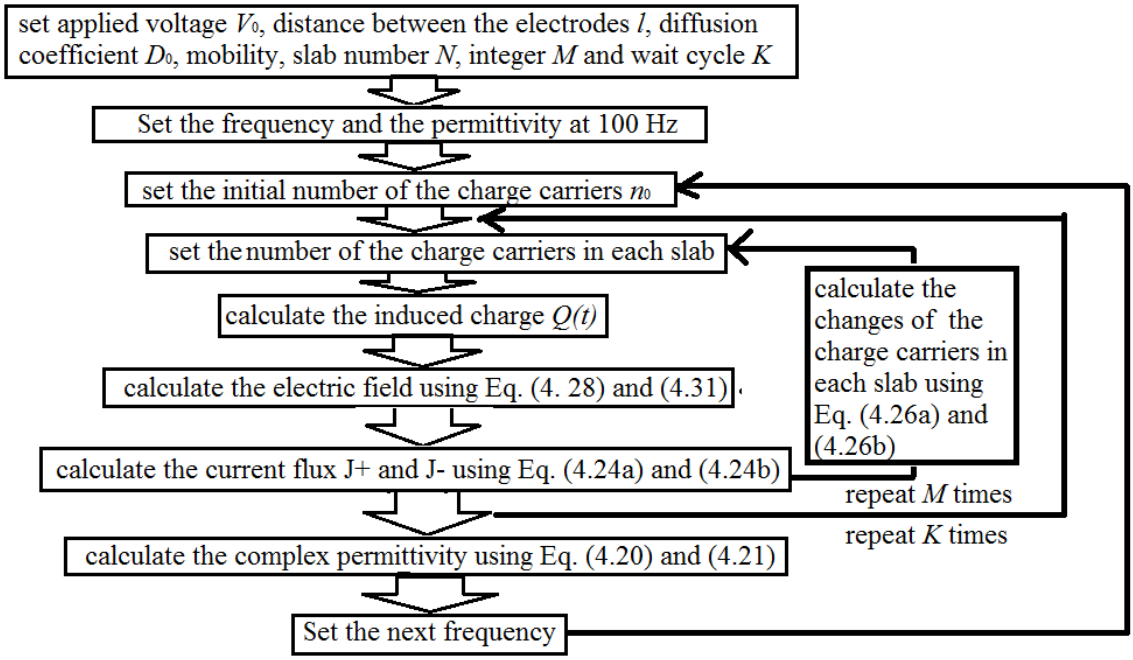

Fig. 4.2 Flow chart of numerical calculation for the calculation of the complex permittivity

4.3 Frequency response of mineral oil and simulation based on PNP model

The quantity of the induced charge on the electrodes is determined by the uneven distribution of the charge carriers between the two parallel electrodes. Sawada has already investigated various parameters that can influence the simulating result [141-145]. According to his study, the space charge polarization should be added to the frequency response in liquid sample. However, as observed from his simulation, this classic model can only fit the experimental result in certain frequency range (0.1Hz-10 kHz). Here, this classic model with two types of charge carriers that has the same properties but different polarity will be used to simulate the experimental results. Because the only difference

between positive and negative ions is their polarity, these two types of charge carriers into one kind of charge carriers will be categorized as one kind of charge carrier for simplicity in the following sections.

In this model, the distance between the two electrodes is 0.5mm. The total conductivity is calculated from the imaginary part of the complex permittivity using $\sigma = \omega\varepsilon_0\varepsilon''(\omega)$. The relative permittivity ε_s is taken directly from the real part of the complex permittivity at 100 Hz that was measured in the experiments. The mobility of these charge carriers is assumed to be proportional to the reciprocal of the viscosity of the mineral oil and the mobility of the charge carriers in the Terna oil is assumed to be $1\times10^{-9}\,m^2s^{-1}V^{-1}$, which is a typical value of ionic mobility in other reports[155-160]. However, this calculated mobility might not be in a good accordance with its real value. Thus, it would be necessary to investigate how mobility can affect the frequency response. The frequency dependent curves of the real part and imaginary part of complex permittivity under the same condition ($\sigma = 5.2\times10^{-11}\,S/m$, $\varepsilon_r = 2.18$, $E_0 = 2\times10^3\,V/m$ and $d = 5\times10^{-4}\,m$) but with different values of mobility, $10^{-6}m^2/V/s$, $10^{-7}m^2/V/s$, $10^{-8}m^2/V/s$, $10^{-10}m^2/V/s$ and $10^{-12}m^2/V/s$, are shown in Figs.4.3-4.4.

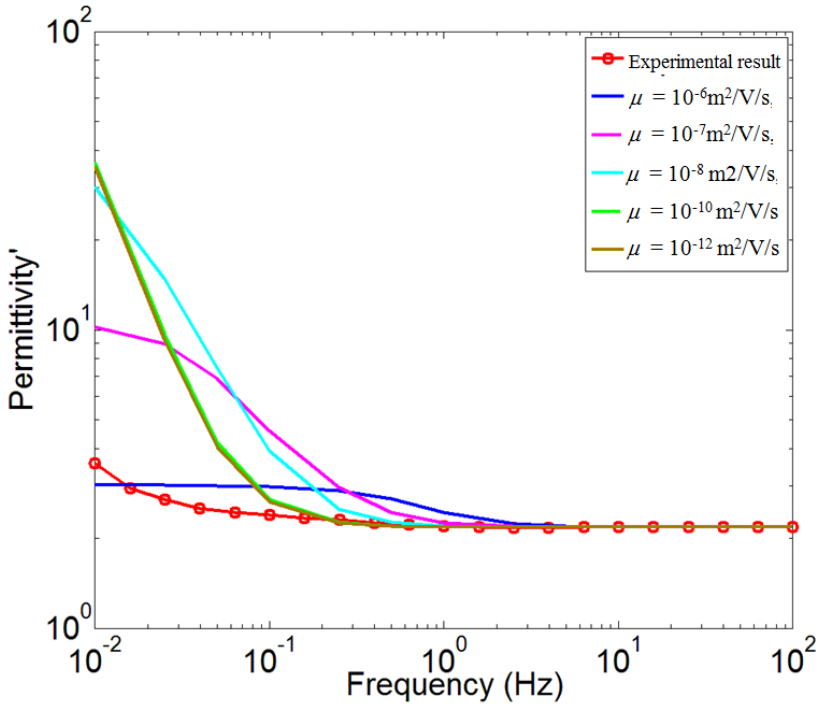

Fig. 4.3 The comparison between simulation result and experimental result of the real part of complex permittivity

In the analysis of the space charge polarization, the distortion of internal field and charge accumulation in the close region of the electrode are the essential factors. The power source in the measurement system supplies counter charges to the electrode and keeps the electric potential between two metal electrodes. The charge carriers in the bulk drift by the electric force and form charge layer in the vicinity of the electrode. The accumulation of charge carriers near the electrode can cause extra polarization, as well as dipole, atomic, or electronic polarization. As found in Fig. 4.3, when the mobility increases, the real part of the complex permittivity shifts towards the high frequency and the maximum value it can reach decreases. It seems if the mobility is lower than 10^{-12} $m^2\ s^{-1}\ V^{-1}$, the frequency response would not change notably. If the charge carriers have a high mobility, they can drift to the electrode in a short time. Thus, the space charge polarization can reach the quasi- equilibrium state earlier if the charge carriers have a higher mobility. However, the real part of complex permittivity change unnoticeably when the frequency is below 1Hz according to the experimental result. This indicates there might be other types of charge carriers in the mineral oil, such as electrons, holes or injected ions.

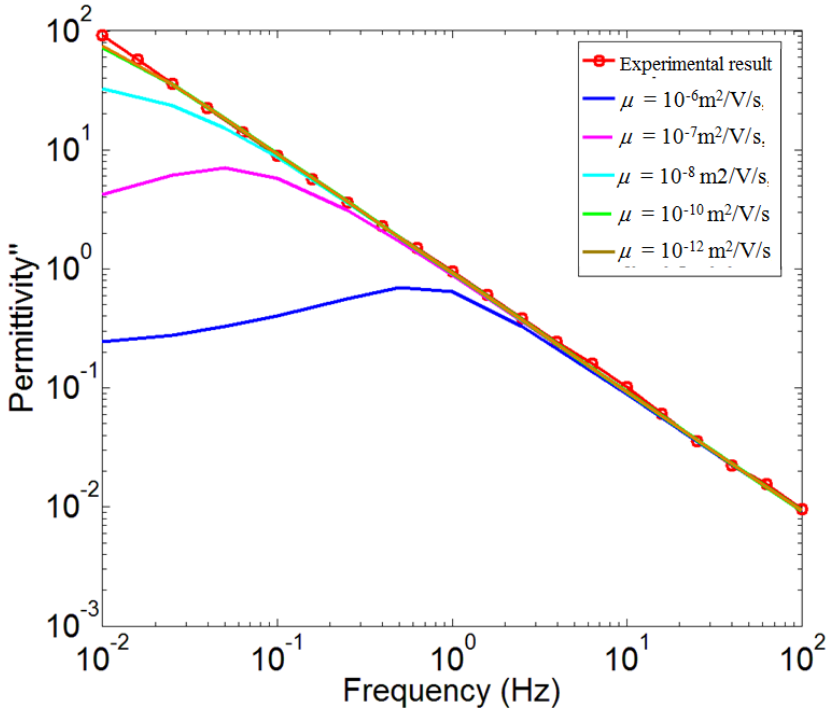

Fig. 4.4 The comparison between simulation result and experimental result of the imaginary part of complex permittivity

As seen from Fig. 4.3, the imaginary part of complex permittivity will reach a maximum peak and then start to decrease. The experimental data shows the imaginary

part always decreases with the frequency with a slope close to -1. A higher mobility can lead to a more serious deviation from the curve that is measured experimentally. The calculated imaginary part of the complex permittivity reaches a maximum value and then starts to decrease as the frequency goes low. When the full polarization has been attained, the dielectric loss can be simply considered as the energy consumed to push total charge carriers form one electrode to the other. Thus, if the charge carriers in the bulk have enough time to get into a region that is close to the electrode, the total energy consumed in every cycle becomes constant and the imaginary part of the complex permittivity will drop to a lower value as the frequency decreases further. In order to make a better fit of the imaginary part of the complex permittivity, a smaller mobility of charge carriers is required.

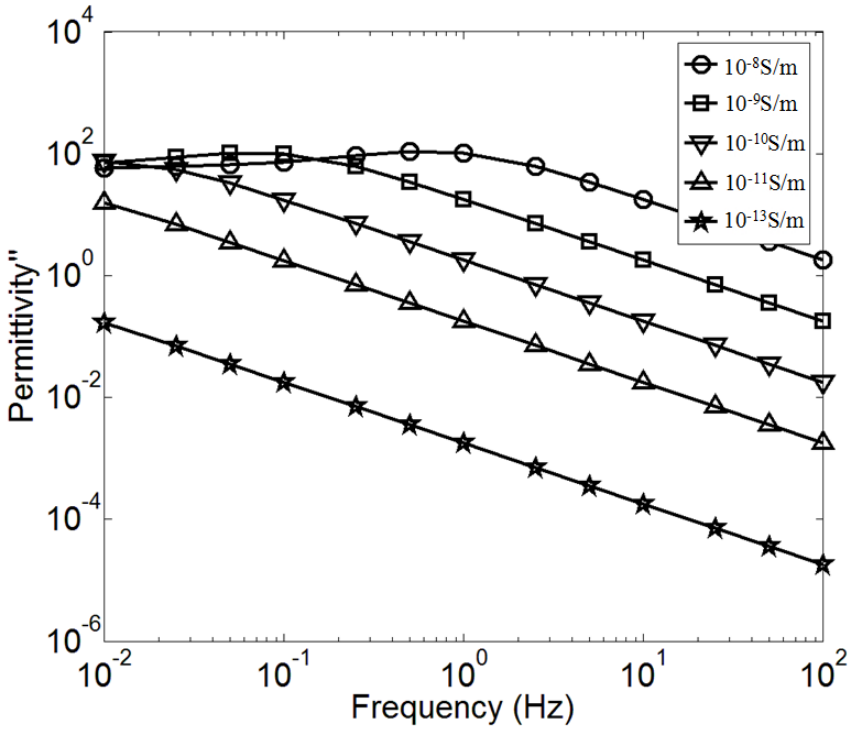

Fig. 4.5 The imaginary part of permittivity with different conductivity

As the two main factors that affect the simulation are the conductivity and mobility, it would also be necessary to understand the influence of the change of the conductivity to the complex permittivity. In our simulation, the mobility of charge carriers is kept constant (10^{-9} m^2 s^{-1} V^{-1}), whilst the total conductivities changes (10^{-8} S/m, 10^{-9} S/m, 10^{-10} S/m, 10^{-11} S/m and 10^{-13} S/m). The frequency responses with different conductivities have been simulated and the simulation results are shown in Figs. 4.5-4.6. As seen in Figs.

4.5 and 4.6, the decrease of the total conductivity can make the frequency response shifts towards the low frequency. The real part of permittivity increases as the frequency goes lower, and finally reaches a very high value at which the real part and does not show any notable change with further decrease of the frequency. When the oil conductivity is below 10^{-9} S/m, the imaginary part of the complex permittivity decreases with the frequency within a medium frequency range (1 Hz- 100 Hz) with a slope that is close to -1. The change of the conductivity only makes the frequency response shift towards high frequency, which is in a good accordance with Sawada's work [141]. As the frequency decreases, the imaginary part of the complex permittivity reaches a maximum value and reveals slightly change if the frequency decreases further. To sum up the change of the conductivity makes the frequency response shift towards high frequency.

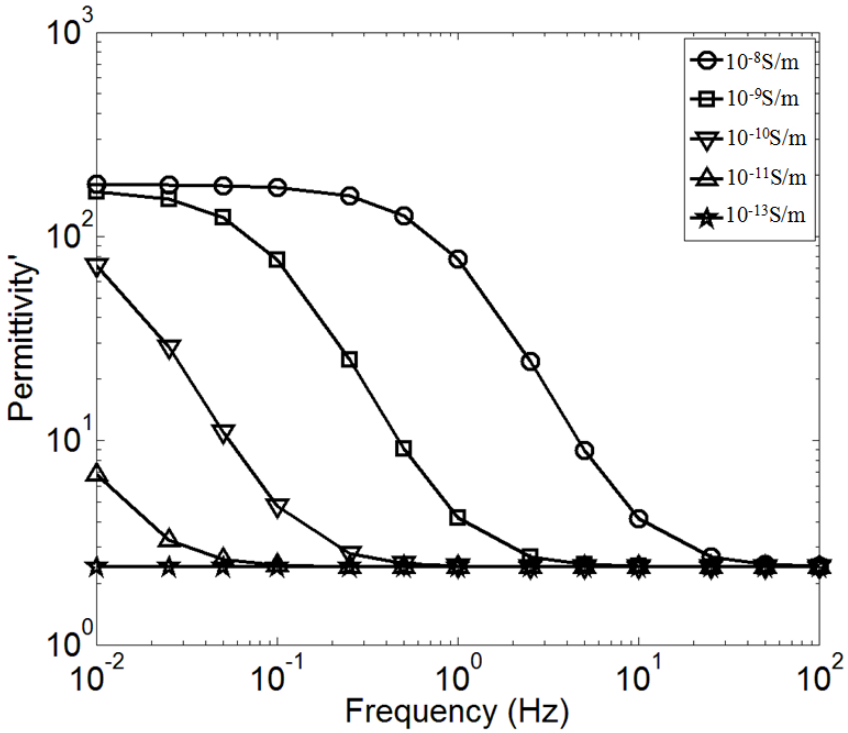

Fig. 4.6 The real part of permittivity with different conductivity

When the simulation result and the experimental result are compared, a dilemma can be found. It needs a higher mobility to have a good fit of the real part of complex permittivity, whilst a lower mobility is the requirement of a better fit of the imaginary part. It suggests that there is other electric conduction process being involved in mineral oil. Therefore, it would be impossible to simulate the dielectric spectroscopy result with the classic space charge polarization model, in other ways, the charge carriers that are created

in the bulk by dissociation is probably not the only cause of the electric conduction in mineral oil.

4.4 Theory of the injection induced polarization

In non-polar liquid, a two-step process can be used to explain the charge injection: A) charge carriers are generated at the metal/liquid interface; B) these newly created charge carriers are forced to drift into the bulk by the electric field. The extraction of these injected charge carriers is affected by the electric drift and the diffusion. Felici studied the injection in hydrocarbon liquid and obtained an analytical solution [37]

$$q_i = q_0 \times \exp(-\frac{e^2}{16\pi\varepsilon_0\varepsilon_r x_B kT}) / (2b \times K_1(2b)) \ , \tag{4.33}$$

with

$$b = \sqrt{(e^3 E / 16\pi\varepsilon_0\varepsilon_r k^2 T^2)} \ , \tag{4.34}$$

where, q_i (C/m^3) is the charge density that is considerably far away from the electrode, x_B (m) is the minimum approach of a charge carrier to the metal electrode, q_0 (C/m^3) is the charge density at x_B and K_1 is the modified Bessel function of the second kind. Here, the assumptions that there is only one kind of injected charge carriers and these injected charge carriers share the same polarity have been made for simplicity. Thus, the recombination of these injected charge carriers does not need to be considered. If the creation of the injected charge carriers in the vicinity of the electrode is much faster than the kinetics of the extraction, the field dependence of the injection current density can be denoted as [35-36]

$$j_i = q_i \mu_i E = q_i^0 \mu_i E / [2b \times K_1(2b)], \tag{4.35}$$

where q_i^0 (C/m^3) is a constant charge density that depends on the nature of liquid and electrode and μ_i is the mobility of these injected charge carriers. When the field is not very high, $2bK_1(2b) \approx 1$. At a low electric field of the order of 10^3 V/m, this injection process can be safely assumed to be autonomous [45-46].

If the diffusion effect, which will be discussed later, can be ignored, and the internal electric field can be approximated as a homogeneous field, the time dependent injection current density j_i *(t)* (A/m^2) in the vicinity of the electrode can be written as

$$j_i(t) = q_i^0 \mu_i E(t) / [2b \times K_1(2b)] \approx q_i^0 \mu_i E(t), \tag{4.36}$$

Thus, the injected current is proportional to the field at the interface of oil/metal electrode in this space charge polarization theory. A few words should be said on the interpretation of the charge injection theory in liquid. Eq. (4.35) has been verified in a large variety of organic solvents and salts up to a field of 20 kV/mm [31-46]. Castellanos pointed out that for a field lower than 4 kV/mm, the injection can be safely assumed to be proportional to the electric field [45-46]. However, Eq. (4.36) can be valid only under the condition that two assumptions have satisfied. First, the injection equation was derived for the case that where the electric field is not too intense, i.e. $\sqrt{e/16\pi\varepsilon_0\varepsilon_r E} >> x_B$. If $\sqrt{e/16\pi\varepsilon_0\varepsilon_r E} >> x_B$, the lower limit of the integration of the total current induced by the motion of the injected charge carriers in the bulk can be approximated as $x = 0$ instead of $x = x_B$ and the solution can be simplified. According to Alj, $x_B \approx 0.3$ nm [35].Thus, $\sqrt{e/16\pi\varepsilon_0\varepsilon_r E} >> x_B$ when a field of 2×10^3 V/m is applied. Second, the distortion of the internal field distribution is negligible and the electric field can be approximated by a homogeneous field [37]. This assumption will be verified later. Besides, if the measurement is carried out under high electric field, more charge carriers will be created and the field distortion can be serious. Therefore, these assumptions are no longer valid under a high electric field. This model can only be used to explain the frequency response of mineral oil under a low electric field.

Since the average injection current is contributed by the motion of all the injected charge carriers, the total injection current density $J_i(t)$ can be described as

$$J_i(t) = \frac{1}{l}\int_0^l j_i(x,t)dt = \mu_i E(t)\rho(t)/l \quad , \tag{4.37}$$

where, $\rho(t)$ (C) is the total amount of the injected charge and l (m) is the distance between two electrodes. There are two different cases for the injection induced polarization. First, the frequency is so high that the charge carriers injected from one electrode are unable to reach to the opposite electrode in a cycle. Second, these injected charge carriers can get to the opposite electrode in a cycle.

Firstly, the polarization due to the motion of these injected charge carriers under the situation that the charge carriers cannot reach the opposite electrodes in a field cycle will be discussed. If the charge carriers can be immediately neutralized once they arrive at the oil/metal interface, the total injected charge can be written as

$$\rho_1(t_0) = \int_0^{t_0} j_i(t)dt = \int_0^{t_0} q_i^0 \mu_i E(t)dt \,. \tag{4.38}$$

When the external voltage applied to the electrodes is $V(t) = V_0 \sin(\omega t)$, Eq. (4.38) becomes

$$\rho_1(t_0) = \int_0^{t_0} q_i^0 \mu_i (V_0 / l) \sin(\omega t)dt = \frac{q_i^0 \mu_i V_0}{\omega l}\left[1 - \cos(\omega t_0)\right]. \tag{4.39}$$

On considering the fact that the injection can take place at both two electrodes, the injection current contributed from the injection at the opposite electrode can be expressed as

$$\rho_{oppo}(t_0) = \frac{q_i^0 \mu_i V_0}{\omega l}\left[1 + \cos(\omega t_0)\right], \tag{4.40}$$

in which, $\rho_{oppo}(t_0)$ (C) is the total charge that injected from the opposite electrode. Therefore, the total charge $\rho_{tot}(t_0)$ (C) injected from both electrodes should be

$$\rho_{tot}(t_0) = \left[\rho_1(t_0) + \rho_{oppo}(t_0)\right] = \frac{2q_i^0 \mu_i V_0}{\omega l}, \tag{4.41}$$

which means, ρ_{tot} is only depends on the frequency. Thus, the total injection current density from both two electrodes is

$$J_i(t) = \mu_i V(t) \rho_{tot}(t) / l^2 = \frac{2q_i^0 \mu_i^2 V_0^2}{\omega l^3}[\sin(\omega t)] \,. \tag{4.42}$$

After substituting Eq. (4.42) into Eq. (4.21), the average current can be denoted as

$$\begin{cases} \Delta I_{real} = \dfrac{1}{T}\displaystyle\int_0^T \frac{2q_i^0 \mu_i^2 V_0^2}{\omega l^3}[\sin^2(\omega t)]Sdt = \frac{q_i^0 \mu_i^2 V_0^2 S}{\omega l^3} \\ \Delta I_{imag} = \dfrac{1}{T}\displaystyle\int_0^T \frac{2q_i^0 \mu_i^2 V_0^2}{\omega l^3}\sin(\omega t)\cos(\omega t)Sdt = 0 \end{cases} . \tag{4.43}$$

By substituting Eq. (4.43) into Eq. (4.20), the polarization caused by the injection can be denoted as

$$\begin{cases} \Delta\varepsilon'' = \dfrac{2\Delta I_{real}}{\varepsilon_0 \omega E_0 S} = \dfrac{2q_i^0 \mu_i^2 V_0}{\varepsilon_0 \omega^2 l^2} \\ \Delta\varepsilon' = 0 \end{cases} , \tag{4.44}$$

in which, ΔI_{real} and ΔI_{imag} are the integration of the total current that is only contributed by the injection current, whilst $\Delta\varepsilon''$ and $\Delta\varepsilon'$ are the changes of the complex permittivity in imaginary part and real part, respectively. As shown in this theory, if the injected

charge carriers have a low mobility, their motion can contribute to the imaginary part of the complex permittivity and the theoretical frequency dependence of the imaginary part of the complex permittivity is proportional to $1/\omega^2$, whilst the results obtained experimentally that are given in Chapter 3 is proportional to $1/\omega$. Thus, these injected charge carriers might move much faster than normal ions and they might be electrons or holes.

If $\mu_i > \omega l^2 / 2V_0$, the injected charge carriers have enough time to reach the opposite electrode. Here, the assumptions that the injected charge carriers can be neutralized immediately when they can get close enough to the electrode and the internal field can be treated constant are kept. A sinusoidal field with magnitude V_0 and period T is shown in Fig. 4.7. If the injection at one electrode starts at $t = 0$, for the other electrode the charge injection begins at $t = T / 2$. In the following sections, the electrode at which the injection takes place at $t = 0$will be referred as the first electrode and the other electrode will be referred as the second electrode for simplicity.

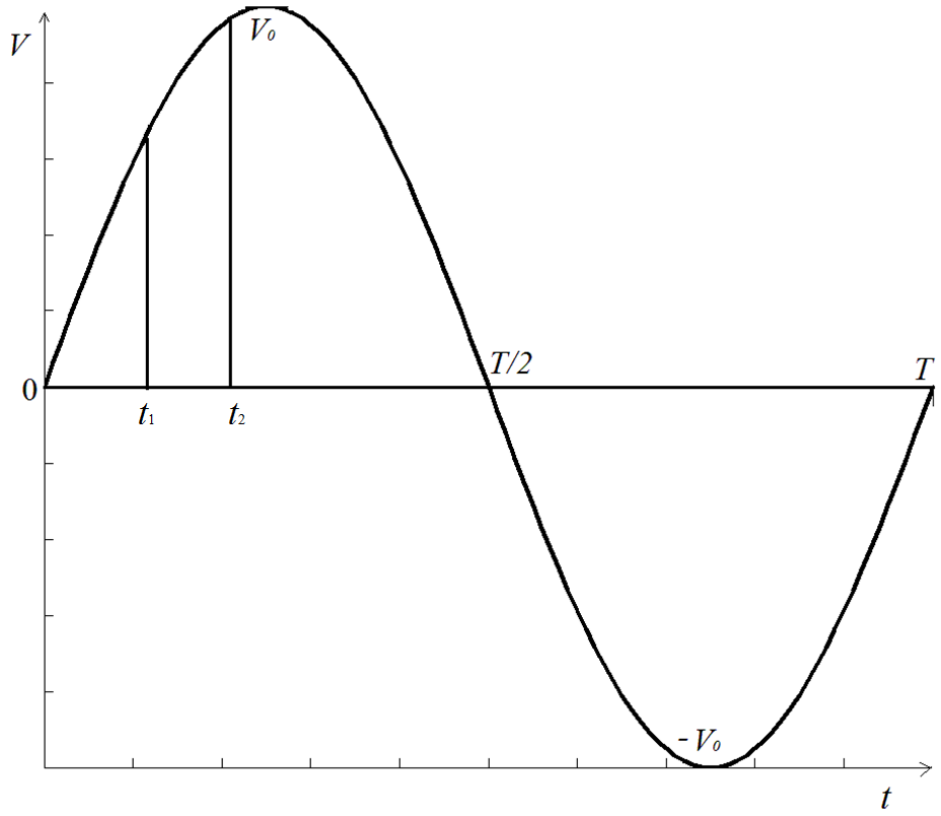

Fig. 4.7 A sinusoidal electric field with magnitude E_0 and period T

For the first electrode, the current density due to the newly generated charge carriers in the vicinity of this electrode can be denoted as

$$\begin{cases} j_i = q_i^0 \mu_i (V_0 / l)\sin(\omega t) & (0 < t < T/2) \\ j_i = 0 & (T/2 < t < T) \end{cases} . \quad (4.45)$$

If the charge carriers injected from the first electrode at t_1 can just reach the second electrode at t_2, the total charge injected from t_1 to t_2 from the first electrode can be written as

$$\rho_1(t2) = \int_{t_1}^{t_2} j_i(t)dt = q_i^0 \int_{t_1}^{t_2} \mu_i (V_0 / l)\sin(\omega t)dt . \quad (4.46)$$

The distance between the two electrodes, *l*, also satisfies

$$l = \int_{t1}^{t2} \mu_i (V_0 / l)\sin(\omega t)dt . \quad (4.47)$$

If Eqs. (4.46) and (4.47) are combined, Eq. (4.46) can be re-written as

$$\rho_1(t2) = q_i^0 l . \quad (4.48)$$

At the very beginning, the injected charge carriers do not have enough time to get close to the second electrode and the minimum time required for the charge carriers injected at $t = 0$ can reach the second electrode is $t_{\min} = \arccos(1 - \omega l^2 / \mu V_0)$.

Thus, the total charge injected from the first electrode at the beginning of a cycle is

$$\begin{aligned} \rho_1(t_0) &= \int_0^{t_0} q_i^0 \mu_i (V_0 / l)\sin(\omega t)dt \\ &= \frac{q_i^0 \mu_i V_0}{\omega l}(1 - \cos(\omega t_0)) \qquad (0 < t_0 < t_{\min}) \end{aligned} . \quad (4.49)$$

When $T/2 > t > t_{\min}$, the charge carriers injected from the first electrode are able to get close to the second electrode and the total charge injected from the first electrode and the amount of this injected charge can be calculated with Eq. (4.48)

$$\rho_1(t) = q_i^0 l \qquad (T/2 > t > t_{\min}) . \quad (4.50)$$

As the electric field reverses at $t = T / 2$, the total injected charge from the first electrode can be simply obtained as $\rho_1(T/2) = q_i^0 l$. After the field reversal, the injected charge carriers will start to be neutralized at the electrode from which they are injected. Therefore, the total amount of charge after the field reversal can be written as

$$\begin{aligned} \rho_1(t) &= q_i^0 l + \int_{T/2}^{T/2+t_{\min}} q_i^0 \mu_i (V(t) / l)dt \\ &= q_i^0 l - \frac{q_i^0 \mu_i V_0}{\omega l}(1 + \cos(\omega t)) \quad (T/2 < t < T/2 + t_{\min}) \end{aligned} . \quad (4.51)$$

Once all these charge carriers have been extracted, the current contributed by the motion of these injected charge carriers will be zero.

To sum up, the total charge due to the injection from the first electrode can be expressed as

$$\begin{cases} \rho_1(t) = \dfrac{q_i^0 \mu_i V_0}{\omega l}(1-\cos(\omega t_0)) & (0 < t < t_{\min}) \\ \quad = q_i^0 l & (t_{\min} < t < T/2) \\ \quad = q_i^0 l - \dfrac{q_i^0 \mu_i V_0}{\omega l}(1+\cos(\omega t_0)) & (T/2 < t < T/2 + t_{\min}) \\ \quad = 0 & (T/2 + t_{\min} < t < T) \end{cases}. \tag{4.52}$$

A similar analysis can be done on the injection from the second electrode, the total charge injected from the second electrode can be denoted as

$$\begin{cases} \rho_{oppo}(t) = q_i^0 l - \dfrac{q_i^0 \mu V_0}{\omega l}(1-\cos(\omega t_0)) & (0 < t < t_{\min}) \\ \quad = 0 & (t_{\min} < t < T/2) \\ \quad = \dfrac{q_i^0 \mu V_0}{\omega l}(1+\cos(\omega t_0)) & (T/2 < t < T/2 + t_{\min}) \\ \quad = q_i^0 l & (T/2 + t_{\min} < t < T) \end{cases}. \tag{4.53}$$

Therefore, in a full circle, it is easy to obtain

$$\rho_{tot}(t) = \rho_1(t) + \rho_{oppo}(t) = q_i^0 l\,. \tag{4.54}$$

Thus, the total injected charge is always constant in the bulk in a full cycle, and it does not depend on the frequency any longer.

The total current from injection is

$$J_i(t) = \mu_i V(t) \rho_{tot}(t)/l^2 = q_i^0 \mu_i (V_0/l)\sin(\omega t)\,. \tag{4.55}$$

By substituting Eq. (4.55) into Eq. (4.21),the complex permittivity contributed by the motion of these injected charge carriers can be denoted as

$$\begin{cases} \Delta\varepsilon'' = \dfrac{q_i^0 \mu_i}{\omega \varepsilon_0}\,. \\ \Delta\varepsilon' = 0 \end{cases} \tag{4.56}$$

If Eqs. (4.44) and (4.56) are put together, the polarization caused by the injection can be expressed as

$$\begin{cases} \Delta\varepsilon' = 0 \\ \Delta\varepsilon'' = \dfrac{q_i^0 \mu_i}{\omega\varepsilon_0} \times \dfrac{2\mu_i V_0}{\omega l^2} & (2\mu_i V_0 / \omega l^2 < 1) \\ \Delta\varepsilon'' = \dfrac{q_i^0 \mu_i}{\omega\varepsilon_0} & (2\mu_i V_0 / \omega l^2 > 1) \end{cases} . \tag{4.57}$$

By substituting Eq. (4.57) to Eq. (4.20), the relative dielectric permittivity with the polarization from the injection being involved can be written as:

$$\begin{cases} \varepsilon'(\omega) = \dfrac{2I_{imag} l}{\varepsilon_0 \omega V_0 S} + \varepsilon_s \\ \varepsilon''(\omega) = \dfrac{2I_{real} l}{\varepsilon_0 \omega V_0 S} + \dfrac{q_i^0 \mu_i}{\omega\varepsilon_0} \times \dfrac{2\mu_i V_0}{\omega l^2} & (2\mu_i V_0 / \omega l^2 < 1) \\ \varepsilon''(\omega) = \dfrac{2I_{real} l}{\varepsilon_0 \omega V_0 S} + \dfrac{q_i^0 \mu_i}{\omega\varepsilon_0} & (2\mu_i V_0 / \omega l^2 > 1) \end{cases} , \tag{4.58}$$

with

$$\begin{cases} I_{real} = f \int_0^{1/f} \dfrac{dQ(t)}{dt} S \sin(\omega t) dt \\ I_{imag} = f \int_0^{1/f} \dfrac{dQ(t)}{dt} S \cos(\omega t) dt \end{cases} . \tag{4.59}$$

In our simulation, the assumption that there are two kinds of charge carriers in our charge transportation model has been made: the first kind is dissociated from the ionic pairs and can be fully blocked by the metal electrode, which is referred as the dissociated charge carriers later; the second kind can be charged from one electrode and discharged at the opposite electrode, which is referred as the injected charge carriers, respectively. It is necessary to define a parameter, α, the ratio of the conductivity that is contributed from the injection over the total conductivity. This ratio is defined as

$$\alpha = \sigma_i / \sigma , \tag{4.60}$$

where, σ_i is the conductivity contributed by the motion of the injected charge carriers. With this definition, Eq. (4.9) can be modified as

$$n_+ = n_- = n_0 = (1-\alpha)\sigma / q(\mu_+ + \mu_-) . \tag{4.61}$$

As seen from the experiment, the imaginary part of the complex permittivity $\varepsilon''(\omega)$ decreases with the frequency in a slope of approximately -1 in a log-log scale, which means $\varepsilon''(\omega)$ is proportional to the angular frequency $1/\omega$. In our previous discussion, if the injected charge carriers are not fast enough to reach the opposite electrode in a cycle,

$\varepsilon''(\omega)$ will be proportional to $1/\omega^2$. If the mobility of the injected charge carriers can travel to the opposite electrode in a cycle at 100Hz, $\varepsilon''(\omega)$ is always proportional to $1/\omega$ with the frequency range studied in this chapter, which is coherent with the experimental result. Thus, a conclusion that the injected charge carriers should have a high mobility so that they can reach the opposite electrode in a cycle can be made. The minimum mobility $\mu_{\min}$ ($m^2\ s^{-1}\ V^{-1}$) required to ensure the charge carriers can get to the opposite electrode can be calculated as

$$\mu_{\min} = \frac{\omega l}{2E} = \frac{100 \times 2 \times \pi \times 5 \times 10^{-4}}{4 \times 10^3} \approx 7.9 \times 10^{-5} (\mathrm{m^2/s/V}) \cdot \tag{4.62}$$

If $\mu_i > \mu_{\min}$, Eq. (4.58) can be simplified as

$$\begin{cases} \varepsilon'(\omega) = \dfrac{2I_{imag} l}{\varepsilon_0 \omega V_0 S} + \varepsilon_s \\ \varepsilon''(\omega) = \dfrac{2I_{real} l}{\varepsilon_0 \omega V_0 S} + \dfrac{q_i^0 \mu_i}{\omega \varepsilon_0} \end{cases} . \tag{4.63}$$

Also, the following expression can be obtained by using Eq. (4.58) and (4.5)

$$\mu_i q_i^0 = \sigma_i . \tag{4.64}$$

As seen from Eq. (4.62), the mobility of these injected charge carriers is much higher than normal ions. Due to its high mobility, the density of these injected charge carriers is low. Frood claimed that there might be small quantity of electrons participating the electric conduction in dielectric liquid [147]. Although Felici's injection theory is developed based on the movement of ionic charge carriers, this high mobility charge carriers injection process can still be explained by his theory. As the density of these injected charge carriers is low, the field distribution may not be significantly affected by the unevenly distribution of these injected charge carriers. On considering the electric field is not intense in this case, Eq. (4.36) is still valid. According to Felici's theory [37], these high mobility injected charge carriers are created at the interface of metal electrode and oil, and then, they will be extracted by electric field and drift into the bulk. However, the existence and the physical meaning of these high mobility charge carriers is not clear, and more research is needed.

However, the computer based simulation discussed above might be time consuming and difficult to be used in daily test. Here, an analytical approach based on Coelho's space charge polarization model will be given.

Firstly, a brief introduction about Coelho's space charge polarization theory will be introduced. In his theory, he assumed that there were parallel plate electrodes contain both positive and negative mobile charge carriers and the diffusion coefficient, the mobility, the density and the charge carried by single charge carrier of positive charge carriers were equal to those of negative charge carriers. In the absence of external voltage, these charge carriers are distributed evenly between electrodes. When a field is applied, these charge carriers are drifting towards the electrodes. These charge carriers can be blocked by the electrode and form charge layers. In his original theory, the distance between the electrodes is 2*d* (m). Please note, this setting has been kept only for simplicity and $l = 2d$.

If $n_+(x,t)$ and $n_-(x,t)$ are the density of positive and negative charge carriers at *x* (m) at time *t* (s) and the charge carried by single charge carrier is *q* (C), the net charge density can be denoted as:

$$\rho(x,t) = q\left[n_+(x,t) - n_-(x,t)\right]. \tag{4.65}$$

When a field is applied, those charge carriers experience the influences from both electric field and thermal diffusion. The current density is given by:

$$j(x,t) = j_+(x,t) - j_-(x,t) \tag{4.66}$$

with

$$j_+(x,t) = qn_+(x,t)\mu_+E(x,t) - D_+q\frac{\partial n_+(x,t)}{\partial t}, \tag{4.67a}$$

$$j_-(x,t) = -qn_-(x,t)\mu_-E(x,t) - D_-q\frac{\partial n_-(x,t)}{\partial t}\ , \tag{4.67b}$$

where, $\mu_\pm$ ($m^2\ s^{-1}\ V^{-1}$) and $D_\pm$ (m^2/s) are the mobility and diffusion coefficients of these two species, respectively. After using Einstein's relationship, the diffusion coefficient can be described as

$$D_\pm = \frac{\mu_\pm kT}{q} \tag{4.68}$$

where, *k* is the Boltzmann's constant, *T* (K)is the absolute temperature.

The equations of charge conservation are given by

$$q\frac{\partial n_\pm(x,t)}{\partial t} + \frac{\partial j_\pm(x,t)}{\partial x} = 0. \tag{4.69}$$

Noting that the electric field must be subject to the Poisson equation

$$\frac{\partial E(x,t)}{\partial x} = q[n_+(x,t) - n_-(x,t)] / \varepsilon_0 \varepsilon_r \ , \tag{4.70}$$

where, ε_0 (F/m) is the dielectric constant of vacuum and ε_r is the relative dielectric constant of the liquid.

If $n_+(x,t)$ and $n_-(x,t)$ do not differ much from their equilibrium values, they can be linearized as

$$n_+(x,t) = n_0 + a(x,t) , \tag{4.71a}$$

$$n_-(x,t) = n_0 + b(x,t) , \tag{4.71b}$$

where, n_0 is the equilibrium value of the density of positive or negative charge carriers and $a(x,t)$ and $b(x,t)$ are much smaller compared to n_0. Here, Coelho assumed that only one type of charge carriers is mobile. Frood and Gallagher further developed Coelho's theory by assuming that both positive and negative charge carriers are mobile and they showed that the current and charge densities have the same form as those with only one kind of charge carriers [146-147].

When the diffusion coefficient and mobility of positive charge carriers are equal to those of negative charge carriers, $D = D_+ = D_-$ and $\mu = \mu_+ = \mu_-$, by substituting Eq. (4.71a) and (4.71b) into Eq. (4.69), the following expressions can be obtained,

$$j(x,t) = \sigma E(x,t) - D\frac{\partial \rho(x,t)}{\partial x} \quad , \tag{4.72}$$

$$\frac{\partial \rho(x,t)}{\partial t} + \frac{\sigma}{\varepsilon_0 \varepsilon_r} \rho(x,t) = D\frac{\partial^2 \rho(x,t)}{\partial x^2} \ , \tag{4.73}$$

where, $\sigma = 2n_0 q\mu$. Assume that in steady state solution of Eq. (4.73) has the form:

$$\rho(x,t) = \rho_\omega(x) e^{i\omega t} \ , \tag{4.74}$$

where ω (rad/s) is the angular frequency. The electric field and current density should also have the same form

$$E(x,t) = E_\omega(x) e^{i\omega t} , \tag{4.75}$$

$$j(x,t) = j_\omega(x) e^{i\omega t} \ . \tag{4.76}$$

Coelho notes that those charge carriers cannot get across the electrodes at $x = \pm d$, thus the current density at the two metal electrodes should follow that

$$\sigma E_\omega(\pm d) = D\left|\frac{\partial \rho_\omega}{\partial x}\right|_{(x=\pm d)} . \tag{4.77}$$

With this boundary condition, the charge density, field and current density can be calculated as:

$$\rho_{\omega}(x) = \frac{\varepsilon_0 \varepsilon_r E_0 \sinh(k_{\omega} x)}{M} \tag{4.78a}$$

$$E_{\omega}(x) = E_0 \frac{\cosh(k_{\omega} x) + i\omega\tau \cosh(k_{\omega} d)}{M}, \tag{4.78b}$$

$$j_{\omega}(x) = i\omega\tau\sigma E_0 \frac{\cosh(k_{\omega} d) - \cosh(k_{\omega} x)}{M}, \tag{4.78c}$$

with

$$\tau = \frac{\varepsilon_0 \varepsilon_r}{\sigma}, \tag{4.79a}$$

$$k_{\omega}^2 = \frac{(1 + i\omega\tau)}{D\tau}, \tag{4.79b}$$

$$M = \frac{\sinh(k_{\omega} d)}{k_{\omega} d} + i\omega\tau \cosh(k_{\omega} d). \tag{4.79c}$$

Note that when $\omega = 0$, $j_0(x) = 0$, therefore, there is no DC conduction in Coelho's model.

The current density in the external circuit can be calculated using the following expression:

$$j_{ext}(\omega) = i\omega(\varepsilon_0 \varepsilon_r - \varepsilon_0) E_0 + i\omega\tau\sigma E_0 \frac{\cosh(k_{\omega} d) - \sinh(k_{\omega} d)/(k_{\omega} d)}{M}. \tag{4.80}$$

The first term of Eq. (4.65) is induced by the displacement current in the media, whilst the second term is induced by the motion of charge carriers. This current density must be equal to the current density in a sample that has a permittivity of $\varepsilon(\omega)$

$$j_{ext}(\omega) = i\omega(\varepsilon(\omega) - \varepsilon_0) E_0 \tag{4.81}$$

Employing Eq. (4.80) in Eq. (4.81) leads to the complex permittivity:

$$\varepsilon(\omega) = \varepsilon_0 \varepsilon_r \left[\frac{1 + i\omega\tau}{i\omega\tau + \tanh(k_{\omega} d)/k_{\omega} d} \right]. \tag{4.82}$$

Eq. (4.82) is Coelho's main result [146].

As discussed in the above paragraphs, it is easy to reach a conclusion that the density of those injected charge carriers is q_i^0 everywhere. If the dissociated charge carriers are present between the two metal electrodes, the internal field is distorted. If the field distortion is not serious, the distribution of the injected charge carriers can also be

linearized. Therefore, if the charge density of those injected charge carriers $\rho_i(x,t)$ does not differ much from their equilibrium values, the distribution of the injected charge carriers can be denoted as

$$\rho_i(x,t) = q_i^0 + \gamma(x,t). \tag{4.83}$$

where $\gamma(x,t)$ is a term that is much smaller than q_i^0. Assuming there are no recombination and dissociation of those injected charge carriers, the current induced by those injected charge carriers can be written as:

$$j_i(x,t) = \rho_i(x,t)\mu_i E(x,t) - D_i \frac{\partial \rho_i(x,t)}{\partial t}. \tag{4.84}$$

Here, an assumption that the amount of the dissociated charge carriers is much more than that of the injected charge carriers has been made and this assumption will be verified later. Thus, the internal field is mainly determined by the distribution of the dissociated charge carriers and can be denoted as

$$E(x,t) = e^{i\omega t} E_0 \frac{\cosh(k_\omega x) + i\omega\tau \cosh(k_\omega d)}{M}. \tag{4.85}$$

If $\gamma(x,t)$ is far smaller than q_i^0, the current due to the motion of these injected charge carriers becomes

$$j_i(x,t) = q_i^0 \mu_i E(x,t) - D_i \frac{\partial \rho_i(x,t)}{\partial x}. \tag{4.86}$$

With conservation of electric charge,

$$\frac{\partial \rho_i(x,t)}{\partial t} + \frac{\partial j_i(x,t)}{\partial x} = 0. \tag{4.87}$$

After using Eq. (4.72), Eq. (4.71) becomes

$$-\frac{\partial \rho_i}{\partial t} = q_i^0 \mu_i \frac{\partial E(x,t)}{\partial x} - D_i \frac{\partial^2 \rho_i}{\partial x^2}. \tag{4.88}$$

Assuming in steady state, the solution for the charge density has the form:

$$\rho_i(x,t) = \rho_{i\omega}(x) e^{i\omega t}. \tag{4.89}$$

Similarly, the current density due to the motion of these injected charge carriers can be denoted as

$$j_i(x,t) = j_{i\omega}(x) e^{i\omega t} \tag{4.90}$$

By substituting Eq. (4.89) into Eq. (4.88), the following expression can be obtained:

$$-B^2\rho_{i\omega}(x)=\frac{\sigma_i}{D_i}\frac{\partial E_\omega(x)}{\partial x}-\frac{d^2\rho_{i\omega}(x)}{dx^2}, \tag{4.91}$$

with

$$\frac{i\omega}{D_i}=B^2. \tag{4.92}$$

After using Eq. (4.85), Eq. (4.91) becomes

$$-B^2\rho_{i\omega}(x)=A\sinh(k_\omega x)-\frac{d^2\rho_{i\omega}(x)}{dx^2}, \tag{4.93}$$

with

$$A=\frac{\sigma_i E_0 k_\omega}{\frac{\sinh(k_\omega d)}{k_\omega d}+i\omega\tau\cosh(k_\omega d)}\times\frac{1}{D_i}. \tag{4.94}$$

Solution of Eq. (4.93) is

$$\rho_{i\omega}(x)=-\frac{A\sinh(k_\omega x)}{B^2-k_\omega^2}+C_1\exp(Bx)+C_2\exp(-Bx). \tag{4.95}$$

If the charge injection can only be affected by the electric field at the two metal electrodes, $x=\pm d$, the current should follow

$$j_i(d,t)=\sigma_i E(d,t), \tag{4.96a}$$

$$j_i(-d,t)=\sigma_i E(-d,t). \tag{4.96b}$$

Using Eq. (4.96) in Eq. (4.95) and solving for C_1 and C_2gives

$$C_1=\frac{q_i^0-\frac{P\sinh(Bd)}{2}+P\exp(Bd)}{\cosh(Bd)}, \tag{4.97a}$$

$$C_2=\frac{q_i^0-\frac{P\sinh(Bd)}{2}-P\exp(-Bd)}{\cosh(Bd)}. \tag{4.97b}$$

Therefore, the charge density of the injected charge carriers becomes

$$\begin{aligned}\rho_{i\omega}(x)=&-\frac{A\sinh(k_\omega x)}{B^2-k_\omega^2}+\frac{q_i^0-\frac{P\sinh(Bd)}{2}+P\exp(Bd)}{\cosh(Bd)}\exp(Bx)\\&+\frac{q_i^0-\frac{P\sinh(Bd)}{2}-P\exp(-Bd)}{\cosh(Bd)}\exp(-Bx)\end{aligned}, \tag{4.98}$$

with

$$P = \frac{2}{(B^2 - k_\omega^2)\sinh(Bd)} \frac{\sigma_i E_0 k_\omega}{\frac{1}{k_\omega d} + i\omega\tau \coth(k_\omega d)} \times \frac{1}{D_i}. \tag{4.99}$$

The current induced in the external circuit by the motion of these injected charge carriers in the mineral oil is the average value of the internal current between the two metal electrodes. The current density in the external circuit can be denoted as

$$\begin{aligned} \frac{1}{2d}\int_{-d}^{d} j_{i\omega}(x)dx = \frac{\sigma_i E_0}{M}\left[\frac{\sinh(k_\omega d)}{k_\omega d} + i\omega\tau\cosh(k_\omega d)\right] \\ + \frac{D_i A \sinh(k_\omega d)}{d(B^2 - k_\omega^2)} - \frac{D_i P \sinh(Bd)}{2d} = \sigma_i E_0 \end{aligned}. \tag{4.100}$$

Thus, even under a non-homogenous field, the current caused by the drift and diffusion of those injected charge carriers can still only contribute to the imaginary part of the complex permittivity.

Using Eq. (4.67), Coelho's space charge polarization theory should be modified as

$$\varepsilon(\omega) = \varepsilon_m\left[\frac{1 + i\omega\tau'}{i\omega\tau' + \tanh(k'_\omega d)/k'_\omega d}\right] - i\frac{\sigma_i}{\omega}, \tag{4.101}$$

with

$$\begin{cases} \tau' = \varepsilon_m/(\sigma - \sigma_i) \\ k'^2_\omega = \frac{1}{D\tau'}(1 + i\omega\tau') \end{cases}. \tag{4.102}$$

4.5 Comparison between experiment and theory

Here, the computer based method and analytical expressions will be used to fit the experimental results of the frequency response of the three different kinds of mineral oil.

The experimental results of Shell ZX-I oil, Hydro Quebec oil and Terna oil are shown in Figs. 4.8-4.13. In all events, the real part of permittivity does not change much within the high frequency range (1Hz-100Hz) and increases significantly when the frequency goes lower and the imaginary part of complex permittivity decreases with the frequency with a slope that is close to -1 in log-log scale. The real parts of the relative complex permittivity of the mineral oil are around 2.1-2.4 in frequency ranges from 1Hz to 100Hz and they does not change much regardless of the AC conductivity. As pointed out by Sawada, the permittivity in this range studied is mainly contributed by electronic, atomic and dipole polarizations and these polarizations have been fully polarized so that the real

part of the complex permittivity seems to be constant [141]. The increase of the real part of the complex permittivity indicates space charge polarization can affect the frequency response in mineral oil when the frequency is below 1 Hz. More charge carriers can be generated during oil degradation. If there are more charge carriers participating the ionic drift and diffusion process, the space charge polarization becomes more significant and a higher real part of the complex permittivity can be observed. Terna oil has been aged for 50 years and it has a high DC conductivity, so the space charge effect in Terna oil is more significant than that in other two oil samples. As seen from Table. 3.1, the AC conductivity of Hydro- Quebec oil that are calculated using the results of the imaginary part of the complex permittivity are 10 times higher than that of Shell ZX-I oil, their experimental results of the real part of complex permittivity are quite similar, which implies that ions may not be the only kind of charge carrier in mineral oil. Besides, the curves of the real part of the complex permittivity shift towards high frequency when the temperature increases, which is due to the increase of density and mobility of charge carriers.

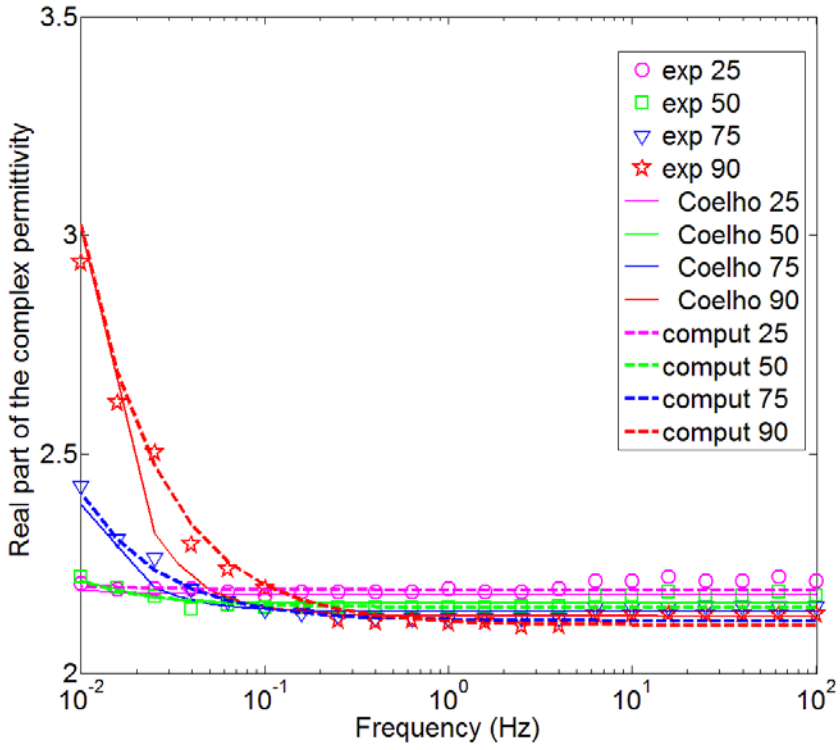

Fig.4.8 Theoretical and experimental results of the real part of the complex permittivity of Shell ZX-I oil.

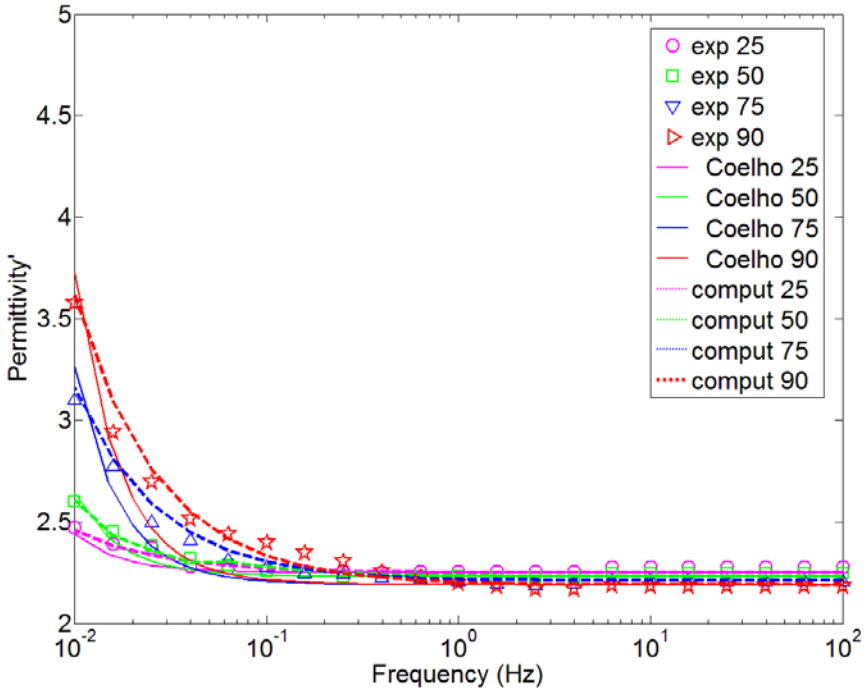

Fig.4.9 Theoretical and experimental results of the real part of the complex permittivity of Hydro Quebec oil.

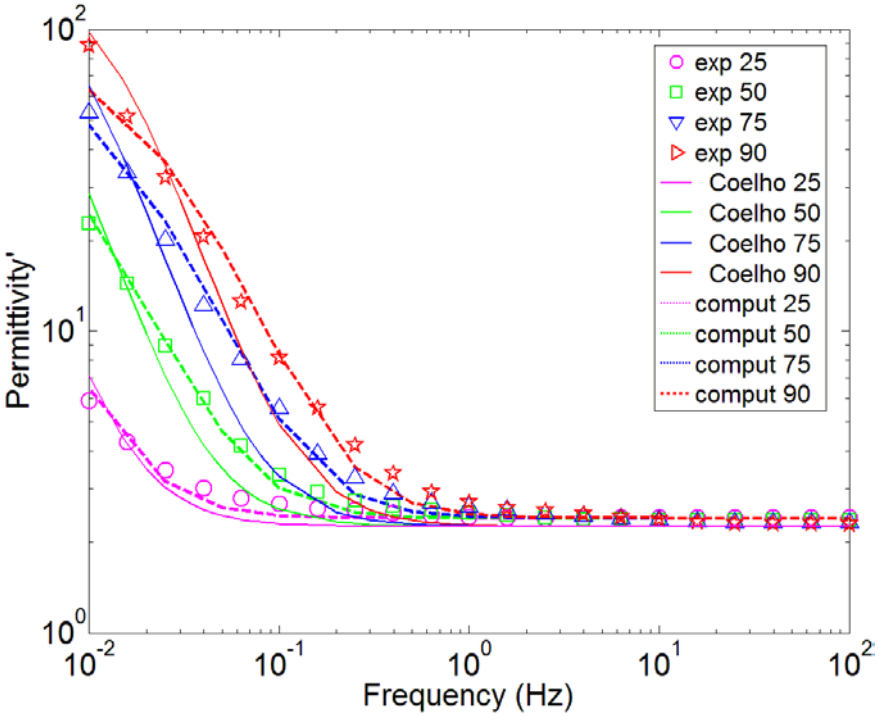

Fig. 4.10 Theoretical and experimental results of the real part of the complex permittivity of Terna oil.

The computer based simulation results of the complex permittivity of these three kinds of mineral oils with different aging times are illustrated in Figs. 4.8-4.13. The dashed lines are the computer based calculated results. Good fits between the observed and the calculated values have been achieved for the frequency-dependent curves of the complex

permittivity. It seems if part of the charge carriers are injected from the electrode, both the real and imaginary part of the complex permittivity can be fitted. The computer based simulation can fit the experimental results of the real part of the complex permittivity of Shell ZX-I oil and Hydro Quebec oil quite well. The simulated results of Terna oil seem to be going to reach a peak value and become lower than the experimental results when the frequency is close to 0.01 Hz. As Terna oil has been aged for around 50 years, more charge carriers will be generated through degradation process. There newly generated charge carriers may not share the same characteristics, thus, there can be charge carriers with different mobility in Terna oil. It has been reported that using two types of charge carriers with different mobility can give a better fit of the experimental results [161].

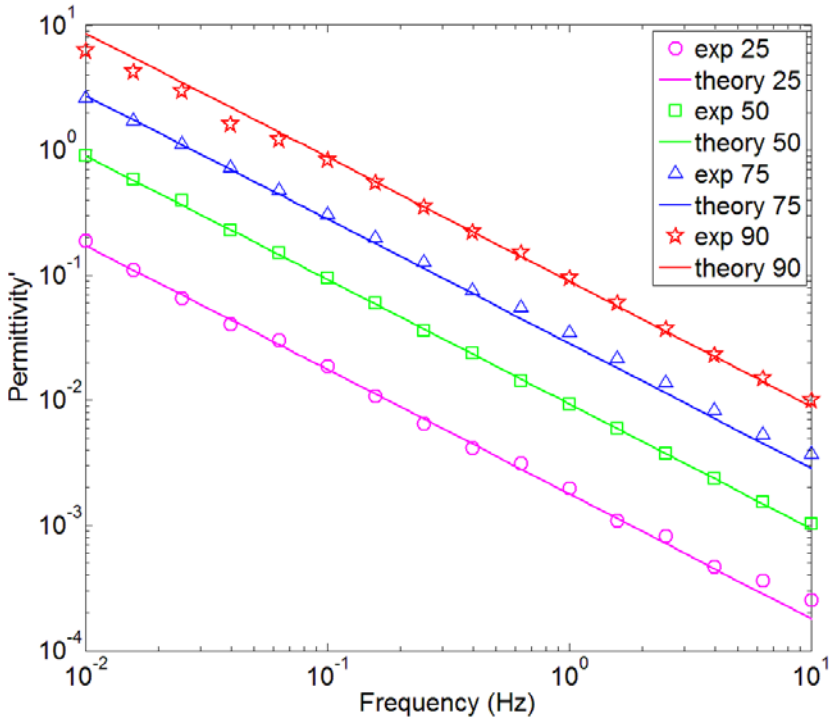

Fig. 4.11 Theoretical and experimental results of the imaginary part of the complex permittivity of Shell ZX-I oil.

The modified Coelho model can also fit the real part and imaginary part of the complex permittivity. In our simulation, there is unnoticeable difference between the calculated result of the imaginary part of the complex permittivity using the computer based simulation and those from the modified Coelho model. Therefore, only the simulated results based on modified Coelho model are illustrated in Figs. 4.11-4.13. However, the computer based method can fit the experimental result of the real part of the

complex permittivity much better than that using the modified Coelho model. The solid lines in Figs 4.8-4.10 are the calculated value from the modified Coelho model. The simulated results of the real part of the complex permittivity based on the modified Coelho model start to increase at a lower frequency and the increasing rate is higher when compared to the experimental data. Although the mineral oil can be treated as weak electrolyte, the amount of the newly dissociated charge carriers should not be simply ignored especially at low frequency. As more charge carriers are generated during the measurement, more charge will be induced at the electrode and the total capacitance can also increase. Therefore, the computer-based calculated value of the real part of the complex permittivity can start to increase at a higher frequency when compared to the calculated results based on the modified Coelho model since more charge carriers are moving to the electrode due to ionic dissociation. Besides, Coelho's model is based on the assumption that the charge distribution can be approximated as homogeneous, which is not true when the frequency goes low. If the frequency is low enough, the charge carriers in the liquid bulk will have sufficient time to reach the interface of oil/electrode and the difference of charge distribution can becomes significant. Therefore, in order to get a more accurate experimental fit, the computer based method is recommended.

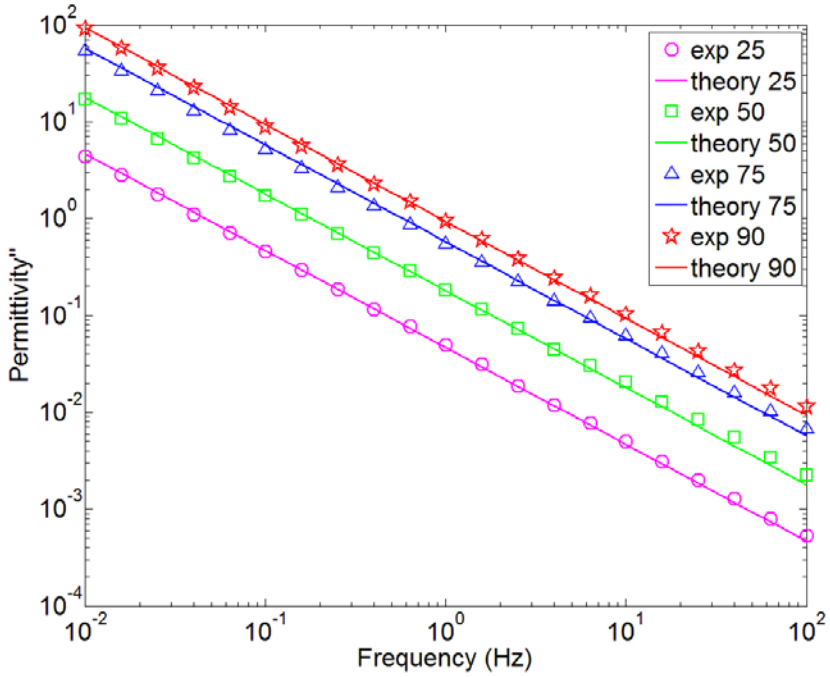

Fig. 4.12 Theoretical and experimental results of the imaginary part of the complex permittivity of Hydro Quebec oil

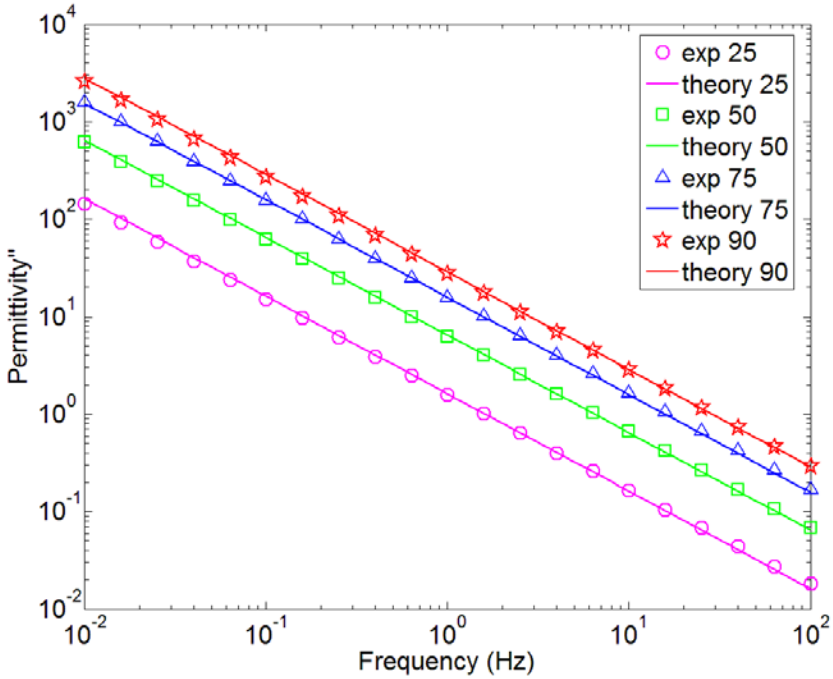

Fig. 4.13 Theoretical and experimental results of the imaginary part of the complex permittivity of Terna oil.

The coefficients 1- α of three different types of mineral oils used in computer based method and modified Coelho model are shown in Table 4.2 and 4.3, respectively. As seen from Table 4.2 and 4.3, it seems when the oil is aged, the injected charge carriers will be the main charge carriers in the mineral oil. Also, a higher temperature can result in a smaller proportion of the first kind of the charge carriers and a larger amount of the second kind of charge carriers. It indicates that the injection can be enhanced by aging and high temperature. These coefficients obtained from two different calculating methods have a good consistence. Since the calculation based on the modified Coelho model is much easier and faster than the computer based method, Eq. (4.101) can be used in daily measurement analysis. However, how the injected charge carriers are generated is still unknown.

Please also note the improved space charge polarization theory is developed based on the assumption that the internal field distortion is not serious. When this frequency-domain measurement is carried out under high electric field, more charge carriers will be created and the field distortion can be significant. Thus, this modified model might not be valid if the field is high. Also, as the frequency goes low, almost all the dissociated charge carriers are able to travel to a region that is close to the electrode and the density of these charge carriers between electrodes can differ much from their equilibrium values

so that Eq. (4.75) and (4.90) are no longer valid if the frequency is too low. Thus, this improved model cannot be used to explain the dielectric behaviour of mineral oil under a very low frequency or a high electric field.

Table 4.2 Coefficient 1- α for three different kinds of mineral oil in computer based method

	25°C	50°C	75°C	90°C
Shell oil	0.9	0.7	0.6	0.45
Hydro Quebec oil	0.4	0.15	0.10	0.065
Terna oil	0.14	0.11	0.08	0.07

Table 4.3 Coefficient 1- α for three different kinds of mineral oil in modified Coelho model

	25°C	50°C	75°C	90°C
Shell oil	0.8	0.45	0.4	0.38
Hydro Quebec oil	0.30	0.11	0.055	0.050
Terna oil	0.105	0.095	0.090	0.080

4.6 Internal field distribution and application of the ratio α

One of the assumption for the injection equation in liquid is the internal field distribution does not change much. Because the heavily aged mineral oil has the highest conductivity, the field distortion will be serious due to a large amount of charge carriers. On considering that the conductivity also increases with the temperature, if the internal field of the Terna oil at 90 °C does not change very much in a whole circle, the internal electric field can be treated evenly distributed between the two electrodes.

Due to the accumulation of charge carriers in the vicinity of the electrode, the electric field close to the electrode could be affected notably by the present of space charge. If the noticeably distorted region is much smaller compared to the rest region, the internal field can still be treated as homogeneous. The distance between two parallel electrodes is l, 5×10^{-4} m, the electric field at 2.5×10^{-5} m($1/20l$), 2.5×10^{-4} m($1/2l$) and 4.75×10^{-4} m($19/20l$) will be calculated. The simulating result is shown is Fig. 4.14. The electric field close to two electrodes are almost the same. Although, the electric field at three different positions are not exactly the same as a sine wave function, the difference

between the sine wave field and all these three curves of the electric field in one circle is really small. When it comes to other types of mineral oil, since there are few charge carriers in the bulk, this kind of difference should be even smaller. Thus, that most of the internal region between two electrodes possesses an approximate evenly distributed field. Therefore, the usage of the injected equation in liquid is valid here.

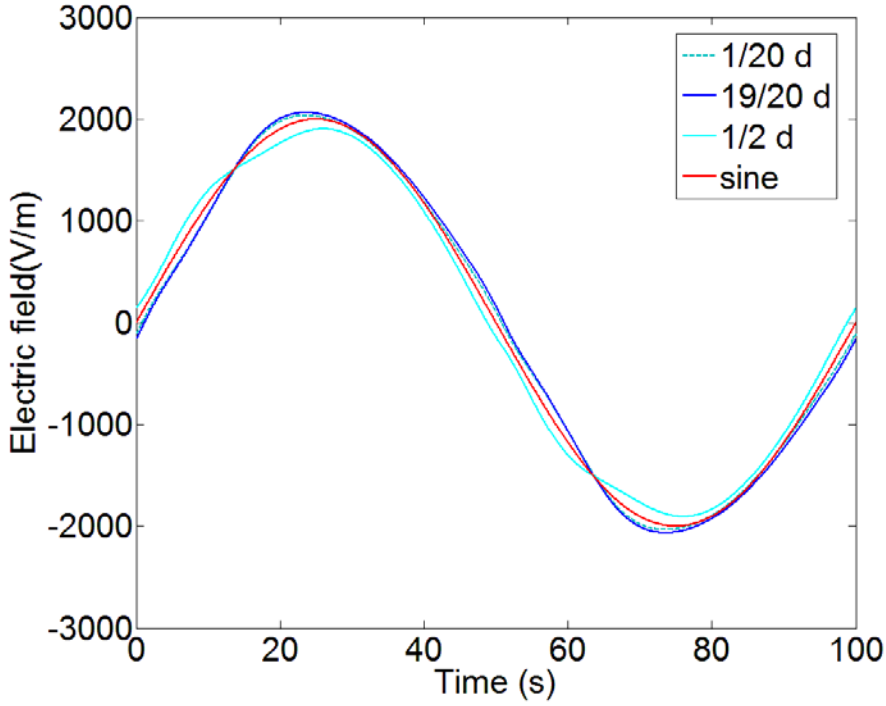

Fig. 4.14 Electric field at certain position between two electrodes in a whole circle

As the ratios α for three different kinds of mineral oil have been calculated, the influence of the second kind of charge carriers on the internal field can be studied. The maximum value of this ratio is 0.95 in our simulation. In our previous discussion, the mobility of those injected charge carriers is higher than 7.9×10^{-5} $m^2/s/V$. The conductivity of the mineral oil measured according to the procedures defined in IEC 61620 is 5.2×10^{-11} S/m. Thus the charge density carried by the injected charge carriers is smaller than 6.2×10^{-7} C/m^3. Assuming that the mobility of the dissociated charge carriers is 1×10^{-8} $m^2/s/V$, which is a typical value that has been reported by other researchers [155-160], the charge density carried by the dissociated charge carriers is 2.6×10^{-4} C/m^3. The charge density of the dissociated charge carriers is much more than that of the injected charge carriers. Thus, the internal field is mainly determined by the distribution of the dissociated charge carriers and Eq. (4.85) is valid.

If the ratio α of the mineral oil is known, the conductivity contributed by the dissociated charge carriers can reveal the condition of the mineral oil as this conductivity depends on the properties of the molecules and the ions. It is well accepted that the dissociation of gas and moisture can increase the conductivity of the mineral oil. If the hydrocarbon molecules in the oil have not suffered from chemical degradation, the dielectric properties of the oil can be significantly improved by removing the dissolved gas and the moisture. However, if the oil is heavily aged and the hydrocarbon molecules have been heavily degraded, it is better to replace the oil rather than going through a reconditioning process. The conductivity contributed by the motion of the dissociated charge carriers, which is going to referred as dissociated conductivity in the following sections, can be denoted as

$$\sigma_d = (1-\alpha)\sigma \tag{4.103}$$

The temperature dependence of the dissociated conductivities of the mineral oils are shown in Table 4.4.

Table 4.4 Dissociated conductivity for mineral oil with different aging period

		25°C	50°C	75°C	90°C
Shell ZX-I oil	σ_d	0.090 pS/m	0.37 pS/m	0.96 pS/m	1.6 pS/m
	σ	0.10 pS/m	0.53 pS/m	1.6 pS/m	3.6 pS/m
Hydro Quebec oil	σ_d	1.1 pS/m	1.5 pS/m	3.2 pS/m	3.5 pS/m
	σ	2.6 pS/m	10 pS/m	32 pS/m	51pS/m
Terna oil	σ_d	13 pS/m	40 pS/m	70 pS/m	110 pS/m
	σ	90 pS/m	360 pS/m	880 pS/m	1500 pS/m

As seen from Table 4.4, the dissociated conductivity increases with the temperature and the oil aging period. Although the initial conductivity of Hydro Quebec oil is about 20 times higher than that of Shell ZX-I oil, the dissociated conductivity of Hydro Quebec oil is about 11 times higher than that of Shell ZX-I oil at 25°C and 1.6 times at 90 °C, which suggested that there might be some highly dissolvable impurities in the Hydro Quebec oil. As the temperature increases, the density of the charge carriers dissociated from these impurities do not change much, consequently, the increasing rate of the dissociated conductivity of Hydro Quebec oil is lower than that of Shell ZX-I oil. In the Terna oil, which has been aged for 50 years, the hydrocarbon molecules have been

severely degraded and smaller molecules are created under electrical, thermal and chemical stresses. As discussed in Chapter 2, some of these newly generated molecules can be dissociated into ions and the total quantity of the dissociated charge carriers increases. Therefore, Terna oil has the highest dissociated conductivity and it might not be worthy to have this oil reconditioned. However, how can the dissociated conductivity be related to the chemical degradation of the hydrocarbon molecules is still not very clear and more research is needed.

IEC 60422 has provided a recommended criterion for dielectric dissipation factor to categorize different oil conditions [162]. The relevant values for good, fair and poor conditions of oil have been given in Table 4.5 [162].

Table 4.5 Application and interpretation of dielectric dissipation factor results (IEC 60042)

Dielectric dissipation factor at 40 to 60 Hz at 90 °C			
Oil condition	Good	Fair	Poor
Power transformer with a nominal system voltage of 170 kV and above	< 0.10	0.10 - 0.20	> 0.20
Power transformer with a nominal system voltage that is below 170 kV	< 0.10	0.10 - 0.50	> 0.50
Description	Oil in norm condition	Oil deterioration detectable	Oil deterioration abnormal

The dielectric dissipation factors for Shell ZX-I oil, Hydro Quebec oil and Terna oil are 0.00059, 0.0083 and 0.25, respectively. Therefore, the Shell ZX-I oil and Hydro Quebec oil can be classified as "good" oil. Due to a high dielectric dissipation factors, Terna oil can be considered as "fair" or "poor" oil depending on the nominal system voltage of the transformer. IEC 60422 states that if oil condition is poor, "reclaim oil or, alternatively, if more economical because other tests indicate severe ageing, replace the oil". As discussed in Chapter 3, the dielectric dissipation factor is mainly affected by its AC conductivity. However, as the adsorbed moisture can significantly increase AC conductivity, high water content may be responsible for high dissipation factor of mineral oil. The dissociated conductivity is related to ions, thus, this new parameter may be used as an indicator for chemical degradation. When an oil sample is in poor condition, it

would be better to replace the oil if it has a high dissociated conductivity. If this oil has a high dielectric dissipation factor but a low dissociated conductivity, it may be worthy for oil reclamation, as its high dielectric dissipation factor may be caused by a high water content.

4.7 Summary

Based on the simulation result, there are probably two kinds of charge carriers in mineral oil. One is dissociated in the oil and can be blocked by the electrode, the other one is created in the vicinity of the electrode. The polarization caused by the drift of the injected charge carriers has been studied. It seems if these injected charge carriers have a high mobility so that they can reach the electrode in a field cycle, the motion of these injected charge carriers can only contribute to the imaginary part of the complex permittivity. A computer based method has been used to fit the experimental data. It seems if part of the total charge carriers are generated at the electrode, both the real part and imaginary part of the complex permittivity measured experimentally can be fitted. Besides, an analytical solution based on Coelho's space charge polarization theory has been developed. Even the field is not homogeneous between the electrodes, the motion of these injected charge carriers can still only contribute to the imaginary part of the complex permittivity. To get an accurate fit, the computer based method is recommended. A new coefficient α, the ratio of the conductivity that is contributed from the injection over the total conductivity has been defined and it decreases with temperature and aging period. The dissociated conductivity has been defined and used to analyse the aging condition of the oil.

Chapter 5 Modelling of DC Conduction in Mineral Oil

When an external DC voltage is applied across the media, a current due to the drift of charge carriers under the electric field can be observed, this is known as the polarization. When this voltage is removed and the subject is short-circuited, the polarization that has been built up in the sample can give rise to the discharge current in an opposite direction. Jaffe provided approximated equations to explain the characteristics of the depolarization current [113]. However, his solutions are quite complex. Macdonald pointed out that Jaffe's assumption was only valid for a low applied voltage (0.2 Volt) , which was much lower than the applied voltage (380 Volts) in Jaffe's experiment, and Jaffe's polarization theory based on ionic drift and diffusion was questionable under a high electric field [134]. Here, a simple model based on charge diffusion has been proposed to estimate the depolarization current in mineral oil.

5.1Basic theory for electric conduction in mineral oil

Let us consider a pair of parallel plate metal electrodes filled with mineral oil, the distance between the two electrodes is l (m). Assuming that the mineral oil can be treated as a liquid in which a small amount of ions are dissociated from ionic- pairs and the density of free ions is far smaller when compared with that of the ionic- pairs, the dissociation and recombination process can be described as

$$\frac{dn_+}{dt} = \frac{dn_-}{dt} = K_d c - K_r n_+ n_-, \tag{5.1}$$

where, c is density of ionic- pairs, n_+ and n_- is density of positive and negative ions in the mineral oil, K_d (s^{-1}) is the dissociation rate and K_r (s^{-1}) is the recombination rate. If cations and anions are distributed evenly between the two metal electrodes in the absence of an external electric field and the diffusion coefficient, the mobility, the density and the charge that is carried by a single charge carrier of positive ions are equal to those of negative ions, the density of positive and negative ions can be denoted as

$$n_0 = \frac{\sigma}{q \times (\mu_+ + \mu_-)}, \tag{5.2}$$

where n_0 is the initial density of positive or negative ions, σ is the conductivity of mineral oil, μ_+ ($m^2\ s^{-1}\ V^{-1}$) and μ_- ($m^2\ s^{-1}\ V^{-1}$) are the mobility of the positive and negative ions, respectively. The recombination rate can be calculated using Langevin approximation [33],

$$K_r = \frac{q \times (\mu_+ + \mu_-)}{\varepsilon_0 \varepsilon_r}, \tag{5.3}$$

in which, ε_0 (F/m) is the permittivity of vacuum and ε_r is the relative permittivity of mineral oil. According to Onsager's field enhanced dissociation theory, the dissociation rate can be written in the following form [34],

$$K_d = K_d^0 \frac{I_1(4b)}{2b} \tag{5.4a}$$

$$b = \sqrt{\frac{q^3 E}{16\pi\varepsilon_0\varepsilon_r k^2 T^2}} \tag{5.4b}$$

where, I_1 is the modified Bessel function of the first kind, K_d^0 (s^{-1}) is the dissociation rate when the electric field is zero, E (V/m) is the electric field, k is the Boltzmann constant and T (K) is the absolute temperature. The dissociation rate in the absence of electric field can be denoted as

$$K_d^0 = K_r n_0^2 / c\,. \tag{5.5}$$

Here, the electric conduction under a medium electric field in which regime the newly generated charge carriers can be extracted within a short time will be discussed. In this regime, the recombination of free ions can be neglected and the current is mainly contributed by the newly generated charge carriers. As indicated by Pontiga and Castellanos, if the internal field can be approximated by the mean electric field, the current induced from dissociation can be written in the form of [45-46]

$$j_d \approx 2K_d clq \tag{5.6}$$

On considering a situation that an electric potential of 1 kV is applied on a liquid sample with thickness of 1 mm, the dissociated charge carriers with a mobility of 1×10^{-9} $m^2s^{-1}V^{-1}$ will drift to a close region near the electrode in less than 1 second. Thus, after one second, all the pre-existing charge carriers can reach the electrode. For a completely blocked electrode, the charge in the vicinity of one electrode can be estimated using

$$\rho_d = \frac{1}{2}\left[Sl\sigma_d / (2\mu_d) + 2K_d clqSt_p \right] \tag{5.7}$$

in which, S (m^2) is the surface area of the metal electrode, σ_d (S/m)is the conductivity contributed by the motion of the dissociated charge carriers, $\mu_d = \mu_+ = \mu_-$ ($m^2\ s^{-1}\ V^{-1}$) is the mobility of the dissociated charge carriers and t_{pol} (s) is the electrification time.

The boundary conditions have been discussed previously by Jaffe et al [113-115]. Assuming that there exists a state of equilibrium concentration at the electrodes in the absence of an applied voltage and the rate of discharge of ions is proportional to the difference between the instantaneous values and the equilibrium value, for the positive ions, the discharge current at the electrode can be denoted as [113-115]

$$\begin{cases} j_d(0,t) = -\xi q(n_+(0,t) - n_+^*) & n_+(0,t) \geq n_+^* \\ j_d(0,t) = 0 & n_+(0,t) < n_+^* \\ j_d(l,t) = \xi q(n_+(l,t) - n_+^*) & n_+(l,t) \geq n_+^* \\ j_d(l,t) = 0 & n_+(l,t) < n_+^* \end{cases} \tag{5.8}$$

Here, ξ represents a rate constant of ionic adsorption and n_+^* is an equilibrium value of the density of the positive ions which depends on the nature of the liquid. If the distribution of the ions are homogeneous between the two parallel electrodes is assumed, then $n_+^* = n_0$.

Therefore, the total charge in the charge layer obeys the following expression,

$$\frac{d\rho_d}{dt} \approx K_d cSl - \xi(n_+ - n_+^*)\Delta V = K_d cSl - \xi(\rho_d - n_+^* \Delta V) \tag{5.9}$$

where ΔV (m^3) is the volume of a region close to the electrode where the charge carriers get accumulated. The first term on the right side represents the newly dissociated charge carriers; the second term describes the process that the dissociated charge carriers are neutralized by the electrode.

On considering that most of the initially dissociated charge carriers are moved to a close region of the electrode within 1 s and only the long-term conductivity will be studied, ρ_d (C) at time t = 0 can be given in the form of

$$\rho_d(0) = \frac{\sigma_d Sd}{4\mu_d q} \tag{5.10}$$

The solution of Eq. (5.9) is represented by

$$p(d,t)=\left(\frac{\sigma_d Sd}{4\mu_d q}-\frac{K_d cSl+\xi n_+^* \Delta V}{\xi}\right)e^{-\xi t}+\frac{K_d cSl+\xi n_+^* \Delta V}{\xi} \tag{5.11}$$

As seen from Eq. (5.11), ξ is also a time constant which indicates the charging time of the charge layer. However, there is no report concerning this parameter in mineral oil. As discussed in Chapter 4, the charge injection cannot be simply ignored even under a low electric field in mineral oil. As the injected charge carriers will have an opposite polarity to the blocked ions in the charge layer, how the injected current can affect the charge layer is not clear. To simplify this issue, an assumption is made that ξ does not change with the electric field. With that assumption, it is easy to obtain $\xi \approx 1/\Delta T$. ΔT is the settling time that is required for the response curve to reach the equilibrium state. As reported by other researchers, the length of the charge layer in the vicinity of the electrode can be estimated by the Debye length of the liquid and the Debye length for non- polar liquid is around several micrometres [163-167]. Here, only the electric conductions in oil of Shell ZX-I oil and Hydro Quebec will be discussed. As seen from Figs. 2.7-2.12, the settling time to reach the quasi-steady state is higher than 100s, therefore $\xi < 0.01$. According to the discussion in Chapter 4, the minimum dissociated conductivity is 0.10 pS/m. If assuming the Debye length is 10 μm ,the following expression can be obtained,

$$\frac{K_d cSl}{\xi n_+^* \Delta V}=\frac{I_1(4b)}{2b}\frac{2\sigma_d Sl}{\varepsilon_0 \varepsilon_r \xi \Delta V} \ll 1 \tag{5.12}$$

In an equilibrium state, the amount of charge in a charge layer can be estimated using the following equation,

$$\rho(\infty)\approx\frac{K_d cSl}{\xi}=\frac{I_1(4b)}{2b}K_r n^2 Sl\Delta T \tag{5.13}$$

However, as the charge layer in the vicinity of the electrode can definitely affect the charge injection process and the nature of the injected charge carriers mentioned in chapter 4 is still not clear, the polarization current will not be studied here.

As discussed in Chapter 4, the injected charge carriers have a high mobility. Thus, when the oil is depolarizing, these injected charge carriers can be extracted in a very short period of time, and the dissociated charge carriers will remain in the oil and start to diffuse into the bulk slowly. Therefore, the depolarization current measurement can help us to gain a better understanding of the motion of these dissociated charge carriers.

Let us consider a parallel electrode system that is filled up with the mineral oil. Assuming the charge carriers can be fully blocked by the electrode and the internal field

can be treated homogeneously. As these charge carriers cannot get through the electrodes, they can only move backwards into the bulk. If the diffusion only happens in 1-D system and there are only positive charge carriers in the mineral oil, the current flux at point x can be denoted as,

$$j(x,t) = qD\frac{dn}{dx}, \tag{5.14}$$

where, $j(x,t)$ (A/m^2) is the current density, q (C) is the charge carried by a charge carrier, D (m^2/s) is the diffusion coefficient and n is the density of charge carriers. With conservation of mass, the dependence of charge density on the time can be denoted as

$$D\frac{\partial^2 n}{\partial x^2} = \frac{\partial n}{\partial t}. \tag{5.15}$$

When the DC field is removed, these charge carriers will diffuse back into the bulk. As the diffusion current is affected by the distribution of charge carriers in the charge layer and currently there is no report concerns on the charge distribution in mineral oil, therefore, a "mirror image" method has been used here to calculate the diffusion current without resorting to the knowledge of charge distribution in charge layer. The scheme of the "mirror image" method is given in Fig. 5.1. The charge in the charge layer always follows an exponential distribution, thus, the charge density that is close to the electrode will be higher than in other regions. As the diffusion flow is determined by the differential of the charge density and it always flows from high density region to low density region, there will be no current flow at the electrode if assuming a completely blocked electrode. Therefore, this "mirror image" method can be safely used since there is also current flow in the middle layer. Jaffe and Adamczewski have independently developed theoretical expressions for ionic diffusion in dielectric liquid. Although their analytical solutions are different, a same exponential term can be found in their expressions [113, 168]. In order to be consistent with their expressions, a length of half the gap of the distance between the two metal electrodes will be used in this "mirror image" method. With this method, the charge distribution between the electrodes has been rearranged and this new distribution of charge carriers is illustrated in Fig. 5.1. Assuming the diffusion in a region that in the middle of these two electrodes can be negligible, the boundary condition can be written as

$$n(0,t) = n(l,t) = 0\ . \tag{5.16}$$

where l (m) is the distance between the two metal electrodes. The charge distribution at the moment that the external field is removed can be described as

$$n(x,0) = f(x)\,. \tag{5.17}$$

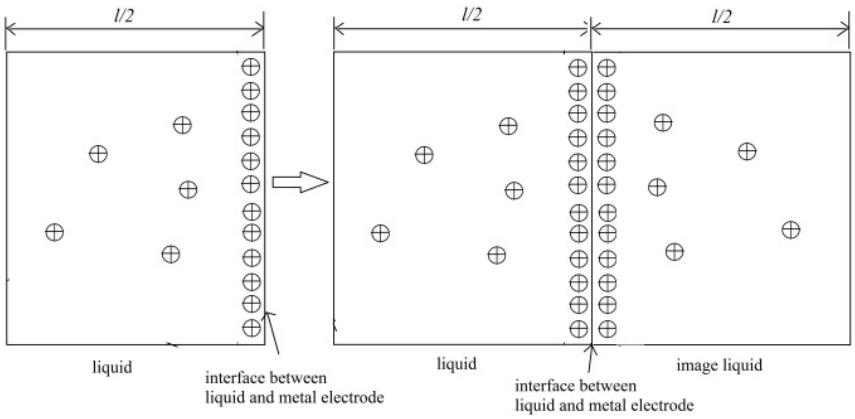

Fig. 5.1 Image method and the distribution of charge carriers.

Assuming that the solution to Eq. (5.15) can be written as

$$n(x,t) = F(x)G(t) \tag{5.18}$$

By substituting Eq. (5.18) into Eq. (5.15), Eq. (5.15) becomes,

$$\frac{\partial n(x,t)}{\partial t} = \dot{G}(t) \times F(x) \tag{5.19a}$$

$$\frac{\partial^2 n(x,t)}{\partial x^2} = G(t) \times \ddot{F}(x) \tag{5.19b}$$

in which, $\dot{G}(t)$ is the first derivative of $G(t)$ and $\ddot{F}(x)$ is the second derivative of $F(x)$.

Re-employing Eq. (5.15),

$$\frac{\dot{G}(t)}{DG(t)} = \frac{\ddot{F}(x)}{F(x)} = -s^2 \tag{5.20}$$

where *s* is a constant.

It is easy to find that Eq. (5.20) can be written in another form

$$s^2 F(x) + \ddot{F}(x) = 0 \tag{5.21a}$$

$$s^2 DG(t) + \dot{G}(t) = 0 \tag{5.21b}$$

The solution to Eq. (5.21a) can be expressed as

$$F(x) = A\cos(sx) + B\sin(sx) \tag{5.22}$$

With the boundary condition of Eq. (5.16), Eq. (5.22) can be solved as

$$F(x) = B_n \sin(\frac{n\pi}{l} x) \tag{5.23}$$

Similarly, the solution to Eq. (5.21b) can be denoted as

$$G(t) = e^{-s^2 Dt} = \exp\left[-\left(\frac{n\pi}{l}\right)^2 Dt\right] \tag{5.24}$$

Therefore, the solution to Eq. (5.15) can be denoted as

$$n(x,t) = F(x) \times G(t) = \sum_{n=1}^{\infty} B_n \sin(\frac{n\pi}{l} x) \exp\left[-\left(\frac{n\pi}{l}\right)^2 Dt\right] \tag{5.25}$$

Employing the initial condition of Eq. (5.17), Eq. (5.25) can be written as

$$\sum_{n=1}^{\infty} B_n \sin(\frac{n\pi}{l} x) = f(x) \tag{5.26}$$

$$B_n = \frac{2}{l} \int_0^l f(x) \sin(\frac{n\pi}{l} x) dx \tag{5.27}$$

On considering the symmetry of the charge distribution in Fig. 5.1, the expression for the charge distribution can be denoted as

$$Q(x,t) = q \times n(x,t) = \sum_{n=1}^{\infty} q \times B_n \times u_n(x,t) \tag{5.28}$$

with

$$\begin{cases} u_n(x,t) = \exp(-((2n-1)\frac{\pi}{l})^2 Dt) \sin((2n-1)\frac{\pi}{l} x) \\ B_n = \frac{2}{l} \int_0^l f(x) \sin((2n-1)\frac{\pi}{l} x) dx \end{cases}, \tag{5.29}$$

where $Q(x,t)$ (C) is the charge density. As the depolarization current at the beginning might be affected by the remaining high mobility charge carriers and the long term current is mainly determined by the ionic diffusion, high order component will not be considered here. After 50- 200s, the magnitude of the depolarization current of Shell ZX-I oil and Hydro Quebec oil approach zero, thus, the maximum depolarization time studied here is 400 s. High order components can affect the short-term conduction, but these component can be negligible in long- term conduction. However, high order components can be involved to increase the accuracy of the fitting. Here, the high order components will be ignored for simplification, thus, the charge density can be written as

$$Q(x,t) = \left(B_1 q\right) \exp(-\frac{\pi^2 D}{l^2} t) \sin(\frac{\pi}{l} x) . \tag{5.30}$$

If the total charge in one charge layer is Q_1, B_1 can be approximated as

$$B_1 \approx 4Q_1 / (lq) . \tag{5.31}$$

As seen from Eq. (5.31), the distribution of the charge carriers in the charge layer does not affect the depolarization current and the depolarization current only depends on the total number of the charge carriers in the charge layer.

With conservation of electric charge

$$\frac{\partial Q(x,t)}{\partial t} = \frac{\partial j(x,t)}{\partial x}, \tag{5.32}$$

the current density can be denoted as

$$j(x,t) = \frac{4\pi D Q_1}{l^2}\exp(-\frac{\pi^2 D}{l^2}t)(\cos(\frac{\pi}{l}x)-1). \quad (0 < x < l/2) \tag{5.33}$$

The total current density that flows in the external circuit can be calculated as

$$J_+(t) = \frac{2}{l}\int_0^{l/2} j(x,t)dx = -\frac{4(\pi-2)Q_1 D}{l^2}\exp(-\frac{\pi^2 D}{l^2}t). \tag{5.34}$$

If there are multiple kinds of charge carriers, this current density can be written as

$$J_+(t) = -\sum_{a=1}^{n}\frac{4(\pi-2)Q_a D_a}{l^2}\exp(-\frac{\pi^2 D_a}{l^2}t), \tag{5.35}$$

in which, Q_a (C) and D_a (m^2/s) are the total charge in the charge layer and the diffusion coefficient for the *a*-th charge carriers. For negative charge carriers, the current can be denoted as

$$J_-(t) = \sum_{a=1}^{n}\frac{4(\pi-2)Q_b D_b}{l^2}\exp(-\frac{\pi^2 D_b}{l^2}t). \tag{5.36}$$

in which, Q_b(C) and D_b (m^2/s) are the total charge in the charge layer and the diffusion coefficient for the *b*-th charge carriers.

Thus, the total current density can be denoted as

$$\begin{aligned} J_{dep}(t) &= J_+(t) + J_-(t) \\ &= -\sum_{a=1}^{n}\frac{4(\pi-2)|Q_a|D_a}{l^2}\exp(-\frac{\pi^2 D_a}{l^2}t) - \sum_{b=1}^{n}\frac{4(\pi-2)|Q_b|D_b}{l^2}\exp(-\frac{\pi^2 D_b}{l^2}t) \end{aligned} \tag{5.37}$$

For simplicity, the diffusion coefficient, mobility and number density of positive ions is assumed to be equal to those of negative ions. The depolarization current density that is contributed by both positive and negative charge carriers can be written as

$$J_{dep}(t) = J_+(t) + J_-(t) = -\sum_{a=1}^{n}\frac{8(\pi-2)|Q_a|D_a}{l^2}\exp(-\frac{\pi^2 D_a}{l^2}t) \tag{5.38}$$

As seen from Eq. (5.38), the exponential terms are similar to that derived by Jaffe and Adamczewski [113, 168].

5.2Experimental fit and analysis

As seen from Figs 2.20-2.23, the depolarization current of Shell ZX-I oil and Hydro Quebec oil decreases with the time. The magnitudes of the depolarization currents for these two kinds of mineral oil at the same temperature are similar regardless of the conductivity, which suggests there is little difference between the total charge in the charge layer in these two kind of mineral oil.

As seen from Eq. (5.38), the curve for depolarization current can be calculated by a formula of the type

$$I_{dep} = J_{dep} \times S = -\sum_{a=1}^{n} C_a \exp(-b_a t) \tag{5.39}$$

in which, C_a and b_a are constants that can be calculated by curve fittings.

Figs 5.2- 5.5 represent the comparison between theory and measurements on the depolarization current in Shell ZX-I oil and Hydro Quebec oil. The constant used in this calculation are given in Table 5.1. It has been seen that the theoretical curves represent the observed data with good accuracy.

Table 5.1Constants used in the calculation of the depolarization current

			30°C			90°C		
Shell ZX-I oil	b_a		1	2×10^{-2}	1×10^{-3}	1×10^{-1}	2×10^{-2}	2×10^{-3}
	C_a	1000V/mm	2.5×10^{-11}	1.6×10^{-11}	1.7×10^{-12}	1.9×10^{-10}	1.9×10^{-10}	2.0×10^{-12}
		2000V/mm	6.0×10^{-11}	3.3×10^{-11}	2.9×10^{-12}	1.0×10^{-10}	2.6×10^{-10}	4.0×10^{-12}
		5000V/mm	5.0×10^{-11}	8.7×10^{-11}	7.2×10^{-12}	6.0×10^{-10}	3.6×10^{-10}	5.0×10^{-12}
Hydro Quebec oil	b_a		1	5×10^{-2}	4×10^{-4}	2×10^{-1}	2×10^{-2}	7×10^{-4}
	C_a	1000V/mm	1.5×10^{-11}	1.0×10^{-11}	1.4×10^{-12}	1.5×10^{-10}	1.6×10^{-10}	2.2×10^{-11}
		2000V/mm	4.0×10^{-11}	1.8×10^{-11}	2.5×10^{-12}	3.9×10^{-10}	3.0×10^{-10}	2.3×10^{-11}
		5000V/mm	1.9×10^{-10}	5.0×10^{-11}	5.4×10^{-12}	8.0×10^{-10}	4.5×10^{-10}	2.9×10^{-11}

With Eq. (5.38) and (5.39), the charge in the charge layers and the mobility of the charge carriers can be denoted as

$$\begin{cases} Q_a = \pi^2 C_a / \left[8S(\pi-2)b_a\right] \\ \mu_a = b_a q l^2 / (kT\pi^2) \end{cases}. \tag{5.40}$$

in which, Q_a (C) and μ_a ($m^2\ s^{-1}\ V^{-1}$) are the amount of the total charge in charge layer and the mobility of *a*-th charge carriers.

Then the correlation between the dissociated conductivity and the total charge in the charge layer can be described as

$$\frac{I_1(4b)}{2b} K_r n^2 qSl\Delta T = Q_a S . \tag{5.41}$$

where, I_1 is the modified Bessel function of the first kind and $I_1(x) = \sum_{m=0}^{\infty} \frac{1}{m!\Gamma(m+2)} \left(\frac{x}{2}\right)^{2m+1}$.

The dissociated conductivity can be denoted as

$$\sigma_{d(a)} = 2n\mu_a q = \frac{2b_a q^2 l^2}{kT\pi^2} \sqrt{\frac{2Q_a b}{qI_1(4b)K_r l\Delta T}} \tag{5.42}$$

The field dependence of the mobility and the relevant dissociated conductivity of Shell ZX-I oil and Hydro Quebec oil can be found in Tables 5.2 and 5.3, respectively. As seen from Table 5.2, there are at least three different types of charge carriers in Shell oil at both 30 °C and 90 °C. As the mineral oil is a mixed compound of paraffin, naphthene and aromatic, there should be different kinds of charge carriers in the mineral oil and these charge carriers might not share the same mobility [88-90]. Also, the dissociated conductivity that is contributed by the charge carriers with the same mobility does not change much with the electric field, which indicates that the depolarization process strongly relies on the ionic drift and diffusion. When the temperature increases, the dissociation rate also becomes higher and more charge carriers are generated from ionic pairs. As observed from Table 5.2, the total dissociated conductivity increases with the temperature, which is consistent with the experimental results shown in Chapter 2 and 3. However, the differences among the dissociated conductivity of the charge carriers that have a mobility of 3.83×10^{-6} $m^2/S/V$ are more significant when compared with the differences among the dissociated conductivity of other charge carriers. Because these charge carriers have a very high mobility (3.83×10^{-6} $m^2/S/V$), they might not be the ions. At the very beginning of the depolarization, the remaining fast charge carriers might participate into the conduction process and affect the depolarization current to be measured. Besides, Eq. (5.38) is flawed as it does not take account of the high order component and these high order components will affect the experimental fitting at the beginning of the depolarization process.

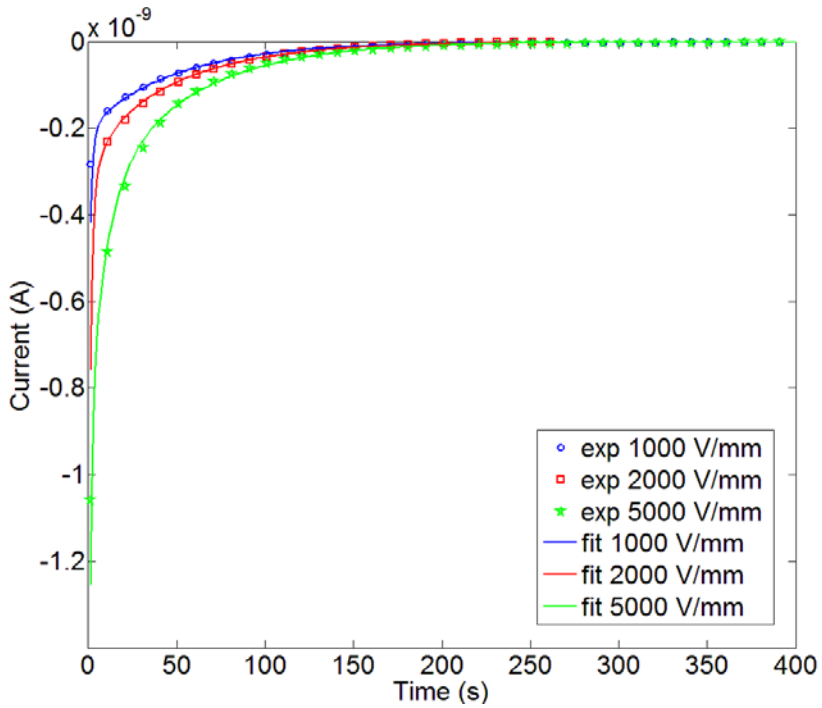

Fig. 5.2 Comparison between theory and measurements on the depolarization current in Shell ZX-I oil at90°C. The drawn-out curves are theoretical value from Eq. (5.38).

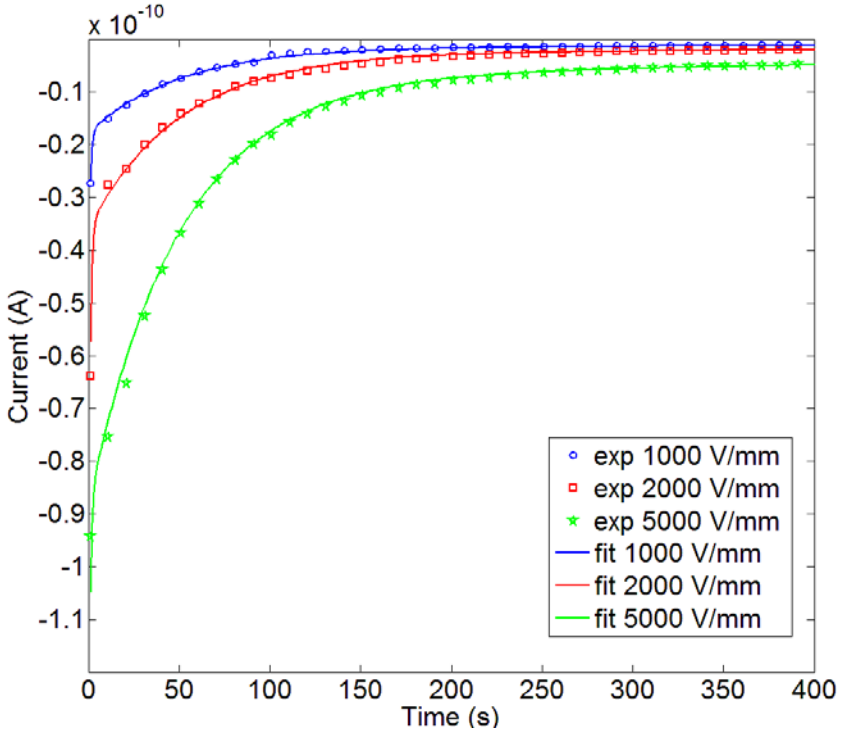

Fig. 5.3 Comparison between theory and measurements on the depolarization current in Shell ZX-I at 30°C. The drawn-out curves are theoretical value from Eq. (5.38).

As seen from Table 5.3, there are also three kinds of charge carriers with different mobility in the Hydro Quebec oil. The dissociated conductivity that is contributed by the

charge carriers with the same mobility does not change much with the electric field and the total dissociated conductivity increases with temperature. As Hydro Quebec oil has been aged for 10 years, this oil has suffered from electric, thermal and chemical stress, therefore the amount of the dissociated charge carriers in Hydro Quebec oil should be higher than that in Shell ZX-I oil. As observed from Table 5.3, the total dissociated conductivity of Hydro Quebec oil is slightly higher than that in Shell ZX-I oil. As observed in Chapter 2, both the steady- state and the initial conductivity current of Hydro Quebec oil experimentally measured are about 10-50 times higher than that of Shell ZX-I oil. Thus, other types of electric transportation should be involved in the polarization period.

Table 5.2 field dependence of the mobility and the dissociated conductivity of Shell ZX-I oil

temperature	μ_a ($m^2/s/V$)	$\sigma_{d(a)}$ (pS/m)			
		1000 V/mm	2000 V/mm	5000 V/mm	average
30 °C	3.83×10^{-6}	0.38	0.49	0.27	0.38
	7.65×10^{-8}	0.31	0.36	0.36	0.34
	3.82×10^{-9}	0.10	0.11	0.10	0.10
90 °C	3.20×10^{-7}	1.36	0.82	1.21	1.11
	6.39×10^{-8}	1.36	1.31	0.94	1.21
	6.39×10^{-9}	0.14	0.16	0.11	0.14

Table 5.3 Field dependence of the mobility and the dissociated conductivity of Hydro Quebec oil

temperature	μ_a ($m^2/s/V$)	$\sigma_{d(a)}$ (pS/m)			
		1000 V/mm	2000 V/mm	5000 V/mm	average
30 °C	3.83×10^{-6}	0.42	0.56	0.79	0.58
	1.92×10^{-7}	0.34	0.38	0.38	0.37
	1.53×10^{-9}	0.16	0.14	0.12	0.14
90 °C	6.39×10^{-7}	1.73	2.27	1.98	1.87
	6.39×10^{-8}	1.77	1.98	1.49	1.75
	2.24×10^{-9}	0.66	0.55	0.38	0.53

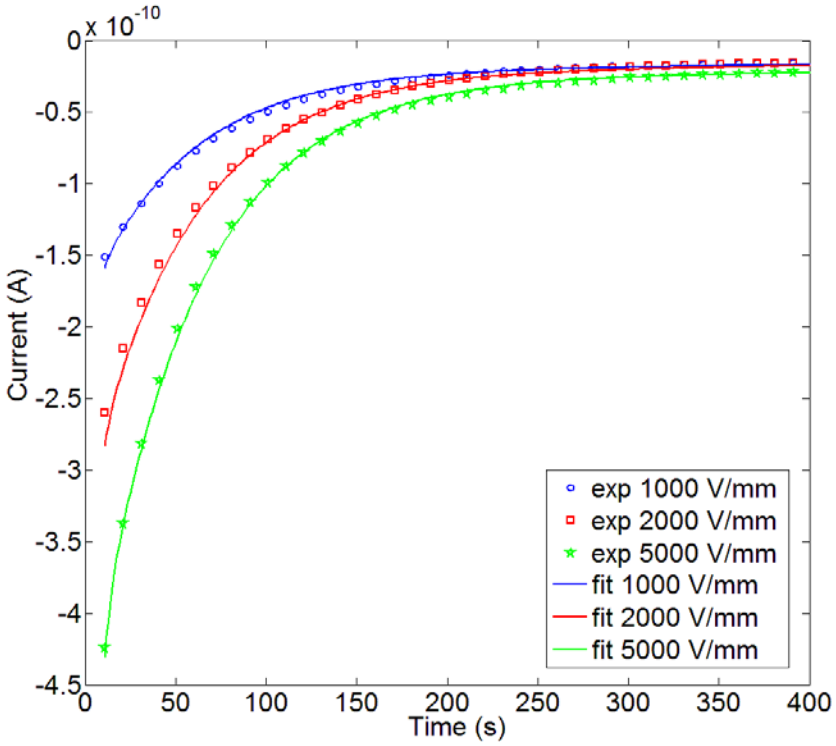

Fig. 5.4 Comparison between theory and measurements on the depolarization current in Hydro Quebec at 90°C. The drawn-out curves are theoretical value from Eq. (5.38).

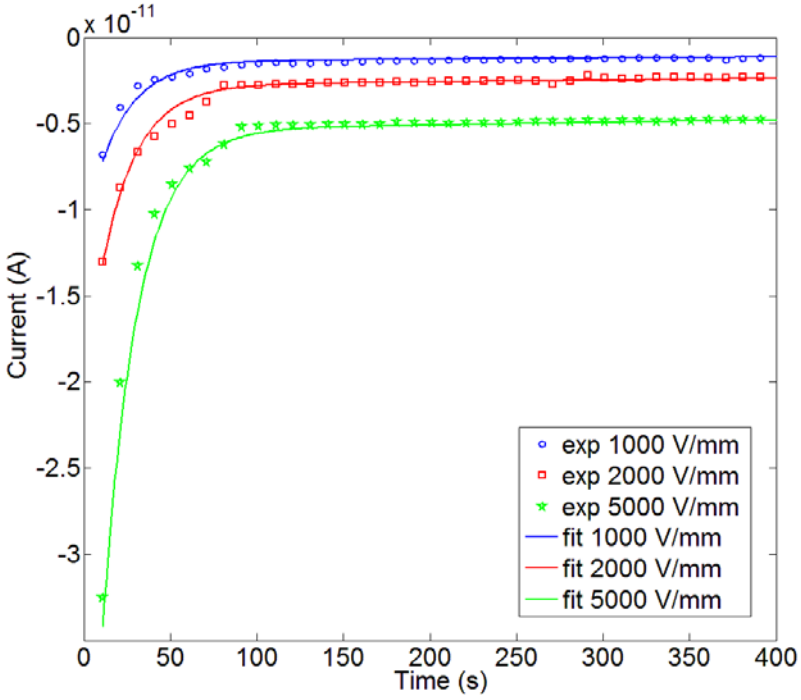

Fig. 5.5 Comparison between theory and measurements on the depolarization current in Hydro Quebec oil at30°C. The drawn-out curves are theoretical value from Eq. (5.38).

Once the ionic charge carriers move to a region that is close to the electrode, they can be neutralized through electrode desorption. As the desorption coefficients for different

types of ions are not the same and the desorption process can surly be affected by the electric field, therefore, the fitted values of the conductivity and mobility are only approximation. How these fitted values can be related to the chemical properties of mineral oil is still not very clear and more research is needed.

In Chapter 4, a modified Coelho model has been proposed, which is given in Eq. (4.101), to explain the dielectric behaviour of mineral oil in frequency domain. As the motion of these injected charge carriers can only affect the imaginary part of the complex permittivity and the real part of the complex permittivity mainly depends on the drift and diffusion of the dissociated charge carriers, the real part of the complex permittivity of Shell ZX-I oil and Hydro Quebec oil should not differ much from each other.

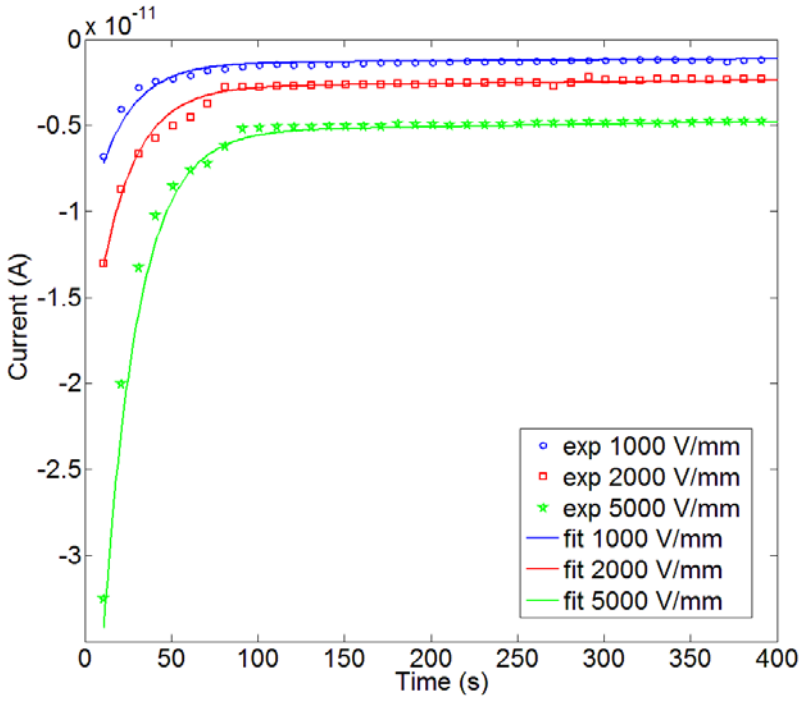

Fig. 5.6 Comparison between theory and measurements on the depolarization current in Hydro Quebec oil at30°C. The drawn-out curves are theoretical value from Eq. (5.37).

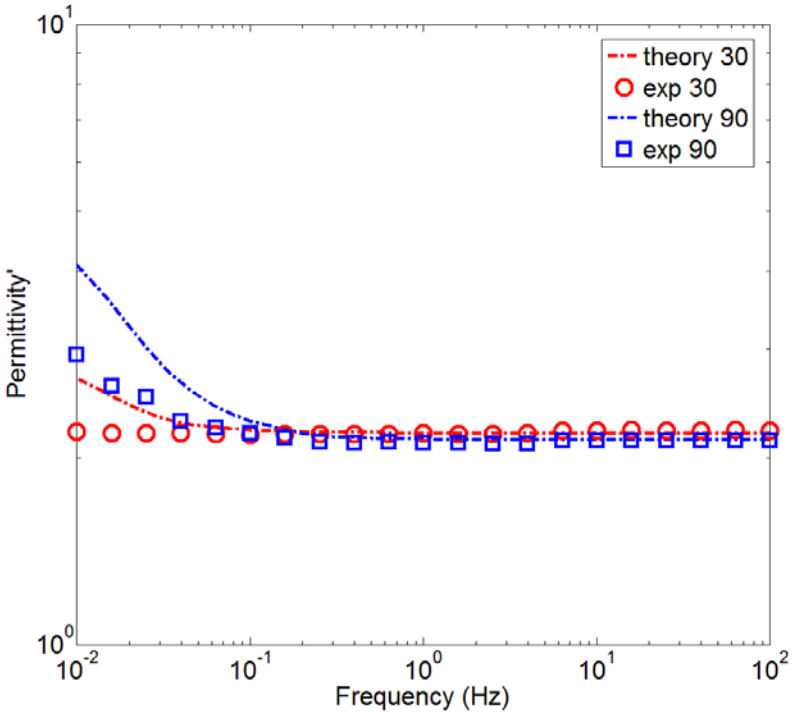

Fig. 5.7.Comparison between theoretical and experimental value of the real part of the complex permittivity of Shell ZX-I oil

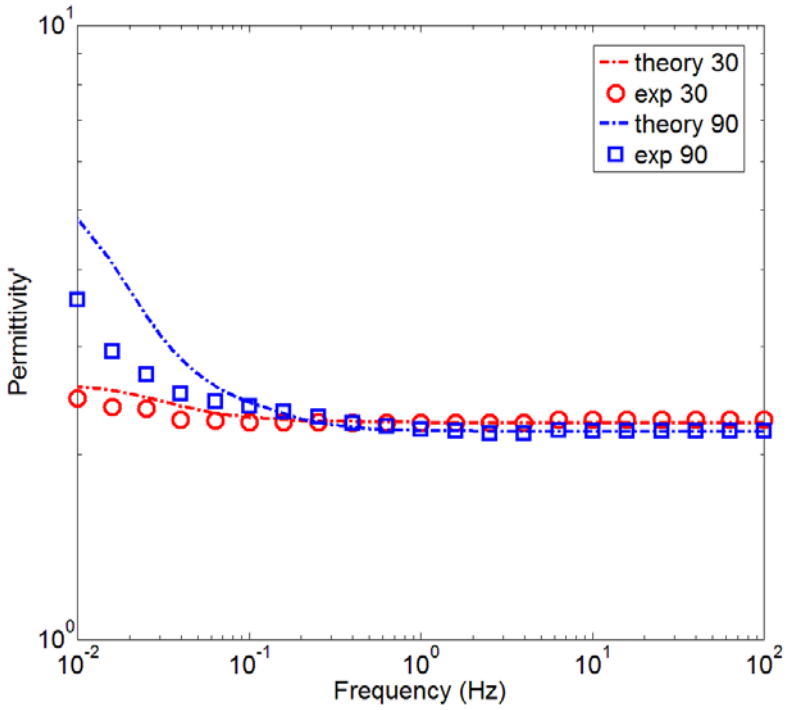

Fig. 5.8.Comparison between theoretical and experimental value of the real part of the complex permittivity of Hydro Quebec oil

The calculated values of the real part of the complex permittivity and the values measured experimentally of Shell ZX-I oil and Hydro Quebec oil are illustrated in Fig. 5.6 and Fig. 5.7, respectively. As seen from Fig. 5.6 and Fig. 5.7, the differences between the experimental values of the real part of the complex permittivity of these two kinds of

mineral oils are not significant, which means the space charge polarizations in Shell ZX-I oil and Hydro Quebec oil can be similar. The calculated complex permittivity using Eq. (4.101) is always higher than the experimental data. The calculated plots do not differ much from each other at the same temperature and this is consistent with the experimental observation.

As Coelho's model does not take account of the ionic adsorption at the electrode, the real part of the complex permittivity calculated using Coelho's model should be higher than the actual value. Besides, Eq. (5.42) used to calculate the dissociated conductivity is not right in a rigid way. When the charge carriers are not evenly distributed between the electrodes, the internal field is distorted by the presence of the space charge. As the knowledge about the distribution of the charge carriers in the vicinity of the electrode is still limited and the non-linearity of the ionic drift and diffusion model, to obtain an analytical solution for the depolarization current with the field distortion being taken into account is not practical and Eq. (5.42) is only an approximation. The depolarization current involves the current contributed from both ionic drift and diffusion, thus, the extraction of charge in charge layer is determined by both the diffusion and drift of charge carriers. As Eq. (5.42) only takes consideration of the ionic diffusion process, the calculated total charge in the charge layer is higher than the actual value, thus, the real part of the complex permittivity calculated using Eq. (4.101) is higher than the experimental results.

Please note, if the field is low, Eq. (5.13) is not valid as the newly generated charge carriers are unable to reach the electrode in a short of time. When the field is high, there are both injected charge carriers and dissociated charge carriers in the mineral oil. These injected charge carriers might react with the dissociated charge carriers or the neutral molecules and generate new charge carriers. Therefore, the analysis method proposed in this chapter is only valid for a medium electric field. In this chapter, the maximum and minimum field used in PDC measurement is 5 kV/mm and 1 kV/mm, respectively. As seen from Table 5.2 and 5.3, the conductivities calculated from the depolarization current do not change much with the electric field, which implies that the majority charge carriers in the charge layer is the dissociated ions. Thus, the injection current may be not high and the medium electric field here means 1 kV/mm- 5 kV/mm. Also, the coefficient of the extraction at the electrode cannot be measured directly by the experiment and this coefficient may change with the electric field. When the field is high, the measured

experimental results are fluctuated due to the non-linearity in the mineral oil and to acquire this coefficient through the method proposed in this chapter becomes difficult.

5.3 Conclusion

The time dependent curves of depolarization current of the mineral oilare well fitted using the exponential equations. The total charge density in the charge layer increases with temperature and aging of the oil. The total dissociated conductivity does not change much with the electric field which indicates that the depolarization process mainly depends on the motion of the dissociated charge carriers. When the temperature increases, the total dissociated conductivity increases. However, the electric conduction in mineral oil is still not very clear and more research is needed.

Chapter 6 Polarization and Depolarization Current (PDC) Measurement of the Oil/Pressboard Insulation

Polarization and depolarization current measurement technique can be used to evaluate the condition of the insulating material in power transformer effectively. The study on this time-domain measurement is still quite limited and an R-C equivalent circuit model has been proposed to explain the dielectric behaviour of oil/pressboard insulation. The dielectric properties of oil/pressboard degrade with time under a combined thermal, electrical, mechanical, and chemical stresses resulting in transformer failure eventually. Properly assessing the insulating properties of oil/pressboard insulation is crucial to the remaining life prediction of a transformer.

Here, PDC measurement has been carried out on oil/pressboard insulation under different pressure, temperature and electric field.

6.1 Experiment procedures

The experimental kit for DC conductivity measurement of oil/ pressboard insulation is the same testing system described in Chapter 2. The experimental procedure follows the recommendation from CIGRE joint working group A2/D1.41 “HVDC transformer insulation: oil conductivity”. First, the pressboard is dried in a vacuum oven at 90°C for at least 2 days. Second, put the pressboard sample in the test cell and then vacuum the test cell. Once the pressure of the test cell is below 100 Pa, inject the mineral oil into the test cell and heat the test cell to 90°C. Fourth, maintain the test cell at 90°C for at least 24 hours and then cool the test cell to the required temperature. Fifth, start the measurement and record the data.

The pressboard used in this experiment is new pressboard with a thickness of 1mm. The oil in which the pressboard impregnated is Shell S3 ZX-I mineral oil. The water content of the mineral oil is 4 ppm before the measurement and 7-9 ppm after the measurement. A DC voltage is applied on the test sample for 3 hours which is required by

CIGRE working group A2/1.41 and then the voltage is removed and the depolarization current is recorded.

6.2 PDC principle theory and classic equivalent circuit model

The PDC measurement is an effective method in the time domain to investigate the slow dielectric polarization in insulating materials[67, 77-85]. When an electric field is applied on the media to be tested, the current density $J(t)$ (A/m^2) flowing through the external circuit can be denoted as

$$J(t) = \sigma E(t) + \varepsilon_0 \varepsilon_r \frac{dE(t)}{dt} + \varepsilon_0 \frac{d}{dt} \int_0^t f(t-\tau) E(\tau) d\tau \tag{6.1}$$

where $f(t)$ is the response function of the dielectric material and σ is the DC conductivity, ε_0 (F/m) is the permittivity of the vacuum, ε_r is the relative permittivity, σ (S/m) is the conductivity and $E(t)$ (V/m) is the electric field. If the sample can be treated as a homogeneous material, the electric field $E(t)$ can be replaced with the external voltage $U(t)$ (V). Then the current can be written as

$$i(t) = C_0 \left[\frac{\sigma}{\varepsilon_0} U(t) + \varepsilon_r \frac{dU(t)}{dt} + \frac{d}{dt} \int_0^t U(\tau) f(t-\tau) d\tau \right] \tag{6.2}$$

where C_0 (F) is the geometrical capacitance of the dielectric material.

If the test object is completely discharged and a step voltage with the following characteristics is applied,

$$U(t) = \begin{cases} 0 & (t < 0) \\ U_0 & (0 \le t \le t_p), \\ 0 & (t > t_p) \end{cases} \tag{6.3}$$

It is easy to notice that the current will be zero when $t < 0$. If $0 \le t \le t_p$, the external voltage U_0 is applied on the sample. The polarization current contributed from the DC conductivity and the different polarizations can be expressed as

$$i_p(t) = C_0 U_0 \left[\frac{\sigma}{\varepsilon_0} + f(t) \right] \tag{6.4}$$

Once the sample is short circuited when $t > t_p$, the relaxation of the polarizations builds up the depolarization current, which can be described as

$$i_{dep}(t) = -C_0 U_0 \left[f(t) - f(t+t_p) \right] \tag{6.5}$$

If the charging time t_p (s) is long enough so that the entire system has entered a quasi-equilibrium state, $f(t+t_p)$ is negligible and the depolarization current is determined by $f(t)$. The R-C equivalent circuit model, which is shown in Figure 3.1, has been suggested to describe the dielectric response of the dielectric sample [69-71, 79-84, 89]. According to this model, the polarization current can be denoted as

$$i_p(t) = \frac{U_0}{R_0} + \sum_i \frac{U_0}{R_i} \exp\left(-\frac{t}{R_i C_i} \right) \tag{6.6}$$

Similarly, the depolarization current can be calculated as

$$i_{dep}(t) = -\sum_i \frac{U_0 \left(1 - \exp\left(-\frac{t_p}{R_i C_i} \right) \right)}{R_i} \exp\left(-\frac{t}{R_i C_i} \right) \tag{6.7}$$

However, please note that the dielectric response function is only valid when the sample can be treated as a homogeneous media. When there are mobile charge carriers in the sample, the electric field can rearrange the distribution of the charge carriers and the charge carriers are no longer evenly distributed in the tested media. Thus, the assumption that the electric field is homogeneous is not correct in a rigid way. When the field is really small, the charge carriers cannot drift far away from their original position and the electric field can be approximated as an evenly distributed field. When the applied field is high, the difference between the density of charge carrier is huge between the two metal electrodes and the field distortion cannot be ignored. However, if the field is high enough, the blocked charge carriers in the vicinity of the electrode are unable to shield the field any longer, the field distortion caused by the charge layer is negligible and the internal field can be treated to be constant again. Besides, the charge injection effect can be significant under a high electric field, which is negligible in the depolarization process. Therefore, the dielectric response function may not be exactly the same in both the polarization and the depolarization process, which will be discussed later.

6.3 Results and discussion

Fig. 6.1 depicts the polarization current measured when the pressboard is subject to a pressure of 2 kPa under different electric fields at 30℃. The polarization current

measured when the applied field is lower than 2 kV/mm does not change much with the time. The current measured at 1 kV/mm is higher than that measured under other electric field except10 kV/mm. The long-term current decreases with the electric field, whilst the long-term current observed under a field of 10 kV/mm is close to that measured under a field of 1 kV/mm. The long –term current reaches a minimum value under a field of 5 kV/mm. The current that flows through the oil impregnated pressboard under a low electric field (below 2 kV/mm) is about 5-10 times higher than that measured in the same mineral oil. If the pressure on the pressboard is low, a tight contact between the pressboard and the electrodes cannot be ensured. Thus, oil gap might exist at the interface of pressboard/electrode and the electric conduction may be affected. However, the mechanism of electric conduction under the condition that the pressboard is subject to a low pressure is not clear and more research is needed.

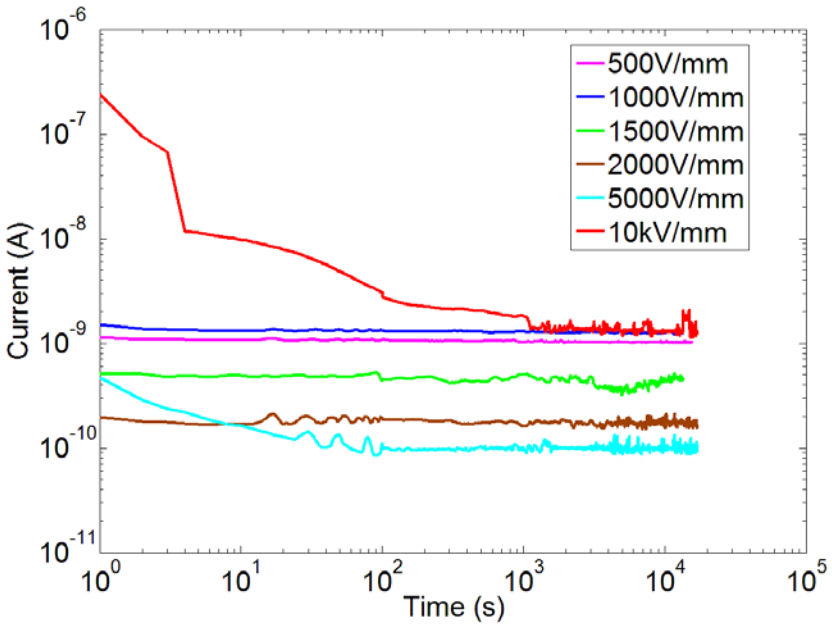

Fig. 6.1 Polarization current of oil/ pressboard with a pressure of 2 kPa on the pressboard at 30°C

According to the requirement from CIGRE A2/1.41 group, a pressure that is close to 10 kPa on the pressboard is required in the DC conductivity measurement. Thus, a lead plate has been added to the electrode system to increase the pressure on the pressboard to 9 kPa. Figs. 6.2-6.3 illustrate the field dependence of the polarization and depolarization current of the oil/pressboard at 30°C when the pressboard is subject to a pressure of 9 kPa. As seen from Fig. 6.2, the long-term current increases with the electric field. In contrast to the experimental data shown in Fig. 6.1, the polarization current always decreases with

the time. The time dependent polarization current under a field of 10 kV/mm becomes noisy after 1000 second. The charge injection can be enhanced by the electric field and the presence of the space charge can distort the internal field leading to a field enhancement between the parallel electrodes, thus, the current flows through the oil/pressboard becomes unstable if the electric field is high.

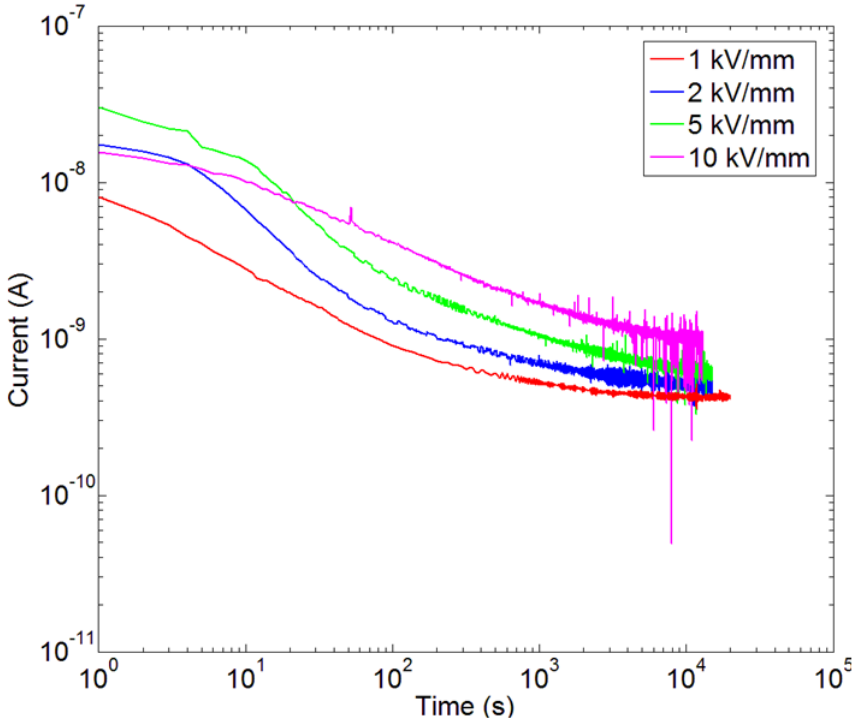

Fig. 6.2Polarization current of oil/ pressboard with a pressure of 9 kPa on the pressboard at 30℃

As seen from Fig. 6.3, the depolarization current decreases with the time. Once the external voltage is removed and the two parallel electrodes are short-circuited, the previous activated polarizations get depolarized resulting in a depolarization current. The magnitude of the depolarization current also increases with the field,as stronger polarizations can be built up in the oil/pressboard insulation under a higher electric field. The initial values of the polarization current are very close to that of the depolarization current. However, how the depolarization process relate to the motion or rotation of the charge carriers in the oil/pressboard insulation is still not clear.

The field dependence of the polarization and depolarization current in oil/pressboard insulation at 90 ℃ with a pressure of 9 kPa on the pressboard is shown in Fig. 6.4-6.5. The initial value and the long –term value of the polarization current both increase with the electric field. The curve of the time dependence of the polarization current under a field of 10 kV/mm is quite noisy, which is similar to that measured at 30 ℃. The initial

values of the depolarization current are also close to that of the polarization current. The long-term current is about 10 times higher when compared to that obtained at 30 °C under the same electric field.

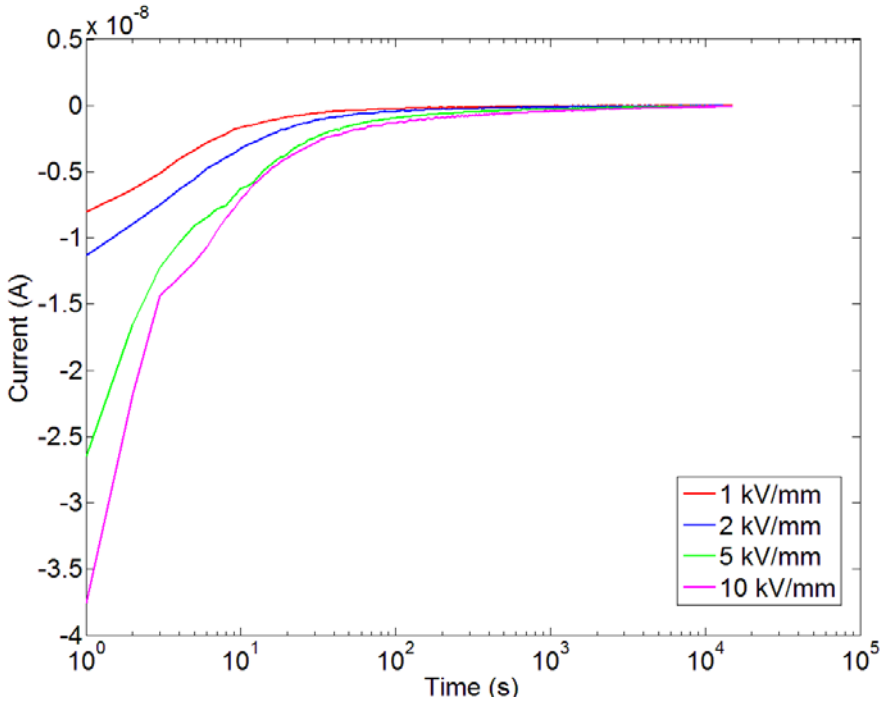

Fig. 6.3Depolarization current of oil/ pressboard with a pressure of 9 kPa on the pressboard at 30°C

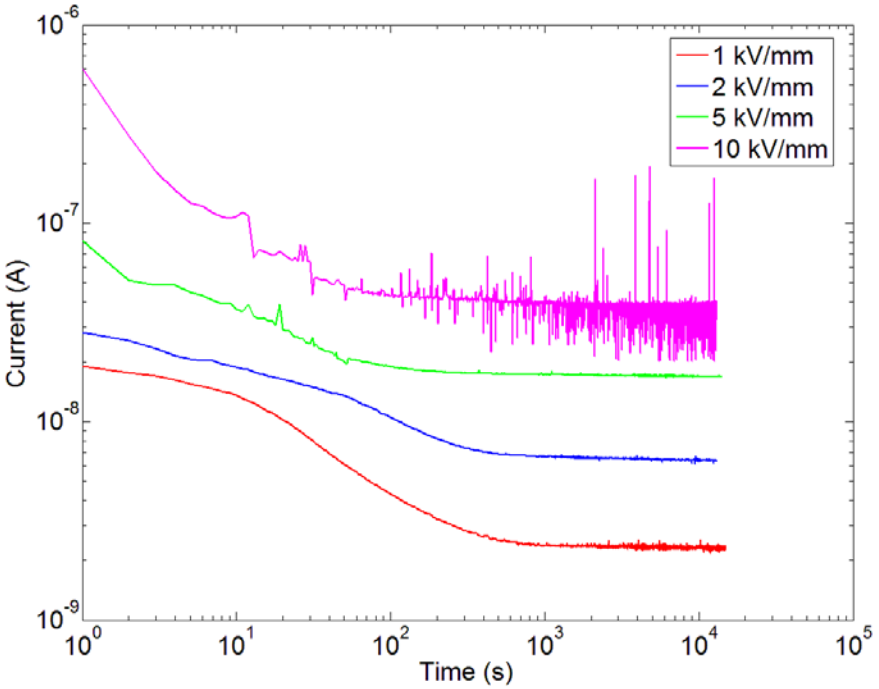

Fig. 6.4Polarization current of oil/ pressboard with a pressure of 9 kPa on the pressboard at 90°C

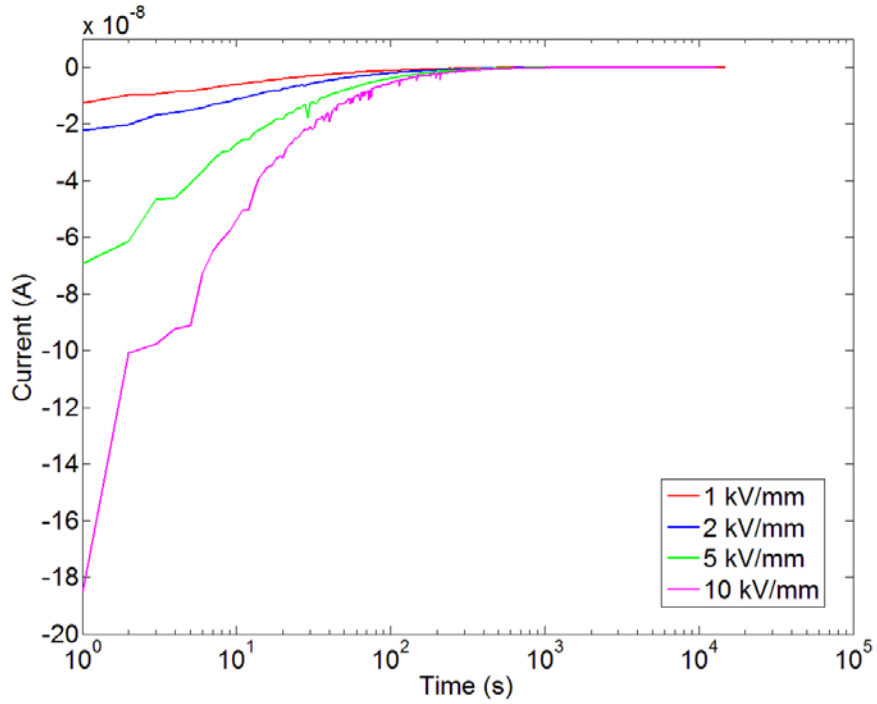

Fig. 6.5Depolarization current of oil/ pressboard with a pressure of 9 kPa on the pressboard at 90℃

Fig. 6.6 shows the field dependence of the long-term conductivity of the oil/pressboard insulation. As seen from Fig. 7.6, the conductivity measured when the pressboard is subjected to a high pressure does not change much with the electric field at both 30℃ and 90℃. The long-term conductivity measured when a high pressure is applied on the pressboard decreases slightly with the electric field at 30 ℃. It seems the conducting current has entered a saturate region. Once the charge carriers are generated in the bulk, it will be immediately extracted by the electric field. Therefore, the polarization current is proportional to the generating rate of the charge carriers. If the generating rate does not change much with the electric field, the increase of the current is negligible and the conductivity will decrease with the electric field. In contrast to the result observed at 30 ℃, the long-term conductivity measured under the same pressure at 90℃ increases with the electric field, which suggests there might be sufficient charge carriers in the oil/pressboard layer or the charge carrier generating rate increases with the electric field. When the pressure is low, the conductivity decreases with the electric field dramatically, reaches a minimum value at a field of 5 kV/mm and then the conductivity starts to increase with the field. If the pressure on the pressboard is low, a tight contact between the pressboard and the electrodes cannot be ensured. Thus, oil gap might exist at the interface of pressboard/electrode and the electric conduction may be affected. However,

the influence of the pressure on the conductivity of oil/ pressboard insulation is still not very clear.

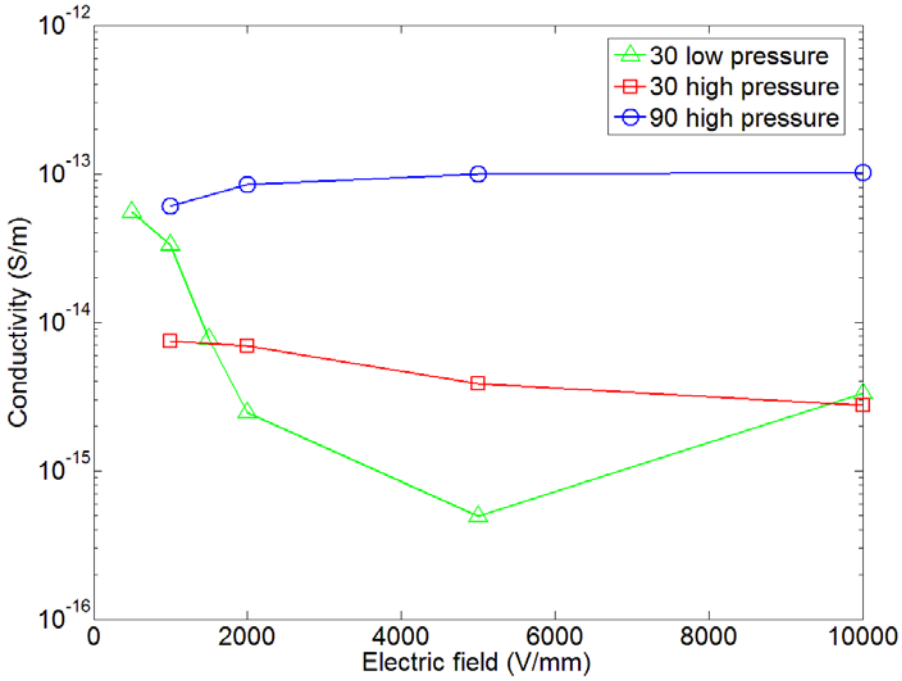

Fig. 6.6Field dependence of the long-term conductivity under different pressures

To sum up, it seems that the polarization and depolarization current increase with the electric field and the temperature. The pressure on the pressboard can affect the PDC measurement of oil/pressboard insulation. However, the mechanism of the electric conduction in oil/pressboard is not clear and more researches are needed.

6.4 Improved R-C equivalent circuit model

The oil conductivity, dielectric response function, pressboard conductivity and the water content between the pressboard and the oil can affect the electric conduction in oil impregnated pressboard insulation system [67-84]. The mobility of the charge carriers in the liquid is usually higher than that in the pressboard and the initial polarization current is supposed to be contributed by the motion of the charge carriers in the liquid, whilst, the drift and diffusion of the charge carriers in the pressboard can be attributed to the long-term DC conductivity [74-76]. Some publications have reported that the steady-state current is determined by the conductivity of the pressboard and the initial current is related to the oil conductivity [74-76].

It is commonly accepted that the dielectric response of the oil/pressboard insulation can be simulated with the R-C equivalent circuit model [69-71, 79-84, 89]. As seen from Fig 3.1, this model consists of a series of connection of capacitor and resistor. The capacitance C_{50} (F)is the total capacitance measured at power frequency. The resistor R_0 (Ω) is the long term DC conductivity. The dielectric polarization processes are represented by different R_i-C_i branches. In our previous discussion, the polarization and depolarization current can be denoted with Eqs. (6.6) and (6.7), respectively. If these two equations are combined together, the difference between the magnitude of the polarization current and depolarization current can be calculated as,

$$i_{diff}(t) = i_p(t) + i_{dep}(t) = \frac{U_0}{R_0} + \sum_i \left[\frac{U_0 \exp\left(-\frac{t_p}{R_i C_i} \right)}{R_i} \right] \exp\left(-\frac{t}{R_i C_i} \right) \tag{6.8}$$

If t_p (s) is larger enough and a quasi-equilibrium state has been reached, Eq.(6.8) becomes

$$i_{diff}(t) = i_p(t) + i_{dep}(t) \approx \frac{U_0}{R_0} \tag{6.9}$$

It seems that the difference between the magnitudes of the time dependent polarization current and depolarization current can be approximated as a constant value under the condition that the electrification time is long enough so that the system has entered a quasi-steady state. However, most of the reports reveal that the difference between the magnitudes of the polarization and depolarization current changes with the time [71-81, 84-89]. Thus, this classic equivalent circuit model, to some degree, still needs to be improved.

To simplify the quantitative analysis, a new parameter, the added depolarization current, $i_{adep}(t)$ (A), will be defined as

$$i_{adep}(t) = \left| -\frac{U_0}{R_0} - \sum_i \frac{U_0 \left(1 - \exp\left(-\frac{t_p}{R_i C_i} \right) \right)}{R_i} \exp\left(-\frac{t}{R_i C_i} \right) \right| \tag{6.10}$$

If the polarization time is long enough, the insulating media will reach the quasi-equilibrium state and the change of the current is insignificant. Then the magnitude of the

added polarization current will be close to that of the polarization current, which can be described as:

$$i_{adep}(t) = \frac{U_0}{R_0} + \sum_i \frac{U_0}{R_i} \exp\left(-\frac{t}{R_i C_i}\right) \approx i_p(t) \tag{6.11}$$

Figs. 6.7 and 6.8 describe the time dependence of the difference between the magnitude of the polarization current and the added depolarization current. As seen from Fig 6.7, almost all the polarization current is higher than the added depolarization current. The polarization current measured at 30 ℃ under a field of 10 kV/mm is lower than the added polarization current at the first few seconds. When the field is high, more charge carriers will be generated and more charge carriers can be blocked at the electrode. Once the tested sample is depolarized, the charge carriers stuck in the vicinity of the electrode will drift backwards to the bulk. Thus, a high charge density in the charge layer can result in a high depolarization current. The added depolarization current decreases faster than the polarization current and can reach the quasi-steady state more quickly, regardless the electric field. As observed from Fig. 6.8, the difference between the polarization current and the added depolarization current is slightly less discernible when compared to that measured at 30 ℃. When the field is 5 kV/mm, the added polarization current is higher than the polarization current. To sum up, the difference between the polarization current and the added depolarization current can be affected by the electric field and the temperature.

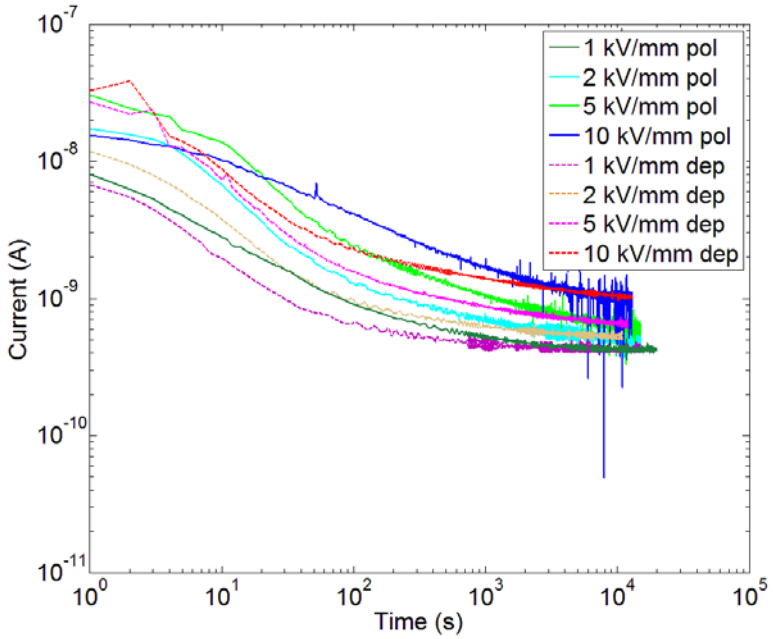

Fig.6.7 Time dependence of the magnitude of the polarization current and the added depolarization current under different electric field at 30℃

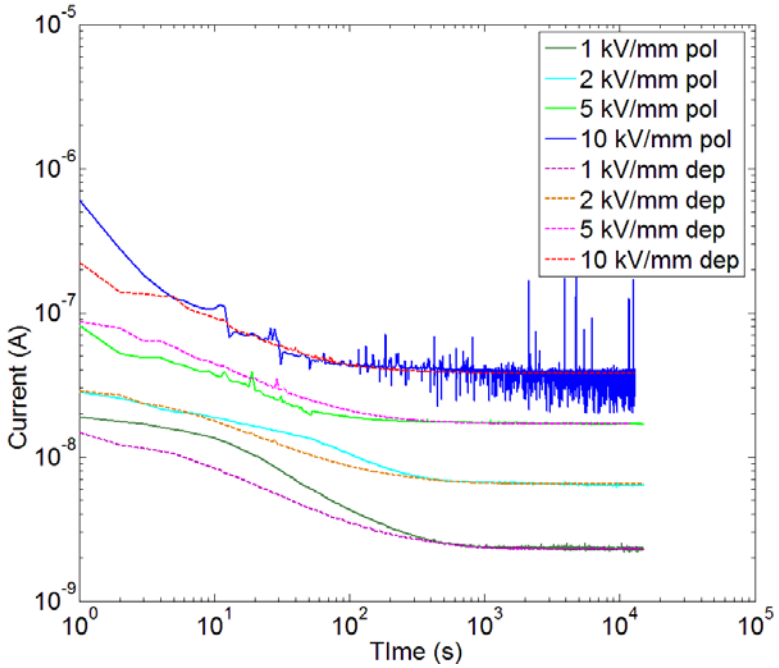

Fig.6.8 Time dependence of the magnitude of the polarization current and the added depolarization current under different electric field at 90℃

Electrode effect is a parasitic effect during dielectric response measurement since it can be added to the real dielectric response making experimental results difficult to understand. This effect originates from the blocking of charge carriers at the liquid/solid interface. This issue has been investigated for over 100 years and many models have been proposed [152, 169-175]. The accumulation of the positive and negative charge carriers in the vicinity of the electrode gives rise to an extra polarization [152]. Fricke has studied the electrode effect theoretically and he thought there might be a double layer in the vicinity of the electrode and the electrode effect is actually caused by the charging and discharging of that double layer [169-170]. Later, the correcting methods on the electrode effect have been discussed by Onaral and Schwan. They thought the electrode effect can be analysed by adding an extra R-C circuit to the original equivalent circuit [171-174]. Umino suggested that it is hard to measure the exact capacitance of the sample at very low frequency and he proposed a modified electrode polarization model. [175]

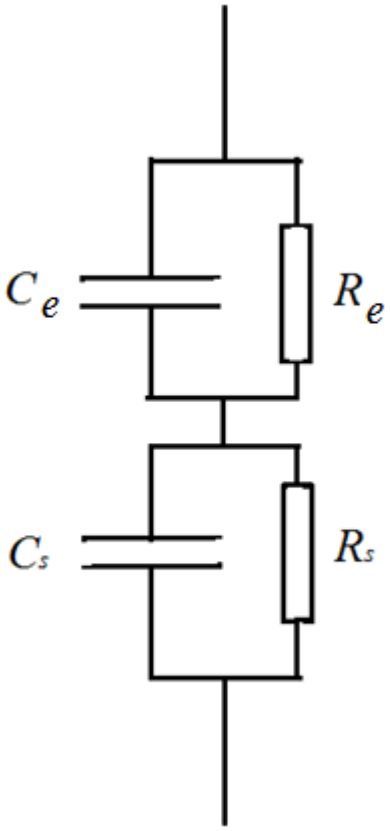

Fig. 6.9 RC model for the electrode effect proposed in [ref 175]

In Fig. 6.9, C_s (F) and R_s (Ω)is the capacitance and resistance for the sample, whilst C_e (F) and R_e (Ω)is the capacitance and resistance for the electrode surface. In the time domain measurement, this effect is more significant as there would be more charge carriers accumulating around the electrode. As the space charge effect has been clearly observed in oil/pressboard sample, it is necessary to add the electrode effect to the classic R-C equivalent circuit model [176-185]. The permittivity at 50 Hz is caused by electronic, dipole, and atomic polarization. When DC field is applied, these polarizations are fully polarized within a very short of time. Thus, this permittivity will not change with or without the charge layer. The long-term conduction in oil/pressboard is not very clear at the moment. For simplicity, an assumption that it cannot be affected by the uneven charge distribution in the bulk will be made. The resistors and capacitors that are represent the dielectric properties of the bulk and the equivalent circuit that stands for the electrode effect should be connected serially. Then the modified R-C equivalent model can be obtained and this model has been shown in Fig. 6.10.

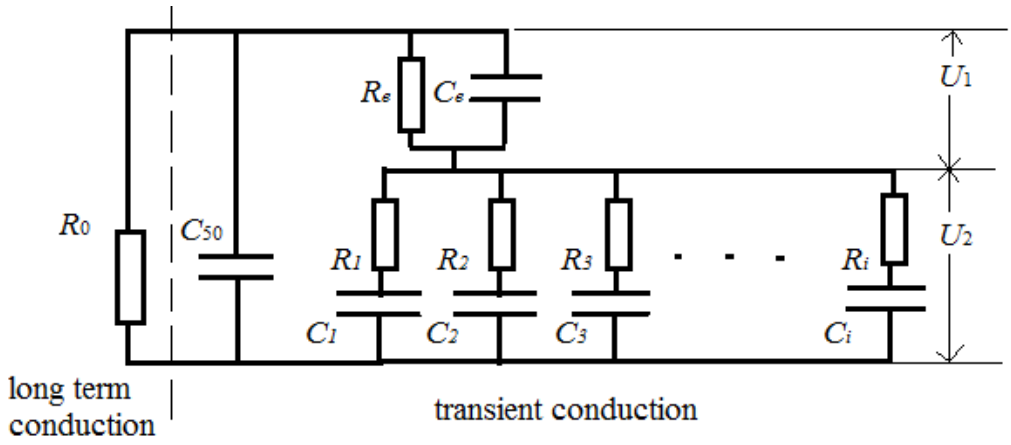

Fig. 6.10 Modified R-C equivalent circuit model for oil/pressboard sample

As seen from Fig 6.10, C_e (F) and R_e (Ω)is the capacitance and resistance to represent the electrode effect. The left part determines the steady- state current. When a step electric potential is applied, the transient conduction will be affected by the right part of this circuit and the transient current will finally become zero if the polarization time is long enough.

First, the total current flowing through this circuit when a step electric potential, U_0 (V), is applied at t = 0 will be discussed.

According to this modified model, the total current can be written as

$$I(t)=\frac{U_0}{R_0}+C_{50}\frac{dU_0}{dt}+\frac{U_1(t)}{R_e}+C_e\frac{dU_1(t)}{dt}. \tag{6.12}$$

With Kirchhoff's circuit law, it is easy to obtain

$$\frac{U_1(t)}{R_e}+C_e\frac{dU_1(t)}{dt}=\sum_i C_i\frac{dU_{bi}(t)}{dt} \tag{6.13}$$

with

$$R_iC_i\frac{dU_{bi}(t)}{dt}+U_{bi}(t)=U_2(t) \tag{6.14}$$

$$U_1(t)+U_2(t)=U_0 \tag{6.15}$$

where, $U_{bi}(t)$ (V) is the electric potential on the capacitance C_i (F). If Eqs. (6.13) - (6.15) are put together, it is a linear system of the differential equations of the first order. If $X(t)=[U_2(t),\ U_{b1}(t),\ U_{b2}(t),\ U_{b3}(t)\ \cdots\cdots U_{bi}(t)]^T$ is defined, the following expression can be obtained,

$$X'(t)=A(t)X(t)+F(t) \tag{6.16}$$

in which,

$$A(t)=\begin{bmatrix} -\frac{1}{C_e}\left(\frac{1}{R_e}+\sum_i\frac{1}{R_i}\right) & \frac{1}{R_1C_e} & \frac{1}{R_2C_e} & \cdots & \frac{1}{R_iC_e} \\ \frac{1}{R_1C_1} & -\frac{1}{R_1C_1} & & & \\ \frac{1}{R_2C_2} & & -\frac{1}{R_2C_2} & & \vdots \\ \vdots & & & & \\ \frac{1}{R_iC_i} & & \cdots & & -\frac{1}{R_iC_i} \end{bmatrix} \tag{6.17a}$$

$$F(t)=[\frac{U_0}{R_eC_e},\ 0,\ 0,\ \cdots,\ 0]^T \tag{6.17b}$$

Once the external electric field is removed and the two metal electrodes are short circuited, the electric potential between the two metal electrodes will be zero. Thus, Eq. (6.15) becomes

$$U_1(t)+U_2(t)=0 \tag{6.18}$$

Using Eqs. (6.13) and (6.14), the system of the first order differential equations for depolarization process can be denoted as

$$X'(t)=A(t)X(t) \tag{6.19}$$

If Eq. (6.19) and (6.16) are compared, it is simple to notice that the solutions for these two equations are different. Apparently, the polarization current and depolarization current calculated from this modified R-C model cannot be exactly the same, which is consistent with previous experimental results.

It is quite feasible to obtain $U_1(t)$ from the above equations. However, this procedure is complicated and it is also quite difficult to calculate the values for the parameters of the modified R-C model with the experimental results. If Eq. (6.19) and (6.16) are closely scrutinized, the solutions for these two expressions should have the following form,

$$U_1(t)=\sum_{n=1}^{i+1}A_n\exp\left(-\lambda_n t\right)+B \tag{6.20}$$

where, A_n and B are constant, λ_n is the eigenvalue of matrix $A(t)$. If $t\to\infty$, $U_1(t)=0$ .Consequently, $B=0$ and Eq. (6.20) becomes

$$U_1(t)=\sum_{n=1}^{i+1}A_n\exp\left(-\lambda_n t\right) \tag{6.21}$$

Similarly, if $t\to\infty$, $U_{bi}(t)=U_0$, Eq. (6.20) becomes

$$U_{bi}(t) = U_0 + \sum_{n=1}^{i+1} A_{n(bi)} \exp\left(-\lambda_n t\right) \tag{6.22}$$

The polarization and added depolarization current can be written as

$$i_p(t) = \sum_{n=1}^{i+1} D_{n(p)} \exp\left(-\lambda_n t\right) + \frac{U_0}{R_0} \tag{6.23a}$$

$$i_{adep}(t) = \sum_{n=1}^{i+1} D_{n(dep)} \exp\left(-\lambda_n t\right) + \frac{U_0}{R_0} \tag{6.23b}$$

with

$$D_n = A_n \left(\frac{1}{R_e} - \lambda_n C_e \right) \tag{6.24}$$

Please note, $D_{n(p)}$ is still equal to $D_{n(dep)}$ if the electrification time is sufficient long, which is similar with that in Eqs. (6.6) and (6.7).

However, as discussed in Chapter 5, the electric field can enhance the dissociation of ionic pairs and more charge carriers will be generated under a higher electric field. If these newly generated charge carriers can be extracted in a very short of time, the current induced by the ionic drift and diffusion is proportional to the dissociation rate. Once the external electric potential is removed, the dissociation rate will have a notable drop, along with the internal field. Also, as the internal field decreases, the velocity of the charge carriers becomes slower. Thus, it is necessary to consider that the difference of the resistors in the R-C equivalent circuit in the polarization and depolarization process. If all the polarization that are represented by the branches in the R-C equivalent circuit is induced from the motion of the charge carriers and the internal field does not change very much, the field dependent resistors can be written as

$$R_e(E) = \frac{R_e(0) K_d(0)}{K_d(E)} \tag{6.25a}$$

$$R_i(E) = \frac{R_i(0) K_d(0)}{K_d(E)} \tag{6.25b}$$

Thus, the matrix $A(t)$ becomes $\frac{A(t) K_d(0)}{K_d(E)}$ and Eq. (6.16) and (6.17) become

$$X'(t) = \frac{\left[A(t) X(t) + F(t)\right] K_d(0)}{K_d(E)} \tag{6.26a}$$

$$X'(t) = A(t) X(t) \tag{6.26b}$$

Please note, $K_d(E)$ (s^{-1}) is not the same dissociated rate introduced by Onsager and how to evaluate this coefficient is still not clear [76]. Apparently, the solution to Eqs. (6.26a) and (6.26b) still obey the same form shown in Eqs. (6.21) and (6.22). Because $A(t)$ does not change, $A(t)$ in Eq. (6.26a) and (6.26b) share the same eigenvalue as that in Eq. (6.21) and (6.22). It is easy to reach the conclusion that the $D_{n(p)}$ is not equal to $D_{n(dep)}$ and consequently, it is reasonable to fit the curve of the polarization current and the added depolarization current with Eq. (6.23a) and (6.23b) with different $D_{n(p)}$ and $D_{n(dep)}$.

Figs. 6.11-6.14 show the result of the analytical fitting method. The light blue, pink, red and blue curve stands for the fitted value of the polarization current or the added depolarization current under a field of 1 kV/mm, 2 kV/mm, 5 kV/mm and 10 kV/mm, respectively. The light blue, pink, red and blue marker represent the measured value of the polarization current or the added depolarization current under a field of 1 kV/mm, 2 kV/mm, 5 kV/mm and 10 kV/mm, respectively. As seen from Figs 6.11-6.14, good experimental fitting can be achieved. The relevant values of the parameters used in our fitting are shown in Table 6.1 and 6.2.

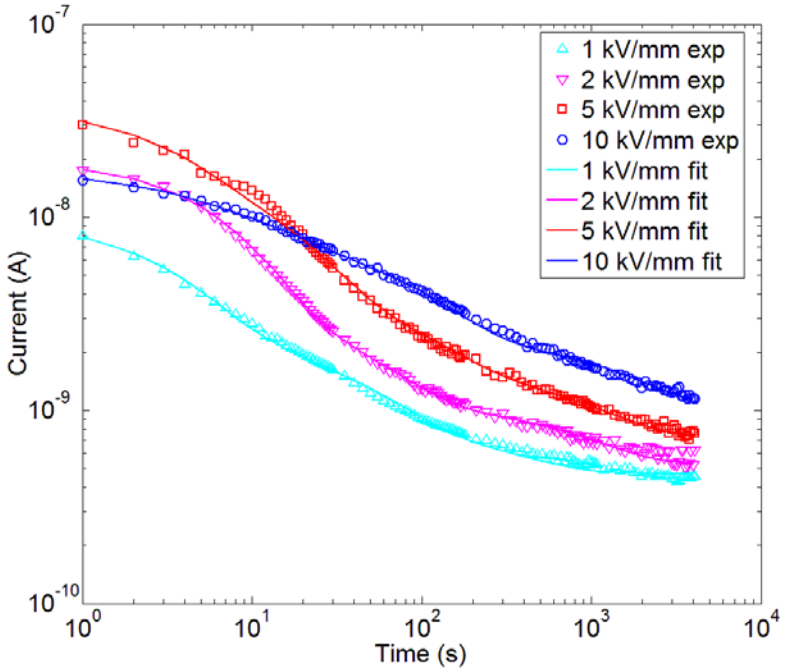

Fig. 6.11 Fit of the polarization current measured at different electric field at 30℃ using Eq. (6.23a)

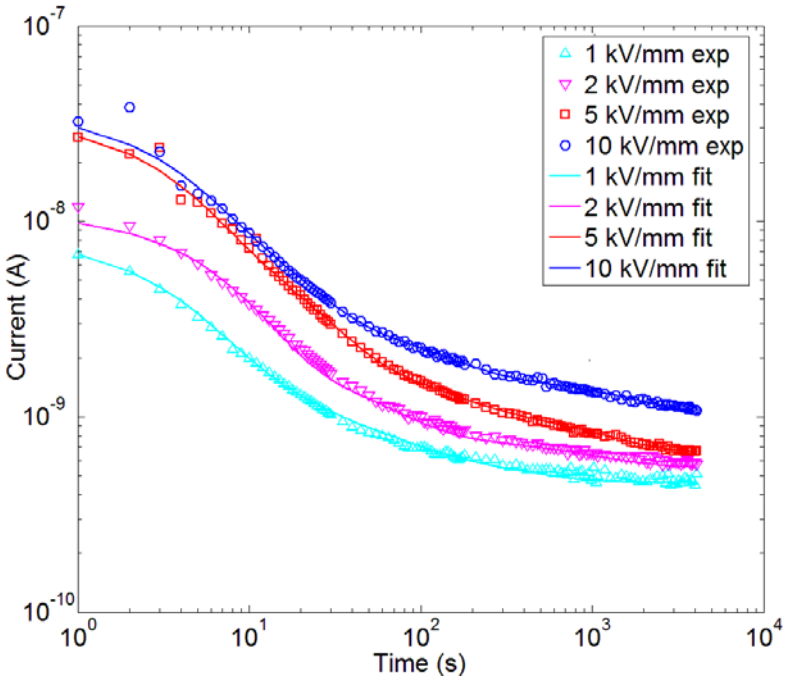

Fig. 6.12 Fit of the added depolarization current measured at different electric field at 30°C using Eq. (6.23b)

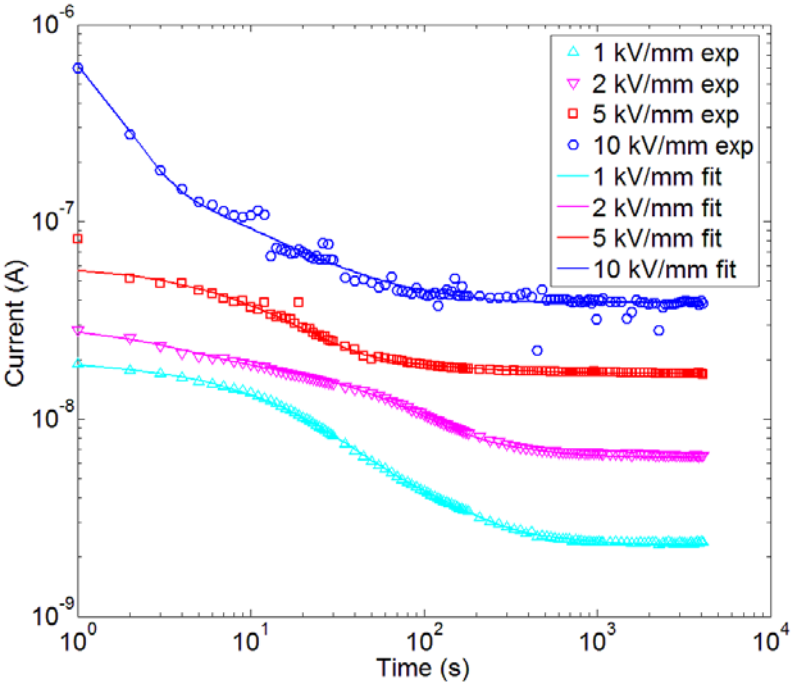

Fig. 6.13 Fit of the polarization current measured at different electric field at 90°C using Eq. (6.23a)

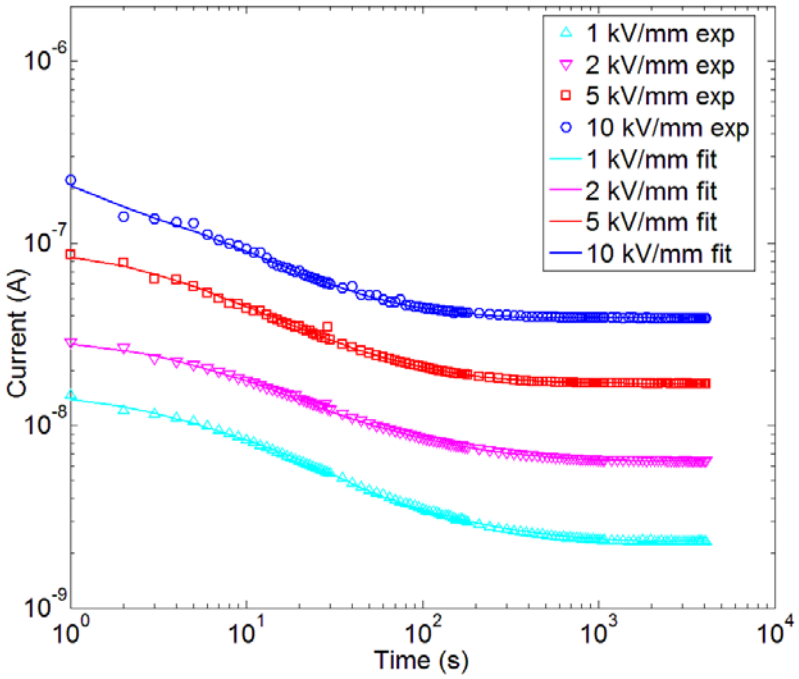

Fig. 6.14 Fit of the added depolarization current measured at different electric field at 90°C using Eq. (6.23b)

Table 6.1Fitting parameters of the polarization and added depolarization current at 30℃

30°C	λ_n	$D_{n(p)}$	$D_{n(dep)}$
1 kV/mm	3.00E-01	6.50E-09	5.60E-09
	1.00E-01	1.00E-09	1.50E-09
	2.00E-02	1.40E-09	6.00E-10
	3.00E-03	3.50E-10	2.20E-10
2 kV/mm	1.50E-01	1.40E-08	9.00E-09
	1.00E-01	2.70E-09	1.00E-09
	2.00E-02	2.20E-09	1.20E-09
	1.10E-03	5.50E-10	2.50E-10
5 kV/mm	3.00E-01	2.00E-08	2.50E-08
	6.00E-02	1.30E-08	7.00E-09
	1.00E-02	2.50E-09	2.50E-09
	1.00E-03	9.00E-10	5.00E-10
10 kV/mm	3.00E-01	4.00E-09	2.50E-08
	7.50E-02	6.00E-09	9.00E-09
	1.00E-02	5.00E-09	1.70E-09
	6.00E-04	1.35E-09	6.50E-10

Table 6.2 Fitting parameters of the polarization and added depolarization current at 90 ℃

90℃	λ_n	$D_{n(p)}$	$D_{n(dep)}$
1 kV/mm	3.00E-01	2.00E-09	5.00E-09
	5.00E-02	1.10E-08	6.00E-09
	1.00E-02	4.00E-09	1.70E-09
	2.00E-03	6.00E-10	6.00E-10
2 kV/mm	3.00E-01	1.00E-08	7.50E-09
	7.00E-02	1.00E-09	1.10E-08
	1.50E-02	1.10E-08	4.50E-09
	3.00E-03	2.00E-09	1.50E-09
5 kV/mm	3.00E-01	6.00E-09	3.50E-08
	7.00E-02	3.30E-08	3.00E-08
	1.50E-02	3.00E-09	1.10E-08
	3.00E-03	1.50E-09	2.00E-09
10 kV/mm	1.20E+00	1.50E-06	1.70E-07
	2.00E-01	8.00E-08	7.00E-08
	5.00E-02	4.80E-08	5.00E-08
	1.00E-02	1.50E-08	1.30E-08

Here, a preliminary study of the field dependence of the fitting parameters has been performed. The field dependences of the fitting parameter are shown in Figs. 6.15 and 6.16. The curves of the parameters λ_n and C_n are shifting towards the upper left corner at 30 ℃ when the electric field increases, whilst those curves are moving towards the upper right corner at 90 ℃. If the discussion in Chapter 4 is recalled, the type of the dominant charge carriers is different at 30 ℃ and 90 ℃ in the electric conduction. When the temperature is low, the electric conduction is determined by the ionic conduction. As the electric field increases, the charge injection will be enhanced and the electric double layer in the vicinity of the electrode can be disturbed. Also, the mobility and the diffusion coefficient of the ionic charge carriers are lower at 30 ℃ so that the diffusion effect is less significant when compared to that at 90 ℃. Therefore, a more intense charge layer can be formed at 30 ℃ and the system needs longer time to reach the equilibrium state. When the temperature increases, more injected charge carriers are generated and the conduction is dominated by the motion of these injected charge carriers. Besides, the ionic charge carriers move faster when the temperature is higher and the electric double layer can reach their equilibrium state more quickly. When the electric field increases, more charge carriers will be generated at the electrode by the injection and the chance of the charge carriers with the opposite polarity in the electric double layer can be neutralized will also increase. Thus, magnitude of the current increases with the electric field. However, the

trend given is Fig. 6.15 and 6.16 are quite chaotic. The modified R-C model still needs further development and the parameters shown here is only for the analytical solution of this model. How to relate this parameter to the resistor and capacitor components in Fig. 6.10 is still not very clear. The electric conduction and the electrode effect in oil/pressboard are still not very clear and more research is needed.

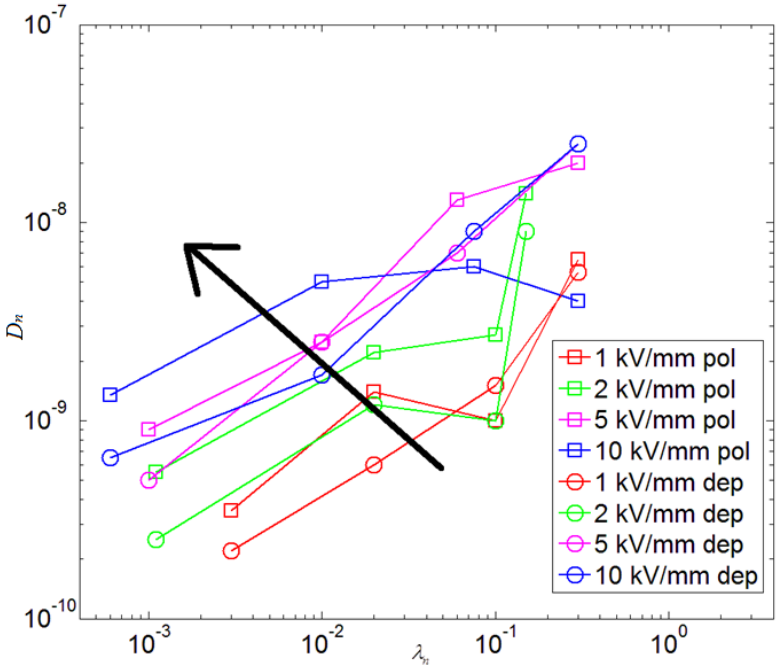

Fig. 6.15 Field dependence of the fitting parameters at 30°C

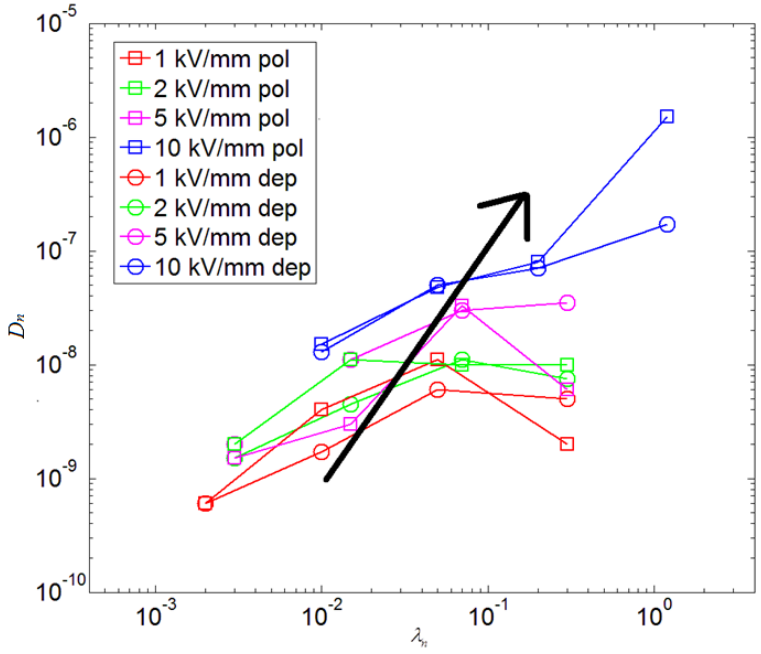

Fig. 6.16 Field dependence of the fitting parameters at 90°C

Please note, the above analysis is only valid at a medium electric field. If the electric field is very low, most of the original charge carriers in the oil/pressboard sample take quite a while to reach the electrode and the conductivity is correlated with the drift timeand the dissociation rate. When the field is very high, the injection induced conduction becomes the dominate conduction and the injection might not be represented by R-C branches. How to obtain the parameters shown in Fig. 6.10 is still not clear and it can be quite difficult to calculate these parameters through the experimental results. Besides, the influence from the aging of the pressboard or oil on this modified R-C equivalent model has not been studied and further researches are required.

6.5 Summary

The polarization and depolarization current measurement has been carried out to evaluate the dielectric properties of the oil/pressboard insulation. The influence of the pressure on the pressboard in the PDC measurement has been studied. If the pressure on the pressboard is low, the metal electrodes and the pressboard may not have a good contact and the polarization current can be significantly affected. The magnitudes of the polarization and the depolarization current increase with the electric field and the temperature. There are differences between the magnitude of the added depolarization current and the polarization, which means the classic R-C equivalent circuit model may not be able to explain the time domain response in the oil/pressboard insulation. The classic R-C equivalent model has been modified with taking consideration of the electrode effect and the field enhanced dissociation effect. The experimental results have been fitted with the exponential equations and good fittings have been achieved and the field dependence of the parameters used in the simulation have been analysed.

Chapter 7 Conclusion and Further Work

7.1 Conclusion

The present work of this thesis is concentrated on the analysis of the result from dielectric spectroscopy and DC current measurement and this thesis aims at understanding the mechanism of transportation of ions in the mineral oil.

As seen from the result of DC conductivity measurement, the DC conductivity of mineral oil increases with its aging time. The initial DC conductivity which is measured at the very beginning of the polarization process (1 s -2 s) does not change much with the electric field and temperature. This indicates that at the very beginning when a DC field is applied, the space charge effect is negligible and the electrical conduction is dominated by the drift of charge carriers. The long-time conductivity of mineral oil decreases with the electric field first(1 kV/mm- 2 kV/mm), and then enters a quasi-constant region. If the electric field increases even higher (above 3.5 kV/mm), an increase of the conductivity can be observed. Terna oil is in a poor condition and needs to be replaced. The time-dependent current of Terna oil can reach a minimum value within 1 hour of electrification and then start to increase. This may be attributed to space charge formation around electrode that can enhance charge injection process. Once measuring electrode and high-voltage electrode are short-circuited, depolarization current can be recorded. The discharge currents simply decay to zero for Shell ZX-I oil and Hydro Quebec oil. When it comes to Terna oil, the magnitude of the depolarization current first decreases and reaches a minimum value. Then the magnitude of this depolarization current increases. This implies a serious distortion in Terna oil and an extra depolarization current is induced from the potential difference between the electrodes. The electrical conduction mechanism in mineral oil is still not very clear.

According to the dielectric spectroscopy test, the characteristics of the frequency response of the mineral oil are similar. First, the real part of the complex permittivity doesn’t change much at high frequency (1Hz-100Hz) and increases significantly when the frequency decreases further. Second, the imaginary part of complex permittivity will

decrease with the frequency with a slope that is close to -1. Third, when the temperature increases, the frequency response of mineral oil will shift towards high frequency region. Also, the conductivity obtained by the dielectric spectroscopy measurement is similar to that measured by time-domain method under a low electric field. The imaginary part of the complex permittivity increases with aging, which means the aged oil has a high dielectric loss. When the oil is aged, more charge carriers will be generated due to chemical, electrical and thermal degradations. If more charge carriers can participate into the electric conduction, the space charge polarization can be more serious and the experimental results have revealed that the value of the real part of the complex permittivity increases with the aging period. However, the space charge effect in mineral oil has not been carefully studied and how to relate the results of the frequency domain measurement with the aging condition of the mineral oil is still not clear.

Based on the simulation result, there are probably two kinds of charge carriers in mineral oil. One is dissociated in the oil and can be blocked by the electrode, the other one is created in the vicinity of the electrode. The polarization caused by the drift of the injected charge carriers has been studied. It seems if these injected charge carriers have a high mobility so that they can reach the electrode in a field cycle, the motion of these injected charge carriers can only contribute to the imaginary part of the complex permittivity. A computer based method has been used to fit the experimental data. It seems if part of the total charge carriers are generated at the electrode, both the real part and imaginary part of the complex permittivity measured experimentally can be fitted. Besides, an analytical solution based on Coelho's space charge polarization theory has been developed. Even the field is not homogeneous between the electrodes, the motion of these injected charge carriers can still only contribute to the imaginary part of the complex permittivity. To get an accurate fit, the computer based method is recommended. A new coefficient α, the ratio of the conductivity that is contributed from the injection over the total conductivity has been defined and it decreases with temperature and aging period. The dissociated conductivity has been defined and used to analyse the aging condition of the oil.

The polarization and depolarization process in mineral oil has been studied. The adsorption of the charge carriers in the vicinity of the electrodes has been studied and an analytical expression to calculate the total charge density in the charge layer near the electrode has been developed. As the depolarization process mainly depends on the motion of the dissociated charge carriers, an analytical solution has been derived to

explain the dielectric behaviour in mineral oil based on the ionic diffusion theory. The time dependent curves of depolarization current of the mineral oil can be well fitted using the exponential equations. The total density in the charge layer increases with temperature and aging of the oil. The dissociated conductivities of three mineral oils have been calculated and the dissociated conductivity does not change much with the electric field. The total dissociated conductivity increases with the temperature. The total dissociated conductivities of Hydro Quebec oil and Shell ZX-I are quite similar, which is consistent with the experimental results from both time domain and frequency domain measurement.

In a guarded electrode system, the field at edge of the guard and guarded electrode can be much higher than the average field between the guarded electrode and high voltage electrode by local field enhancement. Reduce the distance between the measuring electrode and high voltage electrode, *h*, increase the edge radius of the measuring electrode and guard electrode, *r*, or decrease the gap between the measuring electrode and guard electrode, *g*, can lower the maximum field in the test cell. An empirical equation that has been proposed in this thesis can be used to estimate the maximum field. It has been found that the effective surface area of the measuring electrode can be affected by its edge radius. The edge radius of the measuring electrode should be included in the correction equation for the effective radius. If the edge radius or *g/h* is too large, using current effective radius correction equation can lead to a significant error. For DC conductivity measurement for insulating liquid, a ratio of *g/h/r* = 1:3:1 is recommended.

The polarization and depolarization current measurement has been used to test the dielectric properties of oil/pressboard insulation. The influence of the pressure on the pressboard on the PDC measurement has been studied. If the pressure on the pressboard is low, the metal electrodes and the pressboard may not have a good contact and the polarization current can be significantly affected. The magnitudes of the polarization and the depolarization current increase with the electric field and the temperature. There are differences between the magnitude of the added depolarization current and the polarization, which means the classic R-C model may not be able to explain the time domain response in oil/pressboard insulation. The classic R-C equivalent model has been modified with taking consideration of the electrode effect and the field enhanced dissociation effect. The experimental results have been fitted with the exponential equations and good fittings have been achieved and the field dependence of the parameters used in the simulation have been analysed.

7.2Contributions

1) The space charge polarization induced by the motion of the injected charge carriers has been theoretically studied firstly, and it is also the first time that good experimental fittings of frequency response of mineral oil have been achieved based on the ionic drift and diffusion model.

2) The classic DC conductivity has been divided into two new terms: the dissociated conductivity and the conductivity induced by the injection. The dissociated conductivity can be related to the chemical change in mineral oil which may be used in the future as a new parameter in oil condition diagnostics.

3) It is the first time that the electric conduction in frequency domain and time domain can be explained by the ionic drift and diffusion theory simultaneously under the assumption of existence of the fast charge carriers.

4) It is the first time that the local field enhancement in a guarded electrode system for insulating liquid measurement is discovered and quantitatively studied. The classic correcting equation for the effective radius of measuring electrode should be used with caution.

5) The electrode effect has been introduced into the polarization and depolarization theory and an modified R-C equivalent model has been proposed to explain the electric conduction behaviour in oil/pressboard sample.

7.3 Future work

In future, experiments will be designed to confirm the existence of the high mobility injected charge carriers in mineral oil. A selectively permeable film can be coated on the electrode to block certain kinds of charge carriers. As these injected charge carriers might be holes or electrons, at least two different films, one can block the electrodes and the other one can block the holes, need to be used in the dielectric spectroscopy measurement. An improved model with the extraction of charge carriers in the vicinity of the electrode will be developed to obtain a better experimental fitting. As the mechanism of the charge injection discussed in chapter 4 is still not very clear, parameters, such as water content, electrode material, electric field, et al, which can affect this injection, will be studied.

The study of the polarization process in mineral oil will be continued and a polarization theory based on the charge injection and ionic dissociation and recombination will be proposed to explain the dielectric behaviour of mineral oil under DC field. Influence from different parameters, such as, water content, pressure, aging, et al, will be studied. FTIR (Fourier transform infrared spectroscopy) will be used to analyse the quantity of the chemical components in mineral oil. It is possible to relate the dissociated conductivity with different kinds of ions.

The local field enhancement might also exist in other types of guarded electrode system, thus, simulations of the field distribution can be carried out to reduce the maximum field in among other kinds of electrodes. The modification of the Schwarz and Christoffel transformation on rounded corners has been well developed recently and it is possible to obtain an analytical solution of the effective radius with the edge radius being taken into account.

The dielectric properties of oil/pressboard with different aging period will be studied using both frequency- domain and time- domain measurement. The influence of aging on the modified R-C equivalent model will be studied. The electric conduction in oil/pressboard is still not very clear and the knowledge concerns the types of charge carriers in oil/pressboard insulation is limited. Besides, the water content in oil and pressboard can also affect the dielectric properties of oil/pressboard insulation and the procedures for the oil/pressboard DC conductivity measurement is still questionable and needs to be improved.

References

[1] H. M. Ryan, High Voltage Engineering and Testing, The Institution of Engineering and Technology 2001

[2] C. Kim, V. Sood, G. Jang, S. Lim and S. Lee, HVDC Transmission: Power Conversion Applications in Power Systems, Wiley-IEEE Press, 2009

[3] T. J. Hammons, D. Woodford, J. Loughtan, M. Chamia, J. Donahoe, D. Povh, B. Bisewski and W. Long "Role of HVDC Transmission in Future Energy Development" IEEE Power Engineering Review, Vol 20 10-25 2000

[4] K. Meah and S. Ula, "Comparative Evaluation of HVDC and HVAC Transmission Systems", IEEE Power Engineering Society General Meeting, 1-5 2007

[5] M. P. Bahrman and B. K. Johnson, "The ABCs of HVDC Transmission Technologies", IEEE Power and Energy Magazine, Vol 5 32-44 2007

[6] N. Flourentzou, V. G. Agelidis and G. D. Demetriades, "VSC-Based HVDC Power Transmission Systems: An Overview", IEEE Transactions on Power Electronics, Vol 24 592-602 2009

[7] A. Calson, "Specific Requirements on HVDC Converter Transformers," ABB Publication, 96-04-25

[8] E. Takahashi, Y. Tsutsumi, K. Okuyama and F. Ogata, "Partial Discharge Characteristics of Oil-Immersed Insulation Iystems under DC, Combined AC-DC and DC Reversed Polarity Voltage", IEEE Transactions on Power Apparatus and Systems, Vol 95 411-420 1976

[9] J. S. Sajan, K. Dwarakanath and S. N. Moorching, "Comparative Evaluation of Dielectric Strength of Paper-Oil Insulation under AC, DC, Combined, Composite AC/DC and Impulse Voltages", 1998 Annual Report Conference on Electrical Insulation and Dielectric Phenomena, 236-239 1998

[10] T. J. Gallagher, "Simple Dielectric Liquids: Mobility, Conduction, and Breakdown", Oxford University Press, 1975

[11] T. O. Rouse "Mineral Insulating Oil in Transformers" IEEE Electrical Insulation Magazine Vol 14 6-16 1998

[12] J. C. Whitaker "AC Power Systems Handbook, Third Edition", CRC Press, 2006

[13] L. E. Lundgaard, W. Hansen, D. Linhjell and T. J. Painter, "Aging of Oil-Impregnated Paper in Power Transformers", IEEE Transactions on Power Delivery, Vol 19 230-239 2004

[14] A. J. Kachler and I. Hohlein, "Aging of Cellulose at Transformer Service Temperatures. Part 1: Influence of Type of Oil and Air on the Degree of Polymerization of Pressboard, Dissolved Gases, and Furanic Compounds in Oil" IEEE Electrical Insulation Magazine, Vol 21 15-21 2005

[15] IEC 60450 Measurement of the average viscometric degree of polymerization of new and aged cellulosic electrically insulating materials IEC standard 2007

[16] C. Homagk, K. Mossner and T. Leibfried, "Investigation on Degration of Power Transformer Solid Insulation Material", Annual Report Conference on Electrical Insulation and Dielectric Phenomena, 75-79 2008

[17] A. M. Emsley and G. C. Stevens, "Review of Chemical Indicators of Degradation of Cellulosic Electrical Paper Insulation in Oil-filled Transformers", IEE Proceedings on Science, Measurement and Technology, vol 141, 324-334 1994

[18] T. V. Oommen and T. A. Prevost, "Cellulose Insulation in Oil-filled Power Transformers: Part II Maintaining Insulation Integrity and Life", IEEE Electrical Insulation Magazine, vol 22 5-14 2006

[19] A. M. Emsley, X. Xiao, R. J. Heywood, and M. Ali, "Degradation of Cellulosic Insulation in Power Transformers. Part 3: Effects of Oxygen and Water on Ageing in Oil", IEE Proceedings on Science, Measurement and Technology, vol 147, 115-119 2000

[20] J. Fabre and A. Pichon, "Deteriorating Process and Products of Paper in Oil, Application to Transformers", Proceedings of CIGRE conference , paper 137, 1960

[21] D. M. R. Vanegas and S. M. Mahajan, "Correlation Between Hot-spot Temperature and Aging Factor of Oil-Immersed Current Transformers", IEEE Power and Energy Society General Meeting - Conversion and Delivery of Electrical Energy in the 21st Century, 1-5 2008

[22] D. Linhjell, L. Lundgaard and U. Gafvert, "Dielectric Response of Mineral Oil Impregnated Cellulose and the Impact of Aging", IEEE Transactions on Dielectrics and Electrical Insulation, Vol 14 156-169 2007

[23] M. H. G. Ese, K. B. Liland and L. E. Lundgaard, "Oxidation of Paper Insulation in Transformers", IEEE Transactions on Dielectrics and Electrical Insulation, vol 17 939-946 2010

[24] A. M. Franklin, "simpler measurement of relative humidity in electrical insulating oils", Electrical Review, Vol. 194, 373, 1974

[25] IEC 61620 Insulating Liquids –Determination of the Dielectric Dissipation Factor By Measurement Of The Conductance And Capacitance – Test Method IEC standard 1998-11

[26] IEC 60247 Insulating Liquids – Measurement Of Relative Permittivity, Dielectric Dissipation Factor (Tan Δ) And D.C. Resistivity IEC standard 2004-02

[27] ASTM D1169 Standard Test Method for Specific Resistance (Resistivity) Of Electrical Insulating Liquids ASTM Standard 2009

[28] IEC 60093: Methods of Test for Volume Resistivity and Surface Resistivity of Solid Electrical Insulating Materials; IEC Standard 1980-01

[29] ASTM D257: Standard Test Methods for DC Resistance or Conductance of Insulating Materials; ASTM Standard 2007

[30] A. Kuchler, M. G. Berglund and M. Koch "Oil Conductivity Measuring Techniques and Standards" Cigre JWG A2/D1.41 2011

[31] A. Castellanos Electrohydrodynamics Springer Wien New York 1998

[32] P.Debye "Reaction Rates in Ionic Solutions" Journal of the Electrochemical Society Vol 82 265-272 1942

[33] P. Langevin, “Recombinaison et mobilites des ions dans les gaz” Annales de Chimie et de Physique vol 28 433–530 1903

[34] L.Onsager "Deviations From Ohm's Law In Weak Electrolytes" Journal of Chemical Physics, Vol 2 599-615 1934

[35] A. Alj, A. Denat, J. P. Gosse and B. Gosse "Creation of Charge Carriers in Nonpolar Liquids" IEEE Transactions on Electrical Insulation, vol 20 221-231 1985

[36] M. Nemamcha, J. P. Gose, A. Denat and B. Gosse "Temperature Dependence of Ion Injection by Metallic Electrodes into Non-Polar Dielectric Liquids" IEEE Transactions on Electrical Insulation, vol 22 459-465 1987

[37] N. Felici and J.P.Gosse "Injection d'ions par des électrodes métalliques dans les hydrocarbures liquides de résistivité élevée" Revue de Physique Appliquée, vol 14 629-633 1979

[38] N. J. Felici, "A Tentative Explanation of the Voltage-Current Characteristic of Dielectric Liquids" Journal of Electrostatics, vol 12 165-172 1982

[39] A. Denat, B. Gosse, J.P. Gosse, "High Field DC and AC Conductivity of Electrolyte Solutions in Hydrocarbons" Journal of Electrostatics, vol 11 179-194 1982

[40] A. Denat, B. Gosse, J.P. Gosse "Electrical Conduction of Solutions of an Ionic Surfactant in Hydrocarbons" Journal of Electrostatics, vol 12 197-205 1982

[41] A. Denat, B. Gosse, J.P. Gosse "Ion Injections in Hydrocarbons" Journal of Electrostatics, vol 7 205-225 1979

[42] J. C. Lacroix, P. Atten, "Double Injection with Recombination: EHD Linear and Non Linear Stability Study" Journal of Electrostatics, vol 5 453-461 1978

[43] N. Felici "High-Field Conduction in Dielectric Liquids Revisited" IEEE Transactions on Electrical Insulation, vol 20 233-238 1985

[44] C. Brosseau "Interface Influence on the High-Field Conduction Phenomena of a Thin Dielectric Liquid Layer" Journal of Applied Physics, vol 69, 891-895 1991

[45] F. Pontiga and A. Castellanos "The Effect of Field-Enhanced Injection and Dissociation on the Conduction of Highly-Insulating Liquids" IEEE Transactions on Dielectrics and Electrical Insulation, vol 3 792-799 1996

[46] F. Pontiga and A. Castellanos "Electrical Conduction of Electrolyte Solutions in Nonpolar Liquids" IEEE Transactions on Industry Applications, vol 32 816-824 1996

[47] G. Briere And F. Gaspard "Electric Conduction In Nitrobenzene" Chemical Physics Letters vol 1 706-708 1968

[48] A. H. Mufti, A. I. Alessa And A. O. Arafa "The Hydrostatic Effect on Conduction Current in a Transformer Oil Using C8f18 And N2 as Dissolved Gases" Proceedings Of the 5th International Conference on Properties and Applications of Dielectric Materials 25-30 1997

[49] M. Butcher, A. Neuber, M. D. Cevallos, J. C. Dickens and H. Krompholz, "Conduction and breakdown mechanismsin transformer oil", IEEE Transactions on Plasma Science, Vol 34 467-475 2006

[50] E. Occhini and G. Maschio "Electrical Characteristics of Oil-Impregnated Paper as Insulation for HVDC Cables" IEEE Transactions On Power Apparatus And Systems Vol Pas-86 312-326 1967

[51] E. O. Forster "The Metal/Liquid Interface:the Charge Injection Process" IEEE Transactions on Electrical Insulation, vol 19 524-528 1984

[52] A. A. Zaky and R. Hawley, "Conduction and Breakdown in Mineral Oil" P. Peregrinus 1973

[53] E. O. Forster "Electric Conduction in Liquid Hydrocarbons. I. Benzene." The Journal of Chemical Physics, vol 37, 1021-1028 1962

[54] B. S. Harrap and E. Heymann "Theories of Viscosity Applied to Ionic Liquids" Chemical Reviews vol 48 45-67 1951

[55] F. Gutmann and L. M. Simmons "The Temperaute Dependence of the Viscosity of Liquids" Journal of Applied Physics 23 977-978 1952

[56] C. W. Wu and H. Conrad "The Temperature Dependence of the Conductivity of Silicone Oil and Related Electrorheology of Suspensions Containing Zeolite Particles" Journal of Physics D: Applied Physics

[57] T. Iwasawa, T. Sekine, M. Sone and H. Mitsui "Effect of Bound Water Cluster in Liquid Dielectrics on Conductivity" 1996 IEEE Annual Report - Conference on Electrical Insulation and Dielectric Phenomena, 20-23, 1996

[58] S. Itahashi, H. Mitsui, T. Sato and M. Sone "Analysis of Water in Oil-Impregnated Kraft Paper and its Effect on Conductivity" IEEE Transactions On Dielectrics And Electrical Insulation Vol 2 1111-1116 1995

[59] S. Itahashi, H. Mitsui, T. Sato and M. Sone "State of Water in Hydrocarbon Liquids and its Effect on Conductivity" IEEE Transaction on Dielectrics and Electrical Insulation Vol 2 1117-1122 1995

[60] S. Itahashi, H. Sakurai and T. Iwasawa "Effect of Water in Insulating Oil on Conduction Phenomena under High Electrical Field" IEEE Annual Report Conference on Electrical Insulation and Dielectric Phenomena, 917-922 1994

[61] G. Kleinheins "Mobilities of Negative and Positive Charge Carriers Injected from Metal Electrodes into Liquid Benzene" Journal of Physics D: Applied Physics vol 3 75-83 1970

[62] A. W. Stannett "The Conductivity of Hydrocarbon Transformer Oil Containing Water and Solid Conducting Particles" British Journal Of Applied Physics, vol 2 110-114 1951,

[63] B. Craig "Predicting the Conductivity of Water-in-Oil Solutions as a Means to Estimate Corrosiveness" Corrosion vol 54 657-662 1998

[64] K. Wen, Y. Zhou, J. Fu and T. Jin, "A Calculation Method and some Features of Transient Field under Polarity Reversal Voltage in HVDC Insulation" IEEE Transactions on Power Delivery, Vol 8 223-230 1993

[65] T. Nara, K. Kato, F. Endo and H. Okubo, "Study on Dielectric Breakdown at DC Polarity Reversal in Oil / Pressboard-Composite Insulation System" IEEE Conference on Electrical Insulation and Dielectric Phenomena,588-591 2009

[66] H. Okubo, T. Nara, H. Saito, H. Kojima, N. Hawakawa and K. Kato, "Breakdown Characteristics in Oil/pressboard Composite Insulation System at HVDC Polarity

Reversal," in Annual Report Conference on Electrical Insulation and Dielectric Phenomena, 2010

[67] T. K. Saha and P. Purkait, "Investigations of Temperature Effects on the Dielectric Response Measurements of Transformer Oil-Paper Insulation System ", IEEE Transactions on Power Delivery, vol 23 252-260 2008

[68] Y. Du, M. Zahn, B. C. Lesieutre, A. V. Mamishev and S. R. Lindgren, "Moisture Equilibrium in Transformer Paper-Oil Systems" IEEE Electrical Insulation Magazine, vol 15 11-20 2002

[69] J. L. Wei, G. J. Zhang, H. Xu, H. D. Peng, S. Q. Wang and M. Dong "Novel Characteristic Parameters for Oil-Paper Insulation Assessment from Differential Time-Domain Spectroscopy based on Polarization and Depolarization Current Measurement" IEEE Transactions on Dielectrics and Electrical Insulation, vol 18 1918-1928 2012

[70] Y. Sheiretov and M. Zahn "A Study of the Temperature and Moisture Dependent Dielectric Properties of Oil-impregnated Pressboard", Conference on Electrical Insulation and Dielectric Phenomena 487-492 1993

[71] W. S. Zaengl "Applications of Dielectric Spectroscopy in Time and Frequency Domain for HV Power Equipment", IEEE Electrical Insulation Magazine, vol 19 9-22 2003

[72] R. Diabi , J. C. Filippini , C. Marteau and R. Tobazeon "On the Role of Temperature and Impurities in the Low Field Conduction of Insulating Liquids", 12th International Conference on Conduction and Breakdown in Dielectric Liquids, 350-353 1996

[73] J. Hao, R. J. Liao, G. Chen, Z. Q. Ma and L. J. Yang "Quantitative Analysis Ageing Status of Natural Ester-Paper Insulation and Mineral Oil-Paper Insulation by Polarization/Depolarization Current" IEEE Transactions on Dielectrics and Electrical Insulation, vol 19 188-199 2012

[74] A. Setayeshmehr, I. Fofana, C. Eichler, A. Akbari, H. Borsi and E. Gockenbach, "Dielectric spectroscopic Measurements on Transformer Oil-Paper Insulation under

Controlled Laboratory Conditions" IEEE Transactions on Dielectrics and Electrical Insulation, Vol 15 1100-1111 2008

[75] I. Fofana, H. Hemmatjou, M. Farzaneh "Low Temperature and Moisture Effects on Polarization and Depolarization Currents of Oil-paper Insulation" Electric Power Systems Research vol 80 91–97 2010

[76] I. Fofana, H. Hemmatjou and F. Meghnefi "Effect of Thermal Transient on the Polarization and Depolarization Current Measurements of Oil-Paper Insulation" IEEE Transactions on Dielectrics and Electrical Insulation Vol 18 513-520 2011

[77] R. B. Jadav, C. Ekanayake and T. K. Saha, "Impact of Moisture and Ageing on the Dielectric Response of Transformer Insulation" Australasian Universities Power Engineering Conference, 1-6 2012

[78] A. M. Emsley and G. C. Stevens, "A Reassessment of the Low Temperature Thermal Degradation of Cellulose," Sixth International Conference on Dielectric Materials, Measurements and Applications, 229-232 1992.

[79] L. Dag, L. Lars, and G. Uno, "Dielectric Response of Mineral Oil Impregnated Cellulose and the Impact of Aging," IEEE Transactions on Dielectrics and Electrical Insulation, vol 14 156-169 2007

[80] T. K. Saha and P. Purkait, "Understanding the Impacts of Moisture and Thermal Ageing on Transformer's Insulation by Dielectric Response and Molecular Weight Measurements," IEEE Transactions on Dielectrics and Electrical Insulation, vol. 15, pp. 568-582, 2008.

[81] V. D. Houhanessian and W. S. Zaengl, "Time Domain Measurements of Dielectric Response in Oil-Paper Insulation Systems", Conference Record of the 1996 IEEE International Symposium on Electrical Insulation, Vol 1 47-52 1996.

[82] P. Przybylek, "The Influence of Cellulose Insulation Aging Degree on its Water Sorption Properties and Bubble Evolution," IEEE Transactions on Dielectrics and Electrical Insulation, vol 17 906-912 2010.

[83] D. Linhjell, O. L. Hestad, U. Gafvert, and L. E. Lundgaard, "Dielectric Response of Oil-impregnated Cellulose from 0.1 mHz to 3 MHz," IEEE International Conference on Dielectric Liquids, pp. 277-280, 2005.

[84] U. Gafvert, L. Adeen, M. Tapper , P. Ghasemi and B. Jonsson "Dielectric Spectroscopy in Time and Frequency Domain Applied to Diagnostics of Power Transformers", Proceedings Of the 6th International Conference on Properties and Applications of Dielectric Materials, vol 2 825-830 2000

[85] T. K. Saha, Purkait, P. Investigation of polarization and depolarization current measurements for the assessment of oil-paper insulation of aged transformers Dielectrics and Electrical Insulation, IEEE Transactions on (Volume:11 , Issue: 1) 144 - 154 2004

[86] E. Ildstad , U. Gafvert and P. Tharning "Relation between Return Voltage and Other Methods for Measurements of Dielectric Response", IEEE International Symposium on Electrical Insulation 25-28 1994

[87] T. Leibfried and A. J. Kachler "Insulation Diagnostics on Power Transformers Using the Polarisation and Depolarisation Current (PDC) Analysis", IEEE International Symposium on Electrical Insulation 170-173 2002

[88] T. K. Saha, "Review of Time Domain Polarisation Measurements for Assessing Insulation Condition in Aged Transformers", IEEE Transaction on Power Delivery, vol 18 1293-1301 2003

[89] L. Solymar and D. Walsh Electrical Properties of Materials, Oxford University Express, 2003

[90] I. Fofana1, A. Bouaicha, M. Farzaneh and J. Sabau "Ageing Behaviour of Mineral Oil and Ester Liquids: a Comparative Study" Annual Report Conference on Electrical Insulation and Dielectric Phenomena, 87-90, 2008

[91] L. Zhonghua, Z. Jun, Y. Yi, M. Jun, W. Xinsheng, and T. Demin "Formation and Inhibition of Free-Radicals in Insulating Materials Aged by Electrical Field", Proceedings of the 5th International Conference on Properties and Applications of Dielectric Materials, 25-30, 1997

[92] Rashmi Sanghi, "Chemistry Behind the Life of a Transformer", Resonance, 17-23, 2003

[93] H. Tropper "The Effect of Dissolved Gases on the Electrical Conduction and Breakdown of Insulating Oil" Journal of The Electrochemical Society Vol 108 144-150 1961

[94] A. R. Nosseir "Effect of Dissolved Gases, Stress, and Gap Spacing on High-Field Conductivity in Liquid Insulants" IEEE Transactions On Electrical Insulation, Vol 10 58-62 1975

[95] A. Kuchler, M. Libebschner "Evaluation of Conductivities and Dielectric Properties For Highly Stressed HVDC Insulating Materials", Cigré Session 2010, D1_106 2010

[96] H. Li, L. S. Zhong. Q. X. Yu, S. Mori and S. Yamada, "The Resistivity of Oil and Oil impregnated Pressboard Varies with Temperature and Electric Field Strength", IEEE Transactions on Dielectrics and Electrical Insulation, vol 21 1851 2014

[97] J. J. Thomson "Notes on Recent Researches in Electricity and Electromagnetism", Oxford at the Clarendon Press, 1883-48 147

[98] R. Bartnikas "Engineering Dielectrics Volume IIb Electrical Properties of Solid Insulating Materials: Measurement Techniques", ASTM Special Technical Publication, 1987

[99] H. S. Endicott "Guard-Gap Correction for Guarded-Electrode Measurements and Exact Equations for the Two-Fluid Method of Measuring Permittivity and Loss", Journal of Testing and Evaluationvol 4 188-195 1976

[100] I. John and Jr. Lauritzen "The Effective Area of A Measuring electrode" 1963 Annual Report of Conference in Electrical Insulation, 67-73 1963

[101] W. G. Amey and F. Hamburger "Method for Evaluating the Surface and Volume Resistance Characteristics of Solid Dielectric Materials", Proceedings-American Society for Testing Materials, Vol 49 1071-1091 1949

[102] D. G. W. Goad and H. J. Wintle "Capacitance Corrections for Guard Gaps", Measurement Science and Technology, Vol 1 965-969 1990

[103] M. Lisowski "A Effective Area of Thin Measuring Electrode in Determining of Permittivity and Volume Resistivity" IEEE Transactions on Dielectrics and Electrical Insulation, Vol 16 24-31 2009

[104] M. Lisowski and R. Kacprzyk "Changes Proposed for the IEC 60093 Standard Concerning Measurements of the Volume and Surface Resistivities of Electrical Insulating Materials", IEEE Transactions on Dielectrics and Electrical Insulation, 13, 139 -145, 2006

[105] M. Medrano, A. T. Pérez and C. Soria-Hoyo "Design of a Conductivity Meter for Highly Insulating Liquids" Journal of Applied Physics D: applied Physics Vol 40 1477-1482 2007

[106] A. Andersson, "Modified Schwarz–Christoffel Mappings using Approximate Curve Factors", Journal of Computational and Applied Mathematics, Vol 233 1117-1127, 2009

[107] L. Banjai, L.N. Trefethen "A Multipole Method for Schwarz–Christoffel Mapping of Polygons with Thousands of Sides", SIAM Journal on Scientific Computing, Vol 25 1042–1065 2003

[108] A. Andersson, "A modified Schwarz–Christoffel mapping for regions with piecewise smooth boundaries", Journal of Computational and Applied Mathematics, Vol 213 56–70 2008

[109] K. A. Kumar and K. Viswanathan, "Study of UV Transmission through a Few Edible Oils and Chicken Oil" Journal of Spectroscopy, Vol 2013 540417

[110] R. P. Gonçalves, P. H. Março, P. Valderrama "Thermal Edible oil Evaluation by UV–Vis Spectroscopy and Chemometrics", Food Chemistry, vol 163 83-86 2014

[111] R. Ferguson, A. Lobeiras and J. Sabau, “Suspended Particles in the Liquid Insulation of Ageing Power Transformers”, IEEE Electrical Insulation Magazine, Vol 18 17-23 2002.

[112] I. L. Hosier, A. S. Vaughan, S. J. Sutton and F. Davis, "Chemical, Physical and Electrical Properties of Aged Dodecylbenzene: Thermal Ageing of Mixed Isomers in Air", IEEE Transactions on Dielectrics and Electrical Insulation, Vol 14 1113-1124 2007

[113] H. C. Chang and G. Jaffé, “Polarization in Electrolytic Solutions. Part I. Theory”, Journal of Chemical Physics, Vol 20, 1071-1087 1952

[114] G. Jaffé and C. Z. LeMay, “On Polarization in Liquid Dielectrics”, Journal of Chemical Physics, Vol. 21, 920-928, 1953

[115] G. Jaffé and J. A. Rider “Polarization in Electrolytic Solutions. Part II. Measurements” Journal of Chemical Physics, vol 20 1077 1952

[116] A. A. S Akmal, H Borsi, E. Gockenbach and V. Wasserberg "Dielectric Behavior Insulating Liquid at Very Low Frequency", IEEE Transaction on Dielctric and Electrical Inuslation Vol 13 532-538 2006

[117] W. S. Zaengl, "Dielectric Spectroscopy in Time and Frequency Domain for HV Power Equipment, Part I: Theoretical Considerations." IEEE Electrical Insulation Magazine, Vol 19 5-19 2003

[118] R. Bartnikas "Some General Remarks on the Dielectric Loss Mechanisms in Mineral Oils", IEEE Transactions on Dielectrics and Electrical Insulation, Vol 16 1506-1510 2009

[119] R. Z. Syunyaev and V. V. Likhatsky "Effects of Temperature and Pressure on the Phase State of Oils and Asphaltene Solutions Observed Using Dielectric Spectroscopy" Energy Fuels vol 24 2233–2239 2010

[120] C. T. Dervos, C. D. Paraskevas, P. Skafidas "Dielectric Characterization of Power Transformer Oils as a Diagnostic Life Prediction Method" IEEE Electrical Insulation Magazine, Vol 21 11-19 2005

[121] R. Bartnikas “Engineering Dielectrics Vol. III, Electrrical Insulating Liquids”, ASTM, 1994

[122] T. K. Saha "Review of Modern Diagnostic Techniques for Assessing Insulation Condition in Aged Transformers", IEEE Transactions on Dielectrics and Electrical Insulation Vol 10 903-917 2003

[123] R. M. Hill and L. A. Dissado "Debye and Non-Debye Relaxation" Journal of Physics C: Solid State Physics vol 18 3829-3836 1985

[124] R. H. Cole and K. S. Cole "Dispersion and Absoption in Dielectrics I Alternating Current Characteristics" Journal of Chemical Physics Vol 9 341-351 1941

[125] R. H. Cole "On the Analysis of Dielectric Relalxation Measurements" The Journal of Chemical Physics, Vol 23 493-502 1955

[126] S. Havriliak and S. Negami "A Complex Plane Representation of Dielectric and Mechanical Relaxation Process in Some Polymers" Polymer vol 8 161–210 1967

[127] C. D. Paraskevas , P. Vassiliou and C. T. Dervos "Temperature Dependent Dielectric Spectroscopy in Frequency Domain of High-Voltage Transformer Oils Compared to Physicochemical Results" IEEE Transactions on Dielectrics and Electrical Insulation, vol 13 281-284 2005

[128] P. R. S. Jota, S. M. Islam, F. G. Jota "Modeling the Polarization Spectrum in Composite Oil/Paper Insulation Systems", IEEE Transactions on Dielectrics and Electrical Insulation Vol 6 145-151 1999

[129] V. D. Houhanessian, W. S. Zaengl "Time Domain Measurements on Dielectric Response in Oil-Paper Insulation Systems" Conference Record of the 1996 IEEE International Symposium on Electrical Insulation, 16-19 1996

[130] T. K. Saha "Review of Time-Domain Polarization Measurements for Assessing Insulation Condition in Aged Transformers" IEEE Transactions on Dielectrics and Electrical Insulation vol 18 1293-1301 2003

[131] R. Patsch, O. Kouzmine "Return Voltage Measurements – a Good Tool for the Diagnosis of Paper-Oil Insulations" IEEE Russia Power Tech, 27-30 2005

[132] B. Gross "Electret Research - Stages in its Development" IEEE Transactions on Electrical Insulation Vol 21 249-269 1986

[133] B. Ganger and G. Maier "The Resistivity of Insulating Oil in a Direct Voltage Field" Brown-Boveri Review, Vol 56 525-531 1969

[134] J. R. Macdonald, "Theory of ac Space-Charge Polarization Effects in Photoconductors, Semiconductors, and Electrolytes" Physical Review Vol 92 4–17 1953

[135] F. Stern and C. Weaver "Dispersion of Dielectric Permittivity due to Space Charge Polarization" Journal of Physics C: Soild State Physics Vol 3 1736 1970

[136] P. W. M. Jacobs and J. N. Maycock, "Polarization Effects in the Ionic Conductivity of Alkali Halide Crystals. I. AC Capacity" The Journal of Chemical Physics, Vol 39 757 1963

[137] F. C. M. Freire, G. Barbero, and M. Scalerandi, "Electrical Impedance for an Electrolytic Cell" Physical Review E, Vol 73 051202 2006

[138] G. Barbero, A. L. Alexe-lonescu, and I. Lelidis, "Significance of Small Voltage in Impedance Spectroscopy Measurements on Electrolytic Cells", Journal of Applied Physics Vol 98 113703 2005

[139] R. J. Klein, S. Zhang, S. Dou, B. H. Jones, R. H. Colby, and J. Runt, "Modeling Electrode Polarization in Dielectric Spectroscopy: Ion Mobility and Mobile Ion Concentration of Single-Ion Polymer Electrolytes" The Journal of Chemical Physics, Vol 124 144903 2006

[140] A. D. Hollingsworth and D. A. Saville, "A broad frequency range dielectric spectrometer for colloidal suspensions: cell design, calibration, and validation", Journal of Colloid and Interface Science, Vol 257 65-76 2003

[141] A. Sawada "Space-Charge Polarization of a Dilute Electrolytic Cell in the Presence of Diffuse Double Layers" Journal of Applied Physics, vol 112 044104 2012

[142] A. Sawada "Internal Electric Fields of Electrolytic Solutions Induced by Space-Charge Polarization" Journal of Applied Physics, vol 100 074103 2006

[143] A. Sawada "Theory of Space-Charge Polarization for Determining Ionic Constants of Electrolytic Solutions" Journal of Chemical Physics, vol 126 224515 2007

[144] A. Sawada "Dielectric Process of Space-Charge Polarization for an Electrolytic Cell with Blocking Electrodes" Journal of Chemical Physics, vol 129 064701 2008

[145] A. Sawada "Modeling of Electrode Polarization for Electrolytic Cells with a Limited Ionic Adsorption" Physical Review E, vol 88 032406 2013

[146] R. Coelho, "Physics of Dielectrics for the Engineer" Elsevier New York 1979

[147] D. G. Frood and T. J. Gallagher, "Space-Charge Dielectric Properties of Water and Aqueous Electrolytes", Journal of Molecular Liquids, Vol 69 183-200 1996

[148] R. Richert, A. Agapov, A. P. Sokolov "Appearance of a Debye Process at the Conductivity Relaxation Frequency of a Viscous Liquid", The Journal of Chemical Physics, Vol 134 104508 2011

[149] G. Power, M. Nagaraj, J. K. Vij, and G. P. Johari, "Debye Process and Dielectric State of an Alcohol in a Nonpolar Solvent", The Journal of Chemical Physics, Vol 134, 044525 2011

[150] B. A. Mazzeo and A. J. Flewitt, "Two- and Four-Electrode, Wide-Bandwidth, Dielectric Spectrometer for Conductive Liquids: Theory, Limitations, and Experiment", Journal of Applied Physiycs Vol 102 104106 2007

[151] A. Oleinikova, P. Sasisanker, and H. Weinga1rtner "What Can Really Be Learned from Dielectric Spectroscopy of Protein Solutions? A Case Study of Ribonuclease A" Journal of Physical Chemistry B Vol 108 8467 2004

[152] F. Kremer, A. Schonhals "Broadband Dielectric Spectroscopy" Springer 2003

[153] I. Megahed and A. Zaky, "Influence of Temperature and Pressure on Conduction Currcnts in Transformer Oil", IEEE Transactions on Electrical Insulation, vol 4 99-103 1969

[154] A. A. El-Sulaiman, A. R. M. Alamoud, A. S. Ahmed, and M. I. Qureshi, "Effect of Sub-Atmospheric Pressure on the Conduction Current in Transformer Oil", IEEE Conference Record on Conduction Breakdown Dielectric Liquids, 176 -180 1990

[155] U. Gafvert, A. Jaksts, Ch. Tornkvist, L. Walfridson, "Electrical Field Distribution in Transformer Oil," IEEE Transactions on Electrical Insulation, vol 27 647-660 1992.

[156] O. Hjortstam, J. Schiessling, Y. V. Serdyuk, S. M. Gubanski, "Measurements of Ion Mobility in Transformer Oil: Evaluation in Terms of Ion Drift" Annual Report Conference on Electrical Insulation and Dielectric Phenomena. 495-498, 2012

[157] L. Yang, S. M. Gubanski, Y. V. Serdyuk and J. Schiessling, “Dielectric Properties of Transformer Oils for HVDC Applications”, IEEE Transactions on Electrical Insulation, vol 19 1926-1933 2012

[158] M. S. Zadeh, Measurement of Ion Mobility in Dielectric Liquids”, M.Sc. thesis, Chalmers University of Technology, Gothenburg, Sweden, 2011.

[159] A. Denat, "Conduction and Breakdown Initiation in Dielectric Liquids", IEEE internation Conference on Dielectric Liquid, 1-11, 2011.

[160] N. Lavesson, L. Walfridsson, O. Hjortstam, J. Schiessling, "Modelling and Measurement of Field Dependent Resistivity of Transformer Oil" IEEE internation Conference on Dielectric Liquid, 1-4, 2014,

[161] Y. Zhou, M. Hao, G. Chen, G. Wilson and P. Jarman, "Space Charge Polarization in Insulating Mineral Oil", IEEE Conference on Electrical Insulation and Dielectric Phenomena, 587-590, 2013

[162] IEC 60422 "Mineral Insulating Oils in Electrical Equipment - Supervision and Maintenance Guidance", 2013

[163] K. Gopalan "Introduction to Signal and System Analysis" Cengage Learning, 2008

[164] S. Wolny, J. Kedzia, M. Zdanowski "Novel Method of Charge Mobility Assignation in Liquid Dielectrics by Streaming Electrification", Materials Science-Poland, Vol 27 1263-1269 2009

[165] P. A. Von Guggenberg "Experimental Investigation of the Heterogeneity of the Double Layer in Transformer Oil", 1993 Annual Report Conference on Electrical Insulation and Dielectric Phenomena, 68-71 1993

[166] M. S. Vihacencu, A. Ciuriuc, L. M. Dumitran, "Experimental Study of Electrical Properties of Mineral and Vegetable Transformer Oils" UPB Scientific Bulletin Series C: Electrical Engineering and Computer Science, Vol 75 171-182 2013

[167] M. Dong, L. P. Shen, H. Wang, H. B. Wang, and J. Miao, “Investigation on the Electrical Conductivity of Transformer Oil-Based AlN Nanofluid,” Journal of Nanomaterials, Vol 2013, 842963 2013

[168] I. Adamczewski "Ionization, Conductivity and Breakdown in Dielectric Liquids" Taylor & Francis, 1969 159-165

[169] H. Fricke "A Mathematical Treatment of the Electric Conductivity and Capacity of Disperse System I The Electric Conductivity of a Suspension of Homogeneous Spheroids" Physical Review, Vol 24 575-587 1924

[170] H. Fricke "A Mathematical Treatment of the Electric Conductivity and Capacity of Disperse System II The Capacity of a Suspension of Conducting Spheroids Surrounded by a Non Conducting Membrane for a Current of Low Frequency" Physical Review, Vol 26 678-581 1925

[171] H. P. Schwan “Alternating Current Electrode Polarization” Biophysik Vol 3 181-201 1966

[172] B. Onaral and H. P. Schwan "Linear and Nonlinear Properties of Platinum Electrode Polarisation. Part 1: Frequency Dependence at Very Low Frequencies" Medical & Biological Engineering & Computing, Vol 20, 299-306 1982

[173] B. Onaral and H. P. Schwan "Linear and Nonlinear Properties of Platinum Electrode Polarisation II: Time Domain Analysis" Medical & Biological Engineering & Computing, Vol 21 21-216 1983

[174] H. P. Schwan and B. Onaral "Linear and Nonlinear Properties of Platinum Electrode Polarisation.III Equivalence of Frequency and Time Domain Behaviour" Medical & Biological Engineering & Computing, Vol 23 28-32 1983

[175] M. Umino, N. Oda and Y. Yasuhara “Experimental and Theoretical Studies of the Effect of Electrode Polarisation on Capacitances of Blood and Potassium Chloride Solution” Medical & Biological Engineering & Computing, Vol 40 533-541 2002

[176] M. Jeroense and P. Morshuis, "Space Charge Measurements on Impregnated Paper: A Review of the PEA Method and a Discussion of Results," IEEE Electrical Insulation Magazine, vol. 13(3), pp. 26-35, May 1997.

[177] R. Ciobanu, I. Prisecaru and S. Aradoaei, "PEA Measurements upon Cellulose Materials Submitted to Gamma Radiation," in International Conference on Solid Dielectrics, France, 2004.

[178] R. Ciobanu, I. Prisecaru and C. Schreiner, "Space Charge Evolution in Thermally Aged Cellulose Materials," in Solid Dielectrics, 2004. ICSD 2004, Taulorw, France, 2004.

[179] R. Ciobanu, C. Schreiner, W. Pfeiffer and B. Baraboi, "Space Charge Evolution in Oil-paper Insulation for DC Cables Application," in IEEE 14th Intern. Conf. Dielectr. Liquids (ICDL), Massachusetts, USA, 2002.

[180] R. C. Ciobanu, W. Pfeiffer and C. Schreiner, "Charge Packet Evolution in Paper-oil Insulation and Derived Technological Considerations.," in the 7th Intemational Conference on Properties and Applications, Nagoya, Japan, 2003.

[181] Y. Zhou, Y. Wang, G. Li, X. Wang, Y. Liu, B. Li, P. Li and H. Cheng, "Space Charge Phenomena in Oil-paper Insulation Materials under High Voltage Direct Current," Journal of Electrostatics, vol. 67, pp. 417-421, 2009.

[182] Y. Zhou, Q. Sun, G. Li, Y. Wang, X. Jiang, Y. Qiu, J. Li and X. Wang, "Effects of Space Charge on Breakdown Strength and Creeping Flashover in Oil-Paper Insulation," Power System Technology, vol. 33(5), 2009.

[183] C. Tang, G. Chen, M. Fu and R. Liao, "Space Charge Behavior in Multi-layer Oil-paper Insulation under Different DC Voltages and Temperatures," IEEE Transactions on Dielectrics and Electrical Insulation, vol. 17(3), pp. 778-788, 2010.

[184] C. Tang, R. Liao, G. Chen and L. Yang, "Research on the Feature Extraction of DC Space Charge Behavior of Oil-pape Insulation," SCIENCE CHINA Technological Sciences, vol. 54(5), pp. 1315-1324, 2011.

[185] J. Hao, G. Chen and R. Liao, "Effect of Thermally Aged Oil on Space Charge Dynamics in Oil/paper Insulation System," in Joint Colloquium on Transformers, Materials and Emerging Test Techniques, Kyoto, Japan, 2011.